1995

New Porphyrins As Semiconductor Photosensitizers: Molecular Engineering For Solar Energy Conversion

Biswajit Choudhury

NEW PORPHYRINS AS SEMICONDUCTOR PHOTOSENSITIZERS: MOLECULAR ENGINEERING FOR SOLAR ENERGY CONVERSION

by

Biswajit Choudhury

Department of Chemistry

Submitted in partial fulfilment
of the requirements for the degree of
Doctor of Philosophy

Faculty of Graduate Studies
The University of Western Ontario
London, Ontario
December 1994

ISBN 0-315-99249-2

ABSTRACT

The organizing properties of surface-active porphyrins can be employed to obtain large area, ordered arrays of electroactive organic molecules. The design, synthesis, and characterization of two families of surface active porphyrins, possessing variety of side chains, is described. These materials are solid at room temperature and exhibit well-behaved monomolecular films at an air-water interface.

In compressed monolayers, the porphyrin ring appears to be oriented so that the plane of the ring is perpendicular to the surface. The surface pressure-molecular area isotherms change with the length and nature of the side chains in a manner which suggests that a long side chain allows the porphyrin rings to acquire the most ordered packing. A rigid chain structure was found to restrict the orientational flexibility of the porphyrin rings and hence restricted them to acquire well-ordered monolayer.

The solid state photophysical properties of these materials are strongly dependent on their degree of order. Spectroscopic studies of single monolayer films transferred to quartz and SnO_2 slides using the Langmuir-Blodgett technique indicate that increasing the order in porphyrin monolayers leads to increasing spectral shifts in absorption and to decreasing fluorescence quantum yields. On the SnO_2 semiconductor surface, the monolayers exhibit an enhanced fluorescence quenching. This is interpreted as evidence for isoenergetic electron transfer from the porphyrin to the semiconductor. An approximate interfacial electron transfer rate (k_{et}) was estimated on the basis of the fluorescence yields on quartz and SnO_2 surfaces,

respectively.

The surface active porphyrins deposited onto SnO_2 semiconductor surface exhibit an unusual photoelectrochemical effect: a substantial and stable photocurrent/ photovoltage is generated in modified photoelectrode cells which possess porphyrins with electron rich side chains. This is interpreted as resulting from enhanced electron injection at the illuminated interface, resulting from an enhanced through bond electron tunnelling in the electron rich side chains.

An enhanced photocurrent quantum yield was exhibited by all the compounds on diluting their monolayers with dioleoylphosphatidylcholine (DOPC), a non fluorophore surface active compound. This is interpreted as resulting from minimization of the aggregate mediated quenching, which enhances interfacial isoenergetic electron transfer and hence increases the photocurrent yield.

To my parents

ACKNOWLEDGEMENTS

Nature does not often collaborate with men to permit simple repayment, whether the debt is from father to son, from soldier to comrade, or from pupil to master. It may never be possible to pay directly for the gifts of true friendship and therefore, I wish to acknowledge those people who have contributed to my apprenticeship as a scientist.

I thank my advisors, Professor Jim Bolton and Professor Alan Weedon, for providing the opportunity to pursue this work, for their boundless enthusiasm for the subject, and for their patience in allowing a novice to find his own way.

I am greatful to Dr. Lars Forss and Dr. Aitken Hoy for their help with equipment, computers and innumerable insights into the fine art of practising science on a budget.

I would like to thank my fellow graduate students in this department for their support and friendship. Specifically, I thank the following people: Dr. Andreas Rudolph, Dr. David Andrew, Dr. David Oldroyd, Dr. David Wong, Dr. David Hastings, Dr. David Fraser, Dr. Te-Fu Ho, Kelly Hislop, David Maradyn, Paul Krug, Brian DesIslet, Wendy Holden, Tracy Quevillon and Sumit Saha. I am very lucky to gain a number of valued friendships from the "Great Weedon Group".

I would like to convey my deepest appreciation to all the members of the chemistry department, faculty and staff who assisted me in the completion of this work. I am greatful to Cheryl O'Meara and Shannon Woodhouse for the assistance she had provided.

I also wish to acknowledge invaluable and constructive discussions with Drs. B. N. Jagatap, Hemant Sinha and Sujit Roy. I greatly appreciate their contribution to broaden the horizon of my knowledge in basic scientific research.

Finally, I would be a cad, if I were to neglect my wife, Rakhi. But for her confidence in the soundness of the endeavour, her unwavering faith in my abilities and her constant encouragement, this thesis would have remained nothing more than a twinkling in my eye. Her immeasurable contributions are indelibly inscribed in every page of this manuscript. In addition, I would like to thank rest of my family for their love, encouragement and support.

TABLE OF CONTENTS

LIST OF TABLES

LIST OF PHOTOGRAPHIC PLATES

LIST OF FIGURES

LIST OF SCHEMES

LIST OF APPENDICES

CHAPTER 1

GENERAL INTRODUCTION

Mankind has regarded the sun as the source of life and energy since time immemorial. In fact, our traditional energy resources, such as oil and coal, are all products of photosynthesis. With the increasing energy crisis, man is again looking towards the prime energy giver, *the sun*. There is more solar energy that impinges on this earth every hour than could be used by the most greedy and naive society.[1] It is limited in its utility, however, by its low energy density.[2] Harnessing solar energy has therefore attracted the attention of scientists, technologists, economists, sociologists and politicians. All solar energy converters utilize radiation received from the sun. Hence, an understanding of the nature of this radiation is imperative.

The first and most efficient of all solar chemical systems is that of the green plant. The green plant does most of its work with compounds called chlorophylls, which consist of a porphyrin ring with Mg^{2+} complexed at the centre, attached to a long hydrocarbon tail called a phytol. The chlorophyll is not distributed evenly throughout the leaf, but is localized in small units called chloroplasts. Furthermore, the arrangement is not even uniform within the chloroplasts. In a single photosynthetic unit, there is one active center, plus about 300 extra chlorophyll units embedded in a lipid bilayer membrane. The purpose of these extra units is to act as an antenna so that the light absorbed will be delocalized through the system and can,

eventually reach the active center to drive the process of photosynthesis. It is known that the primary photochemical step in green plant photosynthesis involves a one-electron transfer reaction from the excited singlet state of a chlorophyll species to an electron acceptor molecule.[3] The photosynthetic reaction takes place within a reaction-center protein which spans the thylakoid membrane of the chloroplast. This protein functions as a *solar cell*, converting light to electricity, which is then used to drive the slower biochemical reactions, ultimately resulting in the storage of energy as carbohydrates.

In order to fabricate a device that will the mimic photosynthetic process, an understanding of the kinetic and thermodynamic parameters influencing the efficiency of this process is required. An interesting approach is the synthesis and study of donor-acceptor molecules in which photoelectron transfer takes place from a donor moiety to an acceptor moiety.[4] Variation of parameters such as the redox potential difference between the donor and acceptor, the physical distance between them and the nature of the linking molecules has increased the understanding of this process. At present, however, only solution spectroscopic studies and some membrane studies have been conducted to infer photoelectron transfer.

Two distinct types of solar energy conversion devices or systems have emerged over the years: (a) solar thermal conversion devices, which principally use the infrared part of the solar spectrum and (b) solar photoconversion devices, which are based on photons absorbed in the visible/UV region. In the first category, the incident radiation is converted into thermal energy, which is subsequently used for domestic water heating, driving mechanical pumps, thermoelectric generators, etc. The second

category includes the direct conversion of sunlight to electricity, which is an obvious choice since the number of energy wasteful conversion steps is minimized.

Conventional photovoltaic solar cells use inorganic semiconducting materials, such as silicon, to convert sunlight directly into electrical energy. Their simplicity, reliability and favourable power to weight ratio have made them the *preferred* method of providing power for spacecraft over the last thirty years. The physics behind these types of devices also seems to be fairly well understood. However, photovoltaic modules and systems cost too much (typically about four times)[5] to compete effectively with conventional electrical energy from the utility grid. With a goal of finding a more cost effective way of producing electricity, chemists started investigating semiconductor-redox electrolyte liquid-junctions and related photo-electrochemical cells[6,7] as a possible means of solar energy conversion to electricity. In spite of significant problems posed by photocorrosion and surface imperfections/defects in these "wet photovoltaic cells", conversion efficiencies of over 15% have been obtained on solar cells (photoelectrochemical cells) composed of single crystals of Si or GaAs.[8] Techniques are now available to treat the surface imperfections, but photocorrosion still remains a serious problem, limiting the practical application of this type of liquid-junction solar cells.

Oxide semiconductors, such as TiO_2, $SrTiO_3$ or SnO_2 have exceptional thermal and photochemical stability against corrosion, but their large bandgaps reduce the fraction of solar irradiation that can be harvested. In fact, the large bandgap restricts them to the UV portion of the solar spectrum for direct electron transfer on exposure to light. In principle, the spectral response can be improved by doping the

semiconductor with appropriate metal ions. An alternate possibility is to coat the semiconductor surface with highly coloured dye molecules. In the excited state these dye molecules are better donors or acceptors than the ground state, and thus they undergo electron-transfer reactions with nearby substrates, that is, the semiconductor. This process is called *dye sensitization*. The assistance of the dye helps the semiconductor to access the visible portion of the solar spectrum. Sensitization of large bandgap semiconductors using coloured dye molecules has been investigated for many years.[9] There is extensive industrial interest in the field of dye sensitization with possible applications in fields such as photography, photochromic devices and photolithography.[10]

The use of organic, inorganic and organometallic dyes for the semiconductor sensitization process has been cited in many references. A number of groups have employed organic dyes, such as porphyrins[11] and phthalocyanines,[12] for the semiconductor sensitization process. Porphyrins have drawn attention as a dye in this field because of their presence in natural photosynthesis, where chlorophylls act as the absorbers (antenna system) and as the primary electron donors in the photosynthetic membrane. Porphyrins have been a very well-studied group of compounds. The name porphyrin is derived from the Greek πορφυρος (purple). Because of their natural occurrence, stable structure, absorption in the visible range and low oxidation potential, they have been frequent candidates for *organic solar-cell* materials.

1.1 PRESENT RESEARCH : UNDERLYING PRINCIPLE

The present project involves the utilization of the principles of dye sensitization of semiconductors to study the behaviour of a semiconductor liquid-junction photoelectrochemical cell. It is well known that the dye molecules residing in the closest proximity of the semiconductor surface play an important role in isoenergetic electron injection processes. Considerable work has been carried out to determine the dependence of the electron injection rate (and hence the photocurrent yield) on the nature of bonding between the dye molecules and the semiconductor surface. However, the dependence of the electron injection rate on the structure of the dye is not well known. The present work is directed toward the study of the photocurrent quantum yield (or the rate of the isoenergetic electron injection) on the structure of the dye.

In the present work, the study of semiconductor dye sensitization utilized a Langmuir-Blodgett (LB) monolayer film of surface active porphyrin dyes deposited either onto a quartz slide or onto a SnO_2 coated glass slide. As the porphyrin is a highly nonpolar compound, it was made surface active by locating a carboxylic acid group at the end of a side chain attached to the porphyrin ring. When the dye modified semiconductor is placed into an electrochemical cell, it acts as a photoelectrode. It is thus possible to measure directly the photoelectron transfer process by observing the current produced by light impinging on the electrode. Monomolecular layers (monolayers) of LB films are prepared at an air-water interface, since this allows manipulation of the structure on a molecular level. Using porphyrins as the dye in the present work has another advantage. This can lead us

to the direct characterization of the solid state nature of the donor (porphyrin) and acceptor (semiconductor surface) moieties.

In the present work, the idea was to study the relation between the photocurrent efficiency of a porphyrin dye and the nature of the linkage between the porphyrin and the semiconductor surface, which were conceived as logical extensions to the experiments on P-A (see below for nomenclature), which were carried out earlier in our laboratory. To investigate the linkage dependence of photocurrent efficiency, we designed our model compounds for two different kind of studies, (i) to study the distance dependence of the photocurrent quantum yield, where the chemical nature of the chain is same, and (ii) to study the photocurrent quantum yield dependence only on the chemical nature or constituents of the side chain, where the chain length is almost constant. Figure 1.1 shows the porphyrin compounds specifically designed for the present work. The systematic nomenclature of porphyrins[13] is much too cumbersome to be used in written work; instead, each compound will be named using "P" to designate the porphyrin ring, "A" to designate the carboxylic acid group, and appropriate designations for porphyrin substituents and bridging groups.

In Figure 1.1, the compounds of Series-I constitute P-A, P-Me-A, P-Et-A and P-Pr-A, respectively. As we go from P-A to P-Pr-A, the chain length is varied by adding a methylene group, as spacer, between the porphyrin ring and the carboxylic acid group. Hence it was anticipated that, using these compounds, the distance dependence of the photocurrent efficiency can be measured. Moreover, due to the similar chemical nature of these chains (all contain methylene groups only), any

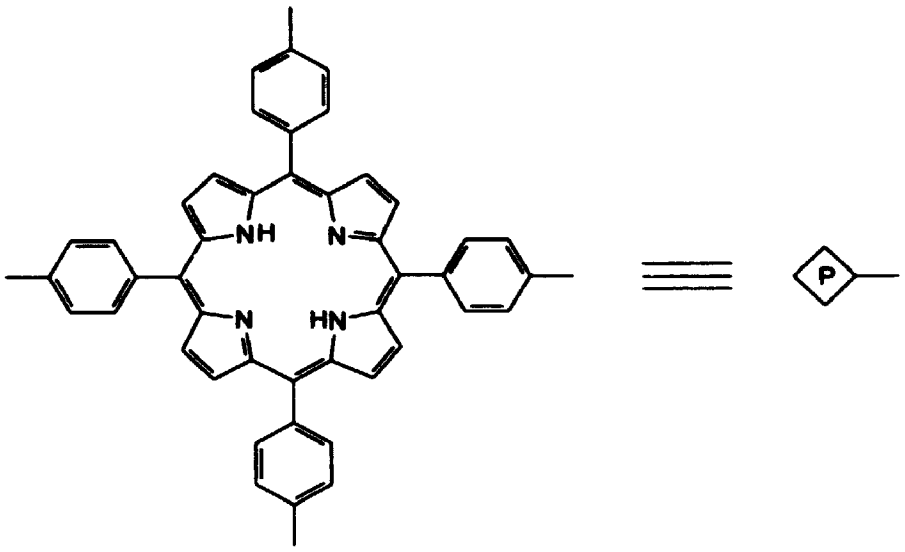

P-A (1)

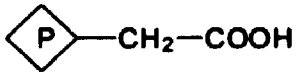

P-Me-A (7)

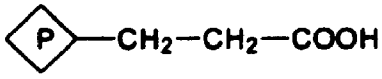

P-Et-A (9)

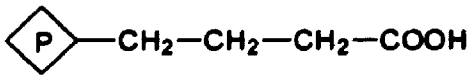

P-Pr-A (25)

Series - I

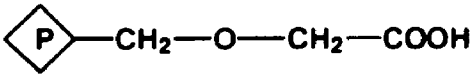

P-Glyco-A (16)

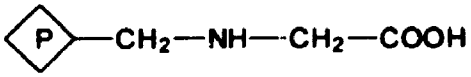

P-Gly-A (11)

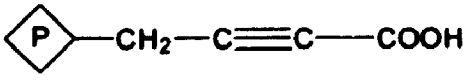

P-Ace-A (23)

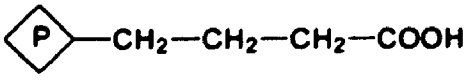

P-Pr-A (25)

Series - II

Figure 1.1 : Designed surface active porphyrin molecules.

variation in the photocurrent efficiency among these compounds can be correlated directly with the chain length. The compounds of Series-II constitute P-Glyco-A, P-Ace-A, P-Gly-A and P-Pr-A, respectively. In all four of these compounds, the distance between the porphyrin ring and the carboxylic acid group is almost same, but the spacer groups are completely different in chemical nature, and hence they possess different electronic environments as well. Thus, the variation in photocurrent efficiency for these compounds reflects different electronic environments possessed by these spacer chains. It was expected that by studying the photoelectrochemical behaviour of all these model dye compounds we would be able to investigate whether isoenergetic electron transfer follows through-space or through bond electron tunnelling mechanisms.

Among all the compounds shown in Figure 1.1, P-A has been previously synthesized and studied by different workers, and in the present study it was used as a standard. The synthetic methodologies for preparing the rest of the six model porphyrin molecules were derived in the present work and all of them were successfully synthesized.

1.2 OUTLINE OF THE THESIS

The thesis is divided into seven chapters, of which this general introduction comprises the first. Chapter 2 is devoted to the synthesis and characterization of the model porphyrin compounds, while Chapter 3 outlines their general spectroscopic properties in solution. A quantitative estimation of their fluorescence quantum yields in four different solvent systems is also presented here. In Chapter 4, the surface

pressure-area isotherms, and general spectroscopic properties are described, and the results are used to estimate the fluorescence quantum yield of these molecules on quartz and SnO_2 surfaces, respectively. The photoelectrochemical properties of these molecules are described in Chapter 5, and the relation of structure to photocurrent efficiency for all the model compounds has been established on the basis of the obtained results. Chapter 6 describes the experimental details of Chapter 2, that is, the synthesis of all the model porphyrin compounds. Finally, Chapter 7 details the conclusions of the present work and some suggestions for further research.

REFERENCES

1. Bolton, J. R. *Solar Energy* **1983**, *31*, 483.
2. Bolton, J. R. *Ann. Rev. Energy* **1979**, *4*, 353.
3. Katz, J. J.; Norris, J. R.; Shipman, L. L.; Thurnauer, M. C.; Wasielewski, M. R. *Annu. Rev. Biophys. Bioenerg.* **1978**, *7*, 393.
4. Bolton, J. R.; Connolly, J. S. In *Photoinduced Electron Transfer*; Fox, M. A.; Chanon, M. (eds.); Elsevier Science Publishers: New York, **1988**, 303.
5. Nolan, J. F. *The Spectrum* **1993**, *6*, 1.
6. Kalyanasundaram, K. *Solar Cells* **1985**, *15*, 93. and references therein.
7. Serpone, N.; Pelizzetti, E. *Photocatalysis: Fundamentals and Applications*, Wiley: New York, **1989**.
8. Heller, A. In *Energy Resources Through Photochemistry and Catalysis*, Grätzel, M. (ed.), Academic Press: Florida, **1983**.
9. (a) Willig, F.; Gerischer, H. *Top. Curr. Chem.* **1976**, *61*, 31. (b) Gerischer, H. *Photochem. Photobiol.* **1972**, *16*, 243. (c) Memming, R. *Photochem. Photobiol.* **1972**, *16*, 243.
10. (a) James, T. H. (ed.) *Theory of the Photographic Process*, 4th ed., Macmillan: New York, **1977**. (b) Weigl, J. W. *Angew. Chem. Internat. Edn.* **1977**, *16*, 374. (c) Charlé, K. -P.; Willig, F. In *Modern Aspects of Electrochemistry*, Convey, B. N.; Bockris, J. O'M.; White, R. E. (eds.), Plenum: New York, **1988**, *19*, 359.
11. For a review, see: (a) Dolphin, D. (ed.) *The Porphyrins*, Academic Press: New York, **1978**, Vol. I-VII. (b) Gouterman, M.; Rentzepis, P. M.; Straub, K. D. (eds.) *Porphyrins, Excited States and Dynamics*: ACS Symposium Series 321;

American Chemical Society: Washington, D. C. 1986.

12. For a review, see: Moser, F. H.; Thomas, A. C. *The Phthalocyanines*, CRC Press: Florida; 1983; Vols. I and II.

13. Bonnett, R. In *The Porphyrins*, Dolphin, D. (ed.), Academic Press: New York, 1978, Vol I.

CHAPTER 2

THE DESIGN, SYNTHESIS AND CHARACTERIZATION OF SURFACE ACTIVE PORPHYRINS

2.1 INTRODUCTION

As discussed in Chapter 1, the purpose of the present study was to establish a relation between the photocurrent quantum yield and the structure of the porphyrin dye, which is present as a monolayer on the semiconductor surface and which is used as the sensitiser. In order to form a monolayer on a semiconductor surface, it is necessary for these porphyrin model compounds to be surface active. Therefore, generation of a surface active group at the end of the porphyrin chain was an important part of the synthesis. As the surface of an SnO_2 semiconductor is comparatively basic, it was anticipated that a carboxylic acid group would be an appropriate surface active group, since it could form an ionic linkage between the semiconductor surface and the porphyrin derivative.

Two different series (Series-I and Series-II) of porphyrin model compounds (Figure 1.1) were designed for the present study. Series-I is comprised of the compounds P-A (1), P-Me-A (7), P-Et-A (9) and P-Pr-A (25). These possess different chain lengths between the relatively nonpolar porphyrin ring and the polar carboxylic acid group. The chain length was varied by changing the number of methylene ($-CH_2-$) groups present in the linkage joining the porphyrin to the carboxyl group. Thus while the chain length was varied, the chemical nature of the chain

remained unchanged. The intention in designing this group of model compounds was to focus on the dependence of photocurrent quantum yield on the distance between the porphyrin chromophore and the semiconductor surface, rather than on the possible electronic conducting nature of the chains.

The members of the Series-II compounds are P-Gly-A (11), P-Glyco-A (16), P-Ace-A (23) and P-Pr-A (25). These possess almost the same chain length between the porphyrin ring and the carboxylic acid group. Different functional groups within the chain were selected such that the effective chain length was not changed but the electronic environment along the chain was changed dramatically. The idea behind designing this group of compounds was to probe how the photocurrent quantum yield depends on the chemical nature of the chain, rather than the chain length.

2.2 EXPERIMENTAL

The detailed synthetic procedures for the preparation of all the desired porphyrin compounds, the instrumental techniques used and the spectroscopic data obtained to characterize the compounds and prove their structures are given in Chapter 6. The references numbers cited in Chapter 6 are given in the reference list of this chapter.

2.3 RESULTS AND DISCUSSION

The synthesis of model porphyrin molecules can be divided into three parts: (i) preparation of the donor molecule i.e., the porphyrin core unit; (ii) linkage of the donor with the chain possessing the desired bridging groups; (iii) generation of a

carboxylic acid group at the end of the linked chain. The preparation of all the model compounds has been achieved as shown in Schemes 1-13. The preparative routes outlined in these schemes are the result of the adaption of literature precedents for the functional group transformations desired.

The tritolyl porphyrin molecules used in the present study were found to be soluble in very few solvent systems. Due to this limitation of solvent choice, literature precedents for functional group transformations had to be modified appropriately in order for them to work for the porphyrin systems. The solvents THF, DMF and $CHCl_3$, as well as various mixed solvents, were frequently used. In addition, zinc porphyrins were often used as starting material, either to protect the protons on the nitrogens of the porphyrin core from any unwanted side reaction, or to increase the solubility of the porphyrins in solvents such as DMF and THF.

All the synthesised compounds were characterized using routine spectroscopic methods. The structures of the target molecules were established from their spectroscopic data by comparison of the data with the predicted values and with data for compounds of analogous structure. All the porphyrins possessing a carboxylic acid group were found to be poorly soluble in most of the organic solvents. Due to this problem, it was often difficult to record good ^1H and ^{13}C-NMR spectra for the compounds containing a terminal carboxylic acid group.

An interesting feature in the ^1H-NMR spectra of the synthesized porphyrins was observed. The coupling of a side chain with the porphyrin moiety led to the splitting of the sharp singlet signal seen for the β-pyrrole protons of tetra-aryl-porphyrin into two different sets of signals. The first set with an integration for six

protons, appeared down-field with respect to the second set, which had an integration of two protons. This presumably arises from destruction of the porphyrin symmetry as well as the change in the electronic environment of the β-pyrrole protons in the vicinity of the attached chain. The two β-pyrrole protons (H_a protons) (Figure 2.1) closest to the side chain apparently become shielded and appear upfield from the other six β-pyrrole protons (H_b protons).

2.3.1 SYNTHESIS OF COMMON STARTING MATERIALS, SCHEMES 1, 2 AND 3

As is evident from Figure 1.1, the molecules targeted for synthesis possess the same tritolylporphyrin unit and different side chains separated by a benzylic unit. A common starting material for the preparation of these compounds ideally should have a good leaving group attached to the methylene carbon of the benzylic group that is attached to the tritolylporphyrin unit. The desired side chain can then be coupled to the benzylic methylene carbon by substituting the leaving group with a nucleophilic adaptation of a suitable side chain in an S_N2 fashion. Hence TTP-Cl (3) (Scheme 3) was considered as the *ideal* common starting material and its synthesis was attempted first. The preparation of TTP-Cl was accomplished by following a series of standard chemical pathways, as shown in Schemes 1-3. P-A (1) was first prepared following a published literature procedure[1] summarized in Scheme 1. It wa. then converted to TTP-OH (2) by reducing the carboxylic acid group to the corresponding primary alcohol group (Scheme 2). Finally TTP-Cl (3) was obtained by converting the alcohol group of TTP-OH (2) to a chloride substituent. ZnTTP-Cl (4) was

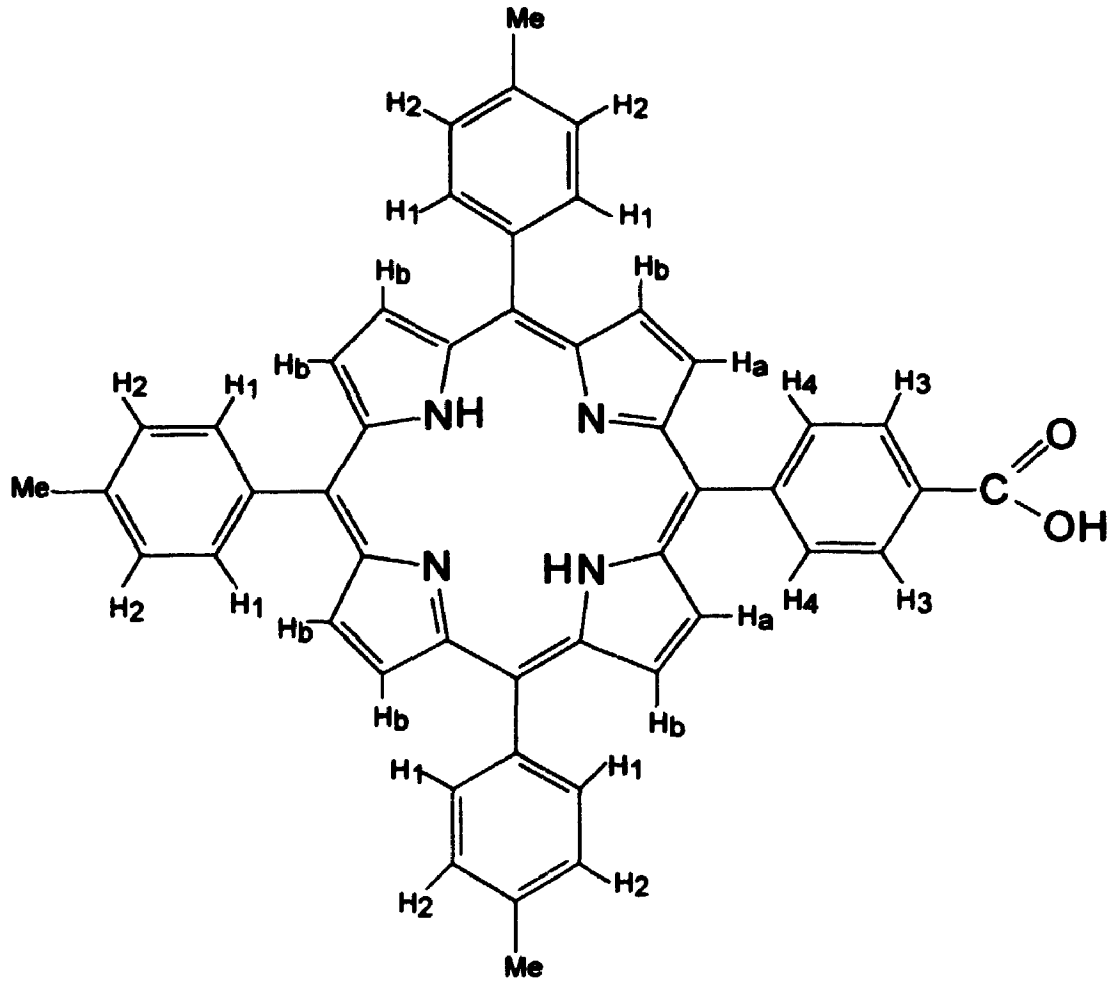

P-A (1)

Figure 2.1 : P-A (1) with labelled ring protons.

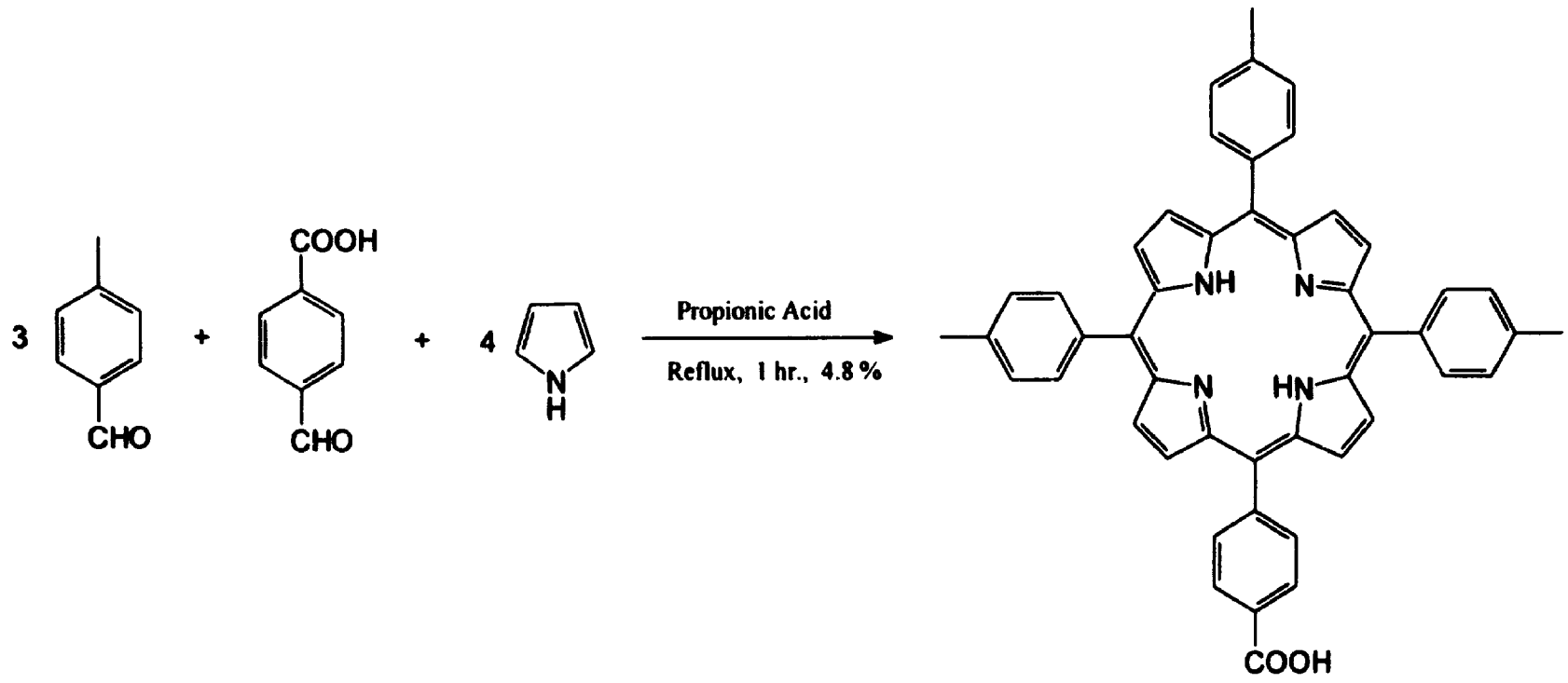

P-A (1)

Scheme 1 : Synthesis of P-A (1)

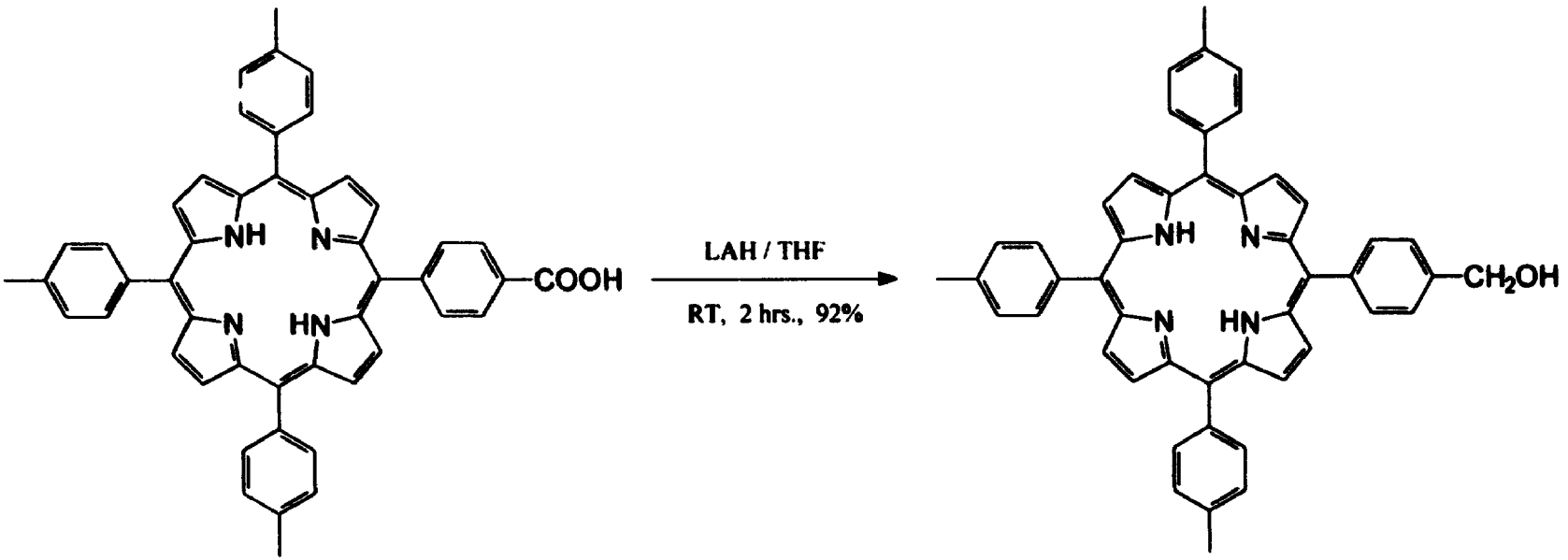

P-A (1)

TTP-OH (2)

Scheme 2 : Synthesis of TTP-OH (2)

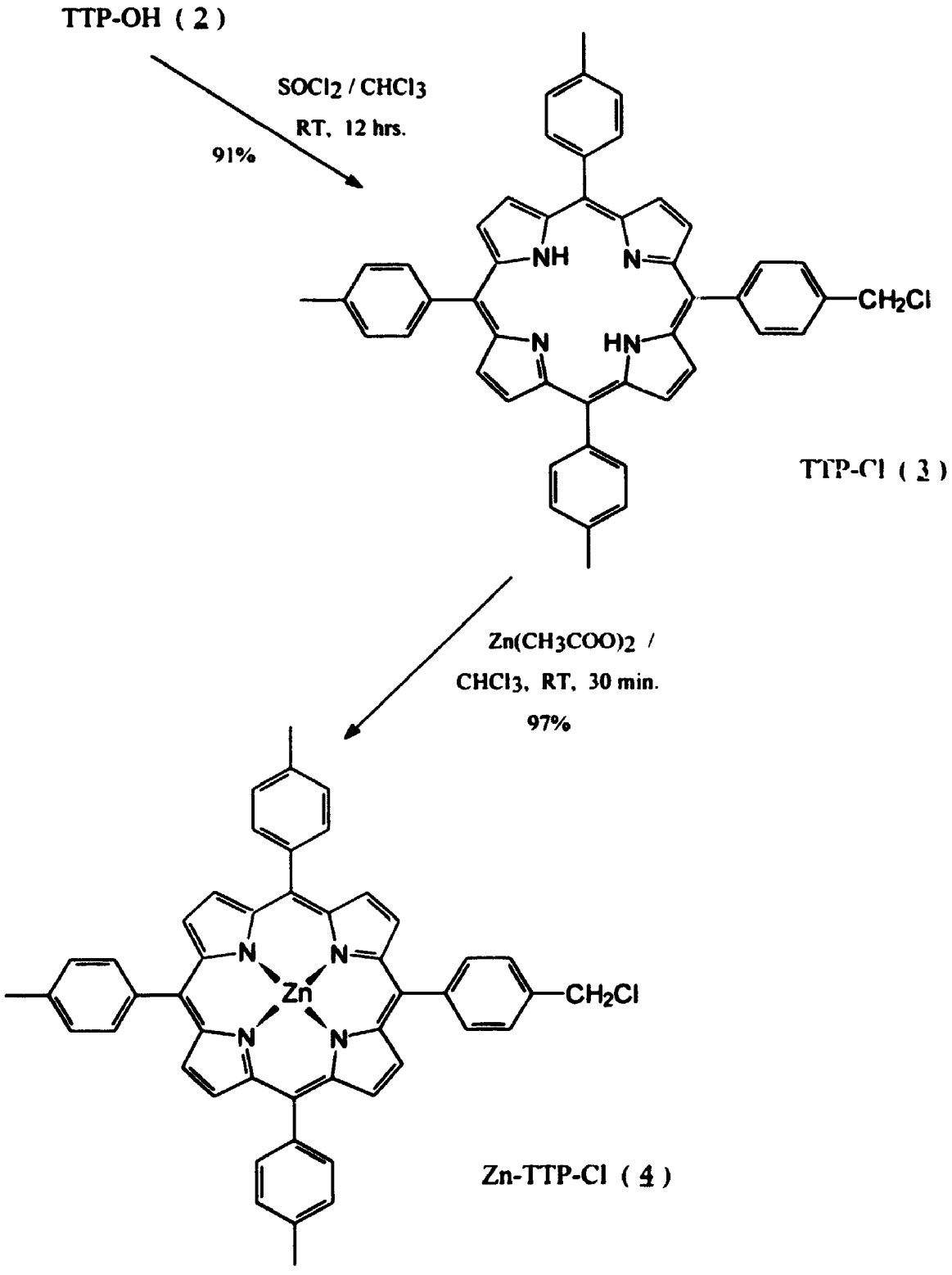

Scheme 3 : Synthesis of TTP-Cl (3) and ZnTTP-Cl (4)

prepared by inserting a Zn^{2+} ion into the porphyrin core of TTP-Cl (3). These syntheses are described in more detail below and the structure of the compounds prepared are proved using their spectroscopic data.

2.3.1.1 Synthesis of TTPa or P-A (1), Scheme 1

5-(4-Carboxyphenyl)-10,15,20-tri(p-tolyl) porphyrin (TTPa) or P-A (1) was prepared by the condensation of p-tolualdehyde, p-carboxybenzaldehyde and pyrrole in propionic acid. The condensation procedure followed was adapted from that reported in the literature[1], where a yield of 2.8% was recorded. An attempt was made to improve the very poor yield of this compound. After several attempts, it was observed that the yield can be maximized to 4.8%, by carrying out the reaction with 1:3:4 mole equivalent ratio of p-carboxybenzaldehyde, p-tolualdehyde and pyrrole. The byproducts of this reaction consist of ~90% tetratolyl porphyrin (TTP) and ~5% of the di- and tri-carboxylic derivatives. The formation of these byproducts has been reported by earlier workers[1].

^{1}H-NMR spectroscopy has been a very valuable tool in assignment of porphyrin core unit. The porphyrin ring protons in the different environments are shown in Figure 2.1. The principal resonances[2] are 8.8 δ (bs, 8H, H_a and H_b protons), 8.3 δ (d, 2H, H_4 protons), 8.1 δ (d, 2H, H_3 protons), 7.7 δ (d, 6H, H_1 protons), 7.5 δ (d, 6H, H_2 protons), 2.7 δ (s, 9H, CH_3 protons) and -2.8 δ (bs, 2H, pyrrole N-H).

In agreement with the above generalization P-A (1) shows the peaks in the expected region. Usually symmetrical porphyrins give a sharp singlet for β-pyrrolic

protons (i.e., H_a and H_b), but a broad singlet is normally observed for P-A (1). This may be inferred as a result of the interaction between H_a, H_4 and H_b, H_1, although the broadening may merely be the result of the loss of symmetry resulting from the presence of a single carboxyl substituent. The tolyl aromatic protons closest to the porphyrin ring (H_1, H_4) are expected to be more shielded than the protons farther from the porphyrin ring (H_2, H_3), and hence the peaks for H_1 and H_4 are expected to be more upfield than H_2 and H_3. The observed result was quite different from the expected one. The chemical shifts of H_2 and H_3 were observed to be more upfield than H_1 and H_4. This suggests that the tolyl rings are not exactly perpendicular to the porphyrin ring, but rather are slightly tilted towards the horizontal plane. The -COOH proton was hydrogen bonded with the water contamination present in the solvent and did not appear separately.

The mass spectrum exhibited ions at 700 (100%), 656 and 350 mass units. These correspond to the calculated molecular weight of 700, as well as the expected fragmentation pattern of the porphyrin compound. The fragment at m/e = 656 is 44 mass units less than the molecular weight suggesting the loss of CO_2. The fragment at m/e = 350 corresponds to a doubly charged (M^{2+}) parent molecule. P-A (1) was also analyzed by infra-red spectroscopy; a carbonyl stretch and a hydroxyl stretch at 1691.8 cm^{-1} and 3314.1 cm^{-1} respectively were observed and confirmed the presence of the carboxyl group.

2.3.1.2 Preparation of TTP-OH (2), Scheme 2

The conventional method[3a] for the reduction of a carboxylic acid group to an alcohol by lithium aluminium hydride (LAH) was followed. A mixture of P-A (1) and LAH in dry tetrahydrofuran (THF) was stirred at room temperature. Refluxing of the reaction mixture is recommended in literature, but in the present case formation of another unidentified byproduct was observed by analytical tlc if these conditions were used. Clean reduction occurred when the reaction was performed at room temperature and a very good yield (92%) was obtained. The formation of the byproduct was also observed on prolonged (>3 hours) stirring of the reaction mixture at room temperature. Hence it was concluded that the temperature and reaction time are very crucial variables to maximize the yield by eliminating the formation of the byproduct.

The ^{1}H-NMR spectra of TTP-OH (2) show the peaks corresponding to the porphyrin core unit and they were assigned similarly as P-A (1). In addition a doublet at δ = 5.05 was observed. This peak is assigned to the new benzylic methylene protons which are coupled with the hydroxyl (-OH) proton of TTP-OH. The chemical shift expected for the methylene protons was calculated according to Shoolery's method[3b] and was predicted to be δ = 4.71; this is in reasonable agreement with the observed value. The hydroxyl (-OH) proton was observed as a hydrogen bonded -OH at δ = 1.54. Addition of D_2O, resulted in the disappearance of this peak (due to deuterium exchange) and the doublet assigned to the methylene group collapsed to a singlet.

The mass spectrum of TTP-OH (2) showed peaks at m/e 686(80%), 670(20%), 343(8%), 335(2%). These were assigned to M^+, $(M - OH)^+$, M^{2+} and $(M - OH)^{2+}$ fragmentations. In the mass spectrometer TTP-OH (2) appears to easily lose an -OH group and pick up a proton to give a fragment equivalent to TTP, i.e. m/e 670. The precise mass of the molecular ion was found to be in reasonable agreement with that calculated for TTP-OH (2). Infra-red analysis of TTP-OH (2) showed disappearance of the carbonyl group of P-A (1) and the presence of an O-H stretch at 3314 cm^{-1}. The disappearance of carbonyl group is evidence of reduction of the carbonyl group of P-A (1) to an alcohol group.

2.3.1.3 Synthesis of TTP-Cl (3), Scheme 3, Step 1

TTP-OH (2) was converted to TTP-Cl (3) by treating it with thionyl chloride at room temperature. The literature procedure[4] for conversion of benzyl alcohol to benzyl chloride was followed for this conversion. The reaction was found to be temperature sensitive and formation of a byproduct occurred at higher temperatures. At room temperature a single product was observed by analytical tlc and there was no sign of the presence of starting material (2). The product was isolated as a green mass which indicates that the porphyrin is in the diprotonated form. The deprotonation of the porphyrin was achieved by dissolving it in chloroform and briefly washing the chloroform solution with water.

The ^{1}H-NMR spectrum showed the expected peaks for the porphyrin core unit and they were assigned similarly as for P-A (1). The peak for the methylene protons appeared at δ = 4.93, which is close to the chemical shift (δ = 4.61)

calculated by Shoolery's method.[3b] This peak was observed as a singlet, presumably because replacement of the hydroxyl group by the chlorine group removes the only proton available for coupling.

The mass spectrum of TTP-Cl (3) showed a highest mass peak at m/e = 670. The expected molecular ion of mass 704 was not observed, even when fast atom bombardment (FAB) and chemical ionization (CI) were used instead of electron impact ionization. The observed highest mass ion presumably arises from the loss of $Cl^{\bullet}$ from TTP-Cl (3) and the formation of tetratolylporphyrin (TTP) by protonation or reduction in the mass spectrometer. Analysis by infra-red spectroscopy revealed the absence of an O-H stretch at 3314 cm^{-1}; a new band at 694.5 cm^{-1} was observed, which is assigned to the C-Cl stretch.

The absorption spectrum showed an intense peak at 418 nm. This is the Soret or B-band of the porphyrin, and possessed a molar extinction coefficient of 4.90×10^5 M^{-1} cm^{-1}. This band is due to the transition from the ground state to second excited singlet state. Four bands were observed at 516 nm, 552 nm, 590 nm and 646 nm. Collectively they are known as Q-bands of the porphyrin and they are assigned to the transition to the first excited singlet state. These transitions correspond to the (0,0) transition and the first vibronic overtone (1,0) resulting in two band spectra. Due to the D_{2h} symmetry of the free-base porphyrin these transitions are each split into X and Y polarized components, giving the characteristic four Q-bands. This pattern was seen for all free base (i.e., unprotonated) and non-metallated porphyrins in this work.

2.3.1.4 Synthesis of ZnTTP-Cl (4) Scheme 3, Step 2

ZnTTP-Cl (4) was prepared from TTP-Cl by adapting a known literature procedure of inserting a Zn^{2+} ion into the porphyrin core.[5] A solution of TTP-Cl (3) in chloroform was mixed and stirred with a methanolic solution of zinc acetate dihydrate at room temperature for 30 minutes. Completion of the reaction was judged by the change in colour of the reaction mixture from deep purple to pink and development of a new spot on analytical tlc. An almost quantitative yield (97%) of the product was obtained. Upon prolonged stirring (>2 hours) substantial change in the yield was not observed.

The ^{1}H-NMR spectra of ZnTTP-Cl (4) showed all the expected peaks of the porphyrin core unit. The chemical shifts observed are 8.91 δ (m, 8H, H_a and H_b protons), 8.28 δ (d, 2H, H_4 protons), 8.16 δ (d, 6H, H_1 protons), 7.82 δ (d, 2H, H_2 protons), 7.60 (d, 6H. H_2 protons), 4.98 δ (s, 2H, benzyl methylene protons), 2.70 (s, 9H, tolyl methyl protons). Down-field shifts were observed for all the protons associated with the π-conjugate system of the porphyrin ring. No down-field shift for tolyl methyl protons and methylene protons was observed. This may be due to the dipolar shift[2] caused by Zn^{2+} ion. In ZnTTP-Cl (4) the formation of a coordinate bond between the nitrogen atoms and the Zn-atom (N→Zn) has occurred; these bonds may possess significant back bonding between the Zn atom and the N-atoms so that the Zn acts as an electron sink. This may cause the deshielding effect for all the protons associated with the porphyrin core. As tolyl methyl protons and methyl protons are not associated with the π-conjugate system, they remained unaffected by Zn^{2+} insertion. Resonances at ~-2.8 ppm was found to be absent due to the removal

of the N-H protons, which is consistent with the insertion of a Zn^{2+} ion into the center of the porphyrin ring.

The mass spectrum of ZnTTP-Cl (4) revealed no molecular ion and the highest mass ion corresponded to the loss of Cl•, as was observed in TTP-Cl (3). Consequently the expected molecular ion (m/e = 767) was not observed and instead the highest mass ion possessed m/e 732 was observed. This mass ion was assigned to ZnTTP, which was formed after the loss of Cl• and reduction or protonation. Infra-red analysis showed the absence of the N-H (3312 cm^{-1}) stretch and the presence of the 695 cm^{-1} C-Cl stretch.

The absorption spectrum of ZnTTP-Cl (4) showed the characteristic Soret band at 420 nm with a molar extinction coefficient of 4.95×10^5 M^{-1} cm^{-1}. Two Q-bands were observed at 550 nm and 594 nm. These correspond to the (0,0) transition and the first vibronic overtone (1,0). The collapse of four-banded spectrum of TTP-Cl (3) to the two-banded spectrum of ZnTTP-Cl (4) is due to the transformation of the symmetry of the porphyrin ring from D_{2h} to D_{4h}. As a result the X and Y polarized components of both the transitions merge to form two Q-bands. This general result was observed for all of the protonated and metallated porphyrins in this work. The two Q-band absorption bands are responsible for the green colour seen for protonated porphyrins; in the case of metallated porphyrins back bonding to the metal shifts the Q-bands, so that the colour can vary. In the case of ZnTTP-Cl (4) the colour was pinkish purple.

2.3.2 SYNTHESIS OF P-Me-A (7), SCHEME 4

P-Me-A (7) is the next member of the homologous series of P-A (1) and the second member of the compounds of Series-I (Figure 1.1). In this compound a methylene group has been added between the porphyrin ring and the carboxylic acid group. To insert the methylene group, a known methodology,[6] as shown in Scheme 4, was adapted. This involved the preparation of a cyano derivative of the porphyrin, from the corresponding porphyrin chloride, and hydrolysis of the cyano group to generate a carboxylic acid group. The literature[6b] suggests that the direct hydrolysis of the cyano group can be very slow and can give a very low yield of the corresponding acid. Therefore methanolysis of the cyano derivative was examined in order to get a high yield of methyl ester, which upon hydrolysis would be expected to give a good yield of the required porphyrin acid.

In order to make this synthetic procedure more efficient direct one-step conversion of TTP-OH (2) to corresponding nitrile was attempted. A published literature procedure[7] for the conversion of benzyl alcohol to benzyl cyanide was followed. In the published procedure treatment of benzyl alcohol with two equivalents of NaCN plus trimethyl silyl chloride (Me_3SiCl) and a catalytic amount of NaI in a 1:1 mixture of DMF/CH_3CN, at 60-65°C for two hours gave a very high yield (98%) of benzyl cyanide. As TTP-OH (2) has a structural similarity with benzyl alcohol, this reaction strategy was applied. However no new product was formed, based upon tlc and ^{1}H-NMR evidence, after eight hours of treatment. The failure of this procedure may be attributed to the poor solubility of TTP-OH (2) in 1:1 mixture of DMF/CH_3CN.

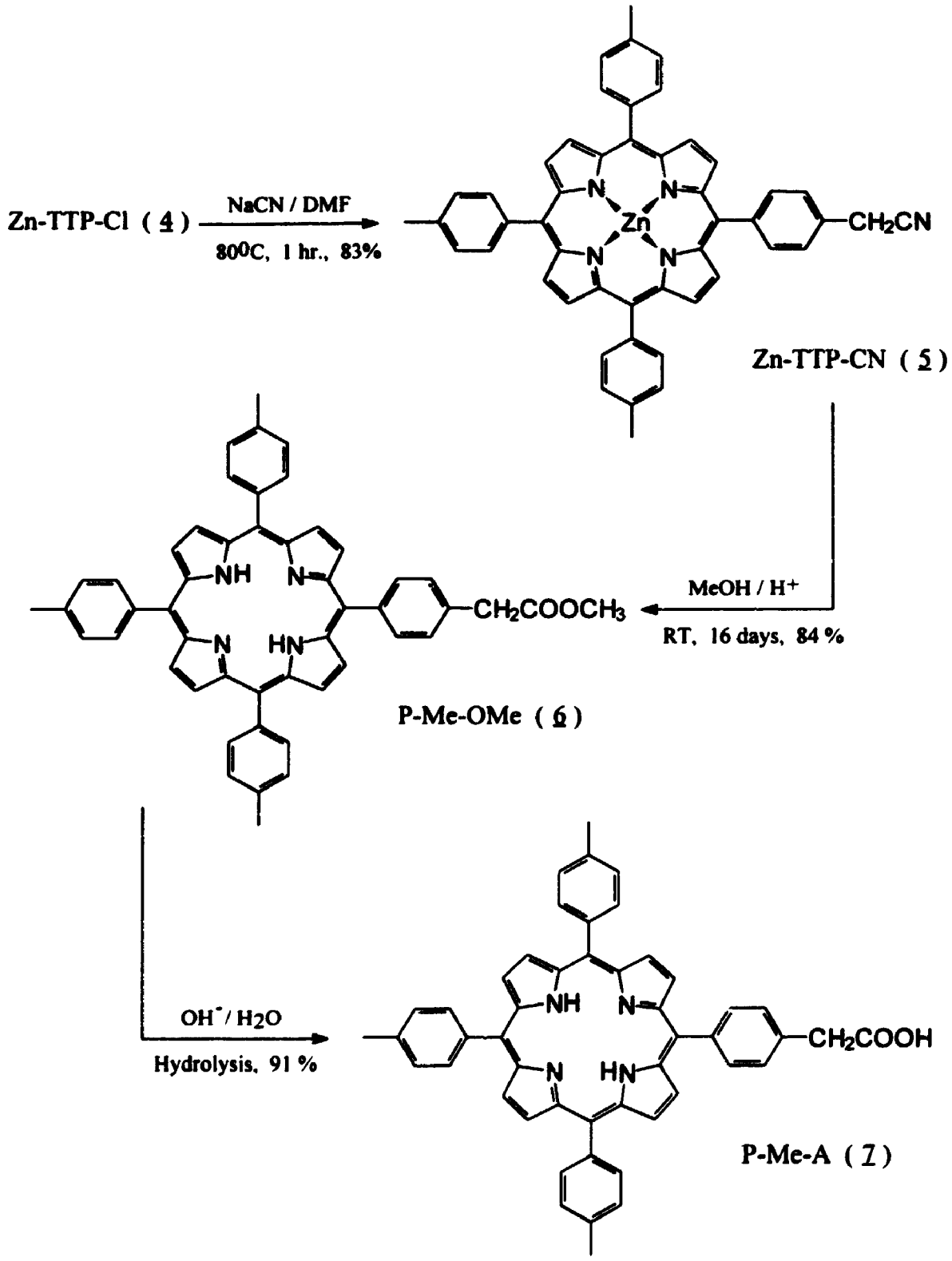

Scheme 4 : Synthesis of P-Me-A (7)

2.3.2.1 Synthesis of ZnTTP-CN (5), Scheme 4, Step 1

ZnTTP-CN (5) was prepared by adapting a known literature procedure for transforming (2-bromoethyl)-vinylporphyrins to the corresponding (2-cyanoethyl)-vinylporphyrins.[6] The use of N-methyl pyrrolidone as solvent has been suggested in the literature but the starting material TTP-Cl (3) was found to be insoluble in it. Therefore DMF, in which TTP-Cl (3) is fairly soluble, was used. A very low yield (21%) of the cyano derivative was obtained. Poor solubility of TTP-Cl (3) in DMF may have accounted for the low yield of the product. The yield of the cyano derivative was improved significantly (83%) by replacing TTP-Cl (3) with ZnTTP-Cl (4) which is very soluble in DMF. Therefore metallation of the porphyrin core is *necessary* for increasing the solubility of the reactant and the product in DMF and hence the conversion yield. Heating the reaction mixture at 50° C was recommended in the literature, but in the present case a quick conversion was only observed at higher temperature (~80° C). For analytical convenience a small quantity of ZnTTP-CN (5) was demetallated[8] to generate TTP-CN (5a) and it was used for all spectral analysis.

The ^{1}H-NMR spectra of TTP-CN (5a) exhibited all the peaks of the protons associated with the porphyrin ring system and they were assigned similarly as P-A (1). β-Pyrrole protons did not come as a multiplet, rather appeared in two different places. All β-pyrrole protons labelled (Figure 5.2) as H_b (δ = 8.88) appeared 0.1 ppm downfield from those labelled as H_a (δ = 8.78) protons. This may be due to the shielding effect caused by the -CN group, resulting in the upfield shift of both H_a protons. The methylene protons of the benzyl group were shifted from 4.93 δ for

TTP-Cl (3) to 4.12 δ for TTP-CN (5a); this exchange is in agreement with the value calculated (δ = 3.78) according to Shoolery's method. This evidence supports the formation of TTP-CN (5a). The presence of a broad singlet at -2.79 δ confirmed the demetallation of the porphyrin core and restoration of its free-base structure.

The mass spectrum of TTP-CN (5a) shows ions at m/e 695(100%), 670(18%) and 335(4%) mass units. These were assigned to M^+, $(M - CN)^+$ and $(M - CN)^{2+}$ fragmentations respectively. TTP-CN (5a) appears able to lose the -CN group and pick up a proton to give a fragment equivalent to TTP (m/e 670). The fragment of mass 335 was assigned to $(M - CN)^{2+}$ fragmentation of TTP-CN (5a) molecule. The observed precise mass was found to be in close agreement with that calculated for TTP-CN (5a). Infra-red analysis of TTP-CN (5a) showed the presence of the C≡N stretch at 2253.0 cm^{-1}. The appearance of the C≡N stretch and the precise mass of the product confirms the formation of TTP-CN (5a).

2.3.2.2 Synthesis of P-Me-OMe (6), Scheme 4, Step 2

P-Me-OMe (6) was prepared by methanolysis of ZnTTP-CN (5) following a published procedure for conversion of (2-cyanoethyl)-vinylporphyrins to harderoporphyrin methyl ester.[6a] Treatment of ZnTTP-CN (5) with saturated methanolic HCl solution at room temperature smoothly converted the cyano group to corresponding methyl ester group and at the same time removed the metal atom. The published procedure suggested overnight treatment of ZnTTP-CN (5) for the conversion, but in the present case complete conversion was only evidenced after 16 days. Upon extraction and purification a high yield (84%) of P-Me-OMe (6) was

obtained. Premature workup resulted in incomplete methanolysis and a mixture of ZnTTP-CN (5) and P-Me-OMe (6) was obtained. Analytical tlc could not be used for monitoring the progress of the reaction as ZnTTP-CN (5) and P-Me-OMe (6) were found to have same R_f values in $CHCl_3$ and in $CHCl_3$/MeOH mixtures. Hence ^{1}H-NMR was used as a tool to monitor the conversion progress. After 16 days the methylene protons of ZnTTP-CN (5) (δ = 4.12) were found to be absent in the spectra, indicating completion of the methanolysis of ZnTTP-CN (5). More vigorous conditions such as heating could not be used to accelerate the reaction as it caused unwanted side reactions of the porphyrin ring.

All the expected peaks of the porphyrin core unit were observed in the ^{1}H-NMR spectrum and they were assigned similarly as P-A (1). The benzyl methylene protons appeared at 3.97 δ, which is in close agreement with the chemical shift (3.63 δ) calculated by Shoolery's method.[3b] The presence of an additional singlet (3.87 δ) for the methyl protons of carbomethoxy group supports the presence of a methyl ester group and hence the formation of P-Me-OMe (6). The presence of a broad singlet at -2.78 δ confirmed the demetallation of the porphyrin core and restoration of its free-base structure. The demetallation occurred due to the treatment of the metallated porphyrin with saturated methanolic HCl solution.

The mass spectrum of P-Me-OMe (6) showed peaks at m/e 728(100%), 697(4%), 670(20%) and 335(5%) mass units. These peaks were assigned as M^+, $(M - OCH_3)^+$, $(M - COOCH_3)^+$ and $(M - COOCH_3)^{2+}$ fragments respectively. P-Me-OMe (6) appears to lose the $-OCH_3$ group easily to give the fragment of m/e = 697, which subsequently loses -CO and picks up a proton to give a fragment (m/e = 670)

equivalent to TTP. The fragment of m/e = 335 was assigned to the M^{2+} fragment of the TTP molecule. The precise mass also supported the formation of P-Me-OMe (6). Analysis of P-Me-OMe (6) by infra-red spectroscopy revealed the absence of the C≡N stretch at 2253.0 cm^{-1} and showed the presence of an ester carbonyl stretch at 1741 cm^{-1}. The presence of the carbonyl group supports the formation of a carbomethoxy group from the cyano compound and thus the formation of P-Me-OMe (6).

2.3.2.3 Hydrolysis of P-Me-OMe (6) to P-Me-A (7), Scheme 4, Step 3

P-Me-A (7) was prepared by the hydrolysis of the carbomethoxy group of P-Me-OMe (6) in basic medium. P-Me-OMe (6) in THF was refluxed with aqueous sodium hydroxide solution for one hour and then it was extracted after acidification. Column purification gave 91% P-Me-A (7), a purple coloured solid compound.

^{1}H-NMR of P-Me-A (7) showed all the expected peaks for the porphyrin core unit and they were assigned similarly as for P-A (1). The methylene protons appeared at 4.04 δ, which is in reasonable agreement with the expected chemical shift (3.67 δ) calculated by Shoolery's method. Due to the hydrolysis of the carbomethoxy group the methyl protons of carbomethoxy group of P-Me-OMe (6) were absent at 3.87 δ. The -COOH proton was not observed separately as it was hydrogen bonded with water contamination present in the solvent.

The mass spectrum of P-Me-A (7) shows ions at 714(60%), 697(100%), 670(42%) and 335(10%) mass units. These peaks were assigned to M^+, $(M - OH)^+$, $(M - COOH)^+$ and $(M - COOH)^{2+}$ fragmentations respectively. P-Me-A (7)

apparently easily lose the hydroxyl (-OH) group from the carboxylic acid group to give a prominent peak of m/e = 697 as the base peak. This subsequently loses the carbonyl group and picks up a proton to give a mass ion equivalent to TTP, which appears at m/e 670. The fragment of m/e = 335 was assigned to the doubly charged mass ion of TTP. The exact mass observed was in close agreement with that calculated P-Me-A (7). Infra-red analysis of P-Me-A (7) shows the presence of a >C=O stretch at 1689.5 cm^{-1} and a new peak at 3421.6 cm^{-1}, which is due to the formation of a hydroxyl (O-H) group. The spectroscopic data indicate the presence of carbonyl and hydroxyl groups and thus confirm the formation of the carboxylic acid group by base hydrolysis of the carbomethoxy ester group of P-Me-A (7).

2.3.3 SYNTHESIS OF P-Et-A (9), SCHEME 5

P-Et-A (9) is another member of the homologous series of P-A (1) and the third member of the compounds of Series-I (Figure 1.1). Two methylene groups have been added between the porphyrin ring and the carboxylic acid group to prepare P-Et-A (9). An established[9] synthetic strategy, as shown in Scheme 5, for the addition of two methyl groups, by using a diethyl malonate derivative was followed for this preparation. A diethyl malonate derivative of the porphyrin was prepared using TTP-Cl (3) as the starting material. The malonate derivative upon hydrolysis and decarboxylation generated the desired monoacid with two methylene groups in the chain.

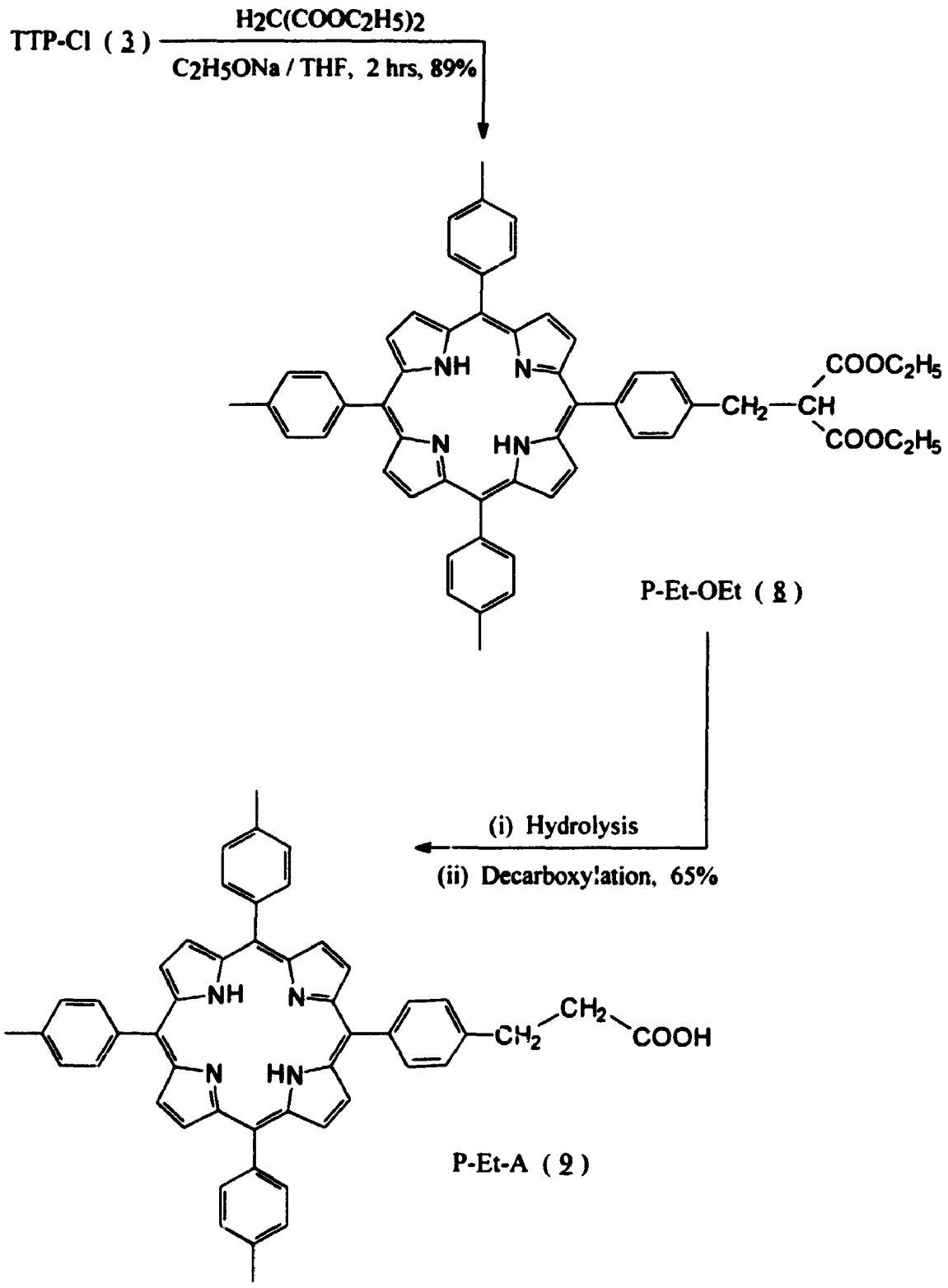

Scheme 5 : Synthesis of P-Et-A (9)

2.3.3.1 Synthesis of P-Et-OEt (8), Scheme 5, Step 1

P-Et-OEt (8) was prepared by the coupling of TTP-Cl (3) and diethyl sodiomalonate. Diethyl sodiomalonate was generated by treating diethyl malonate with sodium ethoxide. Literature procedures[9] suggest overnight reflux, but in the present case the reaction was completed in two hours. Excess diethyl malonate was used in order to avoid the formation of diethyl diporphyrin malonate, which is an unwanted side product. The presence of excess diethyl malonate had another advantage. It ensured the absence of sodium ethoxide in the reaction mixture. Being a better nucleophile than diethyl sodiomalonate, sodium ethoxide can easily react with TTP-Cl (3) to give P-CH_2-O-C_2H_5 and reduce the yield of the desired product. Hence by controlling the factors responsible for the formation of the byproducts, a very high yield (89%) of P-Et-OEt (8) was obtained.

The ^{1}H-NMR spectrum of P-Et-OEt (8) showed the peaks for the porphyrin core protons in the expected regions and they were assigned as for P-A (1). Due to the presence of the diethyl malonate group the β-pyrrole protons were split as it was seen for TTP-CN (5a). In addition peaks at 4.31 δ (q, 4H, ester methylene protons of diethyl malonate group), 3.96 δ (t, 1H, methine proton of diethyl malonate group), 3.56 δ (d, 2H, methylene protons of benzyl group) and 1.35 δ (t, 6H, ester methyl protons of diethyl malonate group) were observed. For diethyl malonate the signals for methyl ester protons, ester methylene protons and malonate methylene protons are observed at 1.28 δ, 4.20 δ and 3.35 δ respectively. The down-field shift of these protons in P-Et-OEt (8) is due to the influence of porphyrin ring current, which deshields the electronic environment of these protons in the diethyl malonate chain.

The mass spectrum of P-Et-OEt (8) showed expected peaks at m/e 828(100%), 756(32%), 682(10%) and 669(46%) respectively. These peaks were assigned as M^+, $(M - C_4H_{10}O)^+$, $(M - C_6H_{10}O_4)^+$ and (M - diethyl malonate chain)$^+$ fragments respectively. P-Et-OEt (8) appears to lose a $-OC_2H_5$ and a $-C_2H_5$ group from the ester group to give a fragment of m/e 756; further loss of -COO and -CO groups from the ester group gives the fragment at m/e 682. Further loss of a -CH group to give a parent TTP unit (m/e 669), which picks up a proton to give a fragment equivalent to TTP (m/e 670). The observed precise mass was in reasonable agreement with the calculated mass for P-Et-OEt (8). Infra-red analysis of P-Et-OEt (8) showed a very intense carbonyl peak at 1688.6 cm^{-1} and a C-O stretch at 1150 cm^{-1}, confirming the presence of ethyl ester group. This evidence supports the formation of P-Et-OEt (8) by the coupling of diethyl malonate anion with TTP-Cl (3).

2.3.3.2 Hydrolysis and decarboxylation of P-Et-OEt (8), Scheme 5, Step 2

The preparation of P-Et-A (9) was adapted from the standard procedure for malonate hydrolysis and decarboxylation.[10] The carboethoxy group of P-Et-OEt (8) was hydrolysed in basic medium. P-Et-OEt (8) in THF was refluxed with aqueous sodium hydroxide solution for two hours and deep violet crystals of the porphyrin diacid were separated out. This is due to the formation of more polar species (i.e., dicarboxylic acid group), which is less soluble in the solvent system. Finally the diacid was isolated as bright violet crystals by acidification of the reaction mixture followed by chloroform extraction.

For decarboxylation of the diacid, to generate a monoacid group, the porphyrin diacid was dissolved in glacial acetic acid and heated at 100°C for one hour. Formation of the monoacid was evidenced on analytical tlc. The R_f values of the porphyrin diacid and the monoacid were found to be significantly different. Based on P-Et-OEt (8), a good yield (65%) of P-Et-A (9) was obtained after routine isolation and column purification.

The ^{1}H-NMR spectrum of P-Et-A (9) could not be obtained due to the poor solubility of this compound in all the solvents examined. Significant self protonation of the carboxylic acid group was observed in $CDCl_3$ and the solution turned green immediately. This is probably due to the increase in chain length between the porphyrin core and the carboxylic acid group. The long chain helps the acid group to come into close proximity with the porphyrin core where the basic pyrrolic nitrogen groups are situated. Self protonation can then give a zwitterionic form of the compound. Due to the protonation of the porphyrin core by the carboxylic acid proton of the chain, the colour of the solution changes from purple to green.

The mass spectrum shows the ions at m/e 728(100%), 711(10%), 683(20%) and 670(25%) mass units. These were assigned to the fragments M^+, $(M - OH)^+$, $(M - COOH)^+$ and $(M - CH_2COO)^+$ respectively. The precise mass data also supported the formation of P-Et-A (9). Infra-red analysis shows the carbonyl peak at 1689.5 cm^{-1} and the peak due to O-H stretch at 3421.9 cm^{-1}. This confirms the presence of carboxylic acid group at the end of the chain linked to the porphyrin ring. The fragmentation pattern and precise mass of P-Et-A (9) supports the presence of a single carboxylic acid group at the end of the chain.

2.3.4 SYNTHESIS OF P-Gly-A (11), SCHEME 6

P-Gly-A (11) is the first member of the compounds of Series-II (Figure 1.1). It was prepared by adapting a standard synthetic procedure (Scheme 6) of linking a methyl glycinate chain to a halogen derivative, followed by the hydrolysis of the methyl ester group to generate the carboxylic acid group.

2.3.4.1 Synthesis of P-Gly-OMe (10), Scheme 6, Step 1

P-Gly-OMe (10) was prepared by coupling of TTP-Cl (3) with methyl glycinate. Methyl glycinate was generated by bubbling ammonia gas through an ice-cold suspension of its hydrochloride salt in dichloromethane. The coupling was done by refluxing TTP-Cl (3) with methyl glycinate in the presence of silver nitrate in chloroform. The reaction was done initially in the absence of silver nitrate, at room temperature as well as under prolonged (40 hours) reflux, but no product was obtained. Addition of silver nitrate yielded the product after overnight reflux and the reaction was complete in 20 hours. The silver nitrate was added to the reaction mixture with a view to catalyze the reaction and after repeated attempts it was found that the yield of the product was dependent on the quantity of the silver nitrate added. The maximum yield (30%) of P-Gly-OMe (10) was obtained by using a 1:5 molar ratio of TTP-Cl (3) and silver nitrate. Silver nitrate may have a number of effects on this reaction, which helps in the coupling. Possibly, it helps to polarize the C-Cl bond by acting as a Lewis acid:

$$\text{Ar-CH}_2^{\delta+}\text{-Cl}^{\delta-} \text{ ---------- } \text{Ag}^+$$

$$\text{Nu}^{\ominus}$$

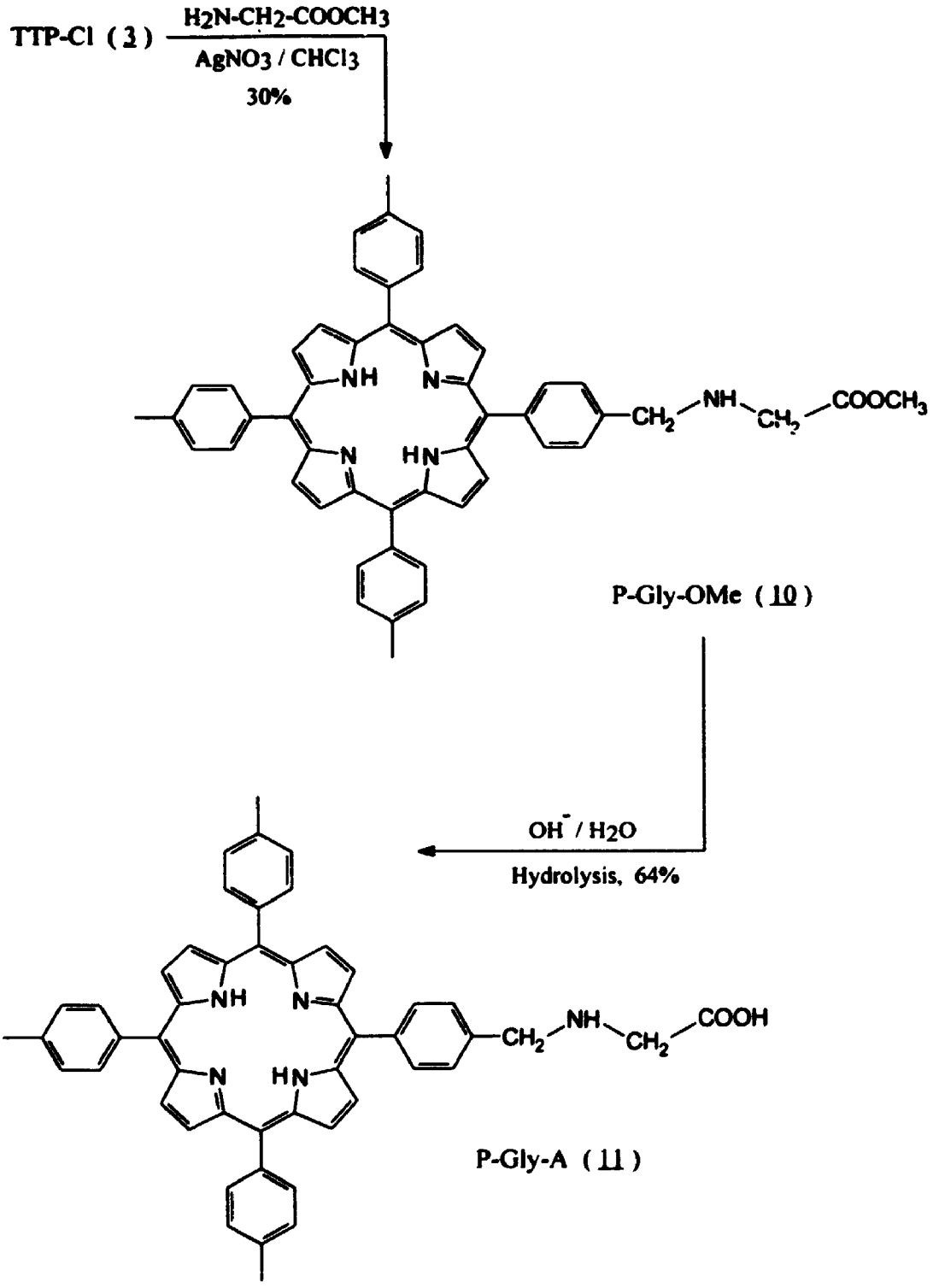

Scheme 6 : Synthesis of P-Gly-A (11)

This acts to speed up the reaction by making Cl a better leaving group.

A very interesting result was observed during the ^1H NMR analysis of P-Gly-OMe (10). The peaks for the porphyrin core protons were obtained in the expected regions and they were assigned as earlier. In addition peaks at 4.14 δ (s, 2H, benzyl methylene protons from porphyrin part), 3.83 δ (s, 3H, methyl ester protons), 3.67 δ (s, 2H, glycyl methylene protons) were observed. The secondary N-H proton of the porphyrin side chain was observed at 3.91 δ. The signals for methyl ester protons and glycyl methylene protons for methyl glycinate are observed at 3.57 δ and 3.28 δ respectively and the down-field shift of these protons on coupling with porphyrin is due to the influence of porphyrin ring current, which deshields the electronic environment of these protons.

The mass spectrum of P-Gly-OMe (10) gave a peak at m/e 760 amu, which is three mass units more than the expected mass 757 amu for P-Gly-OMe (10). This is apparently due to protonation of the pyrrolic nitrogens of the porphyrin ring and the glycyl nitrogen in the mass spectrometer. The observed exact mass was in reasonable agreement with that calculated for P-Gly-OMe (10) plus three protons. This supports the conclusion that coupling of methyl glycinate has occurred with TTP-Cl (3). Infra-red analysis shows a very intense carbonyl peak at 1741.9 cm^{-1}, confirming the presence of the methyl ester group. Moreover the secondary N-H stretching at 3316.1 cm^{-1} was also observed.

2.3.4.2 Hydrolysis of P-Gly-OMe (10) to P-Gly-A (11), Scheme 6, Step 2

The carboxylic acid group was generated from the carbomethoxy group by hydrolysing P-Gly-OMe (10) in basic medium. Upon column purification of the hydrolysed product a yield of 64% was obtained. P-Gly-OMe (10) in THF was boiled with aqueous sodium hydroxide solution on a steam bath for 15 minutes and accumulation of the P-Gly-A (11) as a precipitate was observed. This indicated the formation of a more polar species (i.e. carboxylic acid group), for which the solubility becomes low.

The ^{1}H-NMR spectrum of P-Gly-A (11) could not be obtained owing to the very poor solubility of this compound. A suitable solvent for recording the NMR spectrum could not be found because of its low solubility in all solvents examined. The mass spectrum shows a peak at m/e 699(100%) and 670(98%). The peak at m/e 699 is 44 units less than the expected molecular ion of 743, which is the molecular mass of P-Gly-A (11). The loss of 44 units is due to the loss of CO_2 from the carboxylic acid group. The fragment at m/e 670 indicates the formation of TTP moiety, by the cleavage of the glycine chain attached to the porphyrin ring. Infra-red analysis shows the carbonyl peak at 1689.2 cm^{-1} and the peak due to O-H stretch at 3422.1 cm^{-1}. This confirms the generation of carboxylic acid group at the end of the chain linked to the porphyrin ring.

2.3.5 SYNTHESIS OF TTP-Br (12) AND ZnTTP-Br (13), SCHEME 7

TTP-Cl (3) was used as a starting material for most of the reactions because of its easy preparation and stability under normal conditions. However, in some

reactions the chlorine substituent proved to be an inefficiently good leaving group. This may be due to the fact that the nucleophiles in the reaction mixture are not strong enough to displace chloride group. Hence incorporation of a better leaving group was necessary to carry out the reactions with relatively weak nucleophiles.

At first the preparation of a porphyrin tosylate was attempted. A literature procedure[11] for converting a primary alcohol to the corresponding tosylate, was followed. A solution of TTP-OH (2) in THF was treated with tosyl chloride and KOH at O°C for one hour. After routine workup and purification no new product was evidenced on tlc plate. ^{1}H-NMR showed that the product was nothing but unreacted TTP-OH (2). Therefore it was concluded that for porphyrin (2) the reaction does not occur under these conditions. This may be because the porphyrins solubility prevents attainment of a concentration high enough to compete with hydrolysis of the tosyl chloride by base.

The preparation of TTP-Br (12) was then attempted. As bromide is a better leaving group than chloride, TTP-Br (12) was expected to react better with weaker nucleophilic agents. TTP-Br (12) was synthesized by treating TTP-OH (2) with thionyl bromide at room temperature and in the absence of light. The literature procedure[12] was followed for this conversion. The reaction was found to be light sensitive and formation of four byproducts were observed by analytical tlc, when no precautions were taken to avoid light exposure. A single product was obtained when the reaction was carried out in the dark and almost 100% conversion was indicated by analytical tlc. A green product was isolated because of the presence of porphyrin in the protonated form. Deprotonation of the porphyrin was achieved by briefly

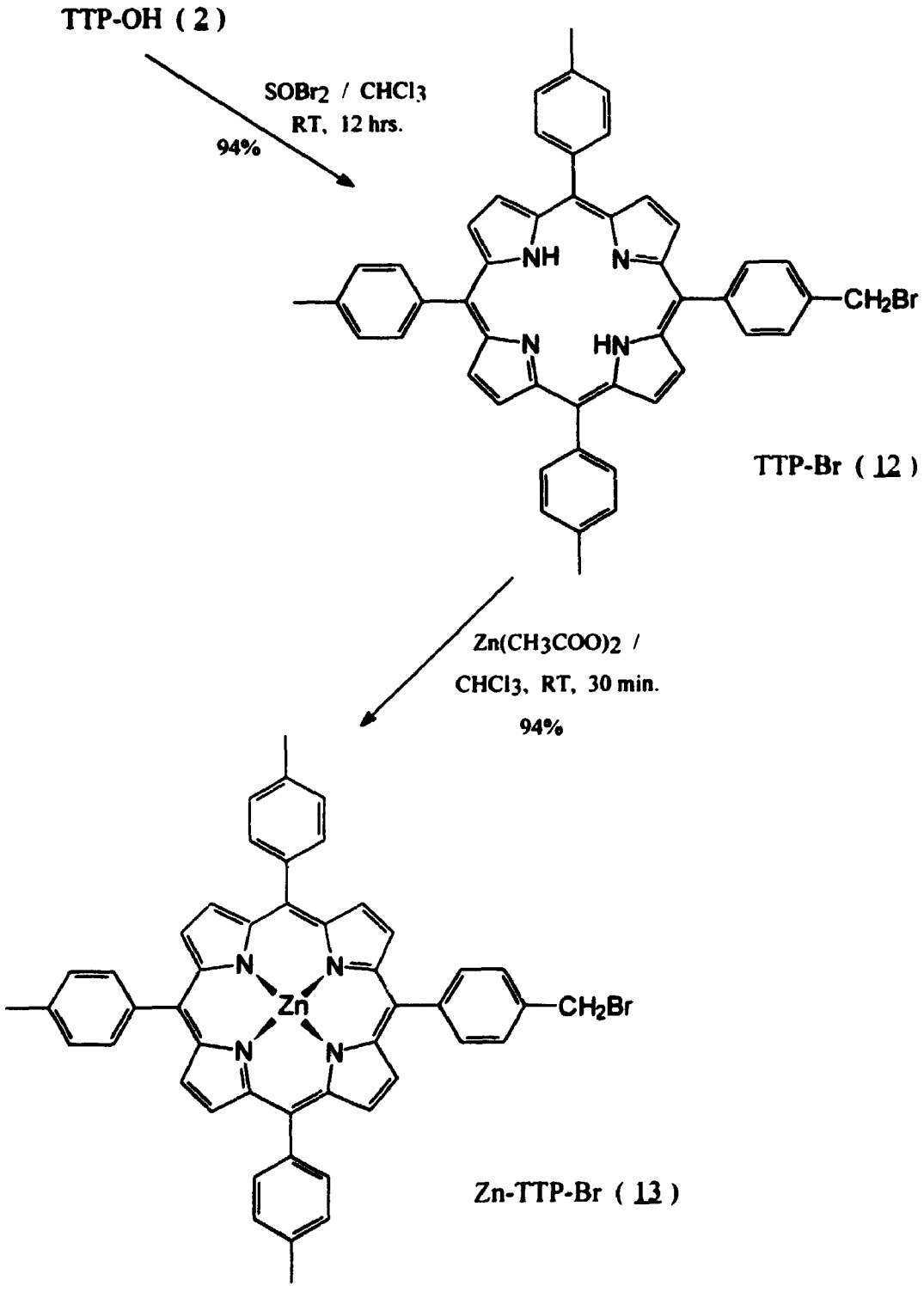

Scheme 7 : Synthesis of TTP-Br (12) and ZnTTP-Br (13)

washing its chloroform solution with saturated sodium bicarbonate solution. Finally it was purified by flash chromatography using chloroform as eluting agent to remove excess HBr and protonated porphyrin.

The ^{1}H-NMR spectrum of the product showed the expected peaks for the protons associated with the porphyrin ring and they were assigned similarly as for P-A (1). The peak for the methylene protons appeared at 4.82 δ, which is close to the chemical shift (4.41 δ) calculated by Shoolery's method. This peak was observed as a singlet, presumably because replacement of the hydroxyl group by a bromine atom removes the only proton available for coupling. The methylene protons were found to be slightly shifted upfield (4.82 δ) in TTP-Br (12) compared to the methylene protons (4.93 δ) in TTP-Cl (3). This is due to the higher electronegativity of chlorine compared to bromine, which therefore deshields the methylene protons slightly more.

As expected the absorption spectrum of TTP-Br (12) was very similar to that of TTP-Cl (3). The characteristic Soret or B-band of prophyrin appeared at 420 nm with a molar extinction coefficient of 5.10×10^5 M^{-1} cm^{-1}; this is due to the transition from the ground state to second excited singlet state. Four distinct Q-bands, which are due to the transition from ground state to the first excited singlet state, appeared at 517, 551, 592 and 643 nm respectively.

The mass spectrum of TTP-Br (12) behaved similarly as TTP-Cl (3). It showed a prominent peak at m/e 670. The expected peak of mass 748 was not observed even when fast atom bombardment (FAB) and chemical ionization (CI) were used instead of electron impact ionization (EIMS). This is apparently due to the formation of tetratolylporphyrin (TTP) from TTP-Br (12), by the loss of bromine

and subsequent protonation of reduction. Analysis by infra-red spectroscopy showed the absence of an O-H stretch at 3314.1 cm^{-1} and a new peak at 551.0 cm^{-1} was observed, which was assigned to the C-Br stretch. Hence from all these data the formation of TTP-Br (12) was confirmed.

TTP-Br (12) was converted to ZnTTP-Br (13) by adapting a known literature procedure,[5] identical to the procedure used for converting TTP-Cl (3) to ZnTTP-Cl (4). A solution of TTP-Br (12) in chloroform was mixed and stirred for 30 minutes with a methanolic solution of zinc acetate dihydrate at room temperature and in the dark. Completion of the reaction was judged by inspection of the absorption spectrum, where the four-banded spectrum, characteristic of a free-base porphyrin collapsed into the two-banded spectrum, characteristic of a metallated porphyrin. The colour change during the formation of ZnTTP-Br (13) from TTP-Br (12) was not very distinct, as it was in the case of ZnTTP-Cl (4). The product was purified by flash chromatography in order to get rid of some protonated porphyrin byproducts and was isolated as a green mass. Conventional column chromatography was not carried out for purification in order to avoid the decomposition of ZnTTP-Br (13), which possesses a very labile -Br group. A very high yield (94%) of the product was obtained. No substantial change in the yield was observed upon prolonged stirring with zinc acetate (>2 hours).

The ^{1}H-NMR spectra of ZnTTP-Br (13) showed all the expected peaks of the porphyrin core unit and they were assigned similarly as ZnTTP-Cl (4). As expected a considerable dipolar shift[2] was observed in ZnTTP-Br (13) for all the protons associated with the π-conjugated system of the porphyrin ring. The tolyl methyl

protons remained unaffected as they are not a part of the π-conjugated system. Resonances at ~ -2.8 ppm were found to be absent because of the replacement of the N-H protons by Zn^{2+} ion. This supports the insertion of the Zn^{2+} ion into the porphyrin core.

The mass spectrum of ZnTTP-Br (13) showed no molecular ion. Instead a strong peak of mass ion 732, due to the loss of Br•, was observed. This is similar to the situation found in ZnTTP-Cl (4). The mass ion 732 was assigned to ZnTTP, which was formed due to the loss of Br• followed by protonation or reduction. Infra-red analysis showed the absence of the N-H stretch at 3317 cm^{-1} and the presence of a C-Br stretch at 552 cm^{-1}, consistent with the formation of ZnTTP-Br (13). The characteristic Soret band was observed in the absorption spectra at 418 nm with a molar extinction coefficient of 4.94×10^5 M^{-1} cm^{-1}. Two Q-bands were observed at 551 nm and 592 nm respectively, which is consistent with the transformation of the ring symmetry from D_{2h} to D_{4h}, due to the insertion of Zn^{2+} in porphyrin.

2.3.6 SYNTHESIS OF P-Glyco-A (16), SCHEME 8

P-Glyco-A (16) is the second member of the compounds of Series-II (Figure 1.1). The synthetic strategy designed for the preparation of P-Glyco-A (16) involves the coupling of ethyl glycolate with a porphyrin halide and subsequent hydrolysis of the ethyl ester group to generate the desired carboxylic acid group. The zinc derivative of the porphyrin was used for the coupling reaction because of its better solubility in the solvents used in the synthesis.

The coupling of porphyrin halide with ethyl glycolate was first attempted by reacting ZnTTP-Cl (4) with ethyl glycolate ($HO\text{-}CH_2\text{-}COOEt$) under basic conditions. A published procedure[13] was followed. The published procedure suggests *in-situ* generation of the sodium salt of ethyl glycolate (14) using ethyl glycolate and NaH in HMPA under ice-cold conditions and then addition of the chloro derivative to the reaction mixture. In the present case HMPA was replaced with THF because ZnTTP-Cl (4) was found to be insoluble in HMPA. ZnTTP-Cl (4) and the sodium salt of ethyl glycolate (14) in dry THF was heated at 60°C for eight hours. A new produce was evidenced on the tlc plate and a significant amount of dark brown polymeric byproduct was also observed in the reaction flask. After isolation, purification and characterization by ^{1}H-NMR and MASS spectroscopy, the new product was found to be ZnP-OC_2H_5, not the desired product ZnP-Glyco-OEt (15). This may be due to the fact that ZnTTP-Cl (4) is insufficiently reactive with ethyl glycolate anion. Kinetically, ethyl glycolate anion may prefer to undergo an intermolecular condensation to generate a glycolate polymer and ethoxide anion. The ethoxide anion thus formed accumulates and displaces chloride from ZnTTP-Cl (4) to give ZnP-OC_2H_5 as the final product. The dark brown polymer thus formed was found to be accumulated on the wall of the reaction flask.

In the second attempt investigated for the preparation of ZnP-Glyco-OEt (15), a relatively non-basic synthetic method was adapted from a published literature procedure.[14] Instead of using the sodium salt of ethyl glycolate (14) to do an S_N2 displacement under strongly basic conditions, ethyl glycolate was used in the presence of silver oxide. Under these conditions, complexation of the halide of the porphyrin

benzyl halide with silver presumably makes S_N2 displacement by an alcohol feasible, and in this case avoids self condensation of ethyl glycolate. A mixture of ZnTTP-Br (13), ethyl glycolate and a catalytic amount of Ag_2O in dry THF was sonicated in a sonicator bath filled with ice water for thirty minutes. After routine isolation and purification no new product was obtained. Almost all (~98%) of the unreacted ZnTTP-Br (13) was recovered. The failure of the reaction to occur may be due to the low concentration of ZnTTP-Br (13) in the reaction mixture. The literature suggests use of 0.1 M concentration of the starting material but it was not possible to achieve that concentration range for ZnTTP-Br (13) because of its low solubility. In the present case only ~10^{-3} M concentration of ZnTTP-Br (13) could be used.

The final and successful method attempted for the synthesis of ZnP-Glyco-OEt (15) involved the preparation and isolation of pure sodium salt of ethyl glycolate (14) and subsequent treatment of it with ZnTTP-Br (13). This modification of the synthetic procedure enabled removal of any sodium ethoxide formed during the reaction of ethyl glycolate with the base. In addition, the greater reactivity of ZnTTP-Br (13) with the sodium salt of ethyl glycolate (14) meant that formation of the desired glycolate ester, ZnP-Glyco-OEt (15) occured before any appreciable condensation of the ethyl glycolate.

2.3.6.1 Synthesis of Sodium salt of Ethyl Glycolate (14)

The preparation was done by adapting a literature procedure for the preparation of lithium salt of ethyl glycolate.[15] In the present work sodium ethoxide was used instead of n-butyl lithium as a deprotonating agent. Ethyl glycolate

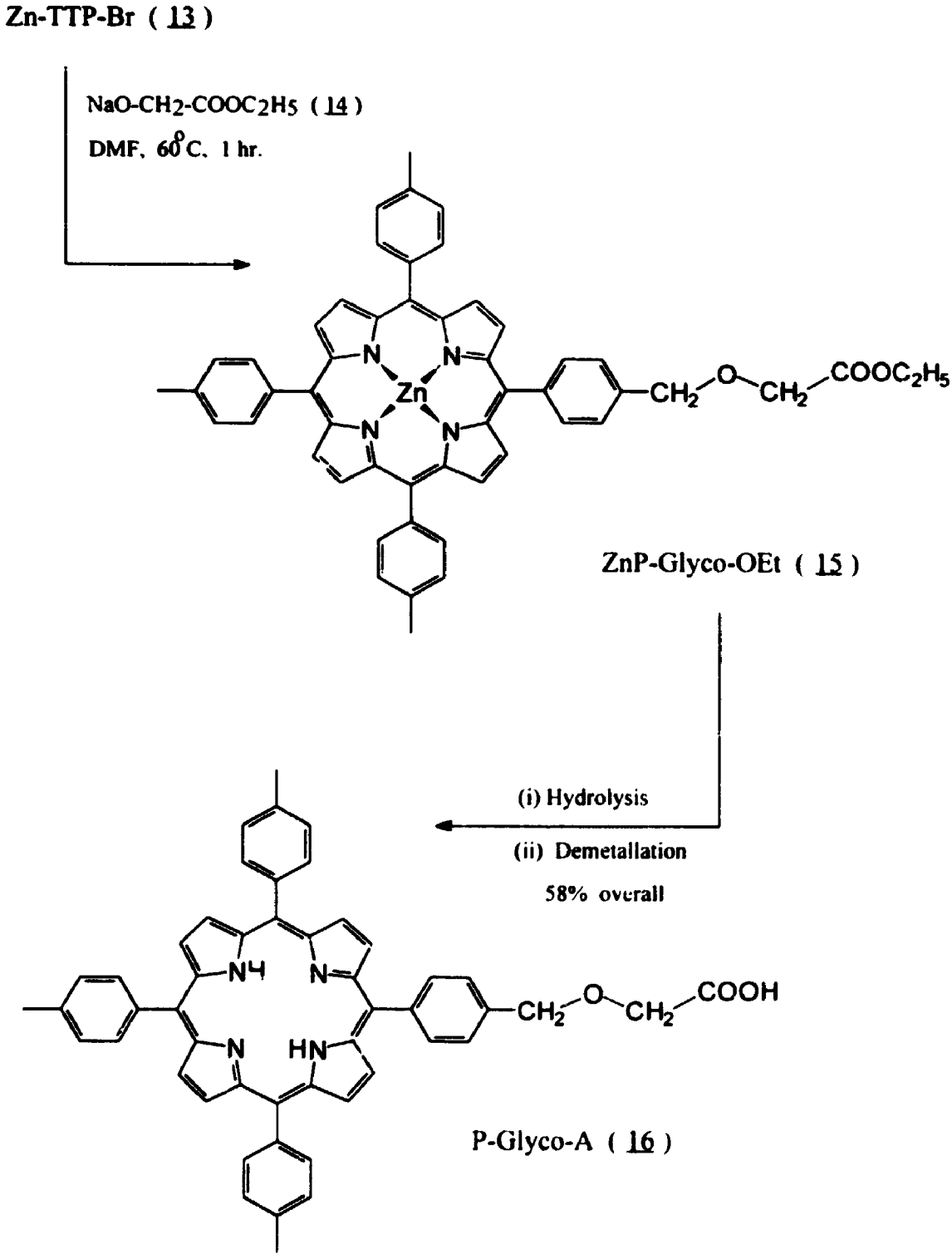

Scheme 8 : Synthesis of P-Glyco-A (16)

dissolved in absolute ethanol was added to sodium ethoxide prepared from metallic sodium and absolute ethanol. After stirring for one hour at room temperature, the reaction mixture was made highly nonpolar by diluting it with pentane. This was done to separate out the desired salt from polar solvent (i.e., absolute ethanol). The sodium salt of ethyl glycolate (14) was isolated as white precipitate immediately. The compound was isolated, washed and dried under vacuum for further use.

2.3.6.2 Synthesis of ZnP-Glyco-OEt (15), Scheme 8, Step 1

As discussed in the previous section ZnP-Glyco-OEt (15) was prepared by modifying a published procedure.[15] ZnTTP-Br (13) and the sodium salt of ethyl glycolate (14) dissolved in DMF were heated at 90°C for one hour under a nitrogen atmosphere. Dry conditions were necessary for the reaction because of the water sensitivity of the sodium salt of ethyl glycolate (14). ZnTTP-Br (13) instead of TTP-Br (13) was used as the starting material as it is more soluble in DMF. The disappearance of the starting material and formation of a new product were evidenced after an hour by analytical tlc. The crude product was not subjected to column purification as considerable hydrolysis of the ester group was observed upon slow elution of ZnP-Glyco-OEt (15) by 3% methanol in chloroform through a column packed with silica gel. To avoid this problem a small analytical amount of ZnP-Glyco-OEt (15) was purified by flash chromatography to give a characterization sample. The purity of the chromatographed product was checked on tlc plate and it was found to be free from any contamination.

The ^{1}H-NMR spectrum of ZnP-Glyco-OEt (15) showed all the expected peaks of the porphyrin ring and they were assigned similarly to ZnTTP-Cl (14). As expected the long glycolate chain caused a distortion of the symmetry of the porphyrin ring so that the signal for the β-pyrrole protons was split. In addition peaks at 3.71 δ (q, 2H, methylene protons of the ethyl ester group), 3.49 δ (s, 2H, methylene protons of the ethyl glycolate chain) and 1.21 δ (t, 3H, methyl protons of the ethyl ester group) were observed. No peak was found at ~ -2.8 δ, consistent with the presence of a metal ion in the center of the porphyrin ring.

The ^{13}C-NMR spectrum of the product was consistent with the structure of ZnP-Glyco-OEt (15). Comparing the observed chemical shifts with predicted values, inspection of the APT ^{13}C-NMR spectrum and comparision with the values observed by Roach[16] for P4Q, which consists of a tetra-aryl porphyrin linked *cis*-1,3 across a cyclobutane ring to a benzoquinone, the following peak assignments were made: A signal at 15.3 δ was assigned to the methyl carbon of the ethyl ester group. A peak at 21.5 δ was assigned to three tolyl methyl carbons i.e., carbons at position 21 of the porphyrin ring (Figure 2.2). Although one of these methyl carbons is in a slightly different environment than the other two, all three are observed coincidently at the same shift. The methylene carbon of benzyl ether group was observed at 29.7 δ. The methylene carbon of the ethyl glycolate chain was assigned to a peak at 66.1 δ. The methylene carbon of the ethyl ester group was assigned to a peak at 72.7 δ. Signals at 120.6 δ and 121.1 δ were assigned to carbons at position 10 and positions 5 and 15 of the porphyrin ring. The carbon at position 20 of the porphyrin ring was assigned to the signal at 121.8 δ. Due to the identical chemical environment of

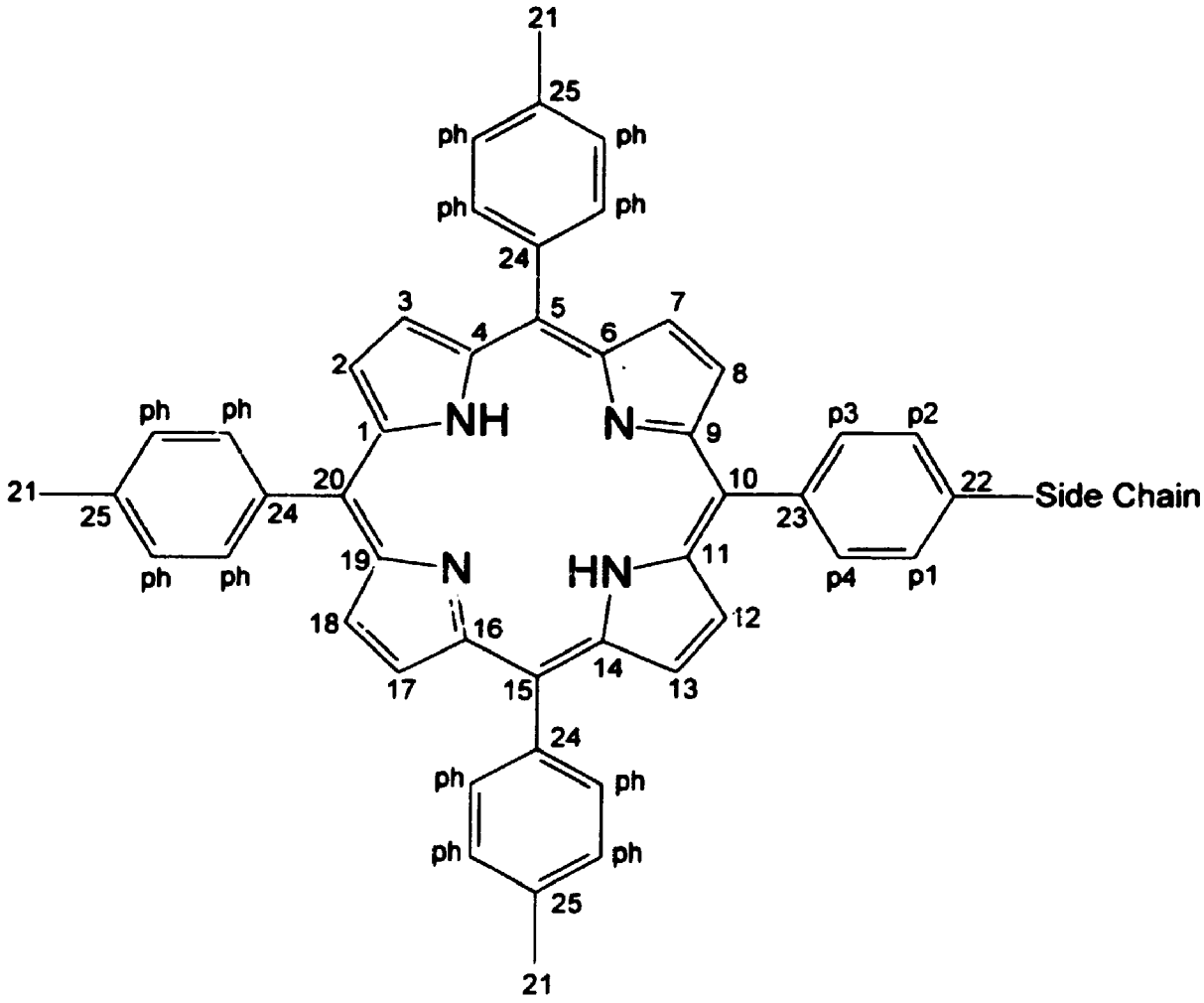

Figure 2.2 : Porphyrin ring skeleton with all the carbons labelled.

carbons at positions 5 and 15 of the porphyrin ring, they appeared as a single signal. The signal at 125.8 δ was assigned to the carbon atoms at positions 2, 3, 7, 8, 12, 13, 17 and 18 of the porphyrin ring (the β-positions of the pyrrole rings). Although these carbons may be divided into pairs each with a slightly different environment, they are observed to be coincident. The aromatic ring carbons bearing the protons of tolyl groups and the phenyl group linking the porphyrin and the glycolate chain were observed as two signals at 127.2 δ and 134.4 δ. Again these carbons are coincidentally at the same shifts. The carbons at positions 1, 4, 6, 9, 11, 14, 16 and 19 of the porphyrin ring (the α-positions of the pyrrole rings) were observed at 131.7 δ and 131.9 δ. Normally a broad signal is observed for the carbons at α-positions, but due to the presence of the glycolate chain their environment was changed and they appeared as two different peaks. The tolyl ring carbons bonded to the porphyrin ring i.e., carbons at positions 24 of the porphyrin ring were assigned to a signal at 137.0 δ. A signal at 137.5 δ was assigned to the carbon of the aromatic ring linking the porphyrin and the glycolate chain bonded to the porphyrin ring i.e., the carbon at position 23 of the porphyrin ring. The tolyl ring carbons bonded to the methyl groups i.e., carbons at positions 25 were assigned to the signal at 139.9 δ. The carbon of the aromatic ring linking the porphyrin and glycolate chain, bonded to the glycolate chain i.e., the carbon at position 22 of the porphyrin ring was assigned to the signal at 142.3 δ. Finally the carbon of the carbonyl group of the ethyl ester was assigned to the signal at 151.2 δ.

The mass spectrum of ZnP-Glyco-OEt (15) showed the parent mass ion at m/e = 835 amu. The observed peaks were at m/e 835(20%), 791(6%), 749(30%) and

733(100%) respectively. These are assigned to M^+, $(M - OC_2H_5 + H)^+$, $(M - CH_2COOC_2H_5 + H)^+$ and $(M - OCH_2COOC_2H_5 + H)^+$ fragmentations. ZnP-Glyco-OEt (15) seems to lose the ethoxy group very easily and then acquires a H-atom to form the fragment of m/e = 791. After losing the ethoxy group the ether linkage of the glycolate chain is cleaved and the molecule tend to lose the $-CH_2CO-$ fragment and pick up a H-atom to give a fragment of mass 749. Finally the oxygen group is lost to give the base porphyrin moiety, which is structurally similar to ZnTTP. Thus the mass ion 733, which is equivalent to the mass ion of ZnTTP, was observed. The observed precise mass was found to be in close agreement with that calculated for ZnP-Glyco-OEt (15). The infra-red analysis showed a very intense peak at 1729.4 cm^{-1}, confirming the presence the carbonyl group of the ester group. Hence on the basis of the spectroscopic evidence the formation of ZnP-Glyco-OEt (15) was confirmed.

2.3.6.3 Hydrolysis and demetallation of ZnP-Glyco-OEt (15), Scheme 8, Step 2

P-Glyco-A (16) was synthesized from ZnP-Glyco-OEt (15) by base hydrolysis of the carboethoxy group. ZnP-Glyco-OEt (15) in THF was boiled with dilute NaOH solution for 30 minutes. During workup the organic layer was washed with 5% HCl to acidify the medium and demetallate the porphyrin core. For the removal of zinc from the porphyrin core the use of glacial acetic acid has been suggested in the literature.[18] In the present case the use of HCl was found to be more convenient as it solves a dual purpose. HCl easily neutralises excess NaOH left after the reaction and it displaces the central metal ion of the porphyrin core. The displacement of

Zn^{2+} is indicated by the change in the colour of the organic phase, from purple to dark green, which is characteristic of the protonated porphyrin. The deprotonation of the porphyrin ring was done by briefly washing the organic phase with water. After column purification an overall yield of 58% of P-Glyco-A (16) was obtained. Calculation of the yield was based on the total amount of starting material ZnTTP-Br (13) used. As the intermediate product ZnP-Glyco-OEt (15) was not isolated in a pure form the yield for the final step of the reaction could not be calculated.

An expected result was observed in the ^{1}H-NMR spectrum of P-Glyco-A (16). All the protons associated with the porphyrin ring appeared in the expected region and they were assigned as earlier. As expected a split in the peak for the β-pyrrole protons was observed. The β-pyrrole (H_b) protons (Figure 2.2) farther from the glycolate chain appeared at 8.98 δ with an integration for six H-atoms and the two β-pyrrole (H_a) protons closer to the glycolate chain appeared at 8.91 δ. Moreover the methylene protons of the benzyl group was observed at 3.89 δ, which is in reasonable agreement with the predicted value 4.44 δ, calculated according to Shoolery's method. The methylene protons of the glycolic acid chain appeared at 5.46 δ, which is consistent with the value (5.01 δ) predicted by Shoolery's method.[3b] A signal due to pyrollic N-H proton appeared at -2.80 δ confirming the presence of free-base porphyrin. This evidence also proves that 5% HCl can be used for removing zinc from the porphyrin core.

The mass spectrum of P-Glyco-A (16) showed the expected molecular mass ion m/e 744 as the base peak. The fragmentation pattern observed was as follows: m/e 744(100%), 727(70%), 686(68%), 670(40%). These were assigned to M^+, (M -

$OH)^+$, $(M - CH_2COOH)^+$ and $(M - OCH_2COOH)^+$ fragmentations respectively. P-Glyco-A (16) seemed to be very stable under electron bombardment and so M^+ itself appeared as the base peak. The molecule then loses the -OH group from the carboxylic acid group to give the fragment with m/e = 727 amu. The fragment of m/e = 686 was generated by the cleavage of the glycolic acid chain and loss of the $-CH_2$-COOH part of the chain. Finally the molecule loses the entire glycolic acid chain and picks up a hydrogen atom to give the mass ion of TTP that appears at m/e 670. The observed precise mass and that calculated for P-Glyco-A (16) were found to be in agreement with each other. The infra-red spectrum showed an intense peak at 1692.3 cm^{-1} for the carbonyl group and an O-H stretch was also evidenced at 3310.1 cm^{-1}. This supports the presence of a carboxylic acid group. All the spectroscopic evidence suggests the formation of P-Glyco-A (16).

2.3.7 SYNTHESIS OF P-Ace-A (23), SCHEMES 9, 10, 11 AND 12

P-Ace-A (23) is the third member of the model compounds of Series-II (Figure 1.1). Its synthesis was found to be the most challenging of all the syntheses performed in the present work. Several synthetic methodologies were attempted, but most of these attempts proved to be unsuccessful. From all the information obtained from these unsuccessful attempts, the synthetic approach was modified significantly to acquire the target molecule P-Ace-A (23). In this section the unsuccessful attempts will be briefly described and this will be followed by a description of the successful route eventually developed.

In order to synthesize P-Ace-A (23), the synthesis of P-Ace-OH (20) was first attempted. This could then be subsequently oxidised to generate the carboxylic acid group. The preparation of P-Ace-OH (20) was initially attempted by the coupling of a porphyrin benzyyl halide with propargyl alcohol. The initial approach to the coupling reaction, was to prepare a copper acetylide of propargyl alcohol and treat it with the porphyrin halide. A published procedure[17] was followed for this reaction. In DMF, ZnTTP-Br (13), the copper acetylide of propargyl alcohol and a catalytic amount of NaCN was heated at 80°C for an hour. ZnTTP-Br (13) was used as the starting material for two reasons. First it is highly soluble in the reaction solvent DMF and second, it protects the porphyrin core from incorporating Cu-metal, which is present in the reaction medium. After the reaction the formation of a new product was evidenced by tlc. The new product was isolated and purified and was then characterized by ^{1}H, ^{13}C-NMR and MASS spectroscopy. From all these data the structure of the new product was established as ZnP-O-CH_2-C≡CH. The formation of this product with an ether linkage had apparently occurred by nucleophilic attack on ZnTTP-Br (13) by the -OH group of propargyl alcohol copper acetylide, which under the conditions used acts as a better nucleophile than the acetylide function, -C≡C$^-$Cu$^+$. Hence it was concluded that the protection of the -OH group of propargyl alcohol is necessary to achieve the desired acetylenic coupling to get P-Ace-OH (20).

Propargyl alcohol was protected by conversion to its (1'-ethoxy) ethyl ether (see Section 2.2.7.1) and this was converted to its Cu acetylide using the literature procedure.[21] This was then heated with ZnTTP-Br (13) in DMF at 80°C in the

presence of NaCN.[17] After routine workup and purification a new product was isolated in high yield (~81%) along with a small amount of unreacted starting material, ZnTTP-Br (13). Structural characterization by ^{1}H, ^{13}C-NMR and MASS spectroscopy indicated that the new product was ZnTTP-CN (5). Apparently the CN^- ion present in the reaction is a better nucleophile than the acetylide and reacts with ZnTTP-Br (13) to give ZnTTP-CN (5).

A further approach to the coupling reaction was to prepare the sodium acetylide of the -OH protected propargyl alcohol and treat it with a porphyrin benzyl halide. It was hoped that the sodium acetylide would show greater nucleophilicity than the copper analogue. Sodamide was first prepared by dissolving sodium in liquid ammonia containing a catalytic amount of a ferric salt. The protected propargyl alcohol was then added (after removal of NH_3 and addition of THF). ZnTTP-Br (13) dissolved in dry THF was then added. After stirring for 2.5 hours the reaction was worked up to yield a thick brown polymeric mass which was impossible to analyze due to its poor solubility in all the solvents examined. No evidence for the formation of the desired coupled product was found. Failure of the benzylation reaction when sodium acetylide is allowed to react with benzyl chloride has been reported previously.[8] The literature suggests that the sodium acetylide has a tendency to abstract proton from the benzylic methylene position of benzyl chloride. Possibly a carbene is formed leading to the formation of various polymeric products. In the case described here the sodium acetylide of the -OH protected propargyl alcohol may have initiated polymerization by methylene proton abstraction from ZnTTP-Br (13). Hence it was concluded that the sodium acetylide of the -OH

protected propargyl alcohol cannot be used with the present porphyrin system, i.e., ZnTTP-Br (13).

Another approach to the coupling reaction was made by the condensation of porphyrin benzyl halide ZnTTP-Br (13) with the dilithio derivative of propargyl alcohol. The reaction was designed using literature procedures[19] which suggested that the acetylide anion is more nucleophilic than the alkoxide anion in the dilithio salt. BuLi (4 eq) was added to a solution of propargyl alcohol (2 eq) in dry THF and HMPA (6 eq) at -80°C. The temperature was raised gradually to -30°C and maintained for 45 minutes. ZnTTP-Br (13) dissolved in dry THF was added at -30°C and then the reaction mixture was stirred at room temperature for 18 hours. After workup a considerable amount of brown polymer was obtained and no sign of a new product was observed by analytical tlc. The formation of the polymer may be due to proton abstraction by the lithio acetylide of propargyl alcohol from the benzylic methylene protons of ZnTTP-Br (13). Hence it was concluded that the use of any highly basic metal (lithium or sodium) acetylide is not possible with ZnTTP-Br (13) because of the presence of the benzylic methylene protons in the latter.

Finally, a successful coupling reaction was achieved by condensation of ZnTTP-Br (13) with the Grignard derivative of the acetylenic function of the -OH protected propargyl alcohol in presence of a catalytic amount of CuCl. A procedure was devised for this reaction using published procedures for structurally related systems[20] along with the experiences gathered from a series of unsuccessful trial reactions. During the development of the synthetic strategy all the trial reactions were done with benzyl bromide (Ph-CH_2-Br) instead of ZnTTP-Br (13). The model

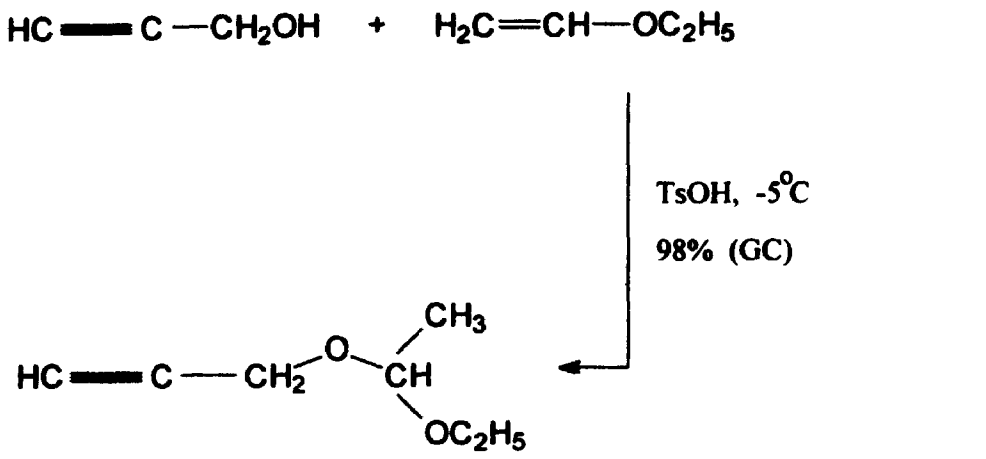

Protected Propargyl Alcohol (17)

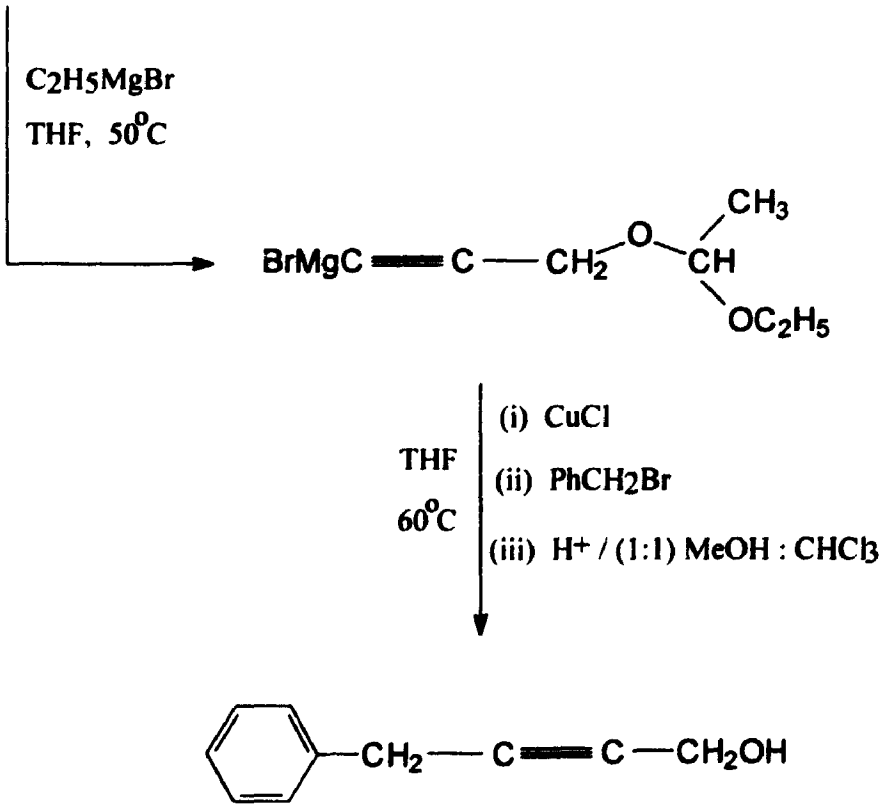

4-Phenyl-2-butyn-1-ol (18)

Scheme 9 : Synthesis of Ph-Ace-OH (18)

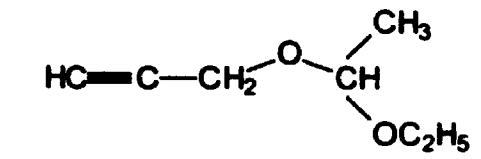

Protected Propargyl Alcohol (17)

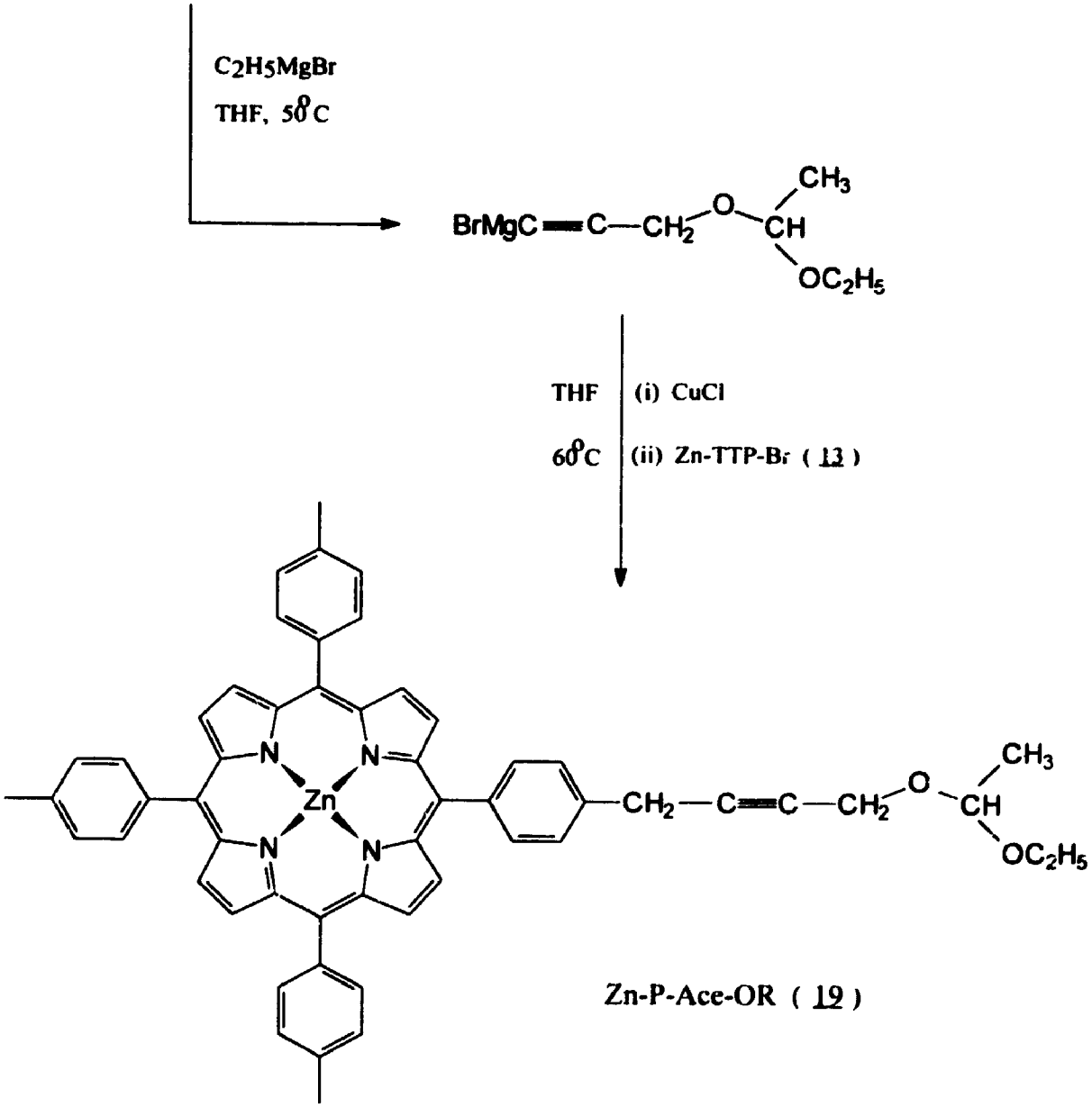

Zn-P-Ace-OR (19)

Scheme 10 : Synthesis of ZnP-Ace-OR (19)

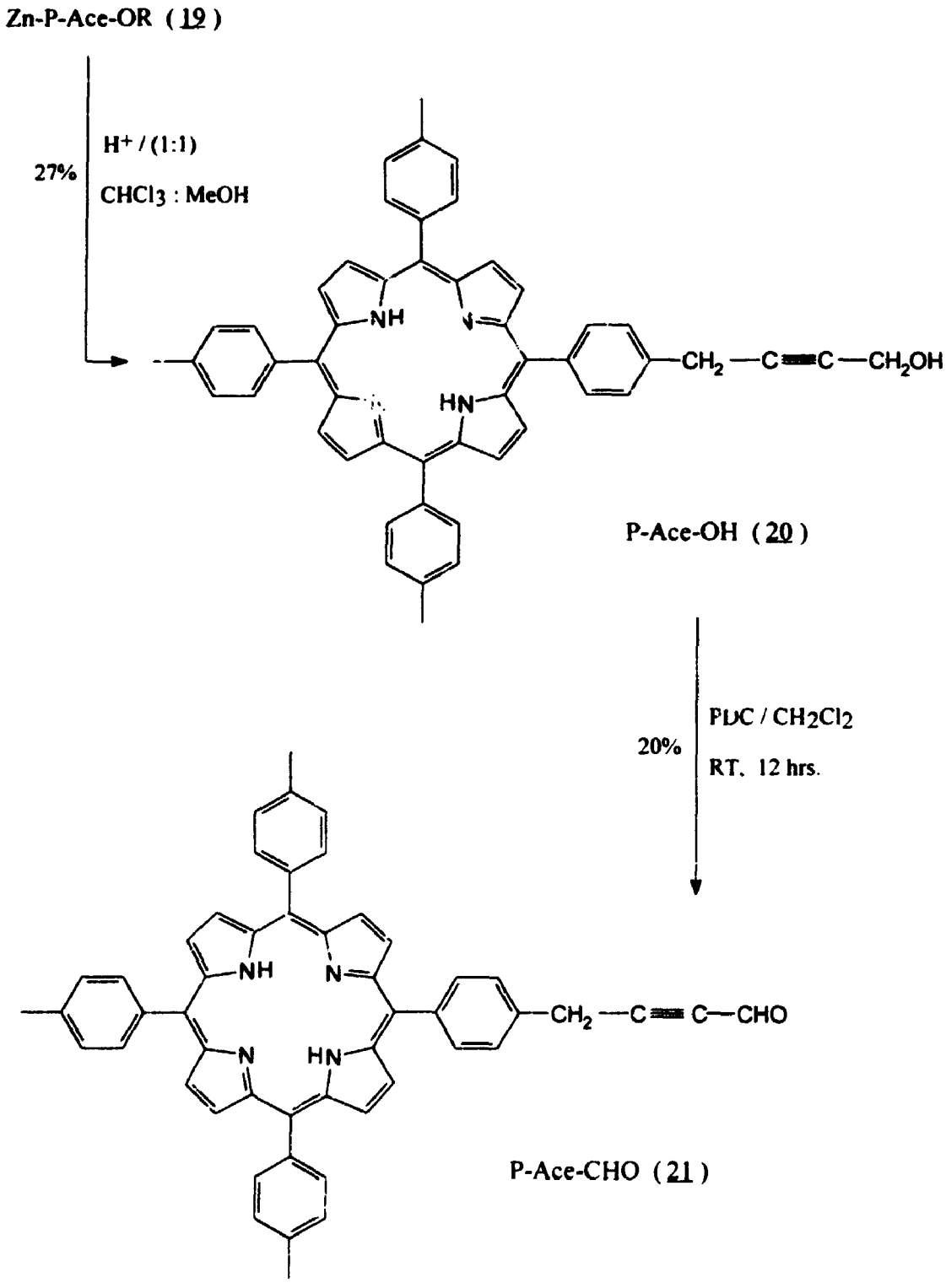

Scheme 11 : Synthesis of P-Ace-CHO (21)

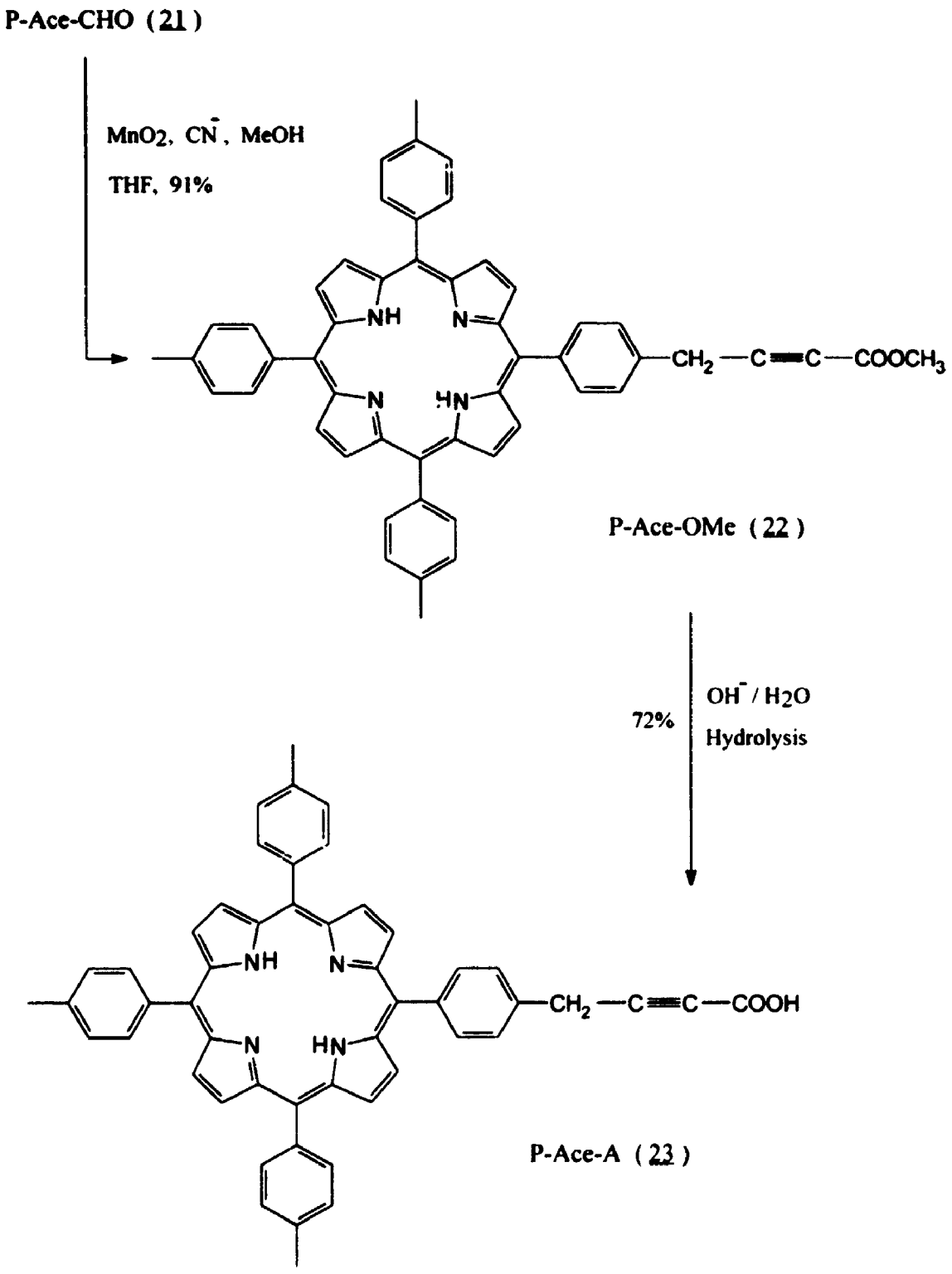

Scheme 12 : Synthesis of P-Ace-A (23)

system was used since the synthesis of ZnTTP-Br (13) requires a series of synthetic steps and consequently supplies of the compounds were low. Benzyl bromide was chosen as the model system for these trial reactions because of its structural similarity with the desired starting material ZnTTP-Br (13). The successful route is summarized in Schemes 9-12 and is described in the following sections.

2.3.7.1 Synthesis of -OH Protected Propargyl Alcohol (17), Scheme 9, Step 1

Frequently in synthetic procedures described in the literature the dihydropyran group has been suggested as the protecting group of choice for alcohols. However ethyl vinyl ether has been found to be a better choice for protecting the alcohol group of propargyl alcohol because it is more easily attached and removed than the dihydropyran group.[21] Propargyl alcohol and ethyl vinyl ether were allowed to react in the presence of p-toluene sulphonic acid at ice-cold temperature for 30 minutes. After work up a good yield (97%) of the -OH protected propargyl alcohol (17) was obtained. The GC analysis showed that the crude product was 98% pure. Distillation of the crude product for further purification is suggested in the literature[21] but in the present case the crude product was used without further purification. This was done because of the high purity of the crude product and also to avoid any decomposition of the product during distillation.

The ^{1}H-NMR spectrum of the -OH protected propargyl alcohol (17) showed all the peaks in the expected region. The assignments were made as follows: 4.73 δ (q, 1H, O-C<u>H</u>< proton of the ethyl vinyl ether part), 4.08 δ (dd, 2H, methylene protons of propargyl alcohol part), 3.61-3.31 δ (m, 2H, methylene protons of ethyl

vinyl ether part). 2.32 δ (t, 1H, acetylenic proton of propargyl alcohol part), 1.20 δ (d, 3H, >CH-C$\underline{H}_3$ protons of ethyl vinyl ether part), 1.08 δ (t, 3H, methyl protons of the ethyl group of ethyl vinyl ether part). Due to the presence of a chiral center (-O-C$\underline{H}$<) in the ethyl vinyl ether part many of the protons were diastereotopic and consequently extra coupling was observed.

The mass spectrum showed the expected mass ion m/e = 127 for the adduct of propargyl alcohol and ethyl vinyl ether (17). The fragmentation pattern observed was: m/e 127(3%), 113(50%), 99(3%), 83(95%), 73(100%) and 56(90%) respectively. The parent mass ion seems to be very unstable and it undergoes loss of H very efficiently to give a low intensity peak of molecular mass 127. In competition the methyl group of the ethyl vinyl ether part cleaves to give a peak of mass 113, which then loses the methylene group of the ethyl vinyl ether part to give a very unstable fragment with m/e = 99. The cleavage of the ether bond associated with the chiral carbon center results in the loss of the ethoxy group from the ethyl vinyl ether part, to give the fragment with m/e = 83, which was observed to be very stable. The observed precise mass also suggested the formation of -OH protected propargyl alcohol (17). The infra-red analysis showed the presence of an intense peak at 1132.4 cm^{-1}, which was assigned to the ether linkage (C-O-C) in the adduct (17). Moreover the presence of the acetylenic ≡C-H stretch at 3294.8 cm^{-1} and the acetylenic C≡C stretch at 2209.4 cm^{-1} was also observed. From this evidence it was concluded that protection of the alcohol group of propargyl alcohol by ethyl vinyl ether had been achieved.

2.3.7.2 Synthesis of 4-Phenyl-2-Butyn-1-ol (18), Scheme 9, Steps 2 and 3

The preparation of 4-phenyl-2-butyn-1-ol (18) using benzyl bromide and the -OH protected propargyl alcohol (17) was attempted first in order to find conditions for the preparation of P-Ace-OH (20). The preparation of 4-phenyl-2-butyn-1-ol (18) has been reported in the literature.[23] However, the literature procedure was inadequate for use with the porphyrin as the starting material. The reported procedure describes the preparation of a Grignard reagent using metallic magnesium and benzyl chloride followed by its treatment with -OH protected 3-bromo propargyl alcohol (Br-C≡C-CH_2OTHP) in the presence of CuBr/Me_2S catalyst. In the present case, Grignard preparation from ZnTTP-Cl (4) and ZnTTP-Br (13) was found to be impossible due to their low solubility in THF. Hence this procedure could not be followed and development of a new synthetic procedure, which can be used for large porphyrin molecules, became necessary.

4-Phenyl-2-butyn-1-ol (18) was prepared following a procedure which was devised by the modification of some published procedures.[20] The Grignard derivative of the acetylenic function of -OH protected propargyl alcohol (17) was prepared by treating a Grignard reagent, ethyl magnesium bromide, with the -OH protected propargyl alcohol (17). The Grignard derivative was then treated with freshly purified[22] cuprous chloride (CuCl) to generate a Grignard-copper complex[20e] with a general structure of (R-C≡C-)$_2$CuMgBr. A distinct colour change was observed during the formation of this complex. Upon addition of CuCl to the Grignard derivative of -OH protected propargyl alcohol (17), a considerable amount of a yellow precipitate was formed first and the colour of the solution turned bright

yellow. After stirring for about 15 minutes at room temperature the precipitate dissolved and the colour of the solution turned light green. These Grignard-copper complexes are known to be very reactive[20e] towards alkyl, aryl and benzylic halides and do not have the tendency to abstract a proton from benzylic methylene protons. Benzyl bromide dissolved in dry THF was then added to this Grignard-copper complex and the mixture was refluxed for 3 hours at 85°C to carry out the coupling reaction. After routine isolation, acid catalyzed deprotection of the alcohol group of the coupled product and column purification a good yield (62%) of 4-phenyl-2-butyn-1-ol (18) was obtained as a colourless liquid.

The ^{1}H-NMR spectrum showed all the peaks in the expected region and they were assigned as follows: 7.36 δ (s, 5H, phenyl protons), 4.62 δ (s, 2H, benzyl methylene protons), 4.18 δ (d, 2H, methylene protons of propargyl alcohol part), 2.47 δ (bs, 1H, alcohol O-H proton).

The mass spectrum showed the expected molecular mass ion m/e = 146. The precise mass of 4-phenyl-2-butyn-1-ol (18) was observed to be in agreement with the calculated value. The infra-red analysis showed the presence of the alcohol O-H at 3311.9 cm^{-1}. The acetylenic ≡C-H stretch which is expected at ca. 3300 cm^{-1} was found to be absent. From all this evidence the formation of 4-phenyl-2-butyn-1-ol (18) was confirmed.

2.3.7.3 Synthesis of P-Ace-OH (20), Scheme 10, Steps 1 and 2; Scheme 11, Step 1

P-Ace-OH (20) was prepared following the same procedure[20] as that used for the preparation of 4-phenyl-2-butyn-1-ol (18) except that benzyl bromide was

replaced with ZnTTP-Er (13). An interesting result was observed during the use of cuprous catalyst (CuCl). Powdered CuCl purified using the previous purification method[23] (i.e. with sulphurous acid) proved to be inadequate for the present reaction since no coupled product was formed. After several attempts it was found that the purification of powdered CuCl using 10% HCl[24] gave fine crystalline CuCl with which the desired reaction was successfully carried out. This may be due to the surface etching of the catalyst which aids formation of the Grignard-copper complex. After the completion of the coupling reaction the crude product was isolated as a purple coloured thick liquid. The liquid appearance of the crude product was probably to the presence of a mixture of excess unreacted -OH protected propargyl alcohol and ZnP-Ace-OR (19), which is the desired coupled product. Deprotection of the alcohol group and demetallation of the porphyrin core using HCl generated the desired free-base porphyrin alcohol (20). Column purification of the crude product using chloroform as eluting agent gave a fair yield (27%) of P-Ace-OH (20) as a dark purple coloured solid. In order to get a better yield an identical reaction was carried out using cuprous cyanide[25] instead of CuCl. However, a lower yield (~10%) of P-Ace-OH (20) was recorded.

The ^{1}H-NMR spectrum of P-Ace-OH (20) showed all the expected peaks for the protons associated with the porphyrin ring and they were assigned as earlier. In addition peaks at 4.47 δ (bs, 2H, benzyl methylene protons) and 4.02 δ (bs, 2H, methylene protons from propargyl alcohol part) were also observed. No alcohol O-H proton was observed, possibly because it exchanged with the water contamination present in the solvent which appeared upfield at ~1.12 δ.

The ^{13}C-NMR spectrum of P-Ace-A (20) showed all the expected peaks for the carbons of porphyrin core and they were assigned as in ZnP-Glyco-OEt (15) (see Section 2.2.6.2). In addition a few more peaks were observed, which were consistent with the product P-Ace-OH (20). Comparing the observed chemical shifts with the predicted values and the APT ^{13}C-NMR spectrum, the following peak assignments were made. The signal at 26.1 δ was assigned to the methylene carbon of the benzyl group. The signal for the methylene carbon connecting the acetylene carbon and alcohol -OH group appeared at 52.5 δ. The signals appeared at 81.8 δ and 84.9 δ were assigned to the acetylene carbon linked to the alcohol methylene group and the benzyl methylene group, respectively. In propargyl alcohol the signal for the methylene carbon attached to the alcohol -OH group appeared at 49.7 δ. The signal for the acetylene carbon atom linked to the methylene carbon was seen at 81.6 δ and that for the terminal acetylene carbon atom it appeared at 73.6 δ. Substantial down-field shift for the terminal acetylene carbon atom has occurred after coupling with the porphyrin moiety and relatively smaller shifts were experienced by other carbons. This is due to the change in the electronic environment of these carbons induced by deshielding nature of the porphyrin ring current.

The mass spectrum showed the expected molecular mass ion m/e = 724. The fragmentations observed were: m/e 724(20%), 707(10%), 686(30%) and 670(100%). These were assigned to M^+, $(M - OH)^+$, (M - acetylene chain + $OH)^+$ and (M - acetylene chain + $H)^+$ respectively. P-Ace-OH (20) seems to have a tendency to lose the -OH group very easily to give a fragment with m/e = 707. This fragment being very unstable loses the entire side chain and picks up a H-atom to give the

porphyrin base moiety with m/e = 670, which is equivalent to TTP. The presence of the fragment m/e = 686 was very surprising. This may be due to a cyclic rearrangement of the side chain which facilitates the incorporation of the •OH radical by the porphyrin moiety to give a fragment of mass 686, which is equivalent to the TTP-OH (2) unit. The observed and calculated precise mass of P-Ace-A (20), were found to be in close agreement with each other. The infra-red spectrum showed the presence of a broad signal due to the alcohol O-H stretch at 3312.4 cm^{-1}. Based on all this evidence the coupling of propargyl alcohol with the porphyrin ring to form P-Ace-OH (20) was confirmed.

2.3.7.4 Synthesis of P-Ace-CHO (21), Scheme 11, Step 2

P-Ace-CHO (21) was prepared by the oxidation of P-Ace-OH (20). Due to the presence of the acetylenic group and the porphyrin ring P-Ace-OH (20) was found to be highly sensitive to oxidation condition. Attempts to convert P-Ace-OH (20) directly to P-Ace-A (23) resulted in over oxidation and consequently milder oxidizing agents had to be used with the aldehyde (21) as an intermediate. Corey[26] has published a variety of excellent synthetic methodologies useful for the efficient oxidation of a wide range of unsaturated alcohols to corresponding carbonyl compounds. One of these procedures was found suitable for the oxidation of P-Ace-OH (20). Pyridinium dichromate and P-Ace-OH (20) were dissolved in CH_2Cl_2 and was stirred for 12 hours at room temperature. The formation of a new product was evidenced by tlc. Routine isolation and purification by flash chromatography gave a low yield (20%) of P-Ace-CHO (21) as a purple coloured solid.

The ^{1}H-NMR spectrum of P-Ace-CHO (21) evidenced all the signals for the protons associated with the porphyrin core in their expected region. They were assigned as earlier. In addition peaks at 9.41 δ (t, 1H, aldehyde -CHO proton) and 4.20 δ (bs, 2H, methylene protons of the benzyl group) were observed. The aldehyde -CHO proton seems to have a long range coupling (J = 0.6 Hz) with the benzyl methylene protons, resulting in a broad singlet signal for the benzyl methylene protons and a triplet signal for -CHO proton. The presence of the broad singlet at -2.78 δ for pyrrole N-H protons of the porphyrin core confirmed the absence of any metallation of the porphyrin core by the pyridinium dichromate.

The ^{13}C-NMR spectrum of P-Ace-CHO (21) showed all the expected peaks for the carbons constituting the porphyrin skeleton and they were assigned as earlier. In addition two signals at 29.7 δ and 173.8 δ were observed. Comparing these observed values with the predicted shifts and the APT ^{13}C-NMR spectrum they were assigned to the benzyl methylene carbon and the aldehyde carbon atoms respectively.

The mass spectrum of P-Ace-CHO (21) showed the expected molecular mass ion at m/e = 722. The observed fragmentations were m/e 722(40%), 694(12%), and 670(100%) and they were assigned to M^{+}, $(M - CHO + H)^{+}$ and $(M - \text{side chain} + H)^{+}$ respectively. P-Ace-CHO (21) seems to lose the aldehyde group very easily and picks up a proton to give a very unstable fragment with m/e = 694. This unstable fragment readily loses the acetylene unit to leave the base porphyrin core, which picks up a proton to give the mass unit equivalent to TTP, i.e., m/e = 670. The observed precise mass was found to be in agreement with that calculated for P-Ace-CHO (21). The infra-red analysis showed the presence of an intense peak at 1695.7

cm^{-1}, confirming the presence of a carbonyl group. Hence from all these data successful oxidation of P-Ace-OH (20) to P-Ace-CHO (21) was concluded.

2.3.7.5 Synthesis of P-Ace-OMe (22), Scheme 12, Step 1

The traditional method for the oxidation of an aldehyde to a carboxylic acid using alkaline silver (I) oxide (Ag_2O) is relatively unsatisfactory for α,β-unsaturated aldehydes, since appreciable base-catalyzed side reactions are occur. In order to avoid this, the conversion of the conjugated aldehyde to corresponding ester group, followed by its hydrolysis to carboxylic acid has been suggested in the literature.[27] According to this published procedure, treatment of a conjugated aldehyde with active MnO_2, NaCN, acetic acid and methanol in THF gives the corresponding methyl ester. Therefore P-Ace-CHO (21), being a conjugated aldehyde was converted to its corresponding methyl ester P-Ace-OMe (22) following the published procedure.[27] P-Ace-CHO (21) dissolved in THF was mixed with NaCN, acetic acid, active magnesium oxide and methanol in a proportion recommended by the literature.[27] The mixture was then stirred at room temperature for 24 hours and formation of a new product was observed by tlc. Routine isolation followed by column purification gave a very high yield (91%) of pure P-Ace-OMe (22), which appeared as a purple solid compound. The duration of the reaction was found to be very crucial. Upon prolonged (>30 hours) stirring significant amounts of brown thick material were deposited along the wall of the reaction flask and the yield of the reaction dropped drastically (~57%).

The ^{1}H-NMR spectrum of P-Ace-OMe (22) exhibited all the porphyrin core protons in the expected region and they were assigned as earlier. Moreover peaks at 4.01 δ (s, 2H, benzyl methylene protons) and 3.86 δ (s, 3H, methyl protons of the methyl ester group) were observed. The chemical shift for the methylene protons was calculated according to Shoolery's method and was predicted to be 3.52 δ, which is in reasonable agreement with the observed value.

The mass spectrum of P-Ace-OMe (22) showed the expected molecular mass ion m/e = 752. The fragmentation pattern observed was m/e 752(20%), 737(12%), 693(36%) and 670(100%) respectively. These fragments were assigned to M^+, (M - CH_3), (M - $COOCH_3$)$^+$ and (M - side chain + H)$^+$ respectively. P-Ace-OMe (22) seems to lose the methyl group readily to give a fragment with m/e = 737, which subsequently loses the CO_2 of the carboxylate group to generate a fragment with m/e = 693. Finally the acetylene group of the side chain is lost to generate the base porphyrin moiety, which acquires a H-atom to generate the fragment (m/e = 670) equivalent to a TTP unit. The precise mass was observed to be in close agreement with that calculated for P-Ace-OMe (22). Infra-red analysis showed an intense peak at 1741.4 cm^{-1}, which was assigned to the ester carbonyl group. Based on this evidence oxidation and esterification of the conjugated porphyrin aldehyde to P-Ace-OMe (22) was confirmed.

2.3.7.f. Hydrolysis of P-Ace-OMe (22) to P-Ace-A (23), Scheme 12, Step 2

The carbomethoxy group of P-Ace-OMe (22) was hydrolysed in basic medium to generate a carboxylic acid group. Upon purification a good yield (72%) of

P-Ace-A (23) was obtained.

The ^{1}H-NMR spectrum of P-Ace-A (23) showed all the expected peaks for the protons of the porphyrin core and they were assigned as earlier. In addition a signal at 4.26 δ (s, 2H, methylene protons of the benzyl group) was observed. No signal for the -COOH proton was observed. This may be because the carboxylic acid proton exchanged with the water contamination present in the solvent and appeared at 1.3 δ. The ^{13}C-NMR spectrum of P-Ace-A (23) could not be obtained owing to the absence of adequate concentration of the sample. The solubility of P-Ace-A (23) was found to be low in all solvents examined. The mass spectrum showed peaks at 694(20%) and 670(100%). The peak at m/e 694 is 44 units less than the expected molecular ion of m/e = 738, which is the molecular mass of P-Ace-A (23). The loss of CO_2 from the carboxylic acid group caused the loss of 44 mass units. The fragment at m/e = 670 indicates the formation of TTP moiety by the cleavage of the acetylene chain attached to the porphyrin ring. Infra-red analysis shows a carbonyl stretch at 1692.1 cm^{-1}, O-H stretch at 3313.9 cm^{-1} and -C≡C- at 2208.9 cm^{-1}. This confirms the generation of a carboxylic acid group at the end of the acetylene chain linked to the porphyrin ring.

2.3.8 SYNTHESIS OF P-Pr-A (25), SCHEME 13, STEPS 1 and 2

The synthetic strategy designed for obtaining P-Pr-A (25) involved the catalytic reduction of the triple bond of P-Ace-OH (20) followed by the oxidation of the alcohol group to corresponding carboxylic acid group. P-Ace-OH (20) was first catalytically reduced to P-Pr-OH (24), which was then oxidized directly to

P-Pr-A (25), without the preparation and isolation of the intermediate aldehyde and ester (21) and (22) respectively.

2.3.8.1 Synthesis of P-Pr-OH (24), Scheme 13, Step 1

P-Ace-OH (20) was converted to P-Pr-OH (24) using a conventional catalytic hydrogenation method. A published literature procedure[27] for catalytic the hydrogenation of an acetylenic triple bond was followed for this preparation. A solution of P-Ace-OH (20) in THF was mixed with catalytic amount of 10% palladium on charcoal and hydrogen was bubbled through the mixture for 3 hours. Normally catalytic hydrogenation reactions are very fast, but in the present case a slow conversion was noticed. This may be due to the low solubility of the porphyrin moiety which inhibits absorption onto the catalyst. After routine isolation and purification an almost stoichiometric amount (98%) of P-Pr-OH (24) was obtained as a purple coloured solid.

The ^{1}H-NMR spectrum of P-Pr-OH (24) exhibited all the porphyrin ring protons in the expected region and they were assigned as earlier. Moreover peaks at 3.82 δ (t, 2H, methylene proton α to the hydroxyl), 2.99 δ (t, 2H, methylene protons of the benzyl group) and 2.08-1.76 δ (m, 4H, methylene protons β and γ to the hydroxyl) were observed. The predicted chemical shifts calculated by Shoolery's method for the α-methylene protons and the benzyl methylene protons, are 3.26 δ and 2.56 δ respectively and they are in reasonable agreement with the observed values. The ^{13}C-NMR spectrum showed all the expected signals for porphyrin ring carbons and they were assigned as earlier. In addition signals at 63.9 δ, 36.6 δ,

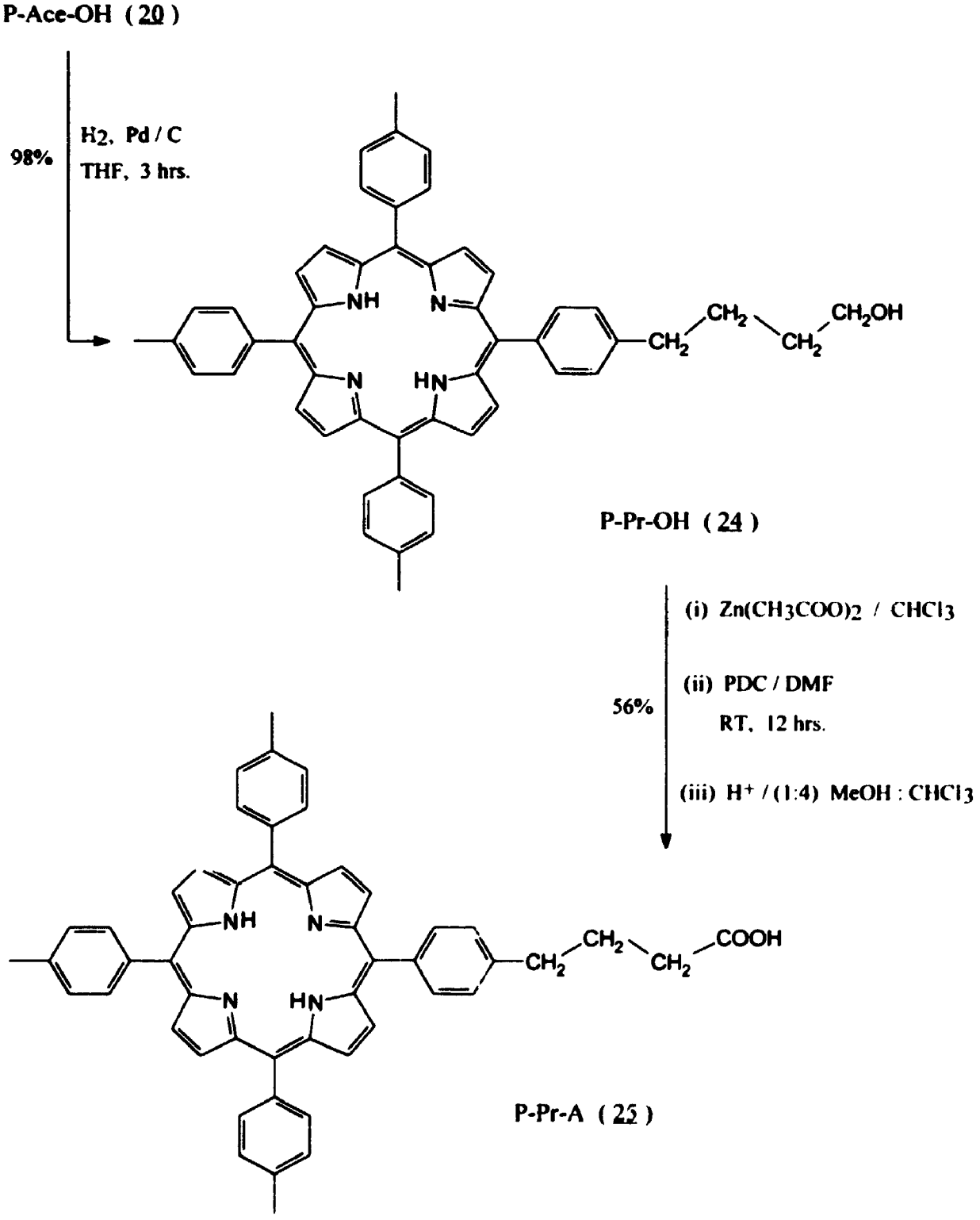

Scheme 13 : Synthesis of P-Pr-A (25)

33.5 δ and 28.6 δ were observed. Comparing the predicted values and the APT ^{13}C-NMR spectrum with the observed chemical shifts and peak multiplicities, the following peak assignments were made: the signal at 63.9 δ was assigned to the α-carbon atom while the β and γ-carbon atoms were assigned to the peaks at 36.6 δ and 33.5 δ respectively. Finally the carbon of the benzyl methylene group was assigned to the signal at 28.6 δ.

The mass spectrum of P-Pr-OH (24) showed the presence of the parent molecular ion at m/e = 728 as the base peak indicating that the compound is quite stable under electron bombardment. In addition peaks at m/e 710(8%), 697(4%), 686(10%) and 670(20%) were observed. They were assigned to $(M - H_2O)^+$, $(M - CH_2OH)^+$, (M - side chain + OH)$^+$, $(M - CH_2CH_2OH)^+$ and (M - side chain + H)$^+$ respectively. P-Pr-OH (24) seems to lose a water molecule to give a low intensity fragment of mass 710. The loss of a water molecule is consistent with a long chain saturated alcohol. In competition with H_2O loss, the molecular ion can undergo loss of the CH_2OH group to give the fragment observed at 697. Finally the entire side chain linked to the porphyrin ring can be lost to give the base porphyrin moiety which picks up a H-atom to give m/e = 670, which is equivalent to TTP unit. The fragment with mass unit 686 may be formed by the recombination of $^{\bullet}OH$ radical with the base porphyrin moiety (m/e = 669) to give a fairly stable fragment, which is equivalent to TTP-OH (2) unit. Most of the long chain porphyrin alcohols synthesized earlier have shown similar behaviour, namely apparent recombination of the $^{\bullet}OH$ radical with the base porphyrin moiety. The observed precise mass supports the formation of P-Pr-OH (24). Infra-red analysis showed a broad peak at

3311.9 cm^{-1}, which was assigned to the O-H stretch of the alcohol group. Thus from this evidence the reduction of P-Ace-OH (20) to P-Pr-OH (24) was confirmed.

2.3.8.2 Synthesis of P-Pr-A (25), Scheme 13, Step 2

P-Pr-A (25) was synthesized by the oxidation of P-Pr-OH (24) to generate a carboxylic acid group at the end of the linked chain. The conventional oxidation procedure[28] recommended for the conversion of a primary alcohol to the corresponding carboxylic acid was found to be very harsh for the porphyrin moiety. Considerable decomposition and unwanted side reactions involving the degradation of the porphyrin ring were observed. This may have occurred due to the acid sensitive nature of the porphyrin. Therefore a modification of the oxidation procedure was required to avoid the use of the harsh acidic condition. An excellent methodology published by Corey,[26] for oxidizing acid sensitive compounds using mild conditions was followed. The application of this procedure requires the use of DMF as solvent and so the zinc derivative of P-Pr-OH (24) was prepared first to increase its solubility in DMF. ZnP-Pr-OH (24a) was oxidized to ZnP-Pr-A (25a) using pyridinium dichromate as the oxidizing agent. Finally demetallation of ZnP-Pr-A (25a) resulted in the formation of the desired product P-Pr-A (25).

P-Pr-OH (24) was converted to ZnP-Pr-OH (24a) following a procedure[5] identical to that used for the preparation of ZnTTP-Cl (4) from TTP-Cl (3) (see Section 2.2.1.4). A distinct change in the colour of the reaction mixture from purple to pink was observed, which indicated the completion of the reaction. Completion of the reaction was also confirmed by the absorption spectrum where the four-banded

spectrum characteristic of a free-base porphyrin collapsed into the two-banded spectrum characteristic of a metallated porphyrin. After isolation and column purification a high yield (92%) was recorded. Pure ZnP-Pr-OH (24a) appeared as a shiny pinkish purple coloured solid.

The ^{1}H-NMR spectrum of ZnP-Pr-OH (24a) exhibited all the expected signals for the porphyrin ring protons and they were assigned as earlier. In addition signals at 3.84 δ (t, 2H, α-methylene protons), 3.01 δ (t, 2H, benzyl methylene protons) and 2.10-1.77 δ (m, 4H, β and γ methylene protons) were observed. No resonances at ~-2.8 δ due to pyrrole N-H protons was observed; this indicates that the insertion of Zn^{2+} ion into the center of the porphyrin ring has occured. This evidence supports the fact that the side chain linked to the porphyrin ring remained undisturbed after the reaction and the metallation of the porphyrin core had occurred successfully.

ZnP-Pr-OH (24a) dissolved in DMF was mixed with pyridinium dichromate and stirred at room temperature for 7 hours. Formation of a new product was evidenced by analytical tlc. During workup the organic layer was washed with 5% HCl solution to remove zinc from the porphyrin core. Column purification of the crude product yielded (56%) pure P-Pr-A (25), which appeared as a purple coloured solid.

The ^{1}H-NMR spectrum of P-Pr-A (25) could not be recorded due to the poor solubility of this compound in all the solvents examined. This was partly due to self protonation of the porphyrin by the side chain carboxylic acid group. The self protonation by the carboxylic acid group may have occurred in the system due to the increase in chain length between the porphyrin ring and the carboxylic acid group.

Such self protonation is not observed in P-A (1). The long chain in P-Pr-A (25) helps the acid group to come in close proximity to the porphyrin core where the basic pyrrole nitrogen groups are situated. The loss of the proton to give a zwitterionic form of the compound becomes possible. Due to the significant protonation of the porphyrin core the purple colour of this compound becomes green in solution.

The mass spectrum of P-Pr-A (25) showed peaks at m/e 742(84%), 728(6%), 697(2%), 684(30%) and 670(100%). These peaks were assigned to M^+, $(M - OH + 3H)^+$, $(M - COOH)^+$, $(M - CH_2CH_2OH + H)^+$ and (M - side chain + H)$^+$ fragments respectively. P-Pr-A (25) showed the expected molecular mass ion as an intense peak at m/e 742 indicating that the molecule is quite stable and is not prone to fragmentation very easily. The ion at m/e = 728 was possibly due to the loss of -OH group of the carboxylic acid group and incorporation of three H^+ ions by the remaining fragment. Two H^+ ions may be incorporated onto the pyrrolic nitrogens of the porphyrin ring while the third H^+ may have been incorporated onto the oxygen of the carbonyl group. Similar behaviour was observed for P-Gly-A (11). The peak at m/e = 697 is assigned to the cleavage of the linkage between the carboxylic acid group and the α-methylene carbon atom, which results in the loss of the carboxylic acid unit. The fragment with mass unit 697 easily loses another methylene group and picks up a H-atom to generate a fragment equivalent to a P-CH_2CH_3 unit with m/e = 684. Finally the last methylene group of the side chain is lost to give the parent porphyrin moiety with a mass unit of 669, which acquires a H-atom to give the peak at m/e = 670. The calculated precise mass P-Pr-A (25) was found to be in close agreement with the observed mass. Infra-red analysis showed an intense peak

at 1693.4 cm^{-1} and a broad peak at 3315.6 cm^{-1}, which were assigned to the C=O stretch of the carbonyl group and the O-H stretch of the carboxylic acid group respectively. Hence from all these data the formation of P-Pr-A (25) was concluded.

REFERENCES

1. Anton, J.A.; Kong, J.; Loach, P.A. *J. Hetrocyclic Chem.* **1976**, *13*, 717.
2. La, Mar; Gerd N.; Walken, J. In *The Porphyrins*; Dolphin, D. ed.; Academic Press, **1979**, *4*, 68.
3. (a) Nystrom, R.F.; Brown, W.G. *J. Am. Chem. Soc.* **1947**, *69*, 2548. (b) Shoolery, J. N. *Varian Technical Information Bulletin*, **1959**, *2 and 3*, Palo Alto, California.
4. Furniss, B.S.; Hannaford, A.J.; Tatchell, A.R. In *Vogel's Textbook of practical Organic Chemistry*, ELBS and Longman Publishers, **1980**, 385.
5. Buchler, J.W. In *The Porphyrins*; Dolphin, D. ed.; Academic Press, **1978**, *1*, 406.
6. (a) Kenner, G.W.; Quirke, M.E.; Smith, K.M. *Tetrahedron* **1976**, *32*, 2753.
   (b) Schwartz, A.; Madan, P. *J. Org. Chem.* **1986**, *51*, 5463.
7. Davis, R.; Untch, K.G. *J. Org. Chem.* **1981**, *46*, 2987.
8. Puppe, L.; Buchler, J.W. *Liebigs Ann. Chem.* **1970**, *740*, 142.
9. Cope, A.C.; Homes, H.L.; House, H.O. *Organic Reactions* **1957**, *9*, 157.
10. Marvel, C.S. *Org. Synthesis* **1955**, *Coll. Vol. 3*, 495.
11. Brandsma, L. In *Preparative Acetylenic Chemistry*, 2nd ed., Elsevier, Amesterdam, **1988**, 256.
12. Kikugawa, K.; Ichino, M. *Tetrahedron Lett.* **1971**, 87.
13. Shiotani, S.; Morita, H.; Ishida, T.; In, Y. *J. Heterocyclic Chem.* **1988**, *25*, 1205.
14. Walkup, R.D.; Cunningham, R.T. *Tetrahedron Lett.* **1987**, *28*, 4019.
15. Anzalone, L.; Hirsch, J.A. *J. Org. Chem.* **1985**, *50*, 2128.

16. Roach, K.J. In *Synthesis and Photochemical Properties of Some Porphyrin derivatives*, Ph.D. Dissertation, The University of Western Ontario, London, Canada, **1990**, 133.

17. Normant, J.F. *Synthesis* **1972**, 63.

18. Ando, T.; Tokura, N. *Bull. Chem. Soc. Jpn.* **1958**, *31*, 351.

19. (a) Cossy, J.; Pete, J.P. *Tetrahedron Lett.* **1986**, *27*, 573. (b) Cossy, J.; Pete, J.P. *ibid.* **1986**, *27*, 2369.

20. (a) Ben-Efraim, D.A.; Sondheimer, F. *Tetrahedron* **1969**, *25*, 2823. (b) Taniguchi, H.; Mathai, I.M.; Miller, S.I. *Tetrahedron* **1966**, *22*, 867. (c) Steen, D.V.; Pabon, H.J.J.; van Drop, D.A. *Rec. Trav. Chim. Pays Bas* **1963**, *82*, 1015. (d) Stoffel, W. *Liebigs. Ann. Chem.* **1964**, *673*, 26. (e) Gensler, W.J.; Mahadevan, A.P. *J. Am. Chem. Soc.* **1955**, *77*, 3076. (f) Osbond, J.M.; Philpott, P.G.; Wickens, J.C. *J. Chem. Soc.* **1961**, 2779.

21. Brandsma, L. In *Preparative Acetylenic Chemistry*, 2nd ed.; Elsevier: Amesterdam, **1988**, 265.

22. Claesson, A.; Sahlberg, C. *Tetrahedron* **1982**, *38*, 363.

23. Keller, R.N.; Wycoff, H.D. *Inorganic Synthesis* **1946**, *2*, 1.

24. Perrin, D.D.; Armarego, W.L.F.; Perrin, D.R. In *Purification of Laboratory Chemicals*; Pergamon Press, **1980**, 486.

25. Heslinga, L.; Pabon, H.J.; Drop, D.A. *Rec. Trav. Chim. Pays Bas* **1973**, *92*, 287.

26. Corey, E.J.; Schmidt, G. *Tetrahedron Lett.* **1979**, 399.

27. Corey, E.J.; Gillman, N.W.; Ganem, B.E. *J. Am. Chem. Soc.* **1968**, *90*, 5616.

28. Burgstahler, A.W.; Widiger, G.N. *J. Org. Chem.* **1973**, *38*, 3652.

CHAPTER 3

ABSORPTION AND STEADY-STATE EMISSION PROPERTIES OF THE NEWLY SYNTHESIZED PORPHYRIN COMPOUNDS

3.1 INTRODUCTION

This chapter begins with a brief summary of the general features of tetra-arylporphyrin absorption and emission spectra. For more detailed information, the reader may refer to the comprehensive review of porphyrin optical spectra by Gouterman.[1] Examination of the absorption and emission spectra of the newly synthesised porphyrin compounds shows that intramolecular complexation between the porphyrin and the attached carboxylic acid group is absent. The fluorescence quantum yields in four different solvent systems, namely 0.1 M sodium hydroxide solution, acetonitrile, dichloromethane and chloroform, were determined. Significant quenching was observed in the case of sodium hydroxide solutions, which is consistent with aggregate formation of the model porphyrin molecules in this solvent.

3.2 EXPERIMENTAL DETAILS

Absorption spectra were recorded using a Hewlett-Packard 8450 UV/Visible absorption spectrometer. This instrument incorporates a microprocessor, so that various spectra can be normalized and compared. A quartz cell of 1.00 × 1.00 cm^2 dimensions was used for measuring the absorption spectra of all the compounds. Emission spectra were recorded using Perkin-Elmer 650-40 fluorescence or PTI

LS-100 photoluminescence spectrometers and were corrected for the instrument response. The same quartz cell of 1.00 × 1.00 dimensions was also used for collecting the emission spectra. Both instruments were microprocessor based, allowing for the comparison of normalized emission spectra.

For absorption and fluorescence measurements, either Fisher or BDH spectroscopic grade solvents were used. A small amount of solid potassium carbonate or ~ 10^{-5} M diethyl amine was added in all the samples to remove the porphyrin dication formed, due to the presence of a removable carboxylic acid proton in all the model compounds.

3.3 RESULTS AND DISCUSSION

3.3.1 Porphyrin Absorption and Emission Spectra

The absorption spectrum of P-A (Figure 3.1) is representative of the free-base porphyrins studied in the present work. The important characteristics are summarized below: (1) All porphyrin absorption bands are interpreted as π-π^* in origin.[1] (2) The bands in the 500 to 650 nm region, collectively referred to as the Q-bands, are assigned to transitions to the first excited singlet state. Four bands are observed in the free-base porphyrins, corresponding to the (0,0) transition and the first vibronic overtone (1,0). Due to the presence of D_{2h} symmetry of the porphyrin ring, the Q-bands are each split into x and y polarized components, giving the characteristic four-banded spectrum. If all four of the pyrrole nitrogen atoms are protonated (giving a dication), the porphyrin ring has a D_{4h} symmetry and the four-banded porphyrin spectrum collapses into a two-banded spectrum. The extinction

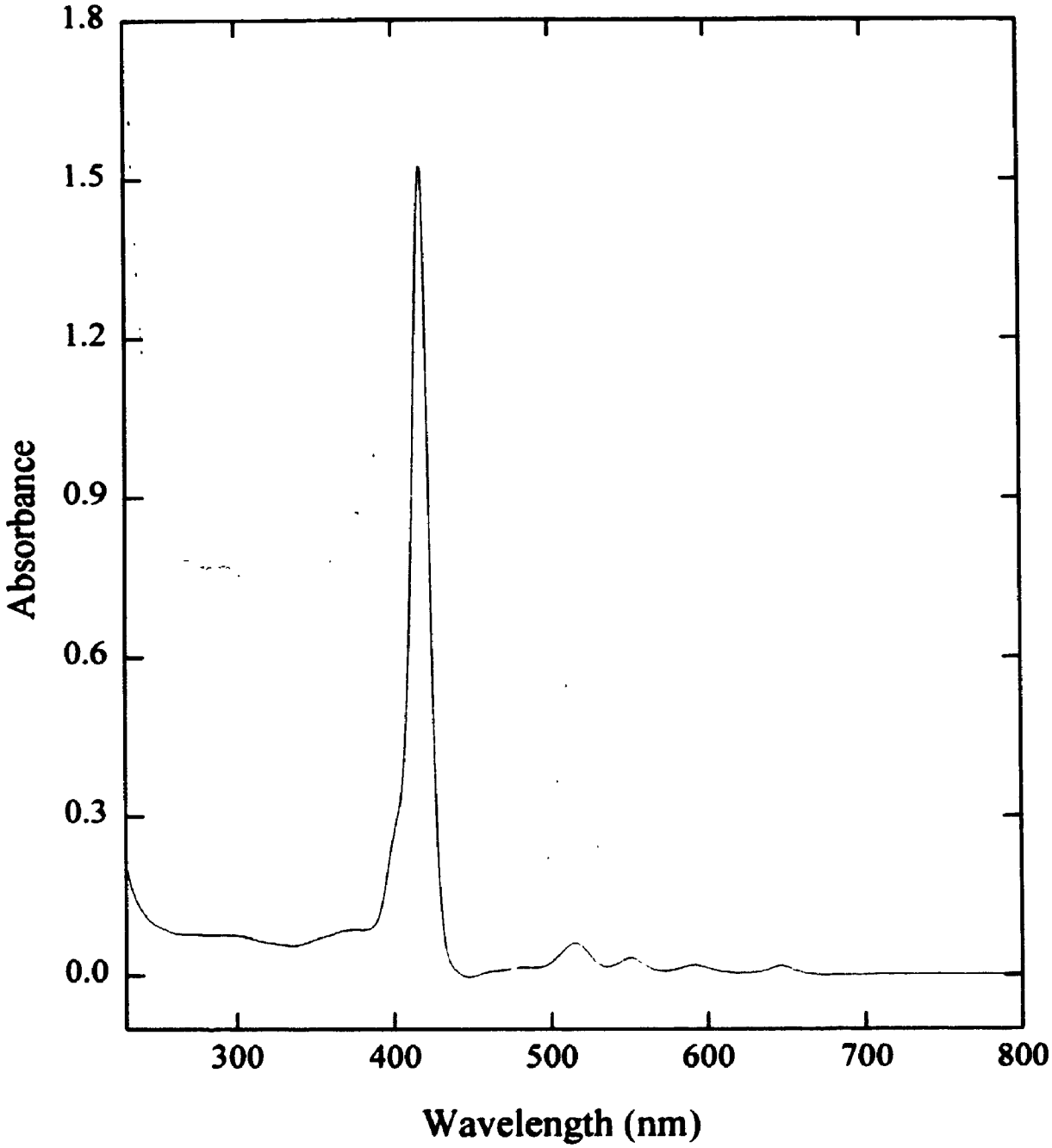

Figure 3.1 : Absorption spectrum of P-A in dichloromethane. The hatched lines are amplified by a factor of ten. Measurement was carried out at 22 ± 2^0C.

coefficients of the Q bands are ≈ 3×10^3 - 2×10^4 M^{-1} cm^{-1}. (3) The most intense absorption, designated as the Soret or B band, occurs in the 420 nm region, with an extinction coefficient ~ 5×10^5 M^{-1} cm^{-1}. It is assigned to the transition from the ground state to the second excited singlet state. (4) To the blue of the Soret band are a number of broad, weakly resolved absorptions with extinction coefficients ≈ 1 -2.5 $\times 10^4$ M^{-1} cm^{-1}. The nomenclature "N", "M", "L", "ζ" and "η" has been adopted to classify these transitions.[1]

All of the model compounds showed very similar absorption spectra as that of P-A. Table 3.1 summarizes the absorption characteristics of all the model porphyrin compounds in the four different solvent systems. From the table, it can be seen that for a given solvent, all model compounds have the same λ_{max} values. This behaviour may be attributed to the absence of any effect from the different chain linkages attached to the porphyrin core system. Hence, all the compounds exhibit the characteristic absorption of the tritolylporphyrin unit only. A uniform change in λ_{max} was observed for all the compounds on changing the solvent system. The differences in the λ_{max} values in different solvents for all the compounds mainly arise from a solvent effect experienced by the porphyrin core unit. In sodium hydroxide solution, all the compounds appear to be aggregated, which results in an absorption at higher wavelength. The difference in the λ_{max} values for different model compounds in sodium hydroxide solution could be attributed to different degrees of cluster formation by these compounds. In acetonitrile, all compounds dissolve completely, resulting in the formation of a homogeneous solution, where all compounds show their characteristic absorption at λ_{max} = 414 ± 2 nm. In CH_2Cl_2

Table 3.1 Absorption characteristics of porphyrin model compounds in different solvent systems.[a]

Compounds	H_2O[b]	CH_3CN	CH_2Cl_2	$CHCl_3$
P-A	444 ± 2	414 ± 2	418 ± 2	418 ± 2
P-Me-A	438 ± 2	414 ± 2	418 ± 2	418 ± 2
P-Et-A	420 ± 2	414 ± 2	418 ± 2	418 ± 2
P-Pr-A	420 ± 2	414 ± 2	418 ± 2	418 ± 2
P-Ace-A	420 ± 2	414 ± 2	418 ± 2	418 ± 2
P-Gly-A	432 ± 2	414 ± 2	418 ± 2	418 ± 2
P-Glyco-A	424 ± 2	414 ± 2	418 ± 2	418 ± 2

[a] Measurements were carried out at 22 ± 2°C and λ_{max} values are given in nm.

[b] 0.1 M NaOH solution.

and $CHCl_3$ all the compounds absorbed at the same wavelength (λ_{max} = 418 ± 2 nm). This shows that a similar solution environment for all the molecules is present in both of these solvents. The difference in the λ_{max} values for all the compounds in acetonitrile and in the chlorinated solvents (CH_2Cl_2 and $CHCl_3$) may arise from a heavy atom effect caused by the chlorinated solvents.

The emission spectrum of P-A is shown in Figure 3.2. No interesting effect in the emission characteristics for all the model compounds in different solvents was observed. All the compounds emitted virtually at the same wavelength (λ_f = 652 ± 2 nm) and showed a similar spectral pattern as for P-A. This clearly indicates that all compounds possess a similar excited singlet state (S_1) deactivation pathway. The presence of different side chains does not cause any disruption of the deactivation process from the excited singlet state.

3.3.2 Fluorescence Quantum Yields

Fluorescence quantum yields were estimated by comparing the integrated emission intensities of samples to that of a standard of known quantum yield. The method is outlined below.

The fluorescence intensity I_f of a sample is given by

$$I_f = I_0(1 - 10^{-A})\phi_f \qquad (3.1)$$

where I_0 is the intensity of the incident light, A is the absorbance of the solution at the excitation wavelength, and ϕ_f is the fluorescence quantum yield. Using the following equation, ϕ_f can be determined by comparing the integrated emission intensity with that of a standard of known quantum yield, ϕ_{fs}.

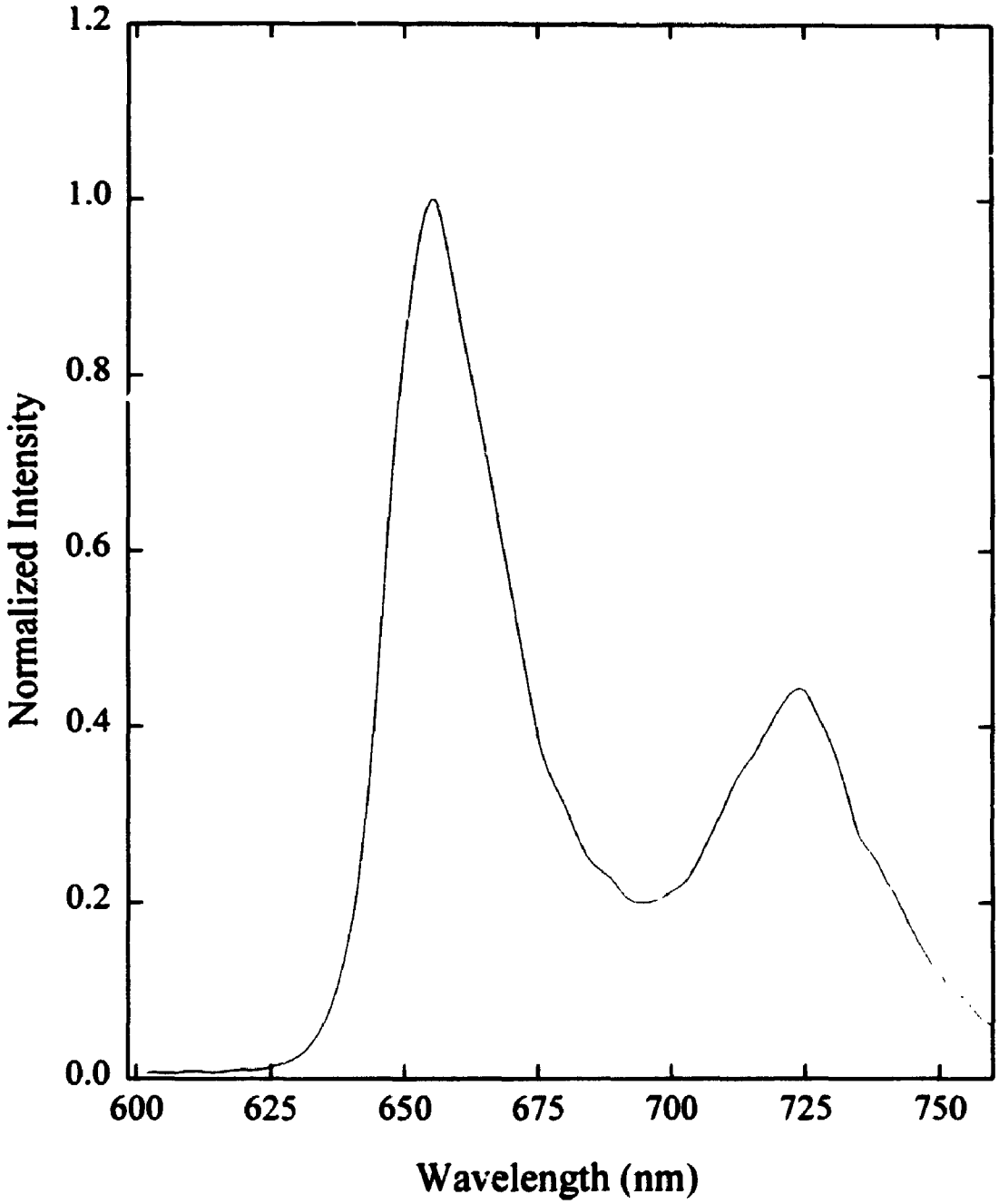

Figure 3.2 : Normalized emission spectrum of P-A in dichloromethane with excitation at 420 nm. Measurement was done at 22 ± 2^0C.

$$\phi_f = \frac{I_f\left(1 - 10^{-A_s}\right)}{I_{fs}\left(1 - 10^{-A}\right)} \phi_{fs} \qquad (3.2)$$

I_{fs} and A_s are the fluorescence intensity and absorbance of the standard. If the absorbance of the sample and that of the reference are less than ~ 0.05, the power series expansion of the 10^{-A} term can be truncated at the second term, and Equation (3.3) can be simplified to

$$\phi_f = \frac{I_f\, A_s}{I_{fs} A} \phi_{fs} \qquad (3.3)$$

Fluorescence quantum yields were estimated for samples in 0.1 M sodium hydroxide solution, acetonitrile, dichloromethane and chloroform respectively. Small amounts of anhydrous sodium or potassium carbonate were added to solutions containing free-base porphyrins to neutralize trace amounts of acid in the solvent, preventing formation of the porphyrin dication species. Presence of the dication form of the porphyrin is indicated by the appearance of either a shoulder or a new band at ~ 440 nm in the absorption spectrum. The concentration of all samples was $\leq 10^{-7}$ M, which gave an absorbance ≤ 0.05 at the excitation wavelength (418 nm). P-A was used as a standard[2] for all the porphyrin compounds studied in the present work. An integrated emission intensity between 600 nm and 800 nm was recorded. Emission intensities were corrected for the response of the photomultiplier tube, although the reference material emitted in the same spectral region as the samples. All samples were sealed with rubber septum caps and deaerated by nitrogen bubbling before recording the emission. The same 1.00 × 1.00 cm^2 quartz fluorescence cell was used

to record the emission of both the sample and the standard.

The estimated fluorescence yields are summarized in Table 3.2. The fluorescence intensities of all the model compounds in a particular solvent are identical to, or slightly quenched relative to each other. Significant fluorescence quenching was observed for all the model compounds when dissolved in sodium hydroxide solution, and a slightly enhanced yield was observed when dissolved in acetonitrile. This indicates that all the model compounds are more fluorescent in acetonitrile and less fluorescent in sodium hydroxide solution, relative to their fluorescent behaviour in dichloromethane or chloroform solutions. Thus, estimates of ϕ_f for acetonitrile solutions should be regarded as upper limits and those for sodium hydroxide solutions should be regarded as the lower limits for all the model compounds.

Table 3.2 Fluorescence quantum yields (ϕ_f) of model porphyrin compounds in different solvent systems.[a]

Compounds	H_2O[b,c]	CH_3CN[b]	CH_2Cl_2[b]	$CHCl_3$[b]
P-A	0.102	0.158	0.130[d]	0.109
P-Me-A	0.093	0.161	0.123	0.110
P-Et-A	0.082	0.168	0.126	0.109
P-Pr-A	0.073	0.185	0.133	0.119
P-Ace-A	0.088	0.197	0.133	0.120
P-Gly-A	0.067	0.182	0.146	0.130
P-Glyco-A	0.019	0.178	0.109	0.093

[a] Measurements were done at 22 ± 2°C.

[b] Errors were in the rage of ±0.002 to ±0.004.

[c] 0.1 M NaOH solution.

[d] ϕ_f for P-A in dichloromethane was taken from reference 2.

REFERENCES

1. Gouterman, M. In *The Porphyrins*, Dolphin, D. (ed.), Academic Press: New York, **1978**, *3*, 1.

2. Siemiarczuk, A.; McIntosh, A. R.; Ho, T. -F.; Stillman, M. J.; Roach, K. J.; Weedon, A. C.; Bolton, J. R.; Connolly; J. S. *J. Am. Chem. Soc.* **1983**, *105*, 7224.

CHAPTER 4

MONOLAYER SURFACE AND PHOTOPHYSICAL PROPERTIES

4.1 INTRODUCTION

The optoelectronic properties of thin films of organic semiconductors such as porphyrins and phthalocyanines have attracted attention for both practical[1] and theoretical[2,3] reasons. The mechanisms of electronic conduction, energy transfer and radiationless deactivation of excited states in single crystals of organic semiconductors are still not well understood.[3] An understanding of these processes in the less well-ordered, but technologically more important, thin films is still in a primitive stage.

In the solid state, porphyrins and many other organic semiconductors, behave as quasi-one-dimensional conductors;[3,4,5] their intermolecular overlap, and therefore their conductivity, is greatest in a direction perpendicular to the molecular planes. Because of the low dimensionality of the conducting pathway, crystal dislocations and bond resistances should have a greater effect on the optoelectronic properties of organic semiconductors than on three-dimensional semiconductors such as silicon. Such considerations led us to synthesize a series of porphyrins possessing surface active properties, in an effort to (a) investigate the effects of order on the photophysical and photoelectrochemical properties of *Langmuir-Blodgett* monolayer films made from these porphyrins and (b) grow large area, well-ordered thin films for use in organic semiconductor devices.

A number of papers dealing with the photophysical properties of porphyrin thin films have appeared. Gouterman *et al.*[6a,b] have studied sublimed films of octaethylporphyrin (H_2OEP) and report that films thicker than ~100 Å have some tendency to crystallize spontaneously. These films showed increased impurity fluorescence, which was attributed to a longer exciton diffusion length in the polycrystalline materials, as compared to the amorphous films. They also noticed a substantial quenching of the Soret band in the fluorescence excitation spectrum of the polycrystalline films,[6a] although this was later thought to be a reflection effect.[6b] These workers later showed[6c] that the emission intensity from both the host and the impurities was enhanced by sublimation onto a heated substrate, rather than at room temperature.

A substantial effort has been devoted to the characterization of monolayer films of porphyrins, both as the pure porphyrins[7,8,9a,c,d] and as mixtures of surfactants.[9b] The optical properties of porphyrins in monolayers resemble those of the dimerized or aggregated species in solution.[7b,8,9a,b] A number of examples of conductivity measurements[7a,9c,d] and photoelectron transfer[7a,c] have also been reported. Kampas *et al.*[10a] prepared both sublimed and spin-coated thin films of a large number of porphyrins for testing in photoelectrochemical (PEC) cells. The amorphous films obtained by spin-coating showed higher quantum efficiencies for photocurrent generation than the polycrystalline films obtained by sublimation, although this result might be explained by the possibility of a large number of pinholes in the polycrystalline layers. Armstrong *et al.*[11] have carefully optimized the sublimation conditions for the deposition of a number of phthalocyanines and have

correlated the changes in the absorption spectra with the type of crystals formed. They obtained the highest efficiencies in PEC cells for films consisting of large crystals which spanned the thickness of the layer.

With the availability of the *newly synthesized porphyrins*, we are now able to exercise more control over the order of the porphyrin chromophore in the monolayer, than was previously possible. This chapter details how the photophysical properties of the newly made porphyrins change as a function of the degree of film order (i.e., aggregation) and the nature of the side chain attached to it. The present work contains the following points: (1) a demonstration that the degree of order of the porphyrins in monolayers depends on the nature of the side chain and the surface of the substrate; (2) a description of the photophysical changes in a system of a single chromophore (tritolylporphyrin) whose degree of order can be almost continually varied due to the different chain lengths attached to it; (3) an explanation of why the porphyrin B absorption band experiences a bathochromic shift in the monolayer; (4) a demonstration that the fluorescence emission quantum yield of the monolayers ϕ_f becomes aggregation (and hence order) and side chain linkage dependant, and (5) a comparison of the photophysical properties of porphyrin compounds with those of the monolayer films and the dissolved species, (i.e., in solution). To the best of our knowledge a number of these points are quite novel.

It should be emphasized that all the porphyrin compounds studied are solid at room temperature. The measurements reported here, unless otherwise noted, were taken at room temperature.

4.2 MONOLAYER TECHNIQUES

Since the pioneering work of Pockels[12] and Langmuir[13] the elegant techniques for the construction and manipulation of monomolecular films at the air-water interface have been extensively studied. The presence of the surface-active molecules at the liquid air interface, develops a tendency to aggregate, arising from the decrease in free energy and the increase of surface tension between them. When such molecules have substantial insolubility in water, yet retain some means of interaction (usually a hydrophillic group), a monomolecular layer may be formed at the water surface. The increase in the surface tension caused by the presence of the monolayer is called the surface pressure, as it may be considered as a two-dimensional analogue of pressure. From a quantitative knowledge of the variation of the available surface area and the amount of the surface-active material present, a surface pressure-area diagram can be constructed. This diagram, made at constant water temperature, is called a *surface pressure-area isotherm*. The presence of a well behaved monolayer can be evidenced by rationalizing the surface pressure-area curve in terms of molecular structure. A typical fatty acid isotherm is shown in Figure 4.1.[14]

Figure 4.2 shows the apparatus usually employed for the production of monolayers at the air-water interface. At first, the trough is filled to the brim with water and the surface-active compound is then spread on the surface as a solution with some volatile, water immiscible solvent such as chloroform. After the solvent has been allowed to evaporate, the surface area of the trough is varied using a movable barrier, which rides along the top of the sides of the trough. The surface tension (or surface pressure) can be measured using a large variety of techniques.

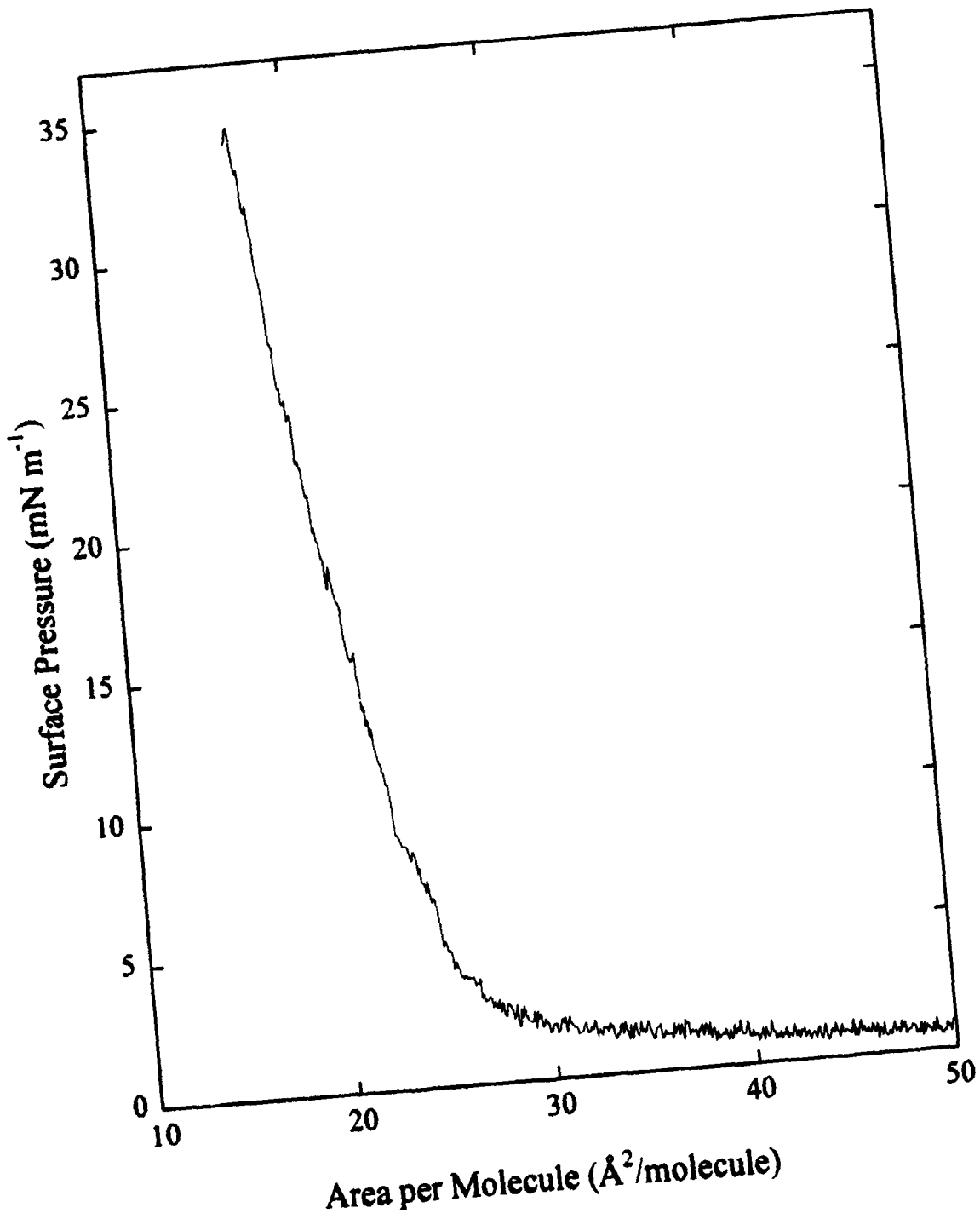

Figure 4.1 : Surface Pressure-Area Isotherm of stearic acid.
Subphase, unbuffered water at 22 ± 2^{0}C.

Figure 4.2 : The Langmuir trough. It consists of a teflon trough (a) of 13 cm × 60 cm × 1 cm deep interior dimensions and 15 cm × 62 cm × 5 cm deep exterior dimensions. A hole (b) 8 cm × 11 cm × 2.5 cm deep is located below the slide deposition apparatus. The teflon trough is screw mounted onto a 2.5 cm thick aluminium base which rests on four leveling screws. A movable teflon barrier (c) rides along the top of the sides of the trough. It is propelled by two arms (d) attached to a worm gear (e) located underneath the base of the trough. The worm gear is powered by a synchronously wound chopper motor (f) via a reduction gear assembly (g). The surface pressure is monitored by a teflon boat (i) of 0.6 cm × 11.1 cm × 0.1 cm dimensions. Seal is made to the sides of the trough by teflon tape (j) which is friction held in a vertical slit on either end of the float and clamped to the sides of the trough with a teflon clamp. The teflon float is attached to the lower arms of a torsion balance (k). The core from a linear transducer is hung from a horizontal arm of the balance and extends into the core of the transducer (l).

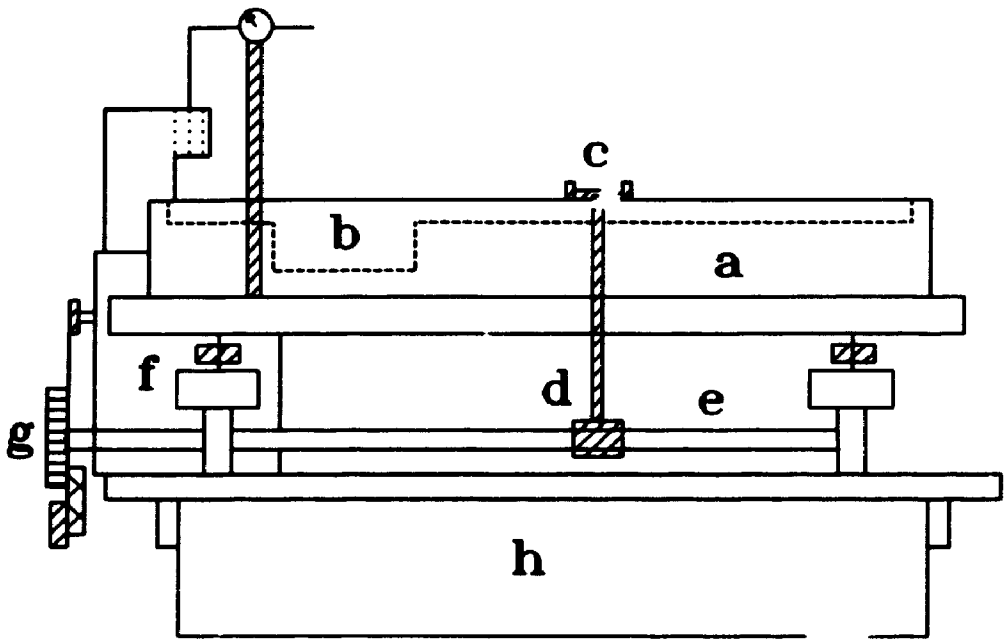
c
b
a
f
d
e
g
h

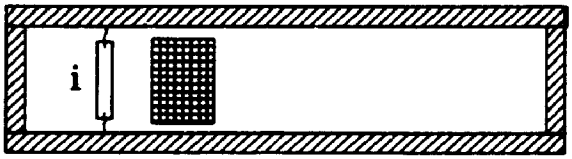
i

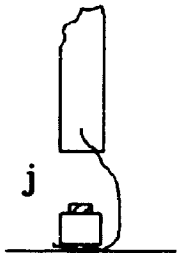
j

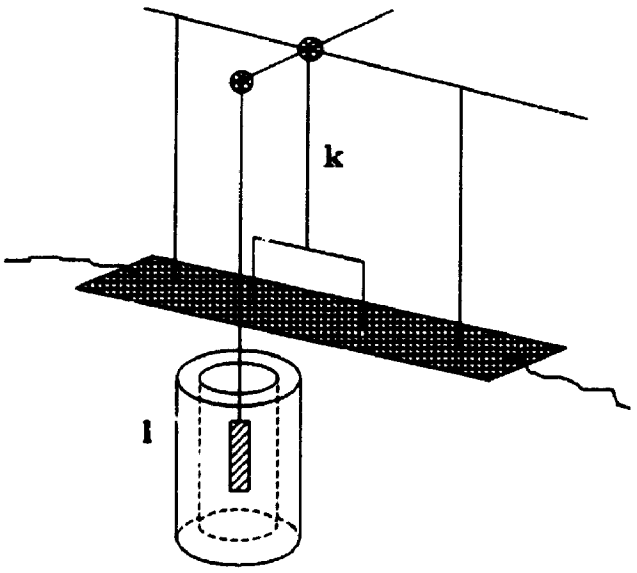
k
l

The method used in the present work utilizes a float-torsion pendulum assembly, which possesses a linear transducer. The twist in the torsion wire is proportional to the difference in surface pressure between the monolayer film on one side of a float and the clean water surface on the other side of the float.

In general, the pressure-area isotherm of a molecule can exhibit several different regions or two dimensional phases. These are shown in Figure 4.3.

(a) In the *gaseous phase* the molecules are well separated due to the high molecular area. Except by direct collision, no other interactions are present between them. Hence the surface pressure is very low.

(b) A *liquid phase* is exhibited in the pressure-area isotherm when the surface area is decreased. This is due to the initiation of interaction between the molecules.

(c) When the surface area is further decreased, the molecules become tightly packed, and the film becomes rigid, resulting in a steep rise of the surface-pressure isotherm. This state is the *solid phase* of the isotherm.

(d) Finally, a further decrease in area results in a folding and buckling of the film leading to *collapse* of the monolayer. The applied pressure overcomes the resisting power of the monolayer, resulting in its destruction.

Not all molecules exhibit all three phases. In some cases, the interaction among the hydrophobic portions is large, so that at low pressure the molecules do not separate, but float about the surface in small islands. This type of behaviour is common for molecules exhibiting only a solid, steeply rising pressure-area curve.

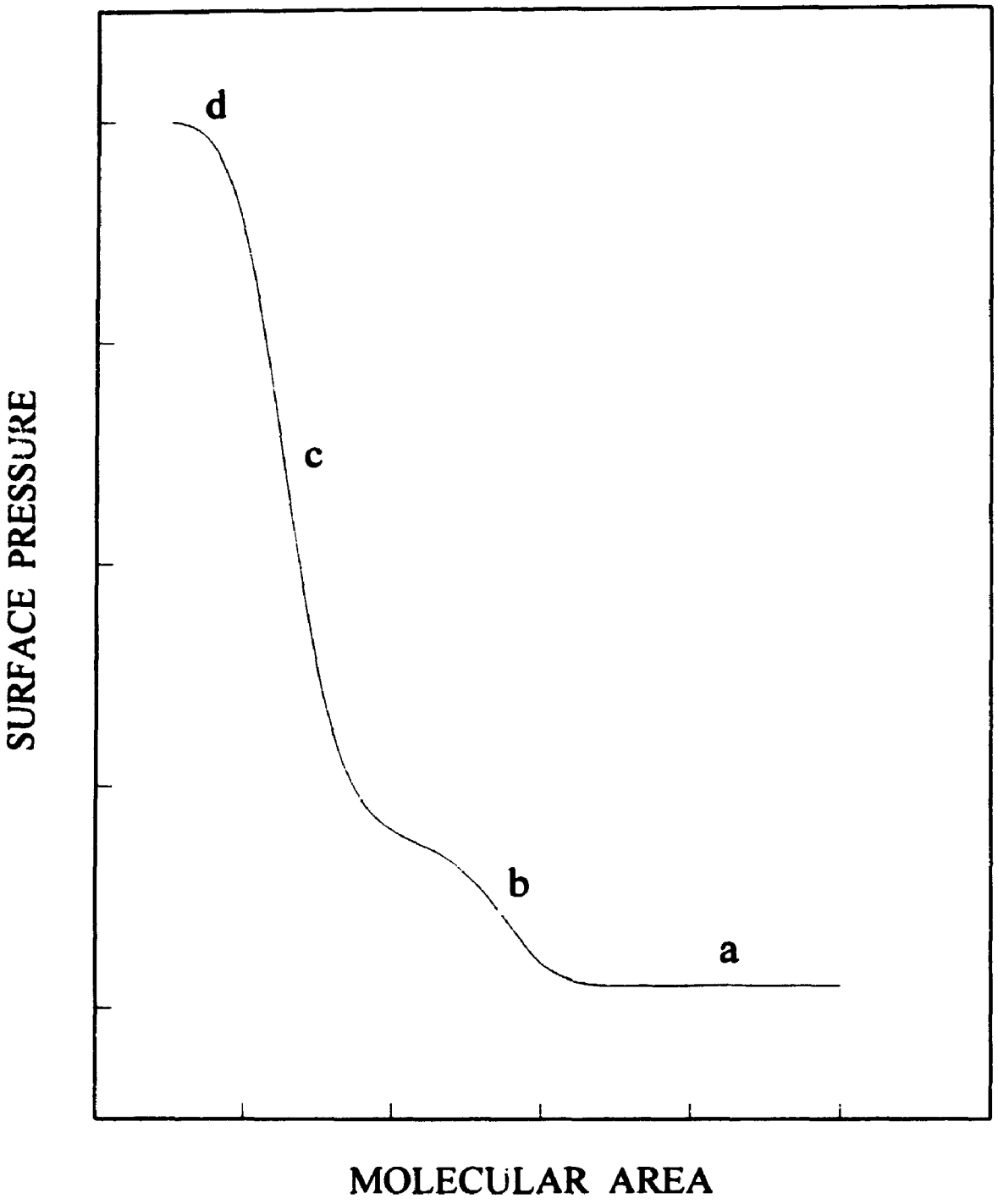

Figure 4.3 : A surface pressure-area isotherm. (a) *gaseous phase*, (b) *liquid phase*, (c) *solid phase* and (d) *collapse*.

Monolayers are known to be formed by numerous types of compounds, some of which are shown in Figure 4.4. Normally these compounds possess distinctive hydrophillic and hydrophobic portions. Fatty acids and long chain (ten or more carbons) alcohols are the *best-studied* group of compounds. Monolayers of a variety of dye molecules have been studied.[15] The hydrophillic group is not limited to long-chain carboxylic acid or alcohols, but to a diverse number of groups. A second group of monolayer forming compounds is the neutral polycyclic compounds, such as abietic acid. The hydrophobicity of this compound is provided by the polycyclic ring system. The third group of compounds, that form monomolecular layers is the naturally occurring lipid soluble materials such as vitamins A, E, K_1 and the chlorophylls. All these compounds contain a hydrocarbon chain and one or more hydrophillic groups.

The formation of well-behaved monolayers has been evidenced by compounds, which do not contain both a distinct hydrophobic and hydrophillic part. Quinquithienyl is such an example, which is known to form monolayers in which the long axes of the molecule stand perpendicular to the water surface, parallel to each other. The stability of the monolayer is attributed to the side-to side interaction of the π-electron systems.[15]

Monolayer formation by free-base porphyrins at the air-water interface has been reported in the literature.[16,17] These compounds have structures in which the hydrophillic groups are situated in varying positions around the porphyrin ring. They were reported to form solid, rigid monolayers where the ring systems are orientated perpendicular to the water surface. Precompression was required to obtain reproducible isotherms. Dick *et al.*[17] have reported the formation of a rigid

Stearic Acid

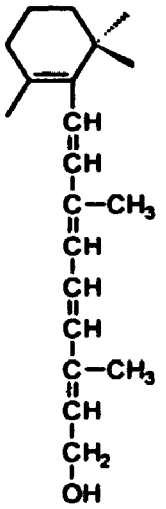

Vitamin A

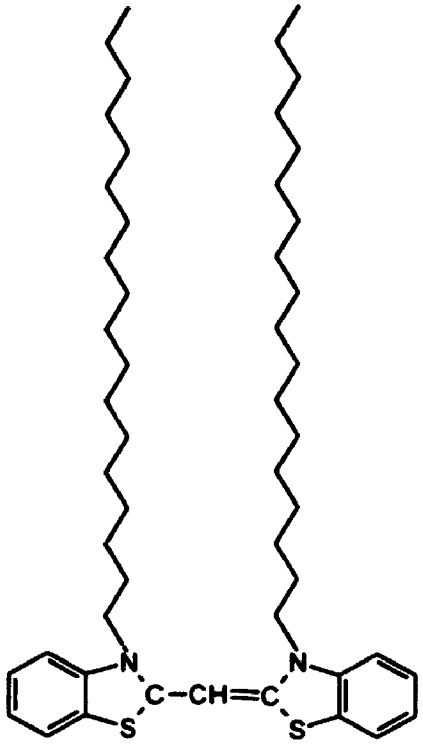

Cyanine Dye

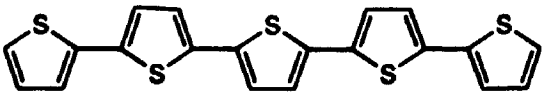

Quinquethienyl

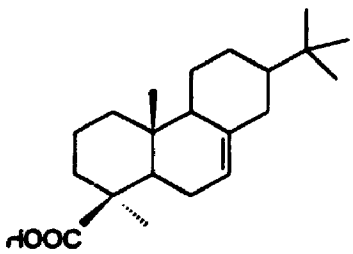

Abietic Acid

Figure 4.4 : Examples of compounds which form monolayers.

monolayer film of 5-(4-carboxyphenyl)-10, 15, 20-tritolylporphyrin at the air-water interface, with an extrapolated area of 79 ± 1 $Å^2$ per molecule at a pressure of 20 mN m^{-1}.

In 1917 Irving Langmuir and Katherine Blodgett published a technique, now known as the Langmuir-Blodgett (LB) technique, for the removal of a monolayer from the water surface to a solid substrate.[18] This removal is accomplished by first compressing the monolayer to some specified surface pressure and then dipping the solid substrate, such as microscopic slide, in and out of the water keeping the surface pressure constant. As the slide is dipped a meniscus is formed, whose direction depends on whether the substrate surface is hydrophillic or hydrophobic. The monolayer is transferred to the slide via this meniscus, as shown in Figure 4.5. Monolayers that transfer only on the downward dip are said to form *X layers*, those that only on withdrawal are called *Z layers* and those that deposit on either form are known as *Y layers*.[19]

4.3 EXPERIMENTAL DETAILS

4.3.1 Langmuir Trough

Monolayers of all the porphyrin model compounds were deposited using a Langmuir trough (Figure 4.2), fabricated from a solid block of teflon. A movable barrier was used to control the surface area taken by the monolayer. The barrier was made of a square iron rod wrapped in teflon and it rode along the top of the sides of the trough oriented perpendicular to the length of the trough. An undercarriage assembly consisting of a worm gear-driven set of forks attached to either end of the

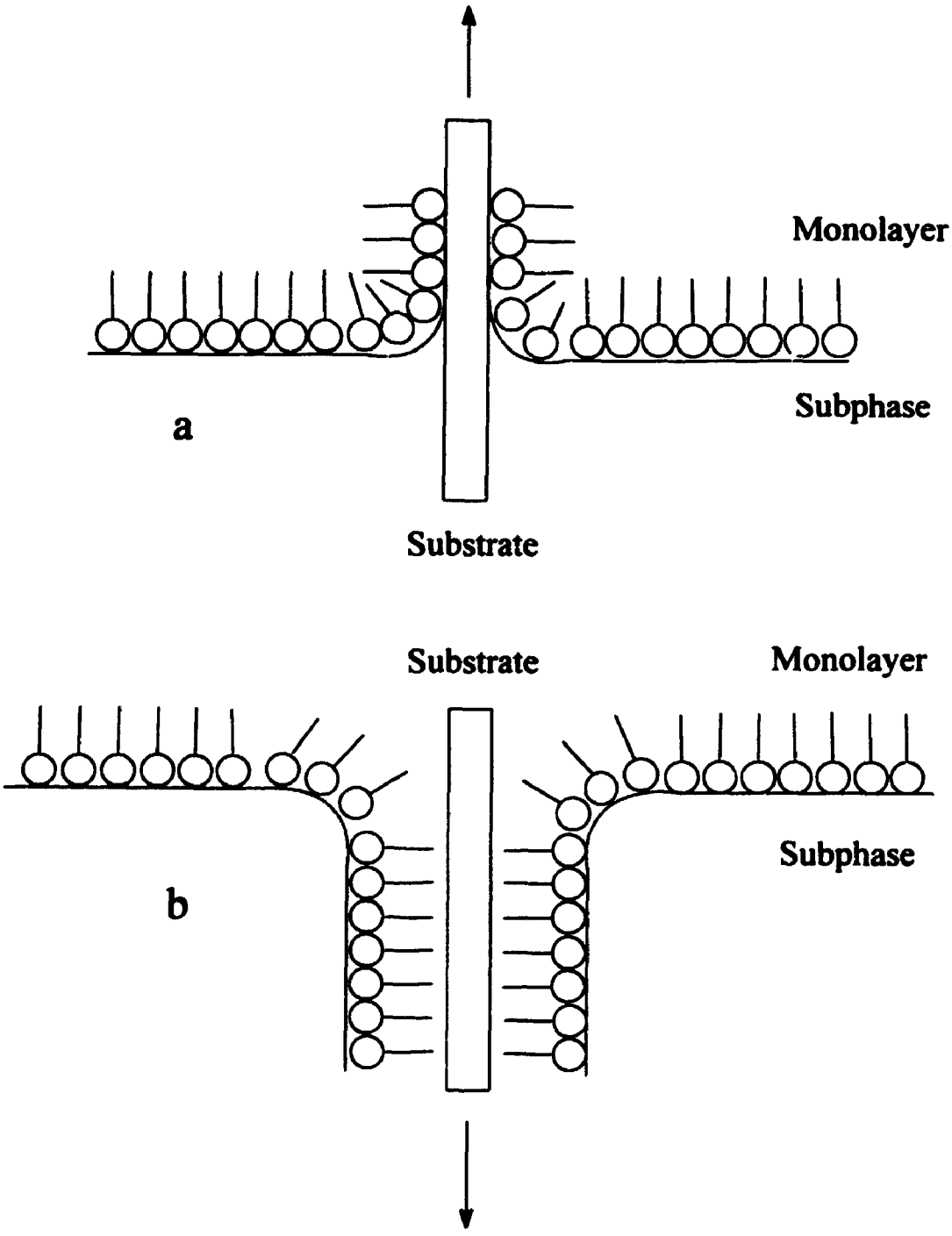

Figure 4.5 : (a) Z layer deposition on withdrawl of a hydrophillic substrate. (b) X layer deposition on insertion of a hydrophobic substrate. Circles represents the hydrophillic portion of the surfactant molecule. Sticks represents the hydrophobic portion.

movable barrier was used to control its movement. A synchronously wound chopper motor (Ithaco Model 382) was used to drive the worm gear, providing a wide range and excellent control of barrier speed. The signal output of the photo-diode mounted along the fly-wheel of the worm gear assembly was used as a reference signal and an external time base for a Nicolet digital oscilloscope (Model 206).

The surface pressure was measured by a floating teflon boat attached to a torsion balance. The movable core from a linear transducer (Hewlett Packard Model 7DCDT-050) was suspended from one arm of the torsion pendulum and extended to the transducer. Care was taken to ensure that the core did not touch the sides of the transducer. This provides a highly sensitive surface pressure-to-voltage converter. The signal was sent to the digital oscilloscope. This voltage plotted against the external time base produced a surface pressure-area isotherm of the monolayer. Finally the data were transferred from the oscilloscope to a PC using GPIB interface and were analyzed by a home made program. Programming techniques in Asyst (version 3.0) were employed for developing all the softwares (Appendix I).

The entire assembly was enclosed in a Plexiglass dust cover with lids on one side, which provide an access for the user. The drive shaft of the dipping motor (American Design Components : Globe CS A1106 reversible motor) was provided with two silk threads, which can be lowered or raised when rotated. The slides were held in place by a teflon slide holder, provided with two anchors to suspend it using the silk threads. The dipping speed could be varied from 0.5 to 9.0 cm min^{-1}. The entire assembly was suspended by screws through the top of the dust cover. All samples were dipped so that the slide was parallel to the length of the trough.

The trough was cleaned periodically by soaking in a solution of a detergent called Decon 75 (BDH Chemicals), followed by through rinsing with filtered water. It was then wiped off using absolute ethanol followed by spectral grade methanol before filling it with the subphase.

4.3.2 The Subphase

Unbuffered water was used as a subphase for all the monolayer depositions. It was purified as follows. House distilled water was passed through scale elimination, deionization and organic removal columns (D8291, D8922 SYBRON/Barnstead) to remove all the possible inorganic and organic impurities. This purified water was then further purified by distilling in a quartz bidistillation apparatus (Bi4, Englehart, Amersil Quartz Division). It was then stored in Pyrex volumetric flasks fitted with inverted ground glass stoppers. The conductivity of the water was measured to be $\sim 10^{-6}\ \Omega^{-1}\ m^{-1}$.

4.3.3 Solvents

The solvent is intended to carry and spread the film quickly. It thus should be volatile, clean, insoluble in water and capable of spreading on water. Chloroform and benzene are good spreading solvents. For the present study, chloroform was used. The samples were made concentrated so that only a few drops of solution were required. In all cases, spectral grade chloroform was used and a blank test of the solvent was made to check for impurities prior to use. A small amount of K_2CO_3 was added to the solution, prior to the deposition, to avoid the formation of the

porphyrin dication (D_{4h}), which shows a shoulder at 450 nm in the absorption spectrum.

4.3.4 The Substrate

Quartz slides (2.5 cm × 7.6 cm) obtained from Corning were used as a substrate for LB films in photophysical studies. Prior to the deposition procedure they were cleaned as follows. At first, the slides were soaked in concentrated chromic acid for three days and then washed (10 rinses) with Branstead filtered water, followed by sonication for 15 minutes in 0.01 M NaOH. This was followed by 5 rinses with filtered water, 5 rinses with triply distilled water and sonication for 15 minutes in the final rinse. The slides were then dried with prepurified nitrogen.

For photoelectrochemical, studies *n-type* Sb-doped SnO_2, in polycrystalline form deposited on a glass sheet was employed as the substrate for the LB monolayer films. It was obtained from Cherry Display Products Corporation. The glass sheets were subsequently cut into 3 cm by 5 cm slides. The sheet resistance was rated at 10 ± 0.5 Ω/sq by the supplier. An estimation by Scanning electron microscopy (SEM) revealed that the SnO_2 film has an average thickness of a 425 nm. SEM also revealed surface texture of ~100 nm^2 dimension. Plate 4.1 shows an SEM micrograph of the SnO_2 surface. The slides were cleaned by soaking in chromic acid for 48 hours, followed by copious rinsing and sonication in bidistilled water. Surface cleanliness was measured by the quality of monolayer deposition.

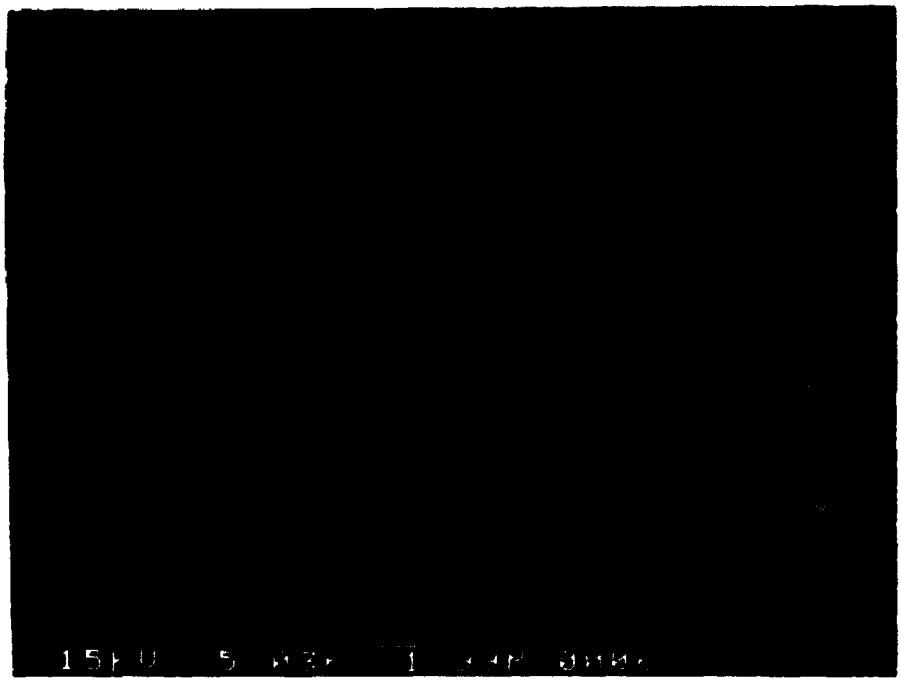

Plate 4.1 : A scanning electron micrograph of the surface of a blank SnO_2 slide.

4.3.5 Monolayer Deposition and Langmuir-Blodgett Film Production

A desired substrate (quartz slide or SnO_2 slide) was dipped into the Langmuir-Biodgett trough prior to any deposition of surfactant porphyrin solution. The solution ($\sim 2.0 \times 10^{-4}$ M) was deposited close to the movable barrier, dropwise on the subphase ($22 \pm 2°C$), using a teflon-sealed *Pressure-Lok* syringe maintaining a minimum of 3 s. between each drop. The trough was then left for 5 min. to ensure evaporation of the solvent before compression was started. Compression of the monolayer was then carried out at a rate of 5.5×10^{17} Å^2 min^{-1}. A surface pressure of 20 mN m^{-1} was chosen for depositing the monolayers. Thus the film was compressed until a surface pressure of 20 mN m^{-1} was reached, at which point the slide was slowly pulled out of the water surface at a rate of 2.0 cm min^{-1}. This was accomplished by the slide dipping assembly powered by a gear motor, which was situated above the trough. The surface pressure was maintained at 20 mN m^{-1} during the transfer of the monolayer. This was done by continual reduction of the surface area, while transferring the monolayer onto the slide. The quality of the deposition was determined by the factor called *deposition ratio*, defined as the ratio of the area covered by the monolayer on the substrate to that lost on the water surface at constant surface pressure. The slides exhibiting a deposition ratio of 1.0 (± 0.1) were the only ones accepted for photophysical studies. Deposition ratios for LB films deposited on SnO_2 slides tended to be slightly higher than unity. Ratios of 1.1 (± 0.3) were accepted for the present study.

4.3.6 Physical Description

The monolayer films of all the model porphyrin compounds were readily visible as a pale yellow-brown film on the transparent substrate, when viewed against the white background of the teflon trough. This was due to the high extinction coefficient and low molecular area of the porphyrin moiety. Specular reflectance is also readily observable when viewed under strong vertical illumination against a black background. The ease with which these films can be observed has proven extremely useful in more clearly defining their surface properties.

Viewing the monolayer by means of specular reflectance is more useful. When a drop of solvent is applied to the surface, it spreads out (the monolayer film appearing on the circumference of the drop) and so a thin band of the film is pushed to the edges of the trough. A second drop produces a second band of film, which is pushed into the first, and under some conditions, a striated film is formed. The observed striations are different shades of purple. When the film is allowed to relax, ensuring complete evaporation of the solvent, it breaks up into islands which drift apart. Upon compression, the floating islands are pushed together to give a film of visually uniform transmittance. The film has enough fluidity so that the islands merge completely. This behaviour is distinct from that observed with porphyrin esters.[16a]

The monolayer is very rigid. Collapse is observed as visible buckling in front of the movable barrier, as the collapse pressure is reached. In addition, if slides are perpendicular to the length of the trough during the dipping, collapse of the film is frequently observed in the region of the slides. This is due to the inability of the film to flow around this barrier. This was avoided by suspending the slides parallel to the

length of the trough during dipping.

4.3.7 Spectral Measurements

Absorbance spectra were measured on a Hewlett-Packard 8450 diode array spectrophotometer. A slide holder was specifically designed to hold the monolayer coated slides vertically against the detector. All the measurements were corrected for reflectance and scattering of the transmitted light by quartz and SnO_2 slides coated with LB film. This was accomplished by a Shimadzu UV-260 double beam spectrophotometer provided with an integrating sphere assembly. The references used were: an uncoated quartz and/or SnO_2 slide depending on the substrate used.

Fluorescence spectra were measured using a PTI LS-100 luminescence spectrometer and a Perkin-Elmer 650 fluorescence spectrometer with data station. Both these instruments feature signal averaging for improved signal to noise ratio on weekly fluorescent samples. The slide was attached perpendicularly to a slide holder especially designed for this purpose. The excitation spectra were recorded from 410 to 470 nm and were corrected for instrument response. Corrected emission spectra were measured over a range of 600 to 760 nm.

All spectral measurements were made on visibly dry samples within 24 hours of fabrication and samples were stored in the dark at room temperature.

4.4 RESULTS AND DISCUSSION

4.4.1 Surface Pressure-Area Isotherm

The surface pressure-area isotherms of Series-I and Series-II (Figure 1.1) of the model compounds are shown in Figures 4.6 and 4.7 respectively. An interesting trend was observed following the porphyrin with different chain systems. The observed molecular areas for monolayers of the model compounds under study, at 20 mN m^{-1} surface pressure and 22 ± 2°C subphase temperature, are tabulated in Table 4.1.

The molecular area for the compounds of Series-I (Figure 1.1), that is, P-A, P-Me-A, P-Et-A and P-Pr-A, followed a decreasing trend as the chain length was increased. During the compression of the monolayer, a smooth transition from the gaseous state to the quasi-liquid state and then to a solid state for all of these compounds was observed. This suggests that these molecules undergo a slow rearrangement to adopt the most suitable orientation of the porphyrin ring to acquire the most ordered packing in the monolayer. Again from Figure 4.6 we can see that P-Pr-A, the compound with longest chain, follows the slowest transition from the quasi-liquid state to the solid state. The smallest area per molecule for P-Pr-A in Series-I suggests the formation of the most aggregated packing of the molecules in this monolayer, and so it remains in the intermediate liquid state for a longer period. In P-A, the porphyrin ring is directly attached to the carboxylic acid group, which is bound to the surface of the subphase. This gives the porphyrin ring of P-A a very few degrees of freedom to arrange itself an efficient packing arrangement in the monolayer, and so P-A occupies the largest area (79.7 ± 0.5 $Å^2$ $molecule^{-1}$) in the

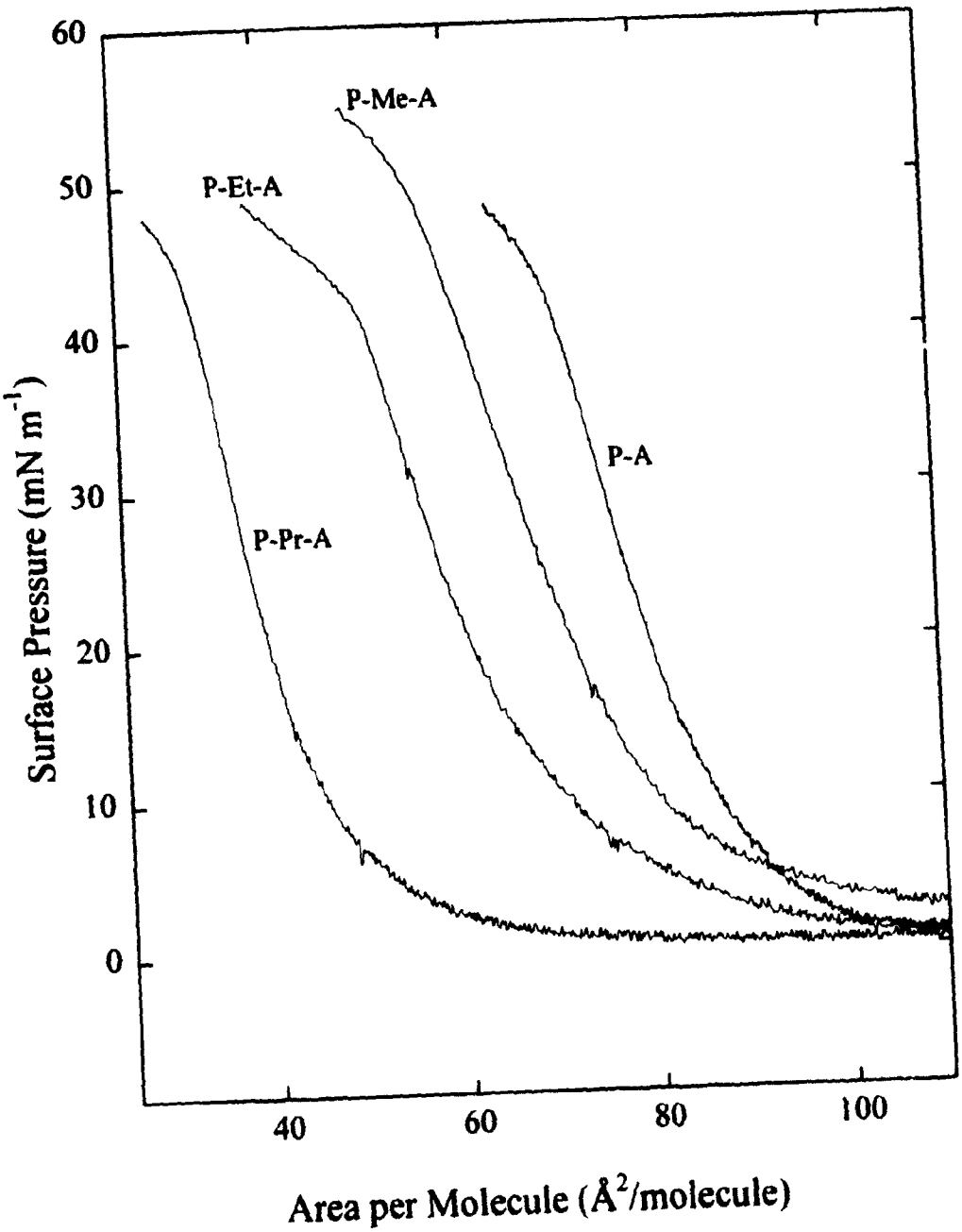

Figure 4.6 : Surface Pressure-Area Isotherm of P-A, P-Me-A, P-Et-A and P-Pr-A. Subphase, unbuffered water at 22 ± 2^{0}C.

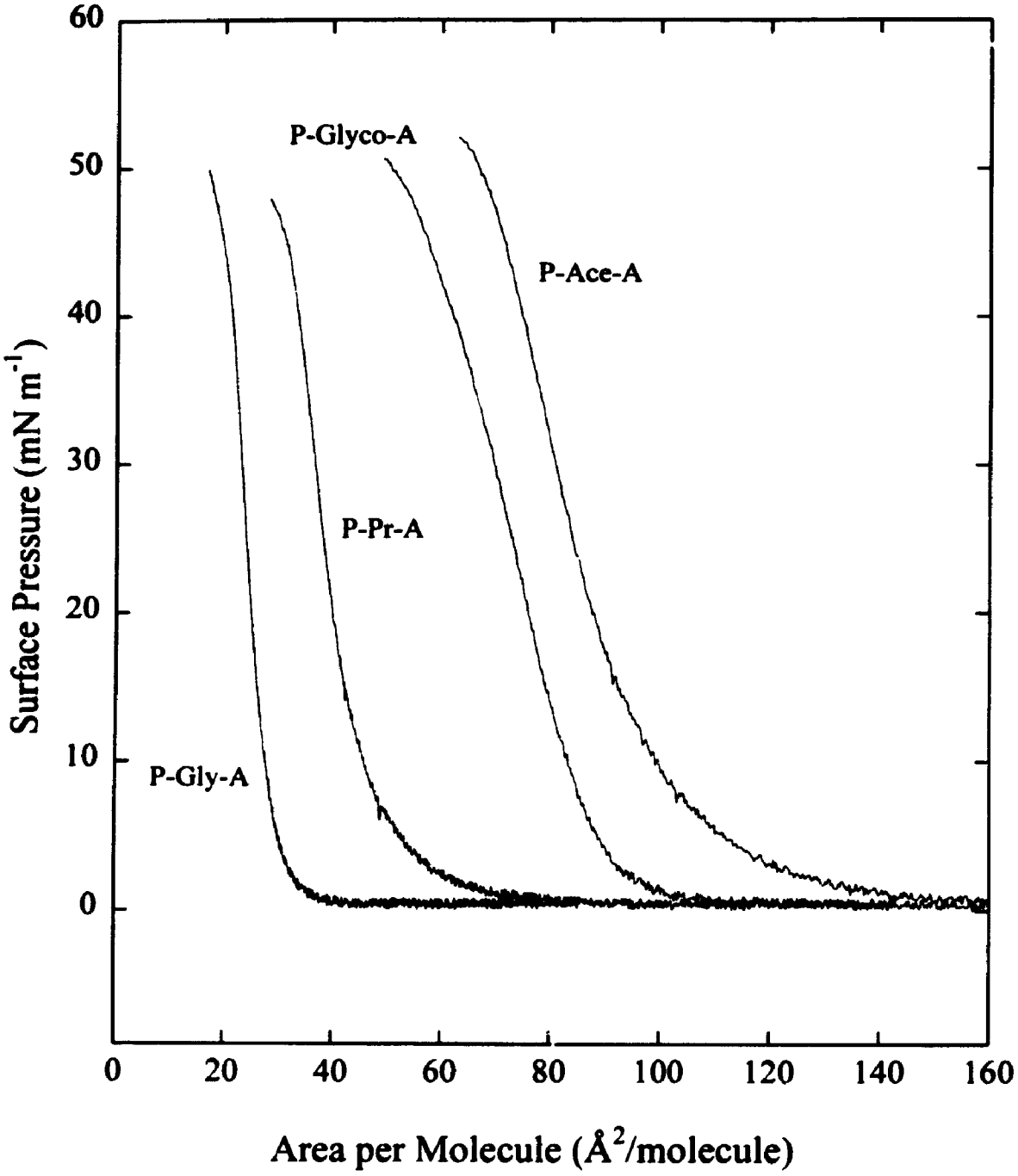

Figure 4.7 : Surface Pressure-Area Isotherm of P-Ace-A, P-Glyco-A, P-Pr-A and P-Gly-A. Subphase unbuffered water at 22 ± 2^{0}C.

Table 4.1 Surface Pressure-Area Isotherms and Absorption characteristics of Porphyrin Model Compounds.[a]

Compound	Area Molecule^{-1} (Å^2 molecule^{-1})[b]	λ_{max} (nm)[c] Quartz	λ_{max} (nm)[c] SnO_2	$\Delta\lambda_{max}$ (nm)
P-A	79.7 ± 0.5	434 ± 2	430 ± 2	4
P-Me-A	70.6 ± 0.4	436 ± 2	432 ± 2	4
P-Et-A	61.4 ± 0.4	438 ± 2	434 ± 2	4
P-Pr-A	39.3 ± 0.3	442 ± 2	436 ± 2	6
P-Gly-A	24.8 ± 0.3	446 ± 2	438 ± 2	8
P-Glyco-A	74.7 ± 0.3	434 ± 2	430 ± 2	4
P-Ace-A	87.0 ± 0.4	432 ± 2	426 ± 2	6

[a] Measurements carried out at 22 ± 2°C.

[b] Areas were measured at 20 mN m^{-1} surface pressure.

[c] λ_{max} were measured using an *integrating-sphere* assembly.

monolayer.[17] The presence of a methylene group between the porphyrin ring and the carboxylic acid group in P-Me-A allows the bulky porphyrin head to rotate itself along the axis of the side chain attached to it. This results in more flexibility of the porphyrin ring, which allows a more ordered conformation of the P-Me-A in the monolayer, and the molecular area drops to 70.6 ± 0.4 $Å^2$ $molecule^{-1}$. Similarly in P-Et-A, due to the presence of two methylene groups in the side chain, the rotational flexibility of the porphyrin head is enhanced, and they tend to arrange themselves face-to-face in close to a sandwich fashion. Hence the molecular area becomes lower than that of P-Me-A. Finally in P-Pr-A the presence of three methylene groups in the chain gives the porphyrin rings an opportunity to arrange themselves in the most ordered fashion and hence will occupy the smallest area (39.3 ± 0.3 $Å^2$ $molecule^{-1}$), in the monolayer. Therefore in the Series-I compounds, an increase in chain length allows the porphyrin rings to approach closer to each other, resulting in a better packing of the molecules in the monolayer, and so a more ordered and aggregated monolayer is formed. Hence, it was concluded that an increase in the chain length contributes to an increasing rotational flexibility of the bulky porphyrin ring and consequently a decreasing orientational hinderance among them. This results in an ordered stacking of the porphyrin heads, which allows them to occupy the lowest possible surface area.

In the previous paragraph, we have discussed that the molecular area of the surfactant molecules in the monolayers is dependent on the chain length. If this holds true for all the molecules, then the molecular areas of the Series-II (Figure 1.1) compounds, that is, P-Gly-A, P-Glyco-A, P-Ace-A and P-Pr-A are expected to be

comparable to each other. From Figure 4.7 and Table 4.1 we can see that the observed result is quite different from the predicted one. P-Pr-A and P-Ace-A have almost the same chain length, and yet their molecular areas differ by almost a factor of two. This difference may be due to the presence of a rigid -C≡C- group in the chain of P-Ace-A. The porphyrin ring attached to a $-CH_2-CH_2-$ group in P-Pr-A is much more flexible than when it is attached to -C≡C- group and so in P-Pr-A it undergoes an ordered stacking and shows a considerably lower molecular area. Again the molecular area of P-Ace-A is expected to be much lower than P-A, as there is no side chain between the porphyrin ring and the carboxylic group in P-A. Surprisingly, a completely different result was observed. This could be attributed to the fact that, during the transition from the quasi-liquid state of the monolayer to its solid state, some of the molecules are trapped in the stacks because of the π-π interaction between the porphyrin π-system and the triple bond π-system. Hence a molecular disorder in the monolayer occurs, and this results in an increase in the effective molecular area of the molecule.

P-Glyco-A also showed an unexpectedly high molecular area, compared to its analogue P-Gly-A. Both these molecules possess an sp^3-hybridized central atom in the chain. The C-N-C bond angle in the sp^3 -NH- group is larger compared to the angle between C-O-C bonds in the sp^3 -O- group. This contributes to a larger bend in the side chain of P-Glyco-A, which contributes to an inefficient aggregation of the porphyrin rings in the monolayer and hence a larger molecular area was observed. Janzen[7d] have reported a similar behaviour for stearic and eladic acids, which possess similar chain lengths. Eladic acid occupies a larger surface area in the monolayer

than stearic acid because of the presence of a double bond in its long chain, which causes a bend in the chain. Due to the absence of a uniaxial chain structure, eladic acid cannot adopt a highly ordered conformation as can stearic acid and hence occupies a large surface area in the monolayer. In a monolayer, P-Gly-A shows a molecular area of 24.8 ±0.3 $Å^2$. This is the smallest value among all the compounds studied. The very small area per molecule suggests the presence of the most aggregated packing of molecules in this monolayer. The long glycinate chain attached to the porphyrin ring in P-Gly-A makes it very flexible and allows the porphyrin rings to approach closer to each other to result in a better aggregation of the molecules.

4.4.2 Absorption Spectra of Porphyrin Monolayers

The absorption and emission properties of porphyrins have recently been reviewed.[20] All the porphyrin model compounds showed identical absorption spectra in chloroform solution. It is well known that porphyrins with a similar ring structure have practically identical spectral properties; the length of the alkyl chains or the substituents have essentially no effect on the photophysical properties.[20] The ring structure only influences the photophysics. Hence it is not surprising that the porphyrins, with different side chains studied in this work, are spectroscopically indistinguishable in dilute chloroform solution.

Figure 4.8, curve 1, shows the Soret or B band region of the absorption spectrum of P-A in chloroform solution. All the other porphyrin model compounds gave identical absorption spectra. The five major absorption bands, in order of increasing energy, are termed the Q_x (0,0), Q_x (1,0), Q_y (0,0), Q_y (1,0) and the B or

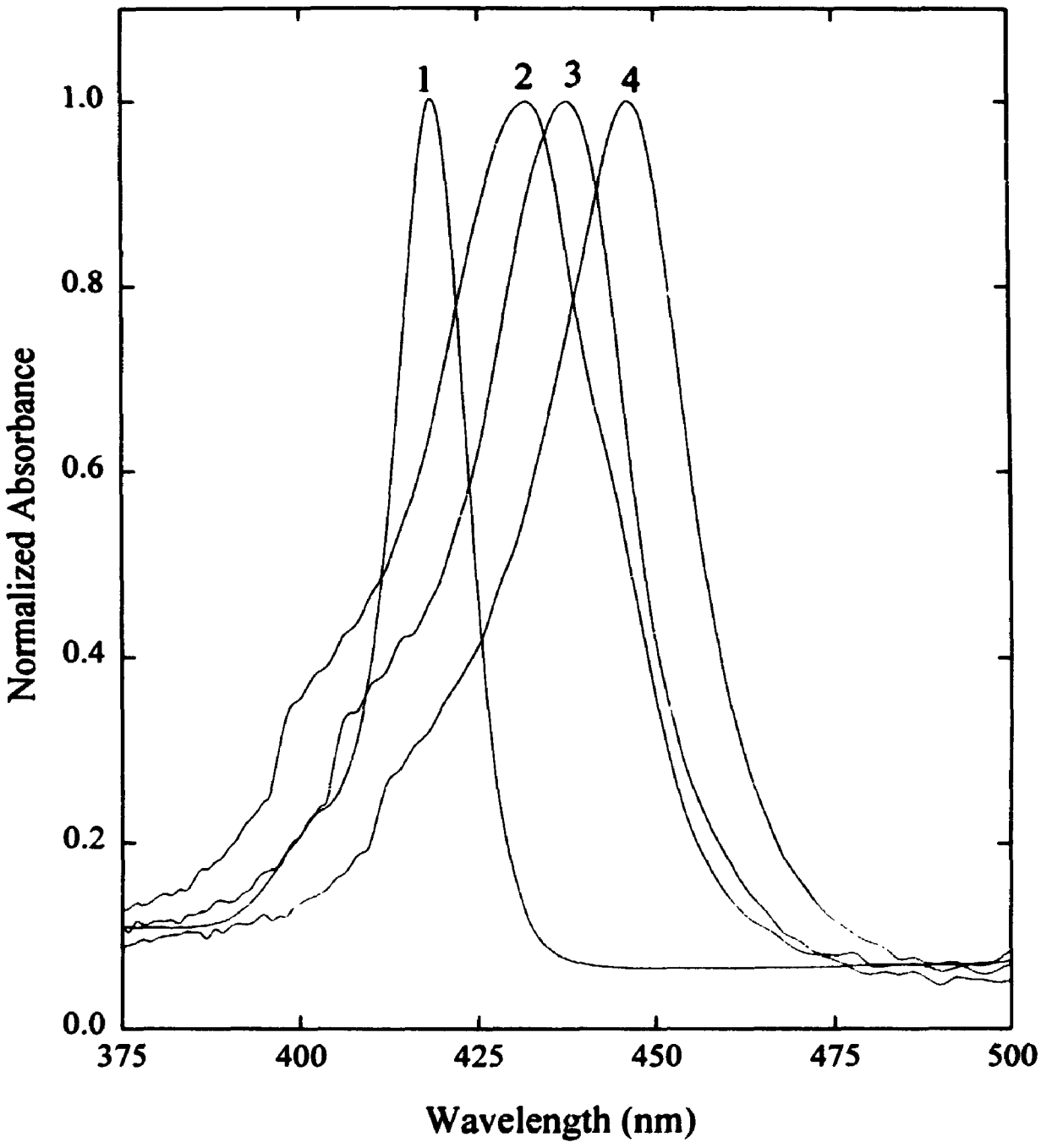

Figure 4.8 : Absorption Spectra : (1) P-A in $CHCl_3$ solution, 1cm cell. (2) P-Ace-A monolayer, (3) P-Et-A monolayer and (4) P-Gly-A monolayer. Spectra are normalized to their λ_{max}. See Table 4.1 for spectral data.

Soret bands. In porphyrin, the Q (0,0) band is the transition to the first excited state (S_1) and the Q (1,0) has one quantum vibrational energy in S_1. Due to the lack of D_{4h} symmetry and the presence of D_{2h} symmetry in free-base porphyrin, the Q-bands are each split into x and y components to give a characteristic four banded spectrum. The B band is the transition to the second singlet state (S_2).[20]

The absorption spectra of the porphyrin monolayers, which depend on the degree of order in the films, depends on the nature of the side chains attached to them. Table 4.1 summarizes the spectral data of the monolayers of all the model compounds. Curves 2, 3 and 4 in Figure 4.8 show the Soret band of the absorption spectra of the monolayer films of P-Ace-A, P-Et-A and P-Gly-A, respectively. As will become apparent from the later results, curve 4 represents a much more highly ordered film than does curve 2 or 3. Although P-Ace-A and P-Gly-A have almost identical chain length, they show a substantially different absorption behaviour because ot their difference in aggregation in the monolayer films, as evidenced from their surface pressure-area isotherms. All the absorption bands have been broadened in the monolayer state relative to the solution and the B bands are red shifted. By examining the data in Table 4.1, a direct relationship between the λ_{max} of the Soret band and the degree of aggregation of different compounds can be established. The more the porphyrin rings in the monolayer becomes ordered, it occupies a smaller surface area and shows a greater red-shift of the Soret band. Bradwell *et al.*[7a,b] and Dick *et al.*[17] have reported a similar red-shift of the B band associated with the aggregate formation. We therefore can explain that, by increasing the chain length, greater conformational mobility of the porphyrin ring is introduced, which results in

a better degree of order in monolayer and a substantial red-shift of the B band. As discussed earlier, P-Ace-A and P-Glyco-A possess a conformational rigidity in monolayer films, as reflected from their surface pressure-area isotherm data and a smaller red-shift of the B band.

The trend of the spectral properties of the model porphyrin compounds were not changed substantially by changing the substrate from quartz to a SnO_2 coated glass plate. From the data summarized in Table 4.1, it is evident that a similar trend in the red-shift of the B band was observed. Using SnO_2 as the substrate, instead of quartz, a consistent blue-shift of the B band was observed for all the model compounds, when the substrate was changed. This can be explained by the difference in surface texture of the substrates. When the smooth surface of quartz is substituted with rough SnO_2 surface, the order of the monolayers gets disturbed and the aggregation of the molecules is diluted. This results in a smaller degree of aggregation, and hence a blue-shift of the B band with respect to its position on quartz was observed. Interestingly, the maximum blue shifts were observed for P-Pr-A and P-Gly-A. This can be explained by the most organized packing nature of these compounds in the monolayer. Both P-Pr-A and P-Gly-A suffer a considerable disorder due to the surface roughness of SnO_2, resulting in a substantial blue-shift of the B band. Hence, it was concluded that, except monolayer disorder, no additional effect was experienced by the porphyrin compounds with different linkages, when deposited on SnO_2 surface.

Spectral shifts, such as those shown here, are similar to those seen in porphyrin[21-24] or phthalocyanine[25-27] dimers or oligomers and in thin films[6,11] and

monolayers.[7b,8,9a,b] In most of these cases, a blue-shift instead of a red-shift of the B band was observed compared with the monomeric species in solutions, and the shifts increase with decreasing interplaner spacing. Recently, Whitten *et al.*[28] have reported a similar blue-shift aggregate formation with a variety of squaraine[28a,b] and fatty acid derivatives of diphenylpolyenes.[28c,d] The shifts are commonly described in terms of the molecular exciton model[29] for excited-state resonance interactions in weekly coupled electronic systems. The coupling splits the absorption bands into a high energy E^+ and a low energy E^- component of which one is usually forbidden. The energy of the absorption peak in the aggregate $E^{\pm}$ is related to its energy in the monomer E^0 by

$$E^{\pm} = E^0 + D \pm V \tag{4.1}$$

where D is analogous to a solvent shift and reflects the change in environment on going from monomer to multimer. This is commonly thought to cause a red shift (i.e., D is negative), although apparently no theoretical calculation of its value has been given.[29d] V is the exciton splitting term, which for a linear, cofacial array of N units tilted at an angle of α from the array axis, is given by[29e]

$$V \approx 2\left|\left[\frac{N-1}{N}\right]\frac{M^2}{R^3}(1 - 3\cos^2\alpha)\right| \tag{4.2}$$

where M is the monomer transition dipole moment and R is the center-to-center distance between the macrocycle units. For a cofacial geometry, the lower energy exciton component E^- is symmetry forbidden[29] and all the oscillator strength is contained in the E^+ component. Thus, the increasing blue-shift of the strongly allowed (large M) B^+ band with increasing order can be explained by (1) a

decreasing interchromophore spacing R, (2) an increasing number of interacting units N and (3) a decreased tilt angle of the porphyrins in the thin film (increasing α). From Equation (4.2) it is evident that V is much more strongly dependent on R than on N or α.

As discussed in the previous section, one can expect a substantial blue shift of the B band by transforming a monomeric chromophore species to an aggregated, well ordered monomer film. The blue shift observed in various molecular thin films is in contrast to the results observed by Bradwell *et al.*[7a,b] and Dick *et al.*,[17] using tritolylporphyrin as the chromophore. Both authors observed a consistent red shift, compared to the corresponding monomeric species in the solution, with increasing aggregation of the porphyrin chromophores. Similar bathochromic shifts were reported for cerium octaethylporphyrin[30a] and vanadyl phthalocyanine[30b] aggregates. Buchler *et al.*[29e] prepared face-to-face double-decker and triple-decker cerium octaethylporphyrins and compared their Soret bands. Interestingly, it was observed that the B band shifts from 378 nm to 387 nm by adding one more porphyrin ring on double-decker, to form the triple-decker. Similarly, in the present study, by allowing the tritolylporphyrin chromophore to form an aggregate in a close to face-to-face fashion, we observed a substantial red-shift, which is directly proportional to the degree of molecular aggregation.

The difference in results observed for different chromophores may arise from differences in the nature of the film and nature of the chromophores. The system of study in all the *blue-shifted* aggregates reported earlier was different from a monomolecular layer. Normally, they varied from spin coated[10] and sublimed[10,11]

thin films to Langmuir-Blodgett multilayers.[28] In a multilayer, the surrounding environment of a chromophore is very similar to that of a single crystal and very different from that in a monolayer because of the presence of an effective inter-layer interaction. These interlayer interactions may affect the D factor in Equation 4.1, which reflects the change in environment on going from monomer to multimer. In our system, perhaps D is negative, and so a bathochromic shift is observed.[28d]

Another explanation for the red-shift can be given on the basis of theoretical calculations,[30c] cited by Law,[30b] in the case of vanadyl phthalocyanine (VOPc) aggregates. The calculations showed that a π-π^* state of VOPc exists, due to the presence of two neighbouring delocalized systems, that is, the macrocyclic phthalocyanine ring and benzene rings. This π-π^* interaction is responsible for the longer wavelength shift of the B band. The alkyl substituent effect in VOPc also contributed to a bathochromic shift.[30b] In cerium octaethylporphyrin,[30a] the presence of a cerium atom sandwiched between the porphyrin ring forms a π-π^* charge-transfer state, which results in the red shift of the B band. Similarly, in the present study , the porphyrin model compounds possess three tolyl rings attached to the porphyrin macrocyclic ring, analogous to the phenyl rings in VOPc. Therefore, there may be a π-π^* charge transfer state present in the monomolecular aggregate of our porphyrin system, which results in the bathochromic shifts. Hence, it was concluded that the chromophore which possess a π-π^* charge transfer state in the molecular aggregate should show a bathochromic shift. Chromophores without these charge transfer states will follow the molecular exciton model[29] and will show hypsochromic shifts in molecular .ggregation.

Broadening of the absorption bands in the solid state, relative to solution, is caused both by the same excitonic interactions that cause the splitting of the bands and by the inhomogeneity associated with the irregular orientation of neighbouring molecules.[31] Thus, as the degree of order increases, the peaks become narrower. In the monolayers of all compounds, the full width at half maximum (FWHM) of the Soret band is close to that observed for the face-to-face zinc porphyrin dimer described by Leighton *et al.*,[23] suggesting that its local environment is quite well-ordered.

The pattern of spectral shifts that emerges in the progression from curves 1 to 4 in Figure 4.8 and along the columns of the λ_{max} values in Table 4.1 can be summarized as follows: The B band is progressively red-shifted as the degree of order of porphyrin rings increases in the monolayer films. A consistent blue-shift is observed when the surface texture of the substrate was changed from smooth to a rough one. From this consistent pattern and from the surface pressure-area isotherm data given earlier, we conclude that these spectral shifts are an indication of the increasing degree of order along this progression.

4.4.3 Emission Spectra and Emission Quantum Yields (ϕ_f)

Figure 4.9 shows the emission spectra of the same solutions and monolayer films as those in Figure 4.8. The emission spectrum of P-A in chloroform solution (curve 1) was taken in a 1 cm cell using the same front face apparatus and conditions as for the monolayers. Table 4.2 shows the fluorescence emission characteristics for all the model compounds on different substrates. The fluorescence emission

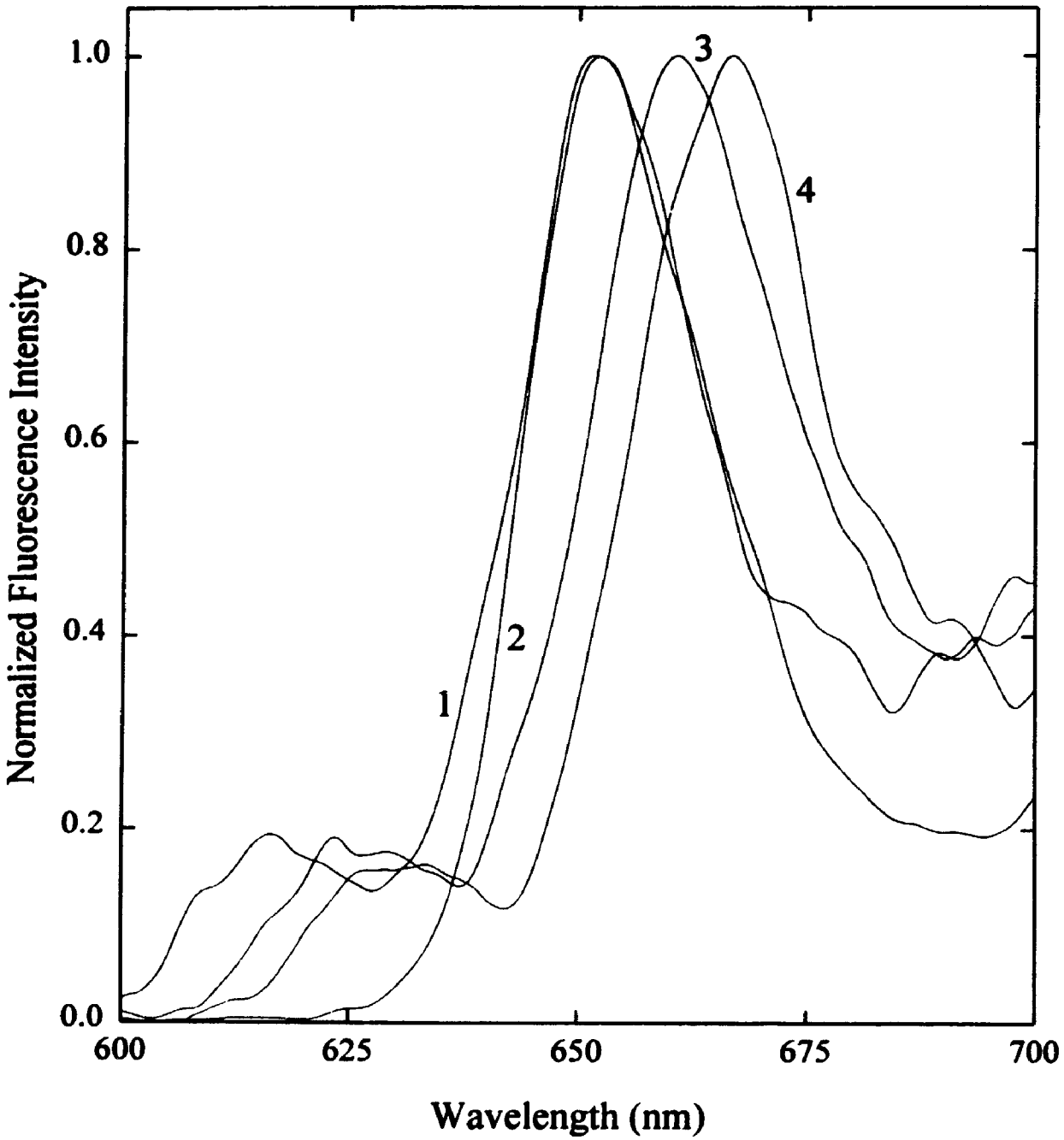

Figure 4.9 : Corrected emission spectra. Numbers correspond to the samples shown in Figure 4.8. The samples were excited at the peak of the B band. Spectra are normalized to their maximum emission intensity at λ_f.

Table 4.2 Absorption and Fluorescence Emission characteristics of Porphyrin Model Compounds on different substrates.[a]

Compound	λ_{max} (nm) Quartz	λ_f (nm) Quartz	λ_{max} (nm) SnO_2	λ_f (nm) SnO_2
P-A	434 ± 2	654 ± 1	430 ± 2	655 ± 1
P-Me-A	436 ± 2	657 ± 1	432 ± 2	658 ± 1
P-Et-A	438 ± 2	661 ± 1	434 ± 2	661 ± 1
P-Pr-A	442 ± 2	664 ± 1	436 ± 2	664 ± 1
P-Gly-A	446 ± 2	667 ± 1	438 ± 2	666 ± 1
P-Glyco-A	434 ± 2	655 ± 1	430 ± 2	654 ± 1
P-Ace-A	432 ± 2	652 ± 1	426 ± 2	651 ± 1

[a] Measurements carried out at 22 ± 2°C.

wavelengths (λ_f) also followed the trend of red shift on both the substrates, as observed for their B bands. Interestingly no blue shifts of λ_f were observed by changing the substrates from quartz to SnO_2. A measure of the relative quantum yield of emission, $\phi_{f,rel}$, of the monolayer films relative to the known quantum yield of P-A in dichloromethane solution ($\phi_f = 0.13 \pm 0.1$),[32] was then obtained by comparing the integrated emission intensities of the monolayers of all the model porphyrin compounds to that of P-A in dichloromethane solution.

The emission spectra shown in Figure 4.9 are corrected for the instrumental response and are normalized at the B band to the absorbance of the corresponding samples. Since the peak absorbances of these monolayer films (and those to be discussed below) are typically > 0.05, the ratio of the amount of light absorbed by a reference to that absorbed by a sample is given by the Beer-Lambert law expression[33]

$$N = (1 - 10^{-A_{\lambda,r}}) / (1 - 10^{-A_{\lambda,s}}) \qquad (4.3)$$

where $A_{\lambda,r}$ and $A_{\lambda,s}$ are the measured absorbances at wavelength λ of the reference and sample spectra, respectively. N is needed to compare quantitatively the emission from different monolayer films of the absorption spectrum with the corresponding emission spectrum. All samples were excited at the peak of the B band. Table 4.3 includes the relative quantum yields of fluorescence for all the monolayers on quartz and SnO_2 surfaces and the surface pressure-area isotherms. The fluorescence emission of a porphyrin dimer, solid film or monolayers, is usually assumed[21,24] to be quenched relative to that of the monomer. Although quenching is a common result of interchromophore interactions,[6,7b,9a,26] there have been several reported systems

Table 4.3 Comparison of Surface Pressure-Area Isotherm and Fluorescence Emission Quantum Yield (ϕ_f) of Porphyrin Model Compounds on different substrates.[a]

Compound	Area Molecule^{-1} (Å^2 molecule^{-1})	ϕ_f (Rel)[b] Quartz	ϕ_f (Rel)[b] SnO_2	$\Delta\ \phi_f$ (rel)
P-A	79.7 ± 0.5	0.417 ± 0.001	0.388 ± 0.001	0.029
P-Me-A	70.6 ± 0.4	0.363 ± 0.004	0.332 ± 0.006	0.031
P-Et-A	61.4 ± 0.4	0.307 ± 0.007	0.282 ± 0.006	0.025
P-Pr-A	39.3 ± 0.3	0.264 ± 0.002	0.202 ± 0.002	0.062
P-Gly-A	24.8 ± 0.3	0.238 ± 0.003	0.167 ± 0.004	0.071
P-Glyco-A	74.7 ± 0.3	0.221 ± 0.007	0.380 ± 0.004	0.159
P-Ace-A	87.0 ± 0.4	0.383 ± 0.003	0.173 ± 0.006	0.210

[a] Measurements carried out at 22 ± 2°C.

[b] All ϕ_f were calculated relative to P-A solution[31] in CH_2Cl_2.

where a dimer is either unquenched[24,28c] or actually emits more strongly[24] than the constituent monomers. In the solid state, for example, ϕ_f for naphthalene single crystals is equal to its ϕ_f in solution,[3a] while for anthracene single crystals the ϕ_f is increased relative to that in solution.[3a,34,35] Quenching seems to be the rule for any system involving a flexible linkage between the chromophores.[24] This can be understood as contributing to an increase in the number of available vibrational modes leading to an enhanced rate of internal conversion. Orientational disorder in the solid state can presumably have a similar effect.

The results in Figure 4.9 and Table 4.3 show that increasing the order of the monolayer film leads to a large decrease in the fluorescence efficiency. On the quartz surface, the least ordered P-A monolayer film fluoresces ~43% as efficiently as the most ordered P-Gly-A monolayer film and only ~8% as efficiently as the P-Ace-A monolayer film. The latter film has a quantum yield for fluorescence comparable to that of the solution species (curve 1, Figure 4.9). Both P-Ace-A and P-Glyco-A possess a comparable surface pressure-area isotherm, but a difference of almost 57% in fluorescence yield was observed between them. This may be due to the lone pair of electrons on the central oxygen atom of P-Glyco-A, which enhances the deactivation of the excited state. Because of differences in reflection effects and film thickness (~1 cm for solution, versus a few μm for the monolayer films), it is difficult to make an exact comparison of quantum yields. However, in all monolayer films of model porphyrin compounds examined, an decrease in fluorescence efficiency with increased order of the film (as seen by a red shift and broadening of the B band) has always been observed. Thus, fluorescence quenching of monolayer films,

at least in the case of tritolylporphyrins, is not a necessary consequence of, but rather is a function of the disordered environment.

Semiconductor surfaces are known to quench the fluorescence of porphyrins.[31] A quenching of 5-15% for the porphyrins on Indium Titanium Oxide (ITO) substrate has been reported.[31] SnO_2 substrates were used because of our ultimate goal to investigate the photoelectron transfer properties of these films. A strong influence of the SnO_2 surface on the fluorescence yields was observed (Table 4.3). All the monolayer films, except that of P-Glyco-A, showed a quenching in the order of 7-55% on changing the substrate from quartz to SnO_2. A steady increase in quenching was observed by increasing the degree of order of the porphyrin rings in the monolayer films. This may be the consequence of increased electron injection behaviour of the long chain porphyrins, which leads to an enhanced deactivation of the singlet (S_1) excited state. As discussed earlier, the SnO_2 surface results in more disorder of the porphyrin monolayer films due to its rough surface and so less quenching and a higher fluorescence yield is expected. Hence, it may be concluded that SnO_2 contributes to considerable quenching by the electron injection process, which overcomes the decreasing quenching effect by the film disorder. For the monolayer film of P-Glyco-A, no quenching was observed, rather an increase in fluorescence yield was recorded. This could be due to its inability to carry out an efficient electron injection and an increased fluorescence yield is contributed by the disorder of the monolayer film on SnO_2 surface. As the deactivation process on SnO_2 surface is a combined effect of both quenching and the electron injection process, we were not able to account for them separately. Thus, we conclude that the additional

fluorescence quenching on SnO_2 surface arises primarily from the electron injection process from the excited state of porphyrin to the conduction band of the SnO_2 semiconductor.

As discussed in the previous paragraph, a substantial increase in the fluorescence yield (~50%) was observed for P-Glyco-A, due to its inability to carry out an efficient electron injection to the semiconductor and increased disorder of the monolayer film on SnO_2 surface. Assuming that, electron injection is not significant for the monolayer of P-Glyco-A, we can say that all the fluorescence quenching is contributed by aggregation only. If the other model compounds also do not undergo an electron injection mediated deactivation of the excited state, then they are expected to show an increased fluorescence yield on SnO_2 surface, almost to the extent of increase that was observed for P-Glyco-A. As no such increase in the fluorescence yield is observed, we assume that the excited singlet state deactivation in these compounds arises from an electron injection process. Hence, using P-Glyco-A as a reference, in which the rate constant of electron injection ($k_{et} \approx 0$) has been assumed to be zero, k_{et} for the other model compounds was estimated.

The estimated k_{et} values for all the model compounds have been tabulated in Table 4.4. An increase in the electron injection rate was observed as one goes from P-A to P-Pr-A, which indicates that an increased alkane chain contributes to an enhanced electron transfer. An unusual result was observed for P-Et-A, as does not follow the increasing trend of the compounds with increasing alkane chain. An increasing k_{et} clearly indicates that as we increase the length of the alkane chain, the electron transfer is facilitated. This may be due to the presence of some kind of

Table 4.4 Comparison of Fluorescence Emission Quantum Yield (ϕ_f) on different substrates and estimated rate of electron injection (k_{et}) in SnO_2 for Porphyrin Model Compounds.[a]

Compound	ϕ_f (Rel)[b] / Quartz	ϕ_f (Rel)[b] / SnO_2	$k_{et} \times 10^7$ (s^{-1})
P-A	0.417 ± 0.001	0.388 ± 0.001	1.5
P-Me-A	0.363 ± 0.004	0.332 ± 0.006	2.1
P-Et-A	0.307 ± 0.007	0.282 ± 0.006	1.2
P-Pr-A	0.264 ± 0.002	0.202 ± 0.002	6.9
P-Gly-A	0.238 ± 0.003	0.167 ± 0.004	10.9
P-Glyco-A	0.221 ± 0.007	0.380 ± 0.004	0
P-Ace-A	0.383 ± 0.003	0.173 ± 0.006	20.4

[a] Measurements carried out at 22 ± 2°C.

[b] All ϕ_f were calculated relative to P-A solution[31] in CH_2Cl_2.

interaction between the orbitals of neighbouring atoms, which helps in an enhanced electron tunnelling, resulting an increased k_{et}. For P-Gly-A and P-Ace-A a very high electron transfer rate was observed. This must be due to their electron rich chains, which facilitates the electron transfer. Hence from the trend of k_{et} of all the model compounds it is obvious that through bond electron tunnelling is a leading cause of the deactivation of the excited state for the compounds with electron rich linkage systems. These concepts will be discussed more in the next chapter.

4.4.4 Excitation Spectra of the Monolayers

Figure 4.10 exhibits the excitation spectra of the same solution and monolayer films as in Figure 4.8. The emission was monitored at ~650 nm to avoid inner filter effects and the spectra were normalized at the peak of the B band. To minimize scattering and reflection, the excitation spectra were measured in an in-line geometry, in which the excitation is incident on the back sample surface at 90° and emission is monitored at 90° to the front sample surface. The excitation spectra of the P-A solution matches the corresponding absorption spectrum (Figure 4.8). This is also true, within experimental error (± 5%), for the monolayer films of all the model compounds. This shows that in the monolayer films, as in solution, the quantum yield for internal conversion from S_2 (B band) to S_1 (Q bands) is unity. However, P-Gly-A, the most highly ordered porphyrin, shows strongly quenched emission when excited near the B band. To minimize scattering, it was necessary to excite the samples near B band in our emission studies.

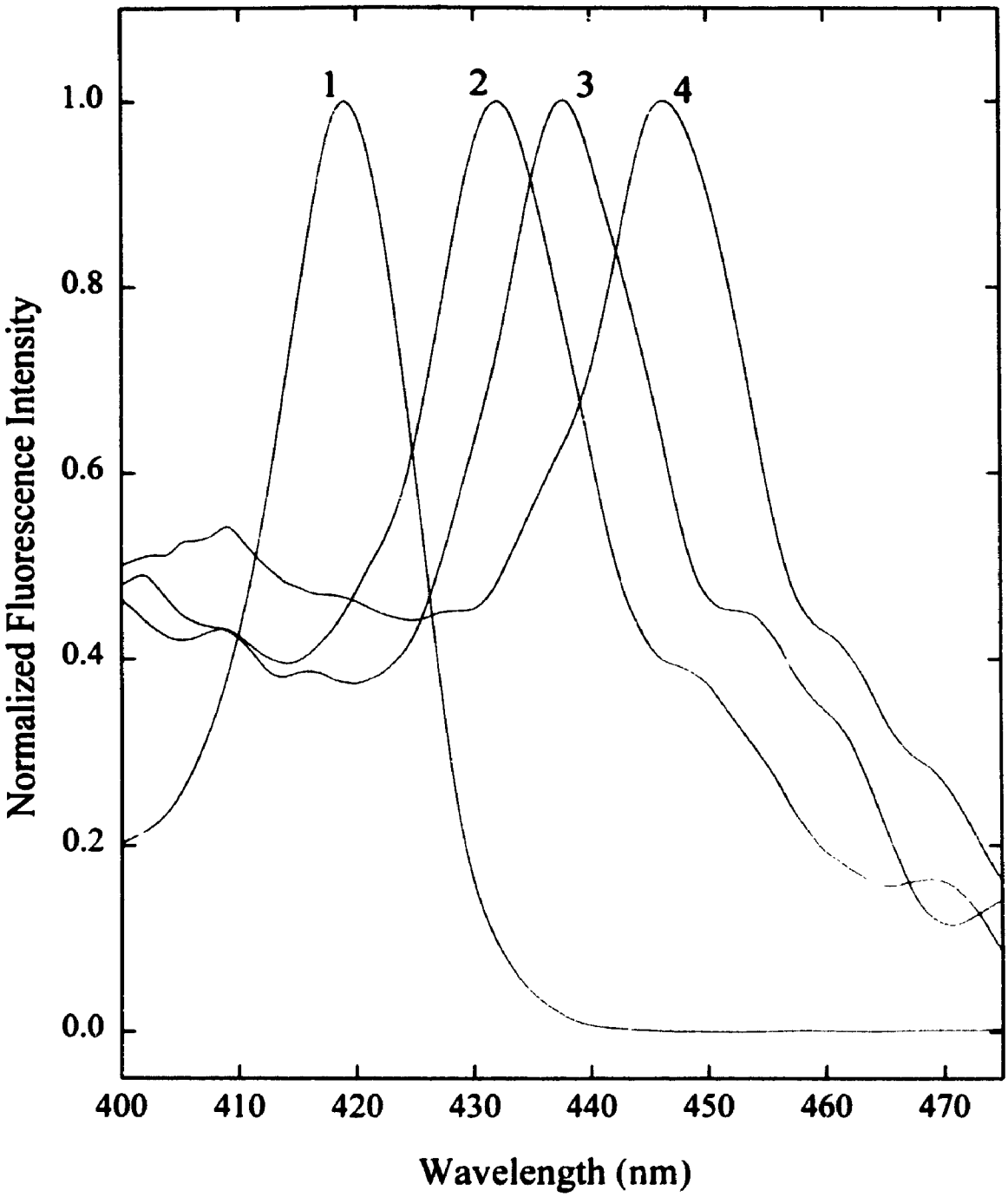

Figure 4.10 : Excitation spectra. Emission monitored at 650 (± 2) nm. Numbers correspond to the samples shown in Figure 4.8. Spectra are normalized at the B bands.

4.5 CONCLUSIONS

The presence of various linkages attached to the tritolylporphyrin ring increases the aggregation of porphyrin rings in monolayer films and the degree of order is a direct function of chain length. This leads to a low surface pressure-area isotherm for P-Gly-A in the monolayer, which possess the best packing in the monolayer. This also shows characteristic changes in the absorption spectra which, for all but the most highly ordered films, can be explained on the basis of a molecular exciton model. The fluorescence quenching, commonly seen in porphyrin monolayers relative to the monomer in solution, is shown to be a result of an increase in molecular order. In disordered films, the fluorescence quantum yield, ϕ_f, becomes comparable to the ϕ_f in solution. In the most highly ordered monolayer of P-Gly-A, the B band is broadened and substantially red-shifted. On a SnO_2 surface, the electron injection process competes with the fluorescence quenching via an internal conversion process, and both of those contribute to a low fluorescence quantum yield. Although disorder of the films on SnO_2 surface decreases the chance of fluorescence quenching by internal conversion, the stronger enhanced quenching by the electron injection process results in a very low fluorescence yield. The compounds with electron rich linkage system undergo an efficient injection process as shown by their k_{et} values. Hence, the photophysical properties of porphyrins with different side chains show that the spectral shifts seen in these monolayers are a function of the organization, not merely the proximity, of the neighbouring chromophores. The nature of the linkage is an important factor for deciding the extent of photoinjection process and hence on the fate of the excited singlet state.

REFERENCES

1. See for example: (a) Loutfy, R. O.; Sharp, J. H.; Hsiao, C. K.; Ho, R. *J. Appl. Phys.* **1981**, *52*, 5218. (b) Loutfy, R. O.; Sharp, J. H. *J. Chem. Phys.* **1979**, *71*, 1211. (c) Leempoel, P.; Fan, F. -R. F.; Bard, A. J. *J. Phys Chem.* **1983**, *87*, 2948. (d) Hackett, C. F. *J. Chem. Phys.* **1971**, *55*, 3178. (e) Meier, H.; Albrecht, W. *Ber. Bunsenges. Phys. Chem.* **1969**, *73*, 86. (f) Musser, M. E.; Dahlberg, S. C. *Thin Solid Films* **1980**, *66*, 261. (g) Lecompte, C.; Boudin, C.; Ruaudel-Teixer, A.; Barraud, A.; Momenteau, M. *Thin Solid Films* **1985**, *133*, 103.

2. Cave, R. J.; Siders, P.; Marcus, R. A. *J. Phys. Chem.* **1986**, *90*, 1436.

3. (a) Pope, M.; Swenberg, C. E. *Electronic Processes in Organic Solids*, Oxford University press: New York, 1982. (b) Simon, J.; Andre, J. -J. *Molecular Semiconductors*, Springer Verlag: Berlin, 1985. (c) Gutmann, F.; Lyons, L. E. *Organic Semiconductors, Part A*, Robert E. Krieger: Malabar, Florida, 1981. (d) Gutmann, F.; Keyser, H.; Lyons, L. E. *Organic Semiconductors, Part B*, Robert E. Krieger: Malabar, Florida, 1983.

4. (a) Piechocki, C.; Simon, J.; Skoulios, A.; Guillon, D.; Weber, P. *J. Am. Chem. Soc.* **1982**, *104*, 5245. (b) Knoesel, R.; Piechocki, C.; Simon, J. *J. Photochem.* **1985**, *29*, 445. (c) Blanzat, B.; Barthou, C.; Tercier, N.; Andre, J. -J.; Simon, J. *J. Am. Chem. Soc.* **1987**, *109*, 6193. (d) Markovitsi, D.; Tran-Thi, T. -H.; Briois, V.; Simon, J.; Ohta, K. *J. Am. Chem. Soc.* **1988**, *110*, 2001.

5. (a) Marks, T. J. *Science* **1985**, *227*, 881 and references therein. (b) Gaudiello, J. G.; Almeida, M.; Marks, T. J.; McCarthy, W. J.; Butler, J. C.; Kannewurf,

C. R. *J. Phys. Chem.* **1986**, *90*, 4917. (c) Schoch, K. F. Jr.; Kundalkar, B. R.; Marks, T. J. *J. Am. Chem. Soc.* **1979**, *101*, 7071.

6. (a) Bonham, J. S.; Gouterman, M.; Howell, D. B. *J. Lumin.* **1975**, *10*, 295. (b) Kampas, F. J.; Gouterman, M. *J. Lumin.* **1976**, *14*, 121. (c) Kampas, F. J.; Gouterman, M. *J. Lumin.* **1978**, *17*, 439.

7. (a) Bradwell, J. A.; Bolton, J. R. *Photochem. Photobiol.* **1984**, *40*, 319. (b) Bradwell, J. A.; Bolton, J. R. *Photochem. Photobiol.* **1984**, *39*, 735. (c) Janzen, F. A.; Bolton, J. R. *J. Am. Chem. Soc.* **1979**, *101*, 6342. (d) Janzen F. A. *Ph.D. Dissertation*, University of Western Ontario, London, **1978**, 200.

8. Zachariasse, K. A.; Whitten, D. G. *Chem. Phys. Lett.* **1973**, *22*, 527.

9. (a) Miller, M.; Knoll, W.; Moewald, H.; Ruaudel-Teixer, A. *Thin Solid Films* **1985**, *133*, 83. (b) Bull, R. A.; Bulkoeski, J. E. *J. Colloid and Interface Sci.* **1983** *92*, 1. (c) Jones, R.; Tredgold, R. H.; Hoorfar, A. *Thin solid Films* **1985**, *123*, 307. (d) McArdle, C. B.; Ruaudel-Teixer, A. *Thin Solid Films* **1985**, *133*, 93.

10. Kampas, F. J.; Yamashita, K.; Fajer, J. *Nature* **1980**, *284*, 40.

11. (a) Kolfta, T. J., Danziger, J.; Lee, P.; Pankow, J.; Nebesny, K. W.; Armstrong, N. R. *J. Phys. Chem.* **1987**, *91*, 5646. (b) Kolfta, T. J.; Sims, T. D.; Pankow, J. W.; danziger, J.; Nebesny, K. W.; Armstrong, N. R. *J. Phys. Chem.* **1987**, *91*, 5651.

12. Pockels, A. *Nature* **1891**, *43*, 437.

13. Langmuir, I. *J. Am. Chem. Soc.* **1917**, *39*, 1848.

14. Goddard, E. D. *Monolayers*; American chemical Society: Washington, D.C., **1975**, 139.

15. Kuhn, H. In *Techniques of Chemistry 1 Physical Methods of Chemistry Part IIIB Spectroscopy in the Infrared, Visible and Ultraviolet*, Weissberger, A.; Rossiter, B. W., Chapter VII, Part I, Interscience: New York, **1972**, 579.

16. (a) Bergeron, J. A.; Gains, G. L. Jr.; Bellamy, W. D. *J. Coll. Interfac. Sci.* **1967**, *25*, 97.; (b) Jones, R.; Tredgold, R. H. *Thin Solid Films* **1983**, *99*, 25.;

17. Dick, H. A.; Bolton, J. R.; Picard, G.; Munger, G.; Leblanc, R. M. *Langmuir* **1988**, *4*, 133.

18. Blodgett, K. B.; Langmuir, I. *Phys. Rev.* **1937**, *51*, 964.

19. Adamson, A. W. *Physical Chemistry of Surfaces*; Wiley-Interscience: New York, **1976**, 183.

20. Gouterman, M. In *The Porphyrins*; Dolphin, D., Ed.; Academic Press: New York, 1978; Vol. 3.

21. (a) Chang, C. K. *J. Hetrocyclic Chem.* **1977**, *14*, 1285. (b) Chang, C. K. *Adv. Chem. Ser.* **1979**, *173*, 162.

22. Collman, J. P.; Anson, F. C.; Barnes, C. E.; Bencosme, C. S.; Geiger, T.; Evitt, E. R.; Kreh, R. P.; Meier, K.; Pettman, R. B. *J. Am. Chem. Soc.* **1983**, *105*, 2694 and references therein.

23. (a) Leighton, P.; Cowan, J. A.; Abraham, R. J.; Sanders, J. K. M. *J. Org. Chem.* **1988**, *53*, 733. (b) Tollin, G.; Salamon, Z. *Photochem. Photobiol.* **1993**, *58*, 730.

24. Boxer, S. G. *Biochim. Biophys. Acta* **1983**, *726*, 265 and references therein.

25. (a) Ciliberto, E.; Doris, K. A.; Pietro, W. J.; Reisner, G. M.; Ellis, D. E.; Fragala, I.; Herbstein, F. H.; Ratner, M. A.; Marks, T. J. *J. Am. Chem. Soc.* **1984**, *106*, 7748. (b) Pietro, W. J.; Ellis, D. E.; Marks, T. J.; Ratner, M. A. *Mol. Cryst. Liq. Cryst.* **1984**, *105*, 273.

26. Kobayashi, N.; Lever, A. B. P. *J. Am. Chem. Soc.* **1987**, *109*, 7433.

27. (a) Fujiki, M.; Kurihara, T. *J. Phys. Chem.* **1988**, *92*, 1281. (b) Biesmans, G.; Van der Auweraer, M.; Cathry, C.; Meerschaut, D.; De Schryver, F. C.; Storck, W.; Willig, F. *J. Phys. Chem.* **1991**, *95*, 3771. (c) Kobayashi, N.; Lam, H.; Nevin, W. A.; Janda, P.; Leznoff, C. C.; Koyama, T.; Monden, A.; Shirai, H. *J. Am. Chem. Soc.* **1994**, *116*, 879. (d) Bi, Z.; Qian, Y.; Zhao, X.; Shen, S.; Yu, J.; Xu, H.; Tien, H. *Photochem. Photobiol* **1994**, *59*, 111. (e) Chau, L. K.; Osburn, E. J.; Armstrong, N. R.; O'Brien, D. F.; Parkinson, B. A. *Langmuir* **1994**, *10*, 351.

28. (a) Kim, Y. S.; Liang, K.; Law, K. Y.; Whitten, D. G. *J. Phys. Chem.* **1994**, *98*, 984. (b) Chen, H.; Herkstroeter, W. G.; Perlstein, J.; Law, K. Y.; Whitten, D. G. *J. Phys. Chem.* **1994**, *98*, 5138. (c) Spooner, S. P.; Whitten, D. G. *J. Am. Chem. Soc.* **1994**, *116*, 1240. (d) Song, X.; Geiger, C.; Furman, I.; Whitten, D. G. *J. Am. Chem. Soc.* **1994**, *116*, 4103.

29. (a) Davydov, A. S. *Theory of Molecular Excitons*, translated by Dresner, S.B.; Plenum Press: New York, 1971. (b) Kasha, M.; Rawls, H. R.; El-Bayoumi, M. A. *Pure Appl. Chem.* **1965**, *11*, 371. (c) Gouterman, M.; Holten, D.; Lieberman, E. *Chem. Phys.* **1977**, *25*, 139. (d) Yan, X.; Holten, D. *J. Phys. Chem.* **1988**, *92*, 409. (e) Kasha, M. In *Spectroscopy of The Excited State*; Di

Bartolo, B., ed.; Plenum Press: New York, 1976.

30. Buchler, J. W.; Cian, A. D.; Fischer, J.; Kihn-Botulinski, M.; Paulus, H.; Weiss, R. *J. Am. Chem. Soc.* **1986**, *108*, 3652. (b) Law, K. Y. *J. Phys. Chem.* **1988**, *92*, 4226. (c) Schaffer, A. M.; Gouterman, M.; Davidson, E. R. *Theor. Chim. Acta.* **1973**, *30*, 9.

31. See, for example, Suto, S.; Uchida, W.; Yashima, M.; Goto, T. *Phys. Rev. B.* **1987**, *35*, 4393.

32. Siemiarczuk, A.; McIntosh, A. R.; Ho, T. F.; Stillman, M. J.; Roach, K. J.; Weedon, A. C.; Bolton, J. R.; Connolly, J. S. *J. Am. Chem. Soc.* **1983**, *105*, 7224.

33. Parker, C. A. *Photoluminescence of Solutions*; Elsevier: Amsterdam, 1968.

34. Wright, G. T. *Proc. Phys. Soc., Ser. B.* **1955**, *68*, 241.

35. Jortner, J.; Bixon, M. *Mol. Cryst. Liq. Cryst.* **1969**, *9*, 213.

CHAPTER 5

THE PHOTOVOLTAIC EFFECT IN PHOTOELECTROCHEMICAL CELL OF SURFACTANT PORPHYRINS

5.1 INTRODUCTION

A number of groups have employed organic semiconductors, such as porphyrins[1] and phthalocyanines,[2] in photovoltaic cells (PVCs),[3] in photoelectrochemical cells (PECs)[4] and in electrophotographic applications.[5] The large visible extinction coefficients, low processing costs, and the possibility of continued improvement in performance through synthetic variation, make the organic semiconductors potentially useful materials for a number of photoelectronic applications. Photoelectrochemical phenomena at the semiconductor/electrolyte interface have been the subject of many investigations, since the pioneering report of Honda *et al.*[6] on the photoelectrolysis of water on TiO_2 electrodes. One of the objectives of these studies has been to find an alternative to solid-state photovoltaic devices for the conversion of solar energy to electricity. In addition, photoelectrochemical cells have the advantage of being able to be configured as photosynthetic cells to produce fuels or other valuable chemicals.

In the previous chapter, we considered the deactivation processes of energy transfer to aggregate porpnyrin species, that resulted in a partial quenching of the excited singlet state of the porphyrin embedded in the LB film. The quartz substrate was thought to play little or no role in this. By replacing the quartz substrate with

the semiconductor SnO_2, an additional fluorescence quenching was observed, which may arise from an isoenergetic electron transfer to the semiconductor. The following section studies this pathway by considering the characteristics of the photocurrent produced in cells, in which the photoactive electrode is a semiconductor, bearing a single monolayer of each of the model porphyrin compounds under study.

5.2 FUNDAMENTALS OF SEMICONDUCTORS

The alliance of solid state physics and electrochemistry has generated the interesting discipline of semiconductor electrochemistry. As a result of this alliance, a common terminology and a convention for representing the semiconductor/ electrolyte interface has arisen. The convention is largely based on the energy band diagrams of solid state physics. Due to the lack of an easy way to represent the chemistry of the surface; all events are described in terms of charges moving between the energy levels, and in fact, most features of semiconductor electrochemistry can be illustrated with this representation. The succeeding development will be qualitative, with important equations given without derivation. A number of good references[7a-f] are available for those interested in assumptions and derivations.

5.2.1 Band Structures in Solids

In the solid state, molecules or atoms exist in close proximity in a lattice structure, and so the interaction between atoms or molecules become important. This interaction causes a splitting of the original energy levels; if N valence levels were originally present, N separate levels would be formed when the lattice is

formed. N is a large number of closely spaced energy levels in the macroscopic solid. The ensemble of these energy levels is called an *energy band*. The energy spacing between adjacent energy levels is so small that energy bands are usually treated as a continuum of energy levels. The continuum has well-defined upper and lower energy limits. The lower (almost fully occupied) band is called the *valence band*, and the upper one (almost vacant) is called the *conduction band*. Any electrons in the conduction band are not bound to a particular atom or molecule, but are free to move under the influence of an electric field. The energy separation between the valence and conduction bands is called the *bandgap*. Energies are measured relative to the vacuum or free-electron level.

In conductors,[8] there is overlap between the valence and conduction bands; thus electrons are free to move throughout the crystal, and will do so in an electric field. Conductors typically have a conductivity of 10^4 to 10^6 Ω^{-1} cm^{-1}. Insulators, on the other hand, have large bandgaps; very few electrons can be thermally excited into the conduction band, and the conductivities are correspondingly low; about 10^{-22} to 10^{-10} Ω^{-1} cm^{-1}. Semiconductors represent an intermediate case; the bandgap is moderate, and at room temperature, an appreciable number of electrons can be thermally excited into the conduction band. Semiconductors generally have conductivities in the range 10^{-1} to 10^3 Ω^{-1} cm^{-1}.

Classically, any number of particles can be accommodated in a given energy level, and according to the Pauli exclusion principle, there can be at most two. Electrons are fermion and thus are governed by the distribution function

$$f(E) = \left(1 + \exp\left[\frac{(E - E_f)}{kT}\right] \right)^{-1} \qquad (5.1)$$

where, f(E) is the occupation density, E is the energy of the electron, k is the Boltzmann constant and T is the absolute temperature. The energy E_f, called the Fermi energy, is the energy at which the probability of finding an electronic orbital filled is exactly ½. The work function Φ (Figure 5.1) is defined as the energy required to remove an electron from the Fermi level to vacuum.

Semiconductors normally are of two types, *intrinsic* or *extrinsic*. In the case of intrinsic semiconductors, the Fermi level lies exactly half way between the conduction and valence bands. Extrinsic semiconductivity arises from the presence of impurities or defects in the solid, which alter the position of the Fermi level. Both cases are shown in Figure 5.1. If the impurity is an electron donor, it will produce a new level within the energy gap, situated just below the conduction band and can donate an electron into the conduction band. This results in a movement of the Fermi level toward the conduction band, and the conductivity is then due to free electrons in this band. This type of material is called an *n-type* semiconductor. If on the other hand, the impurity is an electron acceptor, it will produce a new level within the energy gap close to the valence band, which can accept an electron from the valence band, resulting in a hole in the valence band and movement of the Fermi level toward the valence band. Conduction now occurs by means of holes in the valence band, and the material is called a *p-type* semiconductor. Impurities can be introduced in the semiconductors by means of a technique called *doping*. Careful doping can generate a semiconductor with desired conductivity. In the present study, SnO_2, an *n-type*

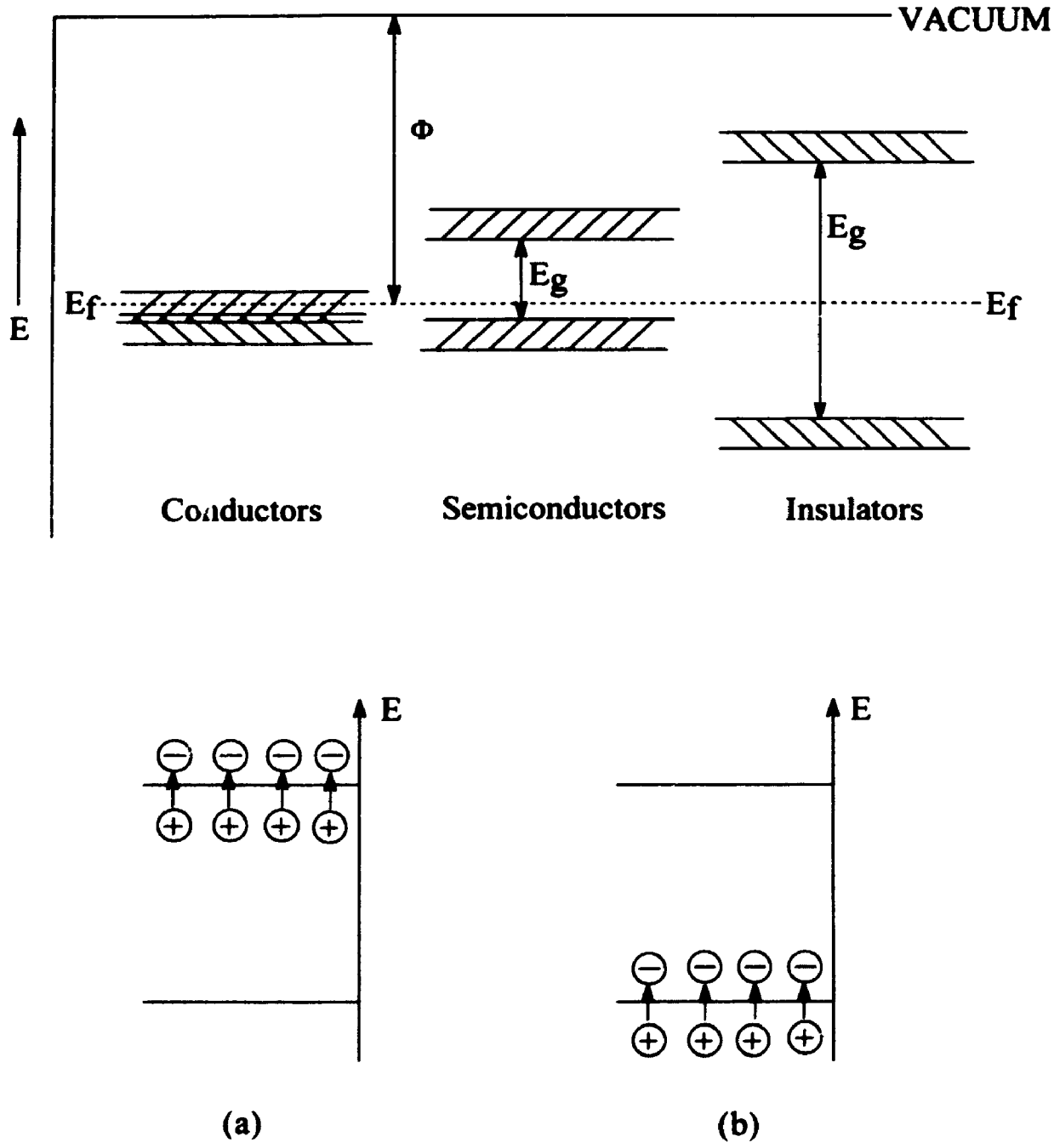

Figure 5.1 : Band structures in solids. E_f is the Fermi level, E_g is the bandgap and Φ is the metal work function. (a) an *n-type* semiconductor, (b) a *p-type* semiconductor.

semiconductor, doped with antimony (Sb), has been used. It possesses a crystal structure analogous to that of rutile, which belongs to the space group D_{4h}, with a unit cell containing two tin and four oxygen atoms.

5.2.2 Photocharacteristics of Semiconductors

The presence of an essentially filled energy band separated from a nearly empty band, leads to very interesting photosensitivity of semiconductors. A photon of light with an energy greater than the bandgap energy can excite an electron from the valence band to the conduction band. The newly created hole and excited electron eventually recombine, but they can be separated by means of electric fields or diffusion and made to perform useful chemical or electrical work. The bandgap energy controls the light absorption characteristics of the semiconductor. In terms of wavelength, light with wavelengths shorter than a threshold wavelength (λ_g) is absorbed to generate charge carriers, while light with longer wavelengths passes unimpeded through the semiconductor. The relationship between λ_g and E_g is:

$$\lambda_g = \frac{1240}{E_g} \qquad (5.2)$$

where λ_g has units of nm, and E_g units of electron-volts. In the solar energy conversion field, the optimum bandgap energy for maximum terrestrial conversion of sunlight to electricity has been estimated to be ~1.4 eV.[9] The present SnO_2 semiconductor has E_g = 3.5 eV or λ_g = 354 nm. Thus SnO_2 alone would require ultraviolet light to produce photocurrent, as it cannot access the lower energy visible light photons. In order to activate such a semiconductor by visible light, a

considerable amount of doping is required to decrease the effective E_g. Dye-sensitization of semiconductor is an interesting alternative to the doping process, which allows such semiconductors to absorb in the visible region.

5.3 SEMICONDUCTOR DYE-SENSITIZATION

Photocurrent may be produced by electron injection from a photoexcited dye located at a semiconductor-electrolyte interface. This technique, called dye sensitization, evolved from the need to produce a photo-electrode stable to oxidation by water.[10] Wide bandgap oxide semiconductor electrodes met this requirement but required ultraviolet light to produce photocurrent. Photocurrent in a conventional semiconductor electrode is produced by electron-hole pair production in or within a diffusion length of the space-charge layer. This involves bandgap excitation. The width of the bandgap for oxide semiconductors stabilizes it chemically but also precludes excitation by visible light. The semiconductor may be sensitized to visible wavelengths by location of a dye at the surface, either by adsorption (electrostatic, hydrophobic or chemical interactions) from solution, evaporation from a solvent or deposition of a thin film (i.e., a monolayer or multilayer). It is required that either the excited or ground state energy of the dye overlap with a semiconductor band. Thus, when the dye is excited by visible light, it may either donate an electron to the conduction band or a hole to the valence band. Except for transient photocurrents, a second reductant, called a *supersensitizer*, is needed to re-reduce the photooxidized dye or reoxidize the photoreduced dye.[11] This supersensitizer takes the place of the second metal contact. A supersensitizer need not always be added to the electrolyte,

since occasionally the conducting medium itself performs this function, as in the case of dye sensitized water splitting.[12] The sensitization scheme is shown in Figure 5.2.

5.4 MONOLAYER COATED CELL VERSES MULTILAYER SANDWICH CELL

The reasons for choosing a semiconductor in an electrochemical cell are pragmatic. In order to study the current due to photoelectron injection, conductive contacts must be made to the thin film spread on the monolayer. The contacts must be made such that an electric field is seen across the film resulting in unidirectional electron flow. One way to do this, would be to sandwich the film between two metal contacts, by first depositing it onto a metal surface using the LB or some other method and then evaporating a second metal layer on the top.[13] This method suffers from two disadvantages. The first is that the electric field exists solely due to the insulating ability of the film. The film must therefore be made perfect, since any holes would create short circuits in the system. Such a device has proven extremely difficult to fabricate. The film must not only be physically perfect but also be chemically pure. Impurities such as oxygen from the air have been known to act as dopants rendering measurements irreproducible. In fact, some measurements under ultra-high vacuum conditions have called into question the basic assumption that electron transfer of the type generally assumed is indeed taking place at all in these sandwich cells.[3h]

The second problem is that the metal contacts have been found to be excellent energy transfer quenchers of the dye excited state.[3h] This might be expected, since the absorption spectrum of the metal extends across the entire visible spectrum and

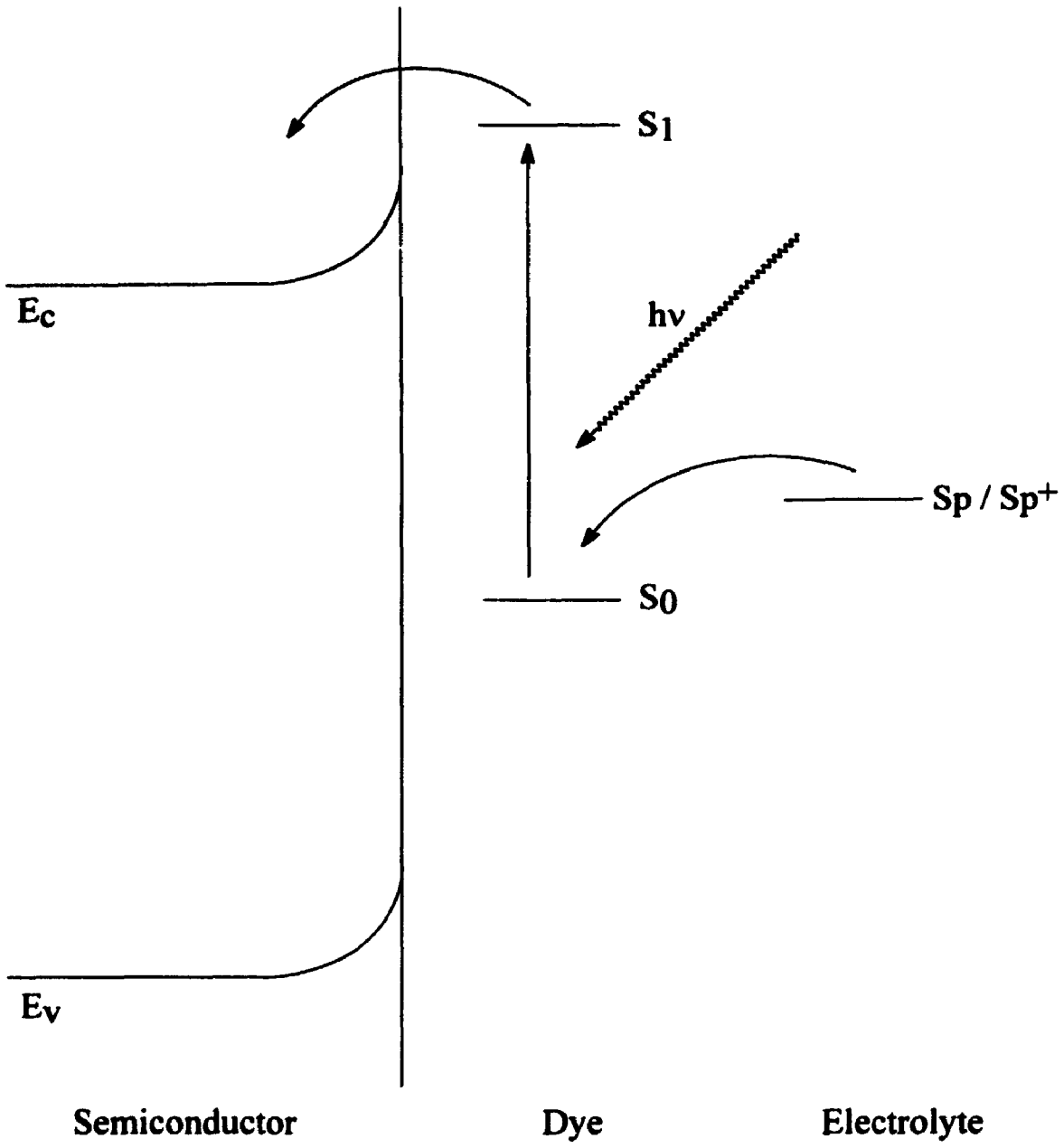

Figure 5.2 : The dye sensitization scheme. Absorption of a photon (h ν) by the dye excites an electron fron the ground state (S_0) to the first excited singlet state (S_1). This is followed by isoenergetic electron transfe. to the conduction band of the semiconductor. The oxidized dye is re-reduced by a supersensitizer (Sp) in the solution.

therefore overlaps well with the dye fluorescence profile. Studies of multilayer sandwich cells have shown that at least three to four monolayers are needed to produce an appreciable photocurrent.[14] Here the middle monolayers find themselves sufficiently separated from the metal for photo-ionization to compete with deactivation by energy transfer to the metal. The problem in this scheme is that the photoionizer is spatially separated from the metal and the electrons must tunnel through the relatively insulating ground state dye molecules before being injected into the metal. These sandwich cells therefore tend to have high resistivities that set a low ceiling on the photocurrent, sufficiently low in many cases to make detection difficult.[14]

A monolayer in the dye sensitization scheme does not suffer from the problems associated with a multilayer sandwich cell and can produce a substantial photocurrent. A single monolayer is thin enough to allow electron tunnelling. Furthermore the spacing between molecules may be large enough to allow ion penetration to the electrode. In either case the resistance of the monolayer will be low, allowing higher currents to pass. Also, in this case, an insulating layer is not required for electric field production, since the semiconductor-electrolyte junction itself produces a field. In fact, most dye sensitization work has been carried out using electrolyte soluble dyes, where those dye molecules that are within a few Å of the electrode to contribute to the photocurrent production. For an *n-type* semiconductor in depletion mode, a positive space charge is formed just below the surface, irrespective of the presence of the monolayer or adsorbed dye. This space charge produces an electric field, which can oxidize the photoexcited dye. Energy transfer

is precluded for wide bandgap semiconductors since their absorption bands are much higher in energy than the fluorescence profile of the dye. The electrolyte also provides a much better contact to the electrode. Rather than being sandwiched between two solid phases the dye covering the electrode surface is accessible and can be affected by changes in electrolyte composition that can be controlled by the experiment. The influence of impurities can be controlled more easily. Furthermore the energetics of the electron transfer process can be studied by varying the redox potential of the supersensitizer.

5.5 ELECTRON ENERGY IN THE CELL

The configuration of the cell used for the photoelectrochemical experiments in the present studies was as follows:

Metal | Semiconductor | Dye Monolayer | Aqueous Electrolyte | Metal

The energetics of this cell is the combination of the energetics of the charge carriers through all five phases and hence each of them contributes to the behaviour of the cell as a whole. As discussed earlier, the Fermi level in a metal is identical to the negative of its work function. The electrochemical potential of an electron resident in a redox couple in solution is the redox potential of the couple. In a solid, the electrochemical potential, which is equivalent to the Fermi level, is measured with respect to vacuum. On the other hand, redox potentials in solution are referenced to the standard hydrogen electrode (SHE). These two can be related by determining the Fermi level of an electron in the platinum wire of the SHE. Theoretical and experimental determinations agree quite well and place it at 4.44 eV below vacuum.[15]

To maintain a zero net current, the electrochemical potential of an electron in all phases of the electrochemical cell must be identical at equilibrium. Therefore when a number of phases of different electrochemical potential are brought into electrical contact, current flows from phases of higher electrochemical potential to phases of lower until the electrochemical potentials of all the phases attain an equilibrium. This builds up charge within certain phases. Potential applied to the leads of the cell destroys the equilibrium to which the cell responds by producing a current. A schematic diagram of the energetics of an electron throughout the entire cell is given in Figure 5.3 and may referred by the reader in the succeeding sections.

5.5.1 Electronic Energy in the Bulk Semiconductor

For semiconductors, the Fermi level (E_f) resides in the bandgap region. The position of the Fermi level determines the electronic state energetics of the bulk semiconductor. According to the Boltzmann statistics,[16] the Fermi energy E_f of an electron in the bulk of a non-degenerate semiconductor is given by

$$E_f = E_c + kT \ln\left(\frac{n_0}{N_c}\right) \tag{5.3}$$

where E_f is the Fermi energy of the electron, E_c is the energy of the conduction band edge, k is the Boltzman constant, n_0 is the density of free electrons at equilibrium in the dark in the conduction band in the bulk, and N_c is the effective density of states at the conduction band edge. Similarly the Fermi level for holes is given by

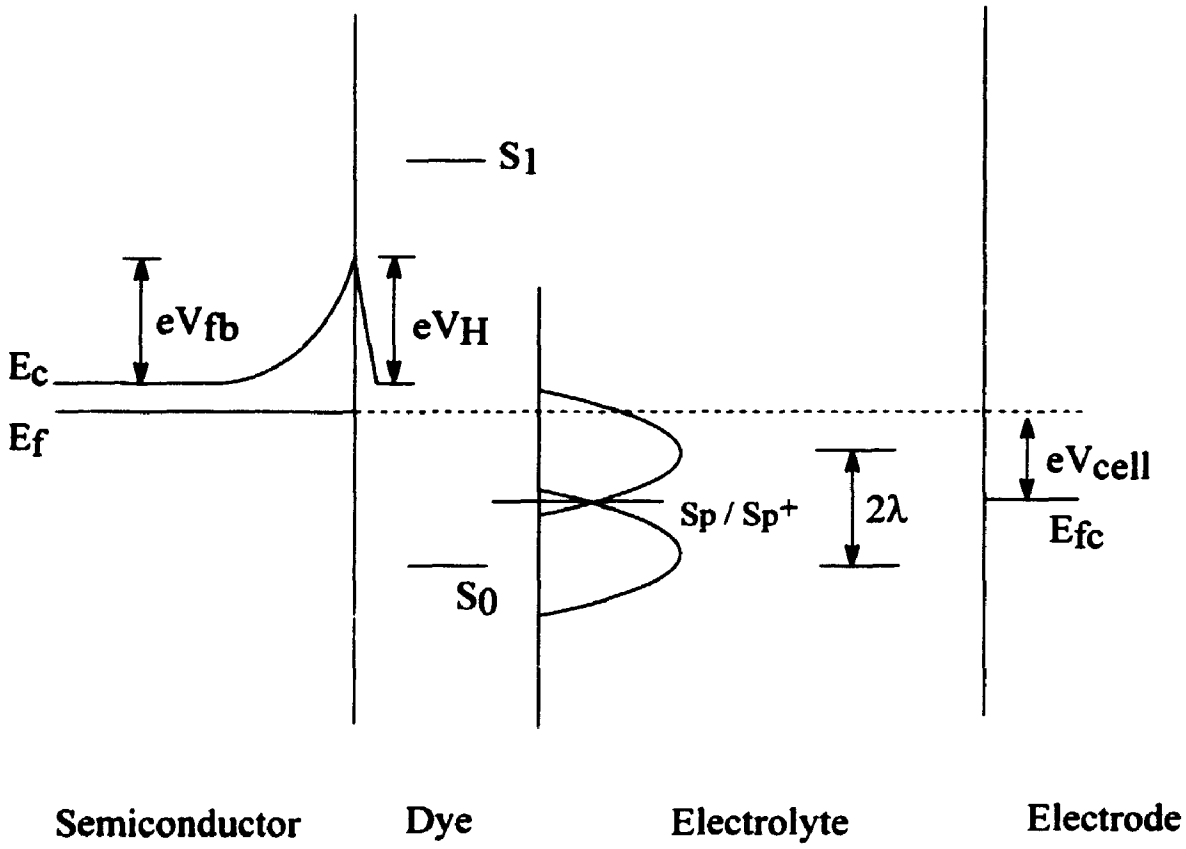

Figure 5.3 : An energy level diagram of the photoelectrochemical cell Here voltage V_{cell} is applied to the cell, E_{fc} is the energy of the Fermi level of the counter electrode, V_{fb} is the flatband potential of the semiconductor and V_H is the Helmholtz potential.

$$E_f = E_v - kT \ln\left(\frac{p_0}{N_v}\right) \qquad (5.4)$$

where E_v is the energy of the valence band edge, p_0 is the density of holes at equilibrium in the dark, in the valence band in the bulk and N_v is the effective density of states at the valence band edge.

In an intrinsic semiconductor, the Fermi level is approximately midway between E_c and E_v. For *n-type* doping, the E_f shifts towards the conduction band edge. In a highly *n-doped* degenerate semiconductor E_f may be located within the conduction band causing it to behave like a metal.

According to equation 5.3, the Fermi level depends on the electron density in the conduction band. If a source or sink for electrons, such as metal lead is attached to the semiconductor and a voltage is applied, the Fermi level will shift accordingly to maintain equilibrium.

5.5.2 Electronic Energy near the Semiconductor Surface

It is well known that at the instant at which a semiconductor electrode is dipped into an electrolyte there is an exchange of electrons between the two phases until the equilibrium conditions are reached.[7a,7c,17] Indeed, electrons are transferred by tunnelling from the phase with the smaller work function to that with the higher work function. For semiconductors, the work function of electrons is given by the Fermi level in the semiconductor. For liquid electrolytes, it is determined by the redox potential of the redox couples present in the electrolyte; these redox potentials are also identified with the Fermi level of the electrolyte. If the initial Fermi level

in an *n-type* semiconductor is above the initial Fermi level in the electrolyte, then equilibration of the two Fermi levels occurs by transfer of electrons from the semiconductor to the electrolyte. This produces a positive space-charge layer in the semiconductor (also called the depletion layer, since the region is depleted of majority charge carriers). If the semiconductor is located in a vacuum, space charge may exist because of surface states, called Tamm states, that are formed by the disruption of the repetitive lattice.[16] As a result, the conduction and valence band edges are bent such that a potential barrier is established against further electron transfer into the electrolyte (Figure 5.4).

For the doped semiconductors the width L_{SC} of the space charge region is given by[7a,18]

$$L_{SC} = \left[\frac{2\epsilon\epsilon_0 V_B}{e N_D}\right]^{1/2} \tag{5.5}$$

where ϵ_0 is the permissivity of free space, ϵ is the relative dielectric constant, e is the electronic charge, and N_D is the effective dopant concentration. The voltage V_B is the band-bending or the potential drop across the space-charge region (Figure 5.4c). The thickness of the depletion layer varies with doping; in typical cases it ranges from 100 Å to several microns. This is in contrast to metal electrodes, where the space-charge layer is infinitesimally small, and changes induced in the electrode essentially reside at the surface. The maximum electric field occurs at the surface and is equal to $2V_B / L_{SC}$. This field can be very high (10^8 V/m) and is the main driving force for separating the electrons and holes created by light absorption. If the position of the Fermi level is changed by applying an external voltage across the electrode, the value

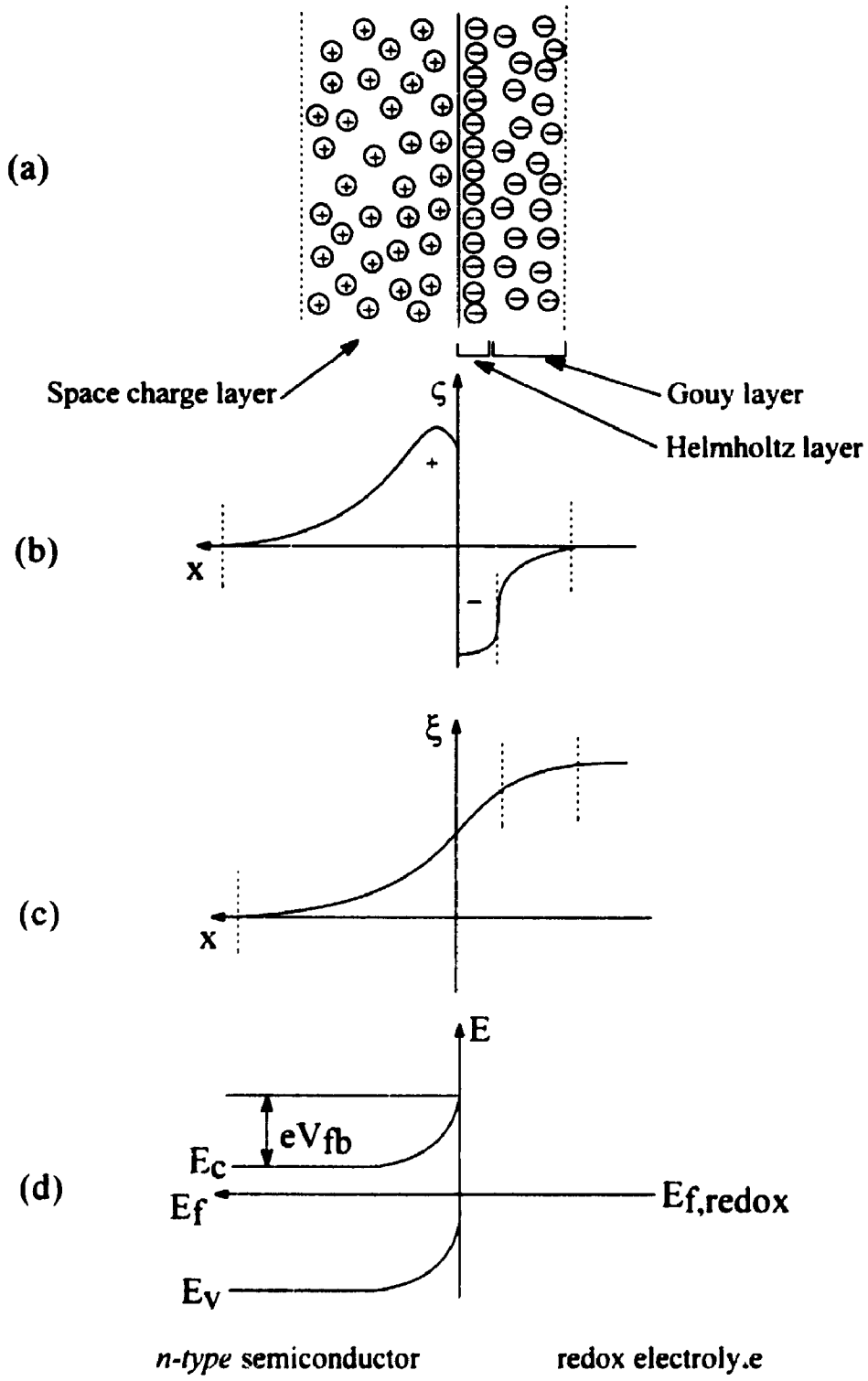

Figure 5.4 : The electrical double layer at the semiconductor-electrolyte interface. (a) The structure; (b) the distribution of charge; (c) the distribution of the potential; (d) the band bending. E_f is the fermi level energy and V_{fb} is the flatband potential of the semiconductor.

of V_B will also change. When the band bending vanishes and $V_B = 0$, the value of the semiconductor electrode potential (vs. reference electrode) is called the flat band potential, V_{fb}. Since V_B is the Galvani potential difference between the surface and bulk of the semiconductor, it cannot be measured directly. However by making certain approximations, it can be measured indirectly.

When an *n-type* semiconductor is brought into contact with a metal of work function greater than that of the semiconductor (lower Fermi energy) electrons flow from the semiconductor to the metal. This produces a positive charge at the semiconductor surface and a negative charge at the metal surface. Since the conductivity of the metal is high, the negative charge all appears at the surface, whereas the positive charge is spread throughout the space charge region of the semiconductor. There is therefore a potential rise in the interfacial region, which rises abruptly on the metal side and more gradually on the semiconductor side. This potential rise represents a barrier to electron flow as shown in Figure 5.5. When an external potential is applied across this interface, the change is seen across the semiconductor space-charge layer, since the conductivity of this phase is lower than that in the metal. The size of the semiconductor side of the barrier is therefore potential dependent but invariant on the metal side. Electrons flowing from the metal to the semiconductor always experience a considerable barrier to flow, whereas the barrier to flow from the semiconductor to the metal may be reduced by an applied potential. The contact therefore becomes rectifying allowing substantial current to pass only from the semiconductor to the metal. If the work function of the metal is less than that of the semiconductor, there is no barrier to flow and the

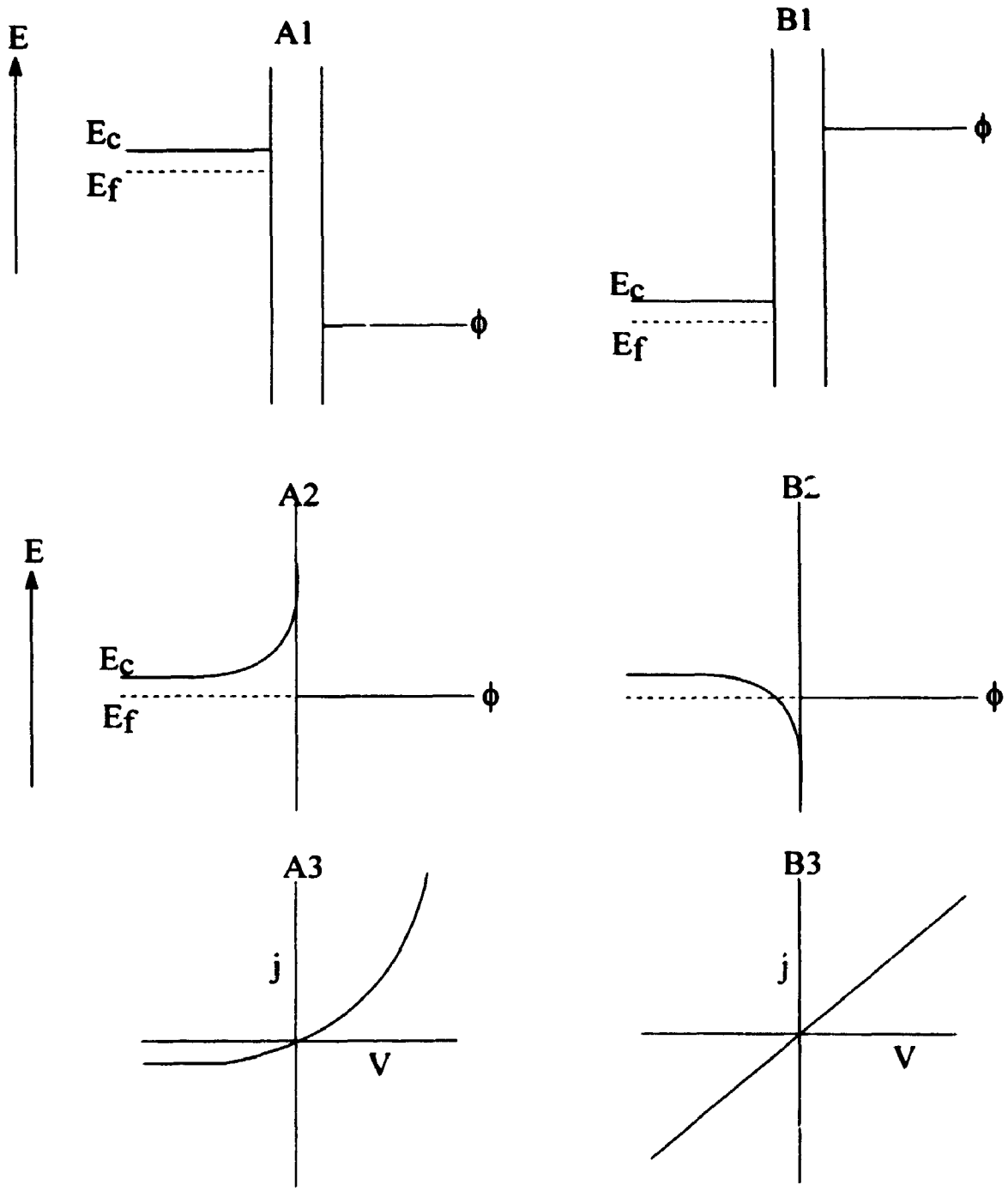

Figure 5.5 : (a) A Schottky barrier junction between a semiconductor with Fermi level E_f and a metal work function ϕ. (A1) Before contact. (A2) After contact. (A3) The current-voltage plot of a Schottky barrier. (b) An ohmic contact. (B1) Before contact. (B2) After contact. (B3) The current-voltage (j-V) plot of an ohmic contact.

contact is said to be ohmic. Figure 5.5 illustrates the current-voltage dependence for the two cases.

The semiconductor electrolyte junction behaves in a manner identical to that of the semiconductor metal junction, provided that the electrolyte is sufficiently concentrated (~0.5 M) so that its conductivity is much greater than that of the semiconductor.[7b] In this case, the work function is replaced by the redox potential of the dominant redox couple and the charge carriers in the electrolyte phase are solvated ions. Surface states may exist at either the semiconductor electrolyte or semiconductor metal junction due to Tamm states or adsorption of impurities. If the surface state density is high enough, equilibrium will be established with the surface states rather than with free carriers in the semiconductor leading to Fermi level pinning in the space charge region.[19]

The metal lead attached to the semiconductor is chosen so that an ohmic contact is formed, since the junction between the semiconductor and the electrolyte is of interest.

5.5.3 Electronic Energy in the Interfacial Double Layers

As discussed in the previous section, when a semiconductor is immersed in an electrolyte solution, a space-charge layer is formed in the interface of the semiconductor. The charged solid surface offers a preferential attractive force to the oppositely charged ions in the electrolyte.[7b] Such a space charge may form even without a surface charge, since the surface is the site of disruption of the geometry of solvation forces acting on the ions in the solution. These ions form a layer or

sheath of ions at the interface (Figure 5.4a). The ion density in the first ion layer near the solid surface is high and gradually decreases as the distance from solid surface increases in the electrolyte. This dense layer is termed the *Helmholtz layer*, while the ions in the diffuse part form the *Gouy layer*. The Helmholtz region begins at the surface and extends to the distance of closest approach of solvated ions. This distance forms a plane called the *outer Helmholtz plane*. The Gouy region begins at the outer Helmholtz plane and extends into the solution bulk. The inner layer (Helmholtz) ions are almost immobile, while in the second layer (Gouy) the ions are mobile. The thickness of the Helmholtz layer is approximately a few Angstroms, controlled by the size of ions.[7e,18a] The thickness of the Gouy layer is also of the order of 1 Å for concentrated solutions. By reasoning similar to that for the semiconductor space charge region, the space-charge potential can be shown to fall off exponentially with distance from the surface. In a sufficiently concentrated electrolyte, the space-charge region disappears, and all the charge is located at the outer Helmholtz plane. In this case, any voltage drop across the solution is located in the Helmholtz region and is linear in this region.

The electrochemical potential in Helmholtz region of a redox active electron, as given by the redox potential of the couple in which it resides, will depend on the size and sign of this space charge and will therefore not be identical with that of the bulk solution. If all the charge resides in the Helmholtz region, the redox potential will coincide with that of bulk solution, since solvated ions cannot exist within it.

5.5.4 Electronic Energy in the Dye Monolayer

The method of dye attachment onto the semiconductor determines whether or not the dye orbital responsible for the photoinjection is located inside or outside the Helmholtz region. In most cases it seems to be located outside. Electrolyte soluble dyes remain outside the Helmholtz plane. If a LB film is deposited, the results can vary depending on whether or not the molecule is oriented in such a way that the dye group is directed toward the surface.[20] If the dye group is oriented away from the surface, then the rest of the molecule may be large enough to place it outside of the Helmholtz plane. The energy of the first excited singlet state (S_1) of a photoelectron injecting dye is estimated by adding the singlet excitation energy from the energy of the ground state, as determined experimentally from its reduction potential. This potential must be sufficiently large that the energy of an electron in the excited state of the dye is greater than that of the conduction band edge, which allows isoenergetic electron transfer to occur into the conduction band.

5.5.5 Electronic Energy in the Electrolyte Bulk

The nature and distribution of electronic states associated with redox couples in solution have been extensively discussed in the literature,[7e,21] and only the most important aspects are reviewed here. In the electrolyte, the electronic energy levels are located at the donors and acceptors that are the reduced and oxidized components of the redox system. There is an important difference between energy levels of delocalized electrons in a crystalline solid and those of localized states in a polar solvent. In the first case, the energy does not depend on whether or not a level

is occupied and in the later case this makes a great deal of difference in the position of the energy level, due to the strong interaction with the solvent. The difference in energy states of the reduced and oxidized components of the redox system can be written as

$$^{0}E_{ox} - \lambda = {}^{0}E_{red} + \lambda = {}^{0}E_{f,\,redox} \qquad (5.6)$$

where $^{0}E_{ox}$ and $^{0}E_{red}$ are the most probable energies for the unoccupied and the occupied quantum states in the solution. The parameter λ represents the activation energy for the process of transforming the solvation shell structure from the equilibrium situation of one species to the most probable structure of the other. λ may vary between 0.2 and 1 eV for redox couples in solution. $^{0}E_{f,redox}$ is the Fermi level of the redox system, which is defined as the energy required to transfer an electron from a redox to the vacuum level. The energy states of reduced or oxidized species are not discrete, but are broadened into a distribution of states due to thermal fluctuations and interactions with the solvent. These distributions of states are denoted by distribution functions W_{red} and W_{ox} for the reduced and the oxidized species, respectively, and can be written as,

$$W_{red} = \exp\left[-\frac{(E - E_{red})^2}{4\lambda kT}\right] \qquad (5.7)$$

$$W_{ox} = \exp\left[-\frac{(E - E_{ox})^2}{4\lambda kT}\right] \qquad (5.8)$$

Figure 5.6 shows the distribution functions in a given medium. The corresponding density of occupied (D_{red}) and unoccupied (D_{ox}) states are given by[7e,18a]

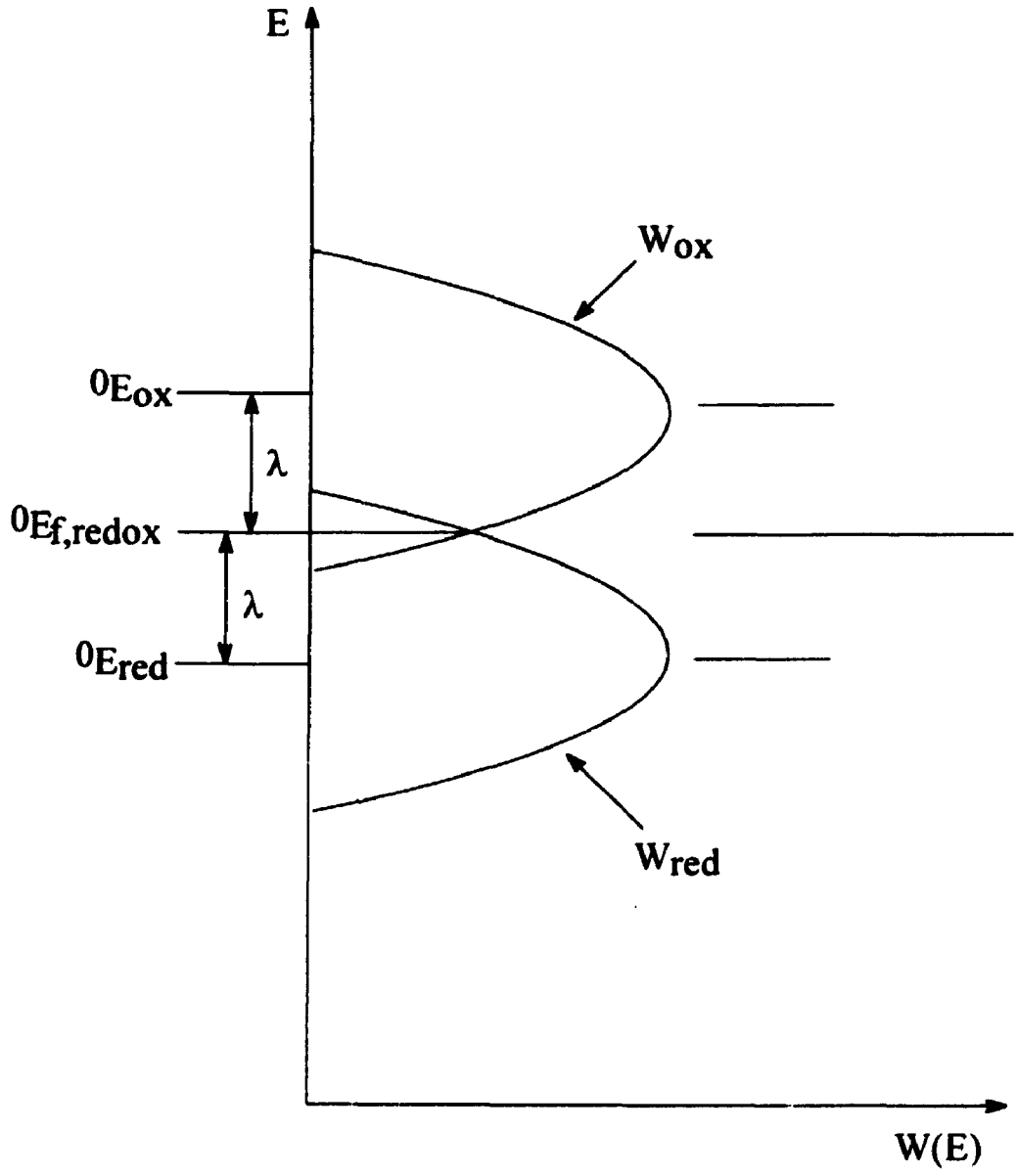

Figure 5.6 : Distribution of the energy states W(E) in a redox electrolyte.

$$D_{red} = C_{red} \; W_{red} \tag{5.9}$$

$$D_{ox} = C_{ox} \; W_{ox} \tag{5.10}$$

where C_{red} and C_{ox} are the concentrations of reduced and oxidized species, respectively. For cases where $C_{red} \neq C_{ox}$, the Fermi level of the redox system differs from the standard ($^0E_{f,redox}$) and is given by,

$$E_{f,redox} = {}^0E_{f,redox} + kT \ln \frac{C_{red}}{C_{ox}} \tag{5.11}$$

The charge transfer between, semiconductor and electrolyte continues until the Fermi level in the semiconductor equals $E_{f,redox}$, at which equilibrium is established.

5.5.6 Electronic Energy at the Metal Electrode

The solution side of the electrolyte metal junction is identical to that for the semiconductor electrolyte junction. Since the metal conductivity is high, any charge that develops in it is confined to the surface. Therefore any potential drop must be located in the Helmholtz region.

Provided that the semiconductor conductivity is low enough compared with the conductivity of the other phases and junctions, changes in the applied potential are seen entirely across its space-charge layer. The voltage changes across the two space-charge regions in the electrolyte then remain invariant with change in applied potential. This may be accomplished by using electrolyte solutions of sufficient concentration.

5.6 pH DEPENDENCE OF FLATBAND POTENTIAL

Many semiconductor surfaces contain acidic or basic groups and maintain equilibria with the electrolyte of the type shown[7e,24]

$$S + H^+ \rightleftharpoons SH^+ \tag{5.12}$$

$$SO^- + H^+ \rightleftharpoons SOH \tag{5.13}$$

where SOH, SO^-, SH^+, and S are the protonated and deprotonated surface acidic and basic groups respectively. Taking the activity of each of these to be unity, the Nernst equations for the corresponding equilibria are

$$V_i = {}^0V_i + \left(\frac{2.303RT}{F}\right)\log[H^+] \tag{5.14}$$

$$= {}^0V_i - 0.059\ pH \tag{5.15}$$

If there is no other adsorption of charged ions, the Helmholtz potential depends on these equilibria and the orientation of molecular dipoles at the surface. There will be a certain pH at which the surface charge will be cancelled by the acidic and basic groups. This point is called the point of zero charge (PZC). At this point the Helmholtz potential arises only from oriented dipoles and will exhibit a potential drop of no more than ~20 mV.

For systems bearing surface acidic and basic groups the flatband potential has been shown experimentally to follow the same pH relation as in equation 5.15[25]

$$V_{fb} = {}^0V_{fb} - 0.059\ pH \tag{5.16}$$

where V_{fb} is the flatband potential with respect to a reference electrode. Neglecting the potential due to oriented dipoles, the Helmholtz potential at a certain pH is the difference between flatband potential at that pH and at the PZC.

5.7 THEORY OF PHOTOCURRENT PRODUCTION: MECHANISM OF REGENERATIVE PHOTOELECTROCHEMICAL CELLS

In principle, there are three types of photovoltaic devices: (1) p-n- junction photocells, (2) Schottky type cells, and (3) regenerative photoelectrochemical cells, where the first two types are pure solid state devices. The basic properties are identical for solid/solid junctions and solid/liquid junctions. The following electrochemical cell is used for the present theoretical discussion, as it is analogous to the photoelectrochemical cell used in the present work.

metal | *n-type* semiconductor | redox electrolyte | metal

The system consists of an *n-type* semiconductor and an inert metal counter electrode, both being in contact with an electrolyte containing a suitable reversible redox system. At equilibrium, the electrochemical potential (Fermi level in the solid) is constant throughout the whole system. Upon light excitation the holes move toward the surface where they are consumed in the oxidation of the reduced species ("red") of the redox system, whereas the electrons move to the ohmic backside contact. Under a certain load, the electrons reach the counter electrode where they are used for the reduction of the oxidized species ("ox") of the redox system. Accordingly, we have

$$red + h^+ \rightarrow ox \quad (\text{at } \textit{n-type} \text{ electrode}) \tag{5.17a}$$

$$ox + e^- \rightarrow red \quad (\text{at counter electrode}) \tag{5.17b}$$

Where h^+ and e^- are the hole and the electron generated by the photoexcitation. Assuming that no other side reactions occur at the semiconductor electrode, this is a cell that operates under completely regenerative conditions.

Similarly, as in solid state devices, the barrier height of a semiconductor-liquid junction is usually large, and thus a redox couple of a relatively positive standard reduction potential should be selected in order to have high band bending at equilibrium. Such a system is easy to find because the energy bands at the semiconductor surface are usually fixed. The basic effects can be illustrated by a detailed energy scheme for semiconductor electrolyte interface, as shown in Figure 5.7a. In the figure, the energy states of the redox system are shown, of which the occupied states (density D_{red}) are located below the Fermi level and the empty states (density D_{ox}) above the Fermi level.

Such a semiconductor-liquid interface is similar to a semiconductor-metal Schottky junction. Differences occur only in the distribution of energy states, which is continuous in a metal, whereas it is limited to a certain energy range in a redox system. The density of occupied states in the electrolyte is given by[7e]

$$D_{red}(E) = D_0 \exp\left[-\frac{(E - E_{f,redox} - \lambda)^2}{4kT\lambda}\right] \qquad (5.18a)$$

and of the empty states

$$D_{ox}(E) = D_0 \exp - \left[-\frac{(E - E_{f,redox} + \lambda)^2}{4kT\lambda}\right] \qquad (5.18b)$$

in which D_0 is a normalizing factor and λ is the reorganization energy. The half-width of this Gaussian type of distribution curve is given by

$$\Delta E_{1/2} = 0.53\ \lambda^{1/2} \qquad (5.19)$$

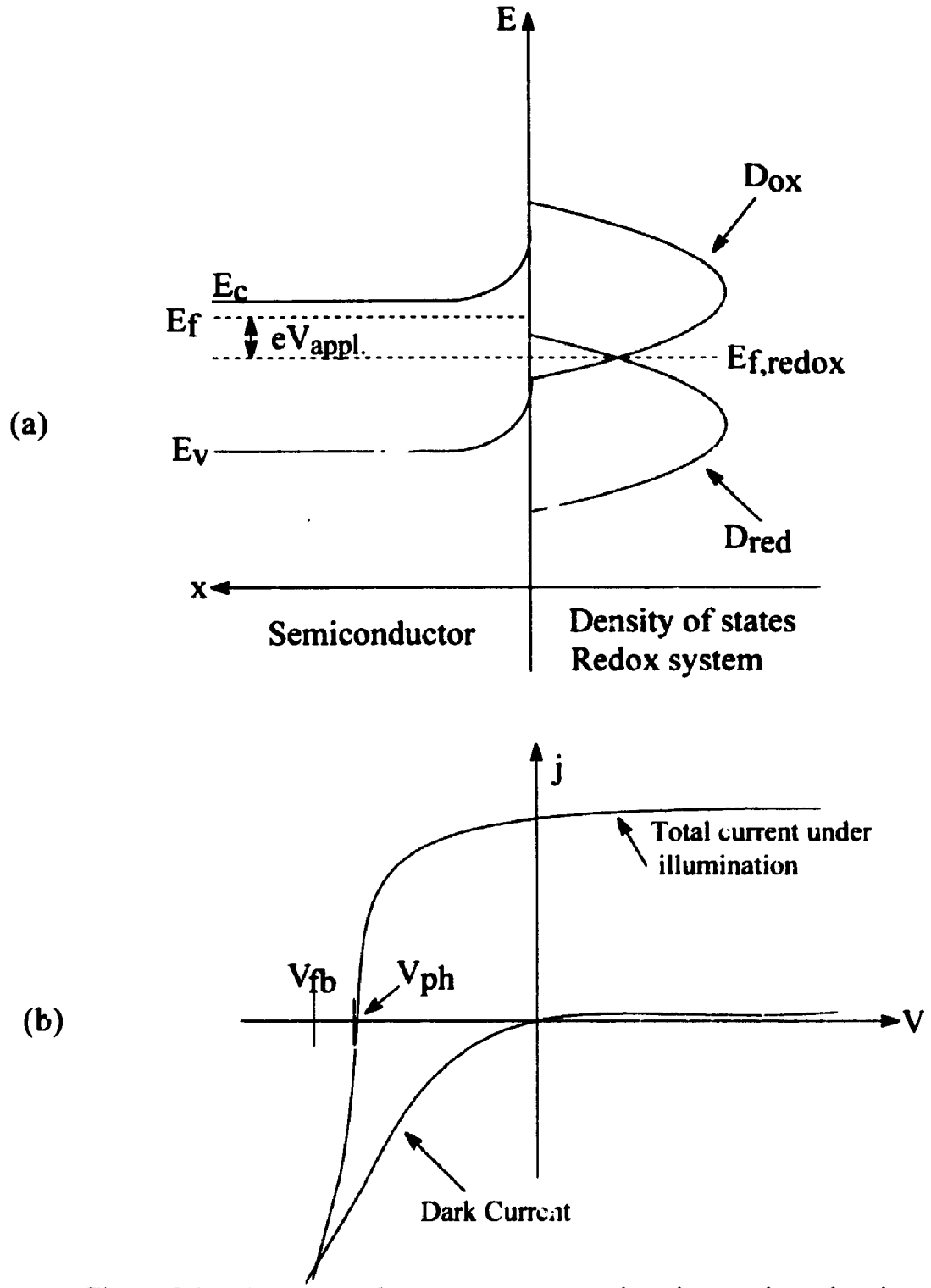

Figure 5.7 : Charge transfer processes at a semiconductor-electrolyte interface (majority carrier device). (a) Energy scheme at forward bias under illumination (b) Current-voltage (j-V) plot. V_{ph} is the photovoltage.

Since the reorganization energy λ varies in the range of 0.5 to 2 eV,[7f] the half width can be on the order of the bandgap of the semiconductor.

Depending on the overlap of the energy states on both sides of the interface, the charge transfer may occur via the conduction or the valence band. This also determines whether a cell is a majority or minority device. Assuming, for instance, that the electron transfer occurs entirely via the conduction band (majority carrier device, Figure 5.7a), the current-potential dependence can be derived as follows.

The cathodic partial current (j_c) is given by[7g]

$$j_c = e\,k_c\,c_{ox}\,n_s = k_c\,c_{ox}\,n_0 \exp\left(-\frac{e\,\phi_{sc}}{kT}\right) \tag{5.20}$$

where c_{ox} is the concentration of the oxidized species of the redox system; n_s and n_0 are the electron density at the surface and in the bulk, respectively; and ϕ_{sc} is the potential across the space-charge layer (Boltzmann equilibrium). The rate constant (k_c) is given by

$$k_c = k_{c,o}\,D_{ox}(E_c) \tag{5.21}$$

where, $k_{c,o}$ is the rate constant for the saturation current, that is, when $D_{ox}(E_c) = 1$. The anodic partial current is determined by

$$j_a = e k_a c_{red} N_c \tag{5.22}$$

which is independent of potential. In this equation, c_{red} is the concentration of the reduced species, and N_c is the density of energy states in the conduction band, whereas the rate constant k_a is given by

$$k_a = k_{a,o} D_{red}(E_v) \tag{5.23}$$

where, $k_{a,o}$ is the rate constant for the saturation current. At equilibrium, that is at

the redox potential, we have

$$j_c = j_a = j_{o,o} = e k_c c_{ox} n_0 \exp\left(-\frac{e\phi_{sc}^0}{kT}\right) \tag{5.24}$$

where $j_{o,o}$ is the partial saturation current and ϕ_{sc}^0 is the potential across the space charge layer at the saturation current. Since the total current is given by

$$j = j_a - j_c \tag{5.25}$$

the dark current can be given by

$$j = -j_{o,o}\left[\exp\left(-\frac{eV}{nkT}\right) - 1\right] \tag{5.26}$$

in which

$$V = \phi_{sc} - \phi_{sc}^0 = V_E - V_{redox} \tag{5.27}$$

On illuminating the semiconductor electrode, holes can be easily transferred to the occupied states of the redox system, leading to a constant anodic photocurrent as long as a field across the space-charge region exists. Thus, assuming that the light does not alter the dark current (the supersensitizer principle) we have,[7g]

$$j = -j_{o,o}\left[\exp\left(-\frac{eV}{kT}\right) - 1\right] + j_{ph} \tag{5.28}$$

Current-voltage curves in the dark and under illumination of such a cell are shown in Figure 5.7b. The forward dark current is mainly determined by the partial saturation current $j_{o,o}$, which depends on the rate constants involved in the surface kinetics, as given in Equation 5.24. It increases linearly with the concentration of the redox system until the current becomes determined by the transport of electrons

through the space-charge layer[7e,23] as given for a metal/semiconductor (MS) Schottky junction, that is, $j_{o,o} \rightarrow j_o$ (MS).[7g] Similarly, as in solid state devices, the photovoltage V_{ph} is then given by (j = 0)

$$V_{ph} = -\frac{kT}{e} \ln\left(\frac{j_{ph}}{j_{o,o}} + 1\right) \tag{5.29}$$

The photovoltage is mainly determined by $j_{o,o}$. As discussed above, $j_{o,o}$ can be relatively small in photoelectrochemical systems, so that the photovoltage may be greater than in pure solid-state devices. These effects have not been studied quantitatively.[27]

5.8 PHOTOCURRENT QUANTUM YIELD

The measurement of the photocurrent quantum yield (ϕ_{PC}) (see section 5.11.5) can give a quantitative idea of the photoconversion efficiencies of different photoelectrochen...al cells. The photocurrent quantum yield depends on various factors. In dye-sensitized, cells it depends on the nature of the dye, the nature of film deposition, the concentration of the supersensitizer, the pH of the electrolyte, etc. Honda *et al.*[28] have reported the direct dependence of the photocurrent quantum yield on the concentration of a supersensitizer in the electrolyte. The second important factor controlling the dye sensitization photocurrent quantum yield is the pH of the electrolyte. In general, it appears that only systems whose flatband potentials vary with the pH exhibit a pH dependence of the photocurrent. For example, CdS, in which there is no equilibrium between adsorbed and solution

protons, exhibits neither a flatband potential nor a dye sensitization photocurrent quantum yield dependence on pH. Dependent systems generally vary logarithmically with the pH with some exceptions.[29]

Watanabe *et al.*[30] have developed a theoretical expression for the pH dependence. They reasoned that the electric field at the location of the dye should depend on the Helmholtz potential drop ($\Delta\phi$). They therefore postulated an ordinary electrochemical rate equation for the photoelectron injection, i_{inj}.

$$i_{inj} \propto \exp\left(\frac{\alpha F \eta}{RT}\right) \tag{5.30}$$

where $$\eta = \text{const.} + \Delta\phi \tag{5.31}$$

and α is the transfer coefficient. Since $\Delta\phi$ is dependent on pH

$$\Delta\phi = \text{const.} - \left(\frac{2.3RT}{F}\right) \text{pH} \tag{5.32}$$

then $$\log i_{inj} = \text{const.} - \alpha\text{pH} \tag{5.33}$$

This predicts the observed exponential dependence on pH.

5.9 LITERATURE REVIEW

There have been many studies of dye-sensitized semiconductor electrodes, and there are some exhaustive reviews are available in the literature.[29a,31] Recently a review has been published[32] describing the sensitization process using various organic and inorganic dyes. For further information, the reader may refer to these reviews. A brief summary of the studies, relevant to the present work is given below.

Laser flash induced photovoltage measurements on an SnO_2 electrode, bearing Rhodamine B as a sensitizing dye and hydroquinone as the supersensitizer, have been reported by Frippiat *et al.*[33] For 10^{-2} M hydroquinone concentrations, they noticed that the photovoltage response could be divided into three parts. For sufficiently anodic prepolarizations, initially the voltage increased very fast, which apparently arose from direct electron injection in the conduction band. This was followed by a slower charging, which they attributed to capture of the electron by surface states, followed by electron tunnelling into the conduction band. At low prepolarization, this slow charging competed with discharging via back tunnelling. Dependence of this slow charging on the hydroquinone concentration indicated that the reduced surface states were competing with the hydroquinone in the reduction of the oxidized dye. Thus, two possible electron injection routes were postulated for this system, one via surface states and another via direct injection. The extent to which the slow charging contributed to the total photovoltage rise varied, depending on which spot on the surface of the electrode was illuminated, indicating that the density of surface states was not uniform across the surface. This inhomogeneity could be eliminated by prepolarization of the electrode at +200 mV. After such a prepolarization, the slow response at different illuminated spots was uniform and large. This was attributed to O_2 chemisorption under anodic bias, leading to the production of a uniformly large number of surface states.

Sequential energy and electron transfer in a bilayer system has been reported by Fromhertz and Arden.[34a] A docosylamine bilayer was deposited on Indium-Tin Oxide (ITO) by depositing two monolayers using the LB technique. Coumarin dye

was incorporated into the outer monolayer and cyanine into the inner. The overlap of the cyanine dye adsorption profile with the fluorescence profile of the coumarin could be controlled through the pH dependence of the position of the fluorescence peak of the coumarin. Therefore a device was realized whose photocurrent was dependent on pH. In order to see the dependence strictly due to the coumarin acid equilibrium, the variation in photocurrent with Helmholtz potential had to be removed. To accomplish this, the photocurrent was measured for each pH at a potential such that the conduction band bending remained constant. Under these conditions, a titration curve for the photocurrent was seen whose pK_a matched that of the coumarin dye. The same system excluding the dye showed no such behaviour. Furthermore, the action spectrum of the photocurrent matched the coumarin dye absorption spectrum.

In an earlier study, Fromhertz and Arden[34b] reported the photocurrent arising from sensitization by cyanine alone embedded in a docosylamine bilayer. Capacitance studies on the system indicated that the bilayer was neither fully insulating nor entirely porous but rather contained some holes. These holes, defined as areas of the electrode that were in direct contact with the electrolyte, were thought to exist due to surface roughness of the electrode.

Thiourea was found to be an excellent supersensitizer for the dye. By simultaneous measurement of the fluorescence, absorption and photocurrent, Fromhertz and Arden[34] were able to monitor the chemical state of the dye during operation. Since there was neither suppression of bleaching nor fluorescence of the dye by the supersensitizer during operation, they concluded that the supersensitization

effect was neither re-reduction of the oxidized dye nor reductive quenching of the excited state. They therefore concluded that the thiourea must be competing with recombination to the dye ground state $D(S_0)$ from an intermediate D^+e state composed of a reduced surface state oxidized dye pair. With these assumptions, they were able to fit the photocurrent to a Stern-Volmer type expression in the thiourea concentration.

Honda and coworkers[35] examined sensitization by organized assemblies of various metallochlorophylls (MChl) on transparent SnO_2 electrodes. The dye layers were deposited by means of the LB technique. Anodic photocurrents were obtained for several MChls, and in all cases the action spectrum generally coincided with the absorption spectrum of the MChl monolayer. The relative photocurrent quantum yield of these MChls was found to be practically zero, which may be due to the occurrence of Förster type energy transfer or aggregate formation. They also found a substantial increase in the quantum yield on high dilution of the monolayers.

Matsumura *et al.*[36] reported anodic photocurrents for ZnO and TiO_2 sensitized by xanthene and by a series of metallated porphyrin dyes in aqueous solution. The xanthene dye exhibited photocurrent quantum yields of ~28%, whereas porphyrins gave only about 0.1 to 2.3%. Fluorescence of the xanthene dyes was totally quenched, whereas the porphyrins exhibited some fluorescence. Correlation was found between the excited state redox potential of the porphyrin and the photocurrent quantum yield. By these results, the authors concluded that a higher barrier to electron injection existed for the porphyrin than for the xanthene dyes allowing deactivation by fluorescence to compete with electron injection. This also

explained the redox potential difference. If the barrier for electron injection from xanthene was sufficiently low, its excited state would overlap completely with the conduction band. The higher barrier in the porphyrin case would mean the that overlap would be partial and dependent on the redox potential of the individual porphyrin.

Minami and Ichimura[37] studied the photoelectrochemistry of metallated monomeric, dimeric and trimeric porphyrins attached together by ester linkages in dimethylformamide solutions at SnO_2 electrodes. Together with the usual hydroquinone dependence, a small variation in the photocurrent with aggregate type was seen but left unexplained. A fairly good correlation between the intersystem crossing yield and photocurrent suggested that the charge injection took place from the triplet state.

Chandrasekaran *et al.*[38] have reported the photoelectrochemistry of a cell possessing a SnO_2 electrode, sensitized by hexadecyltetraaminophenylporphyrin monolayer and multilayers. They observed no photocurrent without the presence of a supersensitizer. This result, as well as flash photolysis results, indicated the presence of a long lived transients for both glass and SnO_2. The following mechanism for the current production was suggested:

$$D + h\nu \rightarrow D^* \qquad (5.34)$$

$$D^* + R \rightarrow D^- + R^+ \qquad (5.35)$$

$$D^- \rightarrow D + e_{cb}^- \qquad (5.36)$$

where D is the dye and R the supersensitizer. In contrast to the usual conclusions regarding this type of system, direct de-excitation of the excited state by the substrate

was thought to be less important than photoreduction of the dye by a supersensitizer.

Breddells and Blasse[39] studied a series of metallated porphyrins deposited onto SnO_2 by solution evaporation. They reported that the anodic photocurrent was dependent on the film thickness, rising to a maximum at a thickness of 50 Å and then remained constant. The photocurrent increased with increasing hydroquinone concentration up to 10^{-2} M. No correlation was found between the photocurrent quantum yield and the redox potentials of the different metallated porphyrins. They rationalized this by the observation that ionization potentials of the solid dyes are relatively insensitive to the type of metal atom present. A better correlation was found between the differing competitive luminescence rates for each porphyrin and the quantum yield for charge injection.

Biesmans *et al.*[40] have examined a photoelectrochemical cell containing xanthene dyes incorporated into LB films deposited onto SnO_2 electrodes. They obtained anodic photocurrents on excitation of the dye. They also observed that the photocurrent quantum yield strongly depends on the applied electrode potential, the regenerator or supersensitizer concentration and the pH of the electrolyte. Interestingly, they found that the photocurrent is nearly independent of the chemical structure of the dye or the amount of dye incorporated into the monolayer. An anodic shift of the flat-band potential on decreasing the electrolyte pH was also reported.

Recently Kay and Grätzel[41] studied the photosensitization of TiO_2 photovoltaic cells by chlorophyll derivatives and related natural porphyrins. On comparison of different chlorophyll derivatives, they reported that free carboxyl

groups are important for adsorption and sensitization on the TiO_2. Conjugation of the carboxyl groups with the π electron system of the chromophore was found not to be necessary for an efficient electron transfer. By using cholanic acid as a coadsorbate for diluting the chromophores on the TiO_2 surface, a substantial improvement of the photocurrent was also recorded.

Very recently, Armstrong and Parkinson[42] deposited highly ordered layers of various phthalocyanines onto SnS_2. A high photocurrent quantum yield was obtained for a monolayer of the sensitizer, but for thicker layers, the yield was found to decrease. Similar results were also observed by Spitler and Parkinson.[43]

An interesting result has been published very recently by Haran *et al.*[44] They studied organized monolayers of octadecyltrichlorosilane (OTS) adsorbed on silicon wafers. Their results show that when the chains in the monolayer are in the *well packed* configuration, the charge transfer efficiency is higher than when the chains have a *gauche* configuration. They have suggested that the increased charge transfer is mediated by electronic coupling through the bonding and antibonding orbitals of the "inert" space layer of the alkyl chain. A similar effect was found by other authors.[45]

5.10 EXPERIMENTAL DETAILS

5.10.1 Monolayer Deposition on SnO_2 Electrodes

The detailed description of the Langmuir-Blodgett monolayer production and its transfer onto SnO_2 semiconductor electrodes has been given in Chapter 4. The physical characteristics of the monolayer is also described there.

5.10.2 Electrical Contacts

In order to make an electrical contact with semiconductor slide, a thin copper wire was glued to the uncovered portion of the SnO_2 slide, using silver paste. A current-voltage plot was taken for the semiconductor slide with two such leads attached, to ensure the establishment of an ohmic contact between the copper wire and the semiconductor slide. A linear plot, as expected, was observed within the current ranges employed in the photoelectrochemical experiments, verifying the ohmic contact.

5.10.3 Chemicals

The surfactant porphyrin compounds used for photoelectrochemical studies were synthesized according to the procedures discussed in Chapter 2. Dioleoylphosphatidylcholine (DOPC), a non fluorophore, surface active lipid was used to dilute the molecular chromophores in the monolayer, The DOPC (Sigma) was weighed on a micro-balance before dissolving it in chloroform. It was then mixed with the porphyrin solutions in the desired proportion using *Pressure Lok Syringes* (Precision Sampling Corporation). BDH spectral grade chloroform was used as the solvent throughout.

5.10.4 The Electrochemical Cell

The electrochemical cell (Figure 5.8) used for all the photoelectrochemical studies consisted of a solid block of Plexiglas into which a 3.5 cm × 1.7 cm hole was drilled horizontally. The hole was sealed by sandwiching a rubber O-ring between

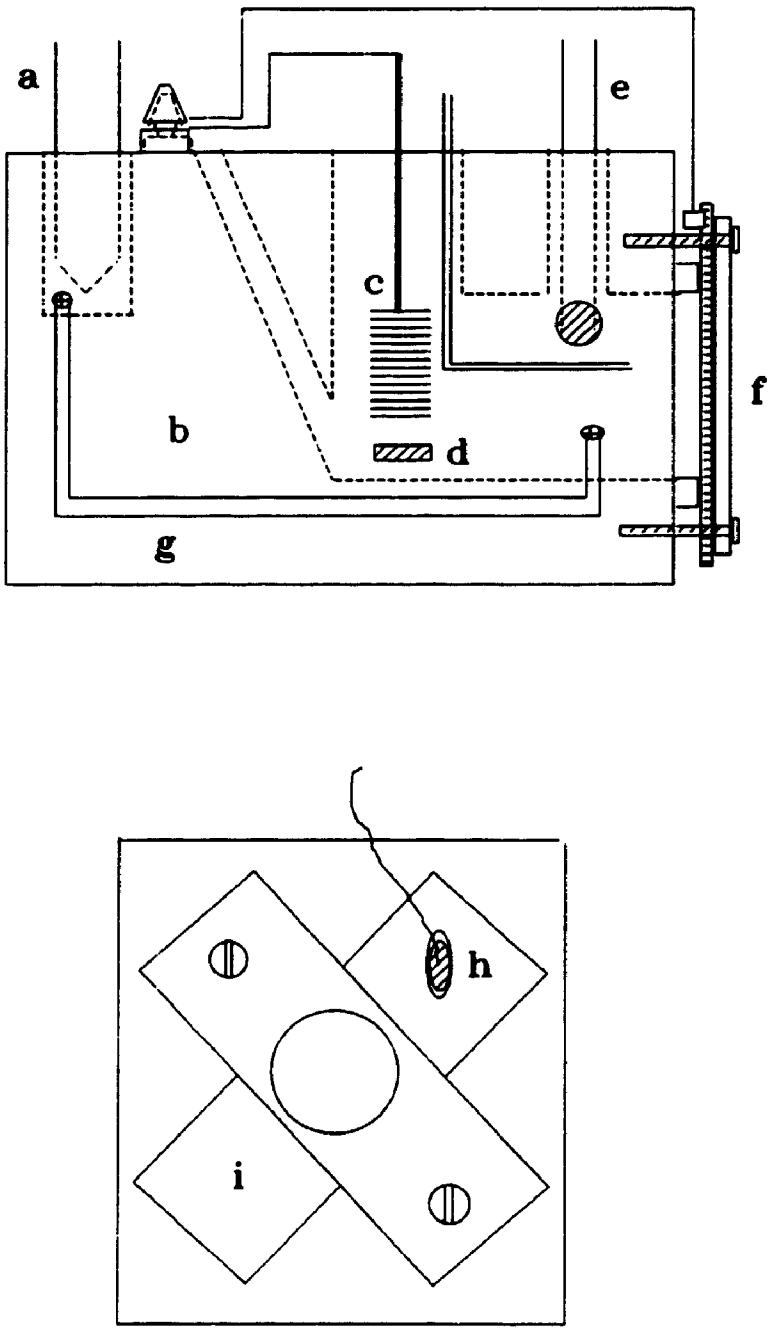

Figure 5.8 : The photoelectrochemical cell (a) Ag/AgCl reference electrode, (b) Plexiglas cell body, (c) platinum grid counter electrode, (d) teflon stir bar, (e) pH electrode, (f) Plexiglas slide holder, (g) Luggin capillary, (h) silver paste, (i) semiconductor slide.

the block and the monolayer bearing side. Other holes were drilled through the block into the compartment to provide access for the counter electrode, a pH electrode and a Luggin capillary which led to a Ag/AgCl reference electrode. The photoactive area of the slide was 2.27 cm^2.

The cell was usually used in the three-electrode configuration (Figure 5.9), in which a platinum grid counter electrode was employed. A Luggin capillary, whose end was placed close to the monolayer coated SnO_2 electrode, provided electrical contact to the Ag/AgCl reference electrode. The current was measured under potentiostatic control, using a shop built potentiostat. The electrical circuit used in applying voltage across the cell and measuring its current is shown in Figure 5.9. Cell voltage was applied by EG&G PARC Universal Programmer (Model 175). The current-voltage plots were scanned at a rate of 1.25 mV/s. The monitoring resistor voltage was recorded by a Nicolet Digital Oscilloscope (Model 206) and then was analyzed by a personal computer. Point-by-point substraction of the monitoring resistor voltage for current-voltage plot was carried out using a home-made program on the computer. Programming techniques in Asyst (version 3.0) was used to analyze the current-voltage plot (Appendix I).

5.10.5 The Electrolyte

A standard aqueous electrolyte was used for all the experimental measurements. The composition of the electrolyte was as follows: 0.5 M NaCl, 0.25 M KH_2PO_4 (buffer), 1.0 M thiourea (supersensitizer) and 0.1 M Na_2SO_3 (oxygen scavenger). The pH of the electrolyte was adjusted with 2 M HCl or NaOH. All

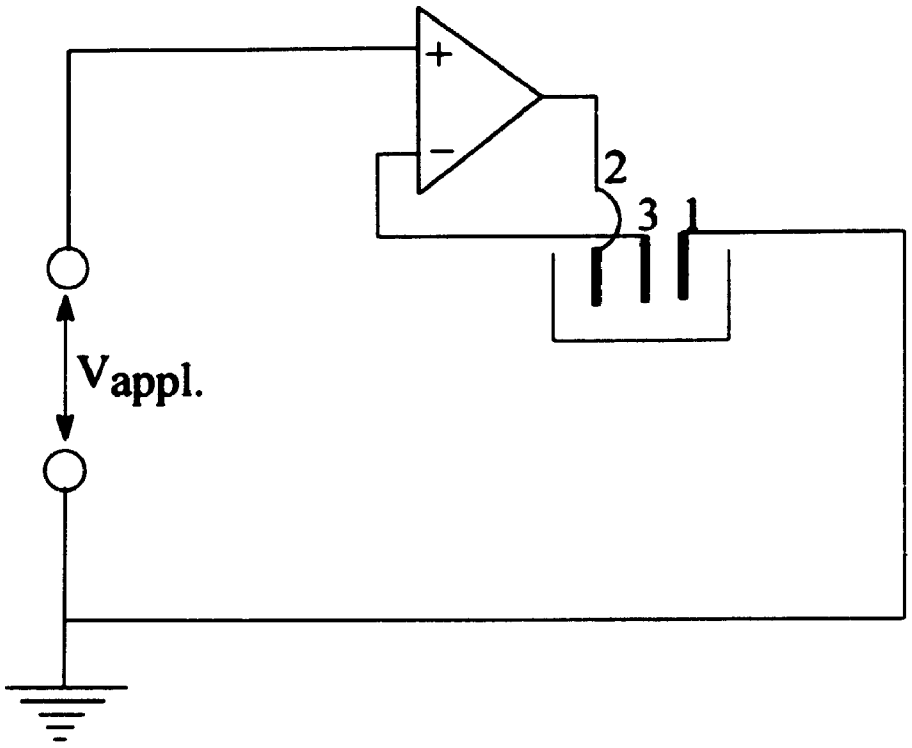

Figure 5.9 : Circuit used to monitor the cell voltage. Current is driven through the cell between the working electrode (1) and the counter electrode (2) by the potentiostat until the voltage between the reference electrode (3) and the working electrode matches the applied voltage, $V_{appl.}$

these chemicals were obtained commercially and used without further purification. In all the experiments, pre-purified nitrogen was bubbled through the electrolyte to ensure the absence of oxygen in the system.

5.10.6 Cell Illumination

The monolayer was illuminated through the transparent slide using a Dolan Jenner Fiber lite (Model 170-D), which contains a tungsten lamp provided with a 5 cm water filter. The spectral irradiance was measured using an International Light radiometer (Model IL1700). The cell and the radiometer detector were mounted on two metal arms, mounted perpendicular to one another on an optical rail. The detector was placed so that the distance between the light source and the cell remained same when either was placed into position in front of the light source. The light irradiance impinging on the cell was controlled by Bausch & Lomb neutral density filters and by positioning of the cell along the optical rail. A 43 cm × 44 cm black plexiglas blind with a sliding shutter was placed across the rail between the light source and the cell. The assembly is shown in Figure 5.10.

A similar setup was used for the measurement of the photocurrent quantum yield (ϕ_{PC}), except that an interference filter having its peak output (λ_{out}) at 432 ($\pm$10) nm was placed in between the light source and the cell. The interference filter provides a narrow band of light around the B-band of the porphyrin and precisely excites the porphyrin chromophore at its λ_{max}. Figure 5.11 shows the transmittance spectra of the interference filter. The irradiance coming through the filter was found to be very steady over a prolonged period (Figure 5.12).

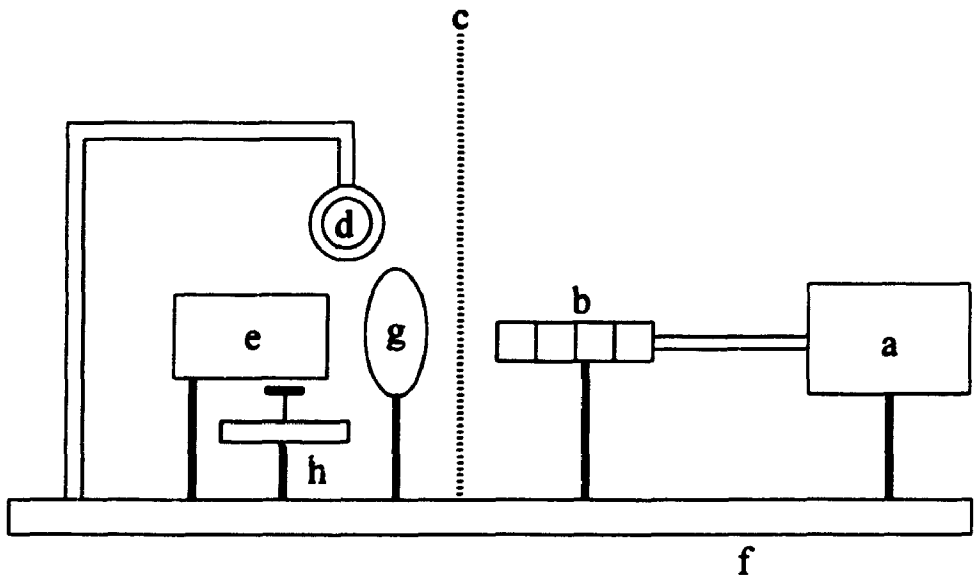

Figure 5.10 : The photoelectrochemical measurement assembly. (a) tungsten light source, (b) neutral density or interference filter, (c) black plexiglass blind, (d) radiometer detector, (e) electrochemical cell, (f) optical rail. (g) fixed apparture mask, (h) magnetic stirrer.

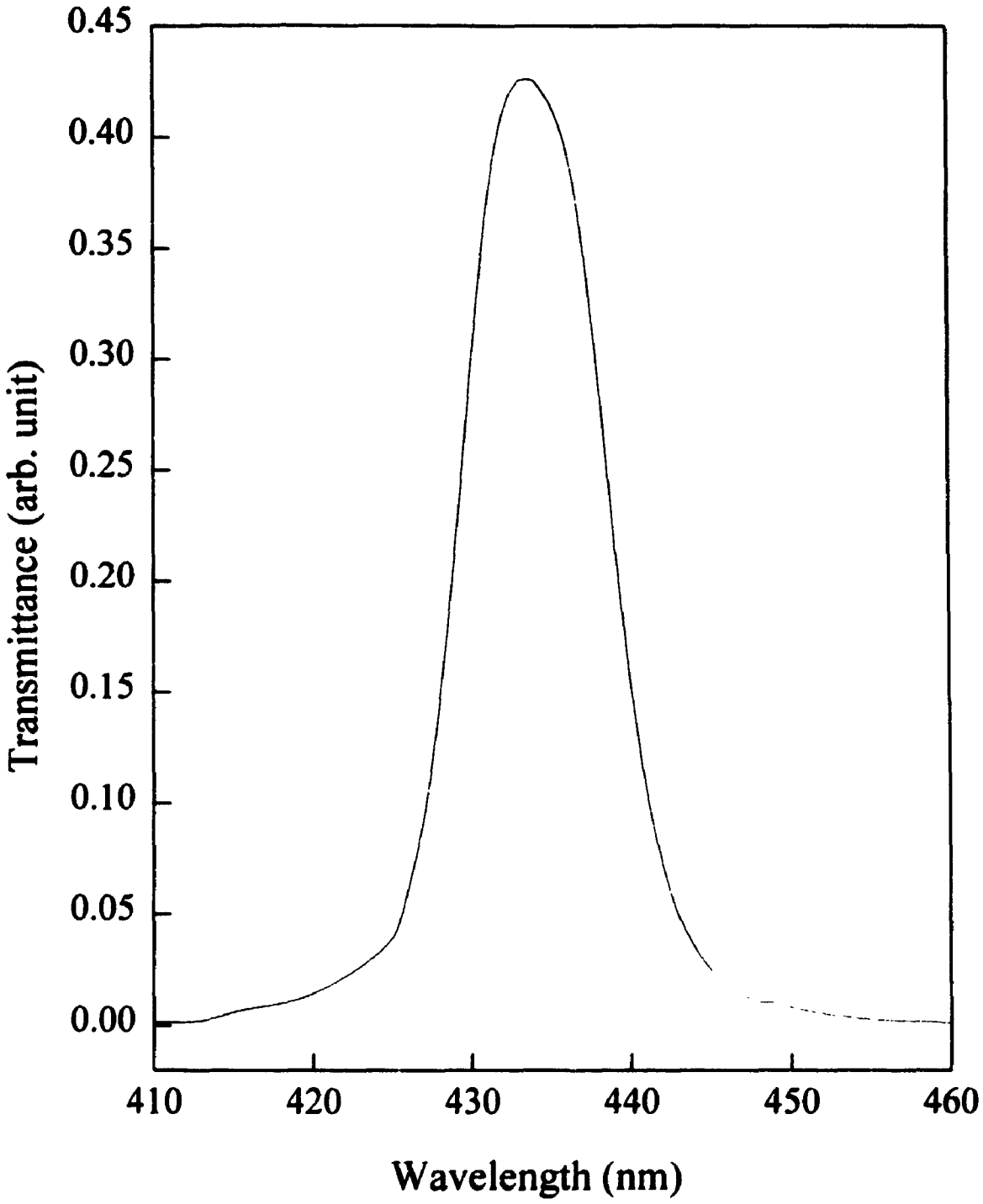

Figure 5.11 : Transmittance spectrum of the *interference filter*.

Transmittance is given in arbitrary units.

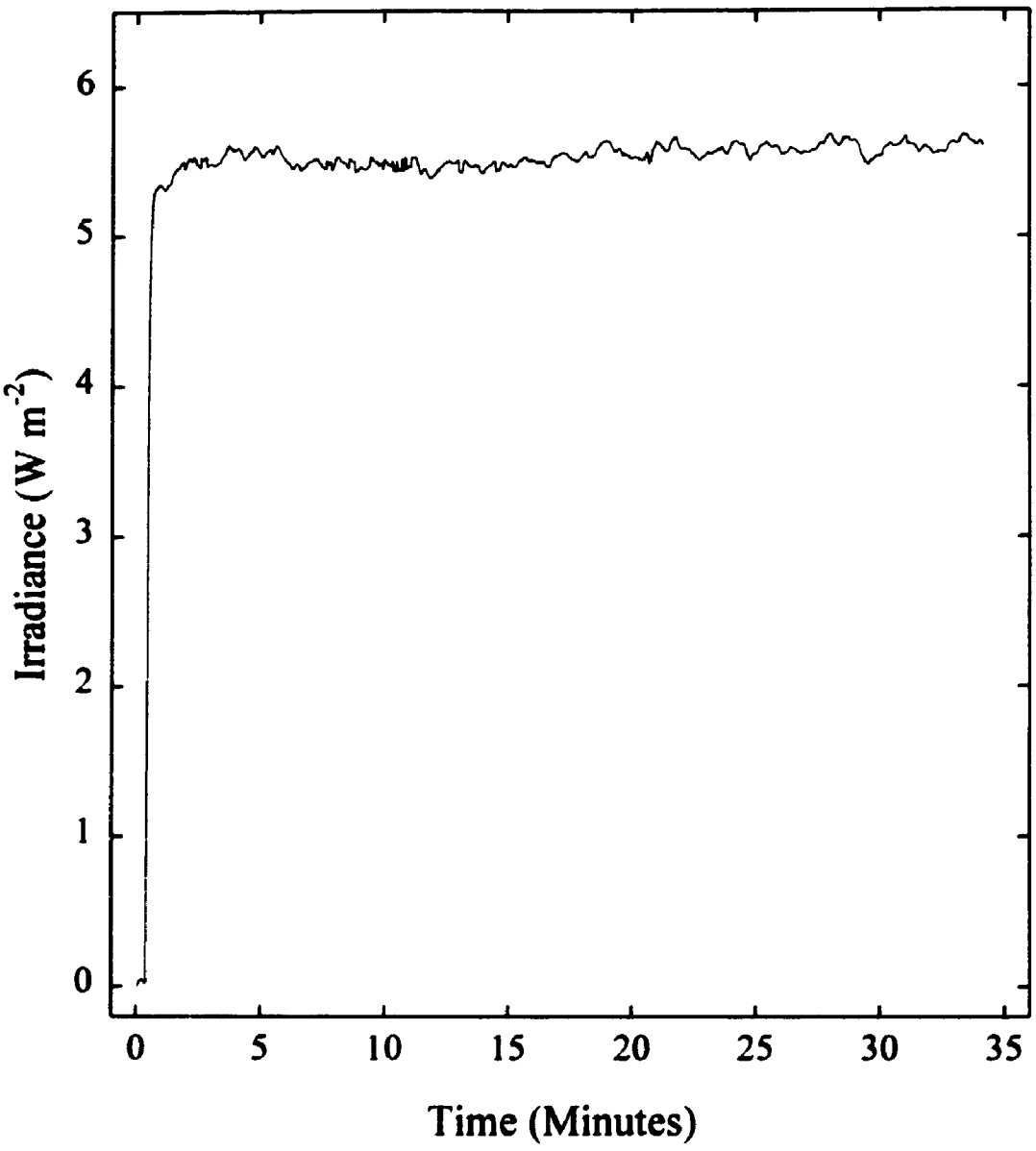

Figure 5.12 : Irradiance of the Dolan Jenner Fiber lite (Model 170-D) tungsten lamp coming through the interference filter. The change in irradiance was 1.3%, over the period of 35 min. with a peak output of 5.7 W m^{-2}.

5.11 RESULTS AND DISCUSSIONS

The photophysical and photoelectrochemical behaviour of the monolayer of P-A, the first compound of Series-I model compounds (Figure 1.1) has been studied extensively in our group. The optimum conditions for obtaining a maximum anodic photocurrent from the photoelectrochemical cell containing a monolayer of P-A on SnO_2 semiconductor surface has been well established by previous workers.[15,46] The following electrolyte composition was recommended by Dick[46] for obtaining the maximum anodic photocurrent:

0.25 M KH_2PO_4, 0.5 M NaCl, 1 M thiourea, 0.1 M Na_2SO_3

where, thiourea (TU) is the supersensitizer and sodium sulphite is the oxygen scavenger. Using only a supporting buffer electrolyte (i.e., NaCl and KH_2PO_4), no difference in the dark current-voltage dependence between blank slides and slides bearing a single monolayer was observed.[46] Addition of TU introduces an anodic dark current component, which probably arises from space-charge tunnelling, since the onset potential is well below the flatband potential. By carrying out oxygen and nitrogen bubbling experiments, it was found that oxygen acts as an electron acceptor both for electrons emitted from the excited state of the dye and from the conduction band of the semiconductor.[46] This fact was also supported by the evidence of an enhanced dark current on oxygen bubbling. Since addition of TU alone produced no anodic photocurrent, oxygen must be acting as a preferential electron acceptor over the conduction band. Bubbling with nitrogen produced a very small anodic photocurrent at anodic voltages and reduced the cathodic photocurrent at cathodic voltage. Addition of sodium sulphite produced this same effect, but much more

strongly. This seems to indicate that the oxygen, which is acting to capture the excited state electron must be adsorbed to the surface of the semiconductor, since bubbling with nitrogen displaces the oxygen from solution and only weakly from the surface, while Na_2SO_3 is capable of scavenging the adsorbed oxygen on the surface more strongly and efficiently.

Following the observations made by Dick,[46] as discussed in the previous paragraph, the recommended electrolyte was used to carry out all the electrochemical experiments in the present study. Although it has been suggested that the bubbling of nitrogen is not necessary in presence of Na_2SO_3, in the present work pure nitrogen was bubbled through the electrolyte for all experiments. This was done to ensure the absence of oxygen in the system as well as to maintain the homogeneity of the electrolyte during the electrochemical reaction, as the magnetic stirrer was not capable of agitating the electrolyte efficiently.

The action spectrum of P-A and P-Gly-A were measured and they overlaped with the corresponding absorption spectrum. This indicates that these compounds generate the photocurrent by absorbing the light at their λ_{max}. As all the model compounds possess similar absorption characteristics, it was assumed that they will exhibit similar action spectrum.

We shall discuss our results in relation to the energy level diagram shown in Figure 5.13. A photon absorbed by P-A in its ground state (S_0) on the SnO_2 surface creates the excited singlet state (S_1) of P-A. S_1 then undergoes oxidation via one of three processes as shown in Figure 5.13. The O_2/O_2^- acceptor level has been placed at +0.5 V vs. SHE as quoted for TiO_2.[47] The TU/TU^+ redox level of thiourea (TU)

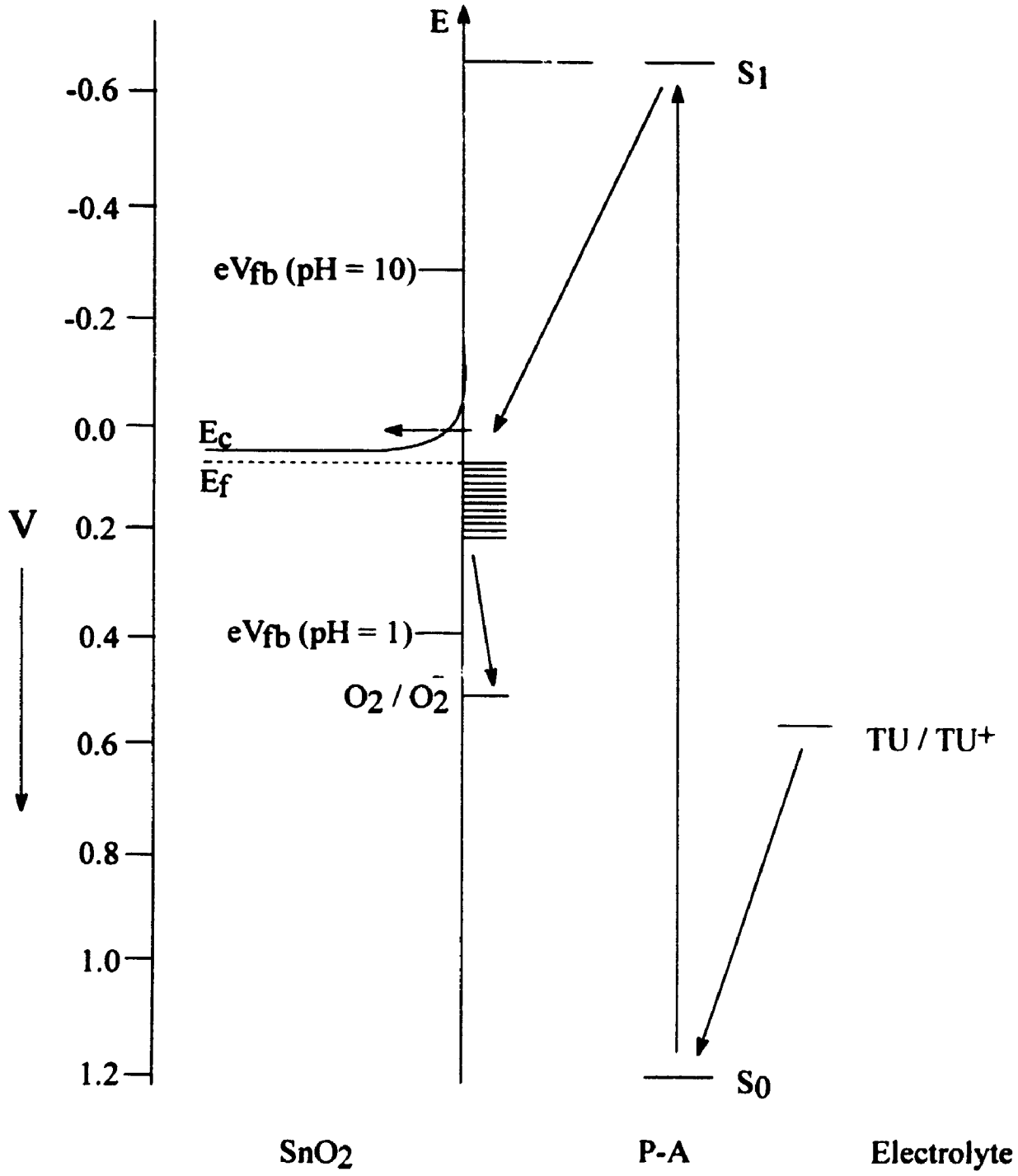

Figure 5.13 : An energy level diagram for the semiconductor-monolayer-electrolyte interface. Arrows indicate possible directions of electron propagation. Energy levels are placed with respect to standard hydrogen electrode (SHE). The scale represents voltage vs. SHE.

used as a supersensitizer has been estimated to be somewhat higher than the potential for the onset of dark anodic photocurrent, since its value is not available in the literature. The reduction potential of the P-A$^+$/P-A couple in the P-A monolayer is taken to be +1.2 V vs. SHE as quoted for free base tetraphenylporphyrin in DMSO.[48] As all the newly synthesized model compounds possess the same porphyrin chromophore as in P-A, their monolayers were assumed to possess the same reduction potential as P-A.

5.11.1 Deposition

In order to carry out the photoelectro-chemical quantum yield studies, mixed monolayers of P-A, P-Ace-A, P-Et-A and P-Gly-A with DOPC were deposited onto the SnO_2 slides. Three mixture ratios, 1:9 (10% DOPC), 3:7 (30% DOPC), and 1:1 (50% DOPC), of DOPC and porphyrin compounds were used and they show almost same deposition ratios. Beyond 50% dilution the signal-to-noise ratio becomes so low that the photocurrent yield was practically impossible to determine.

5.11.2 Current-Voltage (j-V) Curves

Current-voltage curves for all the model compounds were measured. A series of current-voltage plots under identical experimental conditions for P-A, P-Pr-A, P-Ace-A and P-Gly-A are shown in Figures 5.14-5.17. The cell was illuminated with the narrow band light (432 ± 10 nm), rising the interference filter. The pH of the electrolyte was maintained at ~2.0, as suggested by Dick.[46] Interestingly, all the model compounds show similar current-voltage characteristics, except that the

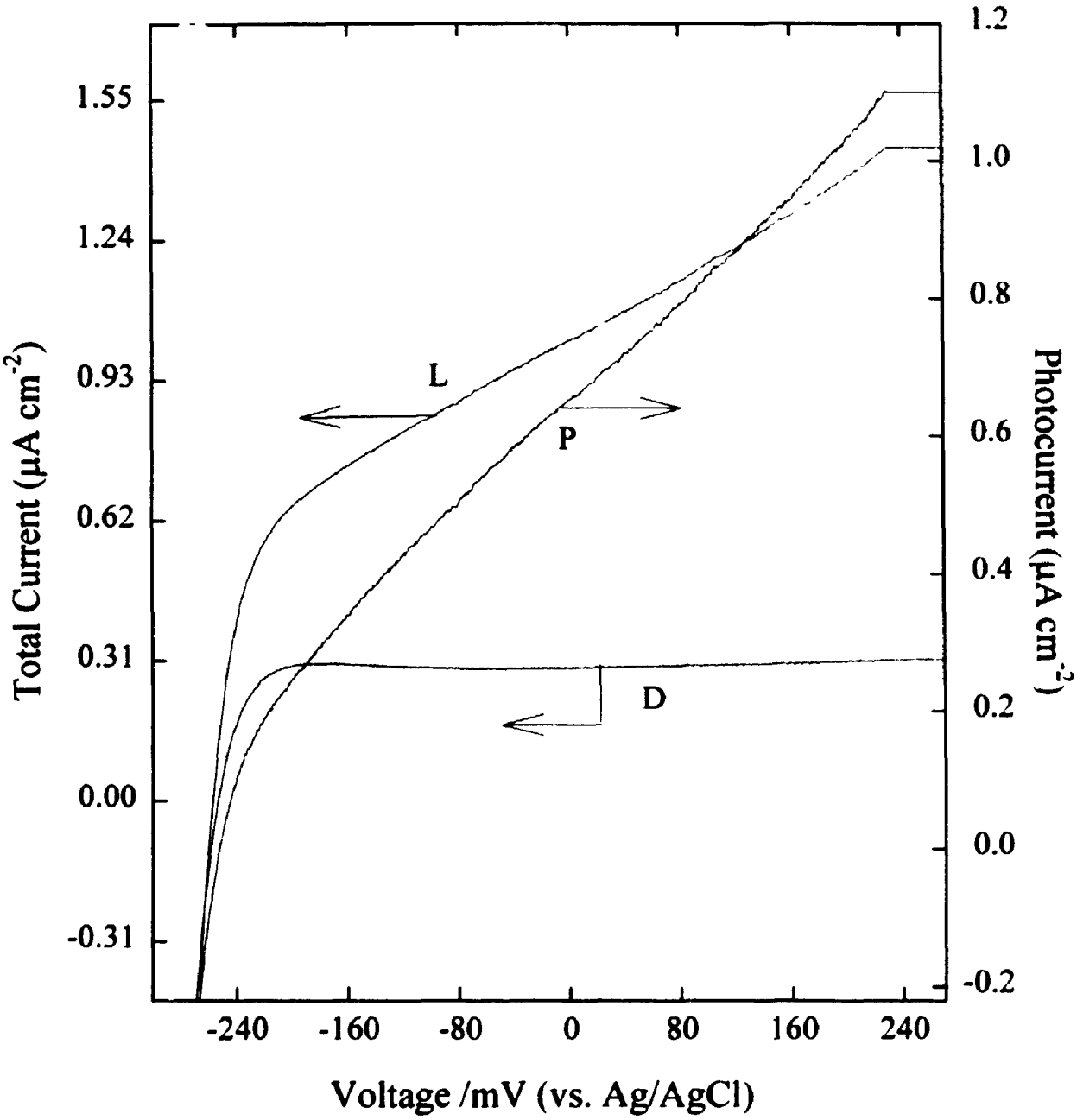

Figure 5.14 : Current-voltage plots of P-A. Electrolyte composition: 0.25 M KH_2PO_4, 0.5 M NaCl, 1 M TU, 0.1 M Na_2SO_3 at pH 2.0. L and D are light and dark current responses. P is the photocurrent response, obtained by subtracting signal D from signal L. V_{fb} = -268 mV at 22 ± 2^{0}C.

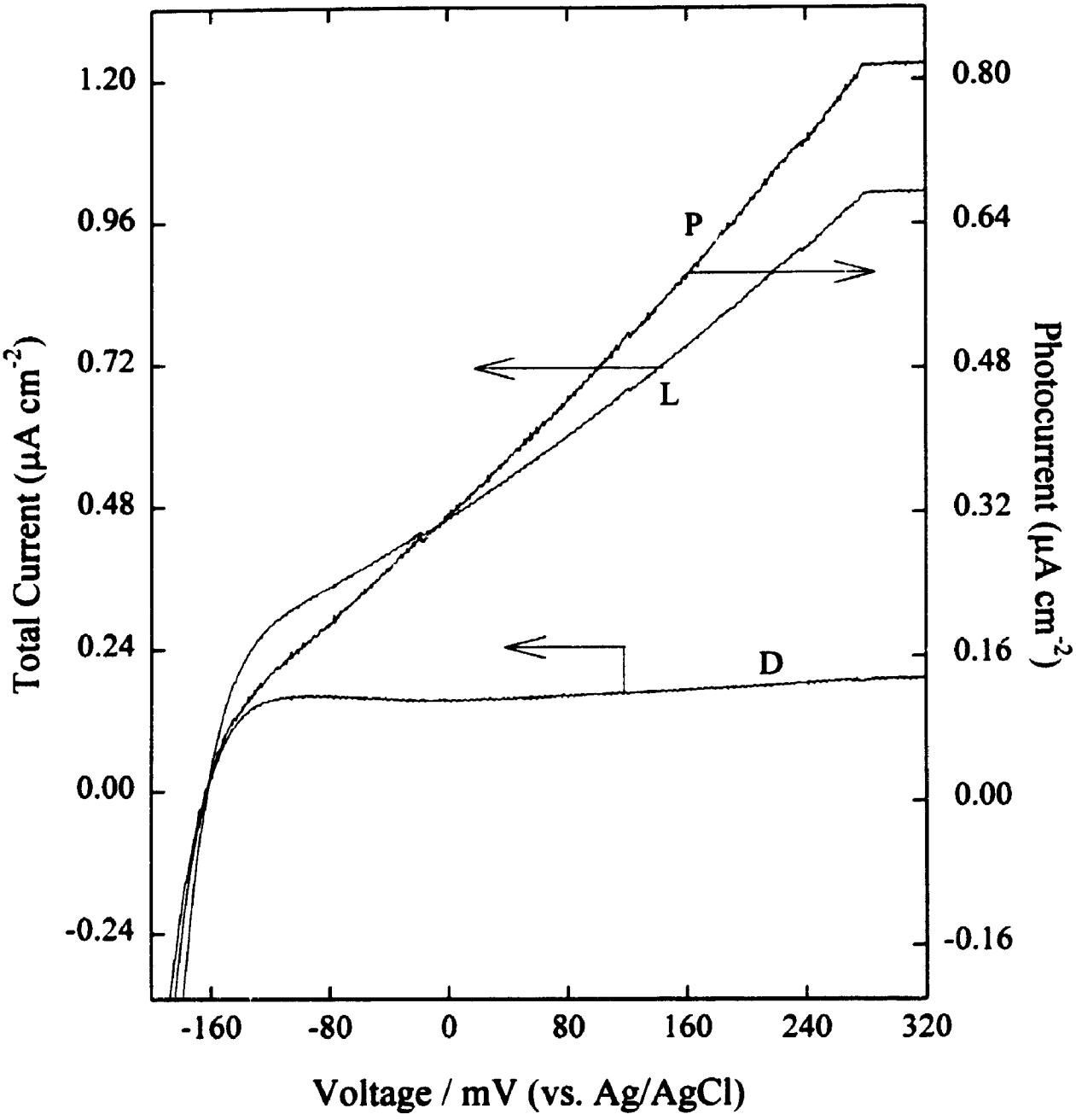

Figure 5.15 : Current-voltage plots of P-Pr-A. Electrolyte composition: 0.25 M KH_2PO_4, 0.5 M NaCl, 1 M TU, 0.1 M Na_2SO_3 at pH 2.0. L and D are light and dark current responses. P is the photocurrent response, obtained by subtracting signal D from signal L. V_{fb} = -161 mV at 22 ± 2^{0}C.

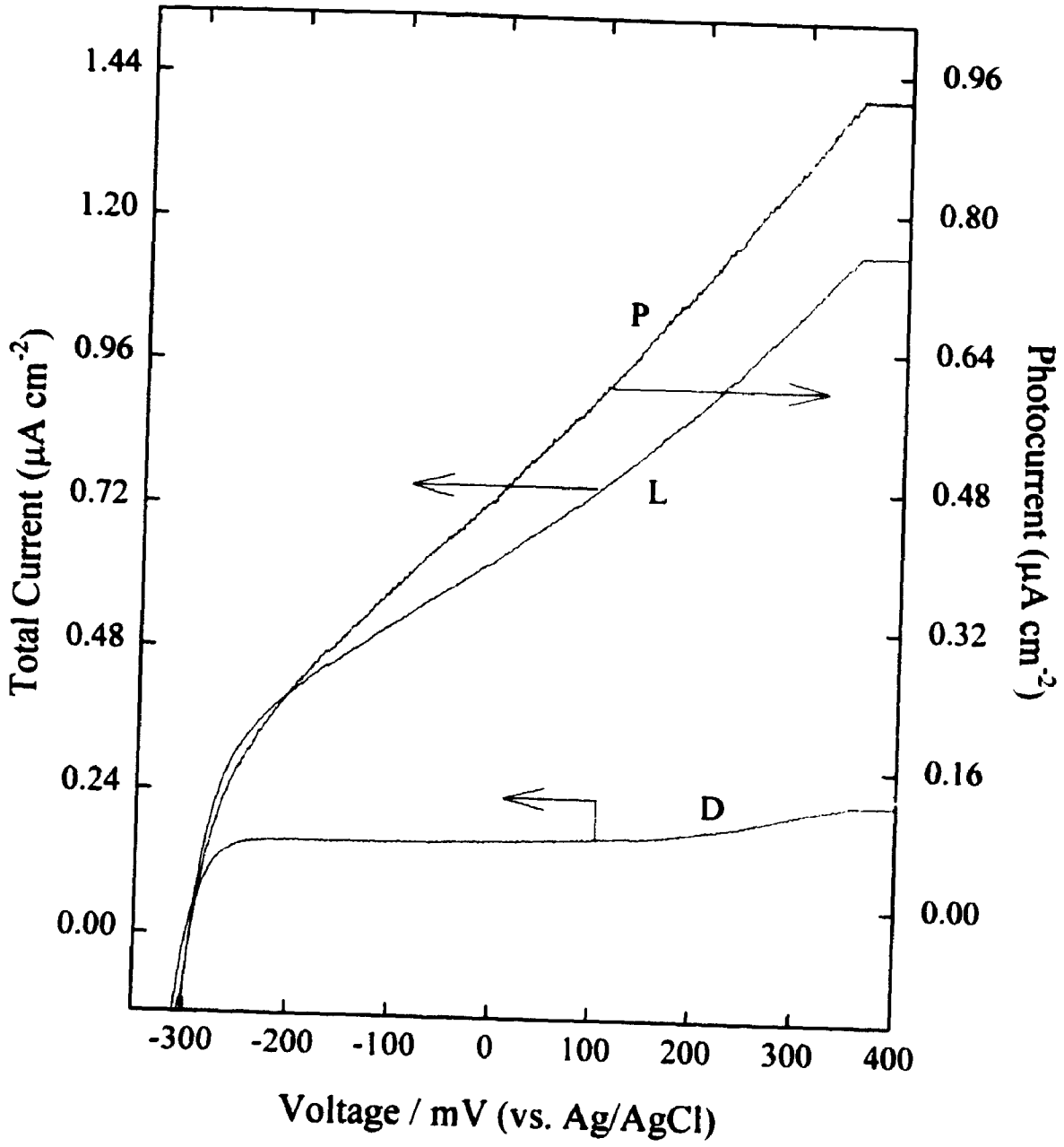

Figure 5.16 : Current-voltage plots of P-Ace-A. Electrolyte composition: 0.25 M KH_2PO_4, 0.5 M NaCl, 1 M TU, 0.1 M Na_2SO_3 at pH 2.0. L and D are light and dark current responses. P is the photocurrent response, obtained by subtracting signal D from signal L. V_{fb} = -291 mV at 22 ± 2^{0}C.

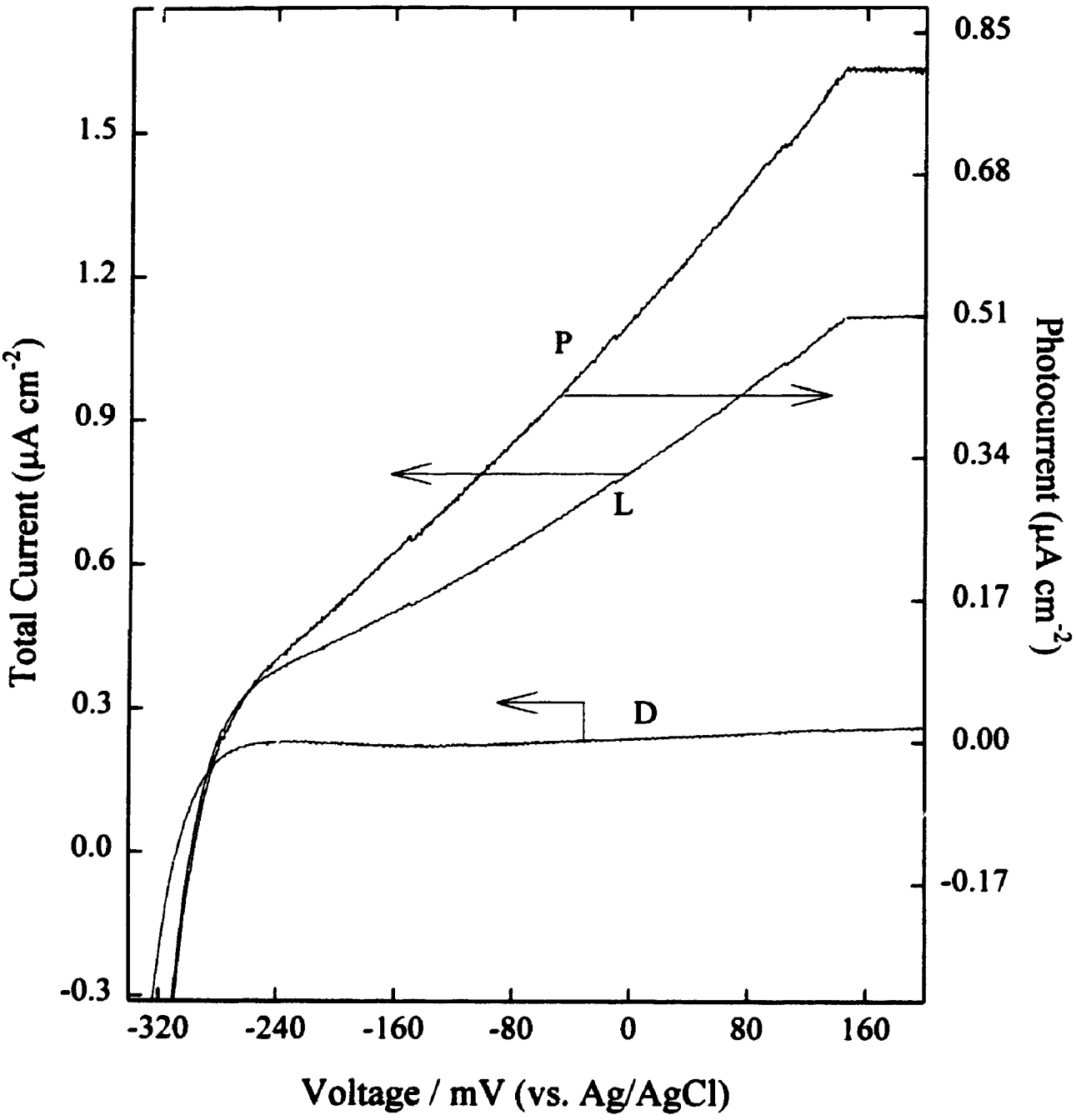

Figure 5.17 : Current-voltage plots of P-Gly-A. Electrolyte composition: 0.5 M NaCl, 0.25 M KH_2PO_4, 1 M TU, 0.1 M Na_2SO_3 at pH 2.0. L and D are light and dark current responses. P is the photocurrent response, obtained by subtracting signal D from signal L. V_{fb} = -286 mV at 22 ± 2^{0}C.

photocurrent yields are different. On removing the interference filter and measuring the current-voltage (j-V) behaviour under white light, an expected increase in the photocurrent yield was observed for all the compounds. No additional change in the pattern of the curves was observed for any of the model porphyrin molecules.

The current-voltage behaviour of a dye sensitized semiconductor electrode mainly reflects the electron injection and excited-state deactivation processes occurring on the electrode. In the present work, as the nature of the j-V curves for SnO_2 electrode was found to be almost identical for all the different sensitizing dyes, it can be anticipated that the sensitizing mechanisms are identical for all the model compounds. For all the porphyrin monolayers, the Soret or B band was selectively chosen for excitation using the narrow band light. This was done in order to make sure that only the singlet excited state of the porphyrin is contributing to the electron injection process and no additional excitation processes are involved in the current production. The different photocurrent yields for different compounds are mainly attributed to their different aggregation in the monolayer caused by different chain lengths, which influences the lifetime of the excited singlet states. Hence, the different chains only affect the photocurrent yield.

5.11.3 Measurement of Flatband Potential

The measurement of flatband potential is normally carried out using the Mott-Schottky technique. However, the Mott-Schottky curves are decidedly non-linear and the intercepts had to be obtained by an extrapolation of the linear portion near the x-axis. In the present work, we have utilized an alternative method,[49] based on the

fact that the photocurrent should go to zero at the flatband condition. This method was used very efficiently in the present study, since both cathodic and anodic photocurrents are observed for all the model compounds at different applied potentials. Figures 5.14-5.17 show a clear crossover from cathodic photocurrent at low potential through zero at the flatband potential to anodic photocurrent at higher potentials. This provides an easy method to calibrate our experiments, as all the potential scales can be related to the flatband potential.

It is well known that the flatband potential is pH dependent. In order to compare different porphyrin compounds, the flatband potentials of all the compounds were measured under identical pH conditions. The flatband potentials for all the model compounds at pH ~2.0 have been summarized in Table 5.1.

5.11.4 pH Dependence of the Photocurrent

The pH dependence of the photocurrent for four different model compounds, P-A, P-Pr-A, P-Ace-A and P-Gly-A, was determined at a fixed applied potential. As P-Me-A and P-Et-A have structural similarity with P-Pr-A, their behaviour can be predicted from the results obtained for P-Pr-A. Similarly P-Glyco-A possesses a structural similarity with P-Gly-A, and it was anticipated that its behaviour can be predicted on the basis of the behaviour of P-Gly-A. Hence, only the above mentioned four compounds were studied. It was found that for all four of them the photocurrent increases markedly below pH ≈ 4. Measurements for all the compounds were carried out at a fixed offset potential (+400 mV) from their respective flatband potentials.

Table 5.1: Flatband potential of all the model compounds at pH ~2.0. The cell was illuminated at $\lambda = 432 \pm 10$ nm. Electrolyte composition: 0.25 M KH_2PO_4, 0.5 M NaCl, 1 M TU, 0.1 M Na_2SO_3 at 22 ± 2°C.

Compound	V_{fb} (mV)
P-A	-268 ± 2
P-Me-A	-242 ± 2
P-Et-A	-238 ± 3
P-Pr-A	-161 ± 2
P-Ace-A	-291 ± 3
P-Gly-A	-286 ± 1
P-Glyco-A	-104 ± 2

Figure 5.18 and 5.19 show the pH dependence of the photocurrent for a SnO_2 electrode covered with a monolayer of P-A, P-Pr-A, P-Ace-A and P-Gly-A, respectively, and illuminated by a tungsten lamp that had virtually no intensity below 400 nm. A similar electrolyte composition, as mentioned earlier, has been used for these measurements. Pure nitrogen was bubbled through the electrolyte for all the measurements.

The similarity in the pattern of the pH dependence curves for the four different compounds indicates that the change of the dye molecule on the SnO_2 semiconductor surface does not alter the electron injection process under the influence of a different pH. The electron injection mechanism associated with all four dyes must be identical and the different chain lengths do not have any effect on it. The different photocurrent yields for all four compounds at a particular pH is merely due to the difference in their quenching behaviour.

An injection scheme has been put forth by Memming[50] to explain low photocurrent quantum yields for heavily doped semiconductors. According to this scheme, direct injection is followed by recombination via back electron tunnelling through the space-charge layer. This predicts the opposite pH effect on anodic photocurrent to that which is observed for our system, since at higher pH back electron transfer should be inhibited due to a thicker space-charge layer. It therefore appears that pH must be identically affecting the initial electron injection step as well as the back tunnelling rate for all four compounds.

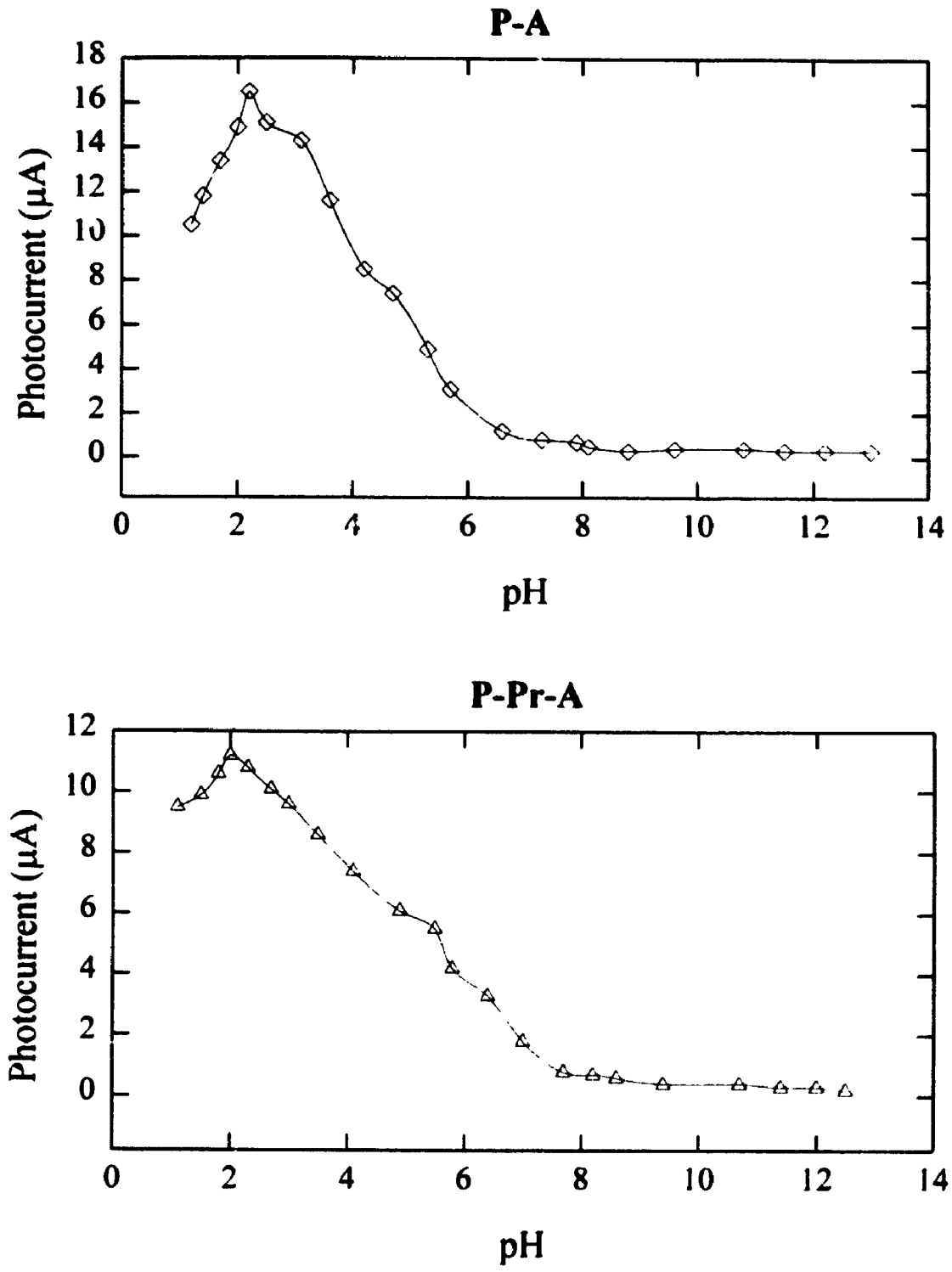

Figure 5.18 : Plots of pH dependence of the photocurrent. Electrolyte composition: 1 M TU, 0.25 M KH_2PO_4, 0.5 M NaCl, 0.1 M Na_2SO_3. Measurements were made at 22 ± 2^{0}C and at fixed offset potential (+400 mV) from the flatband potential of both compounds.

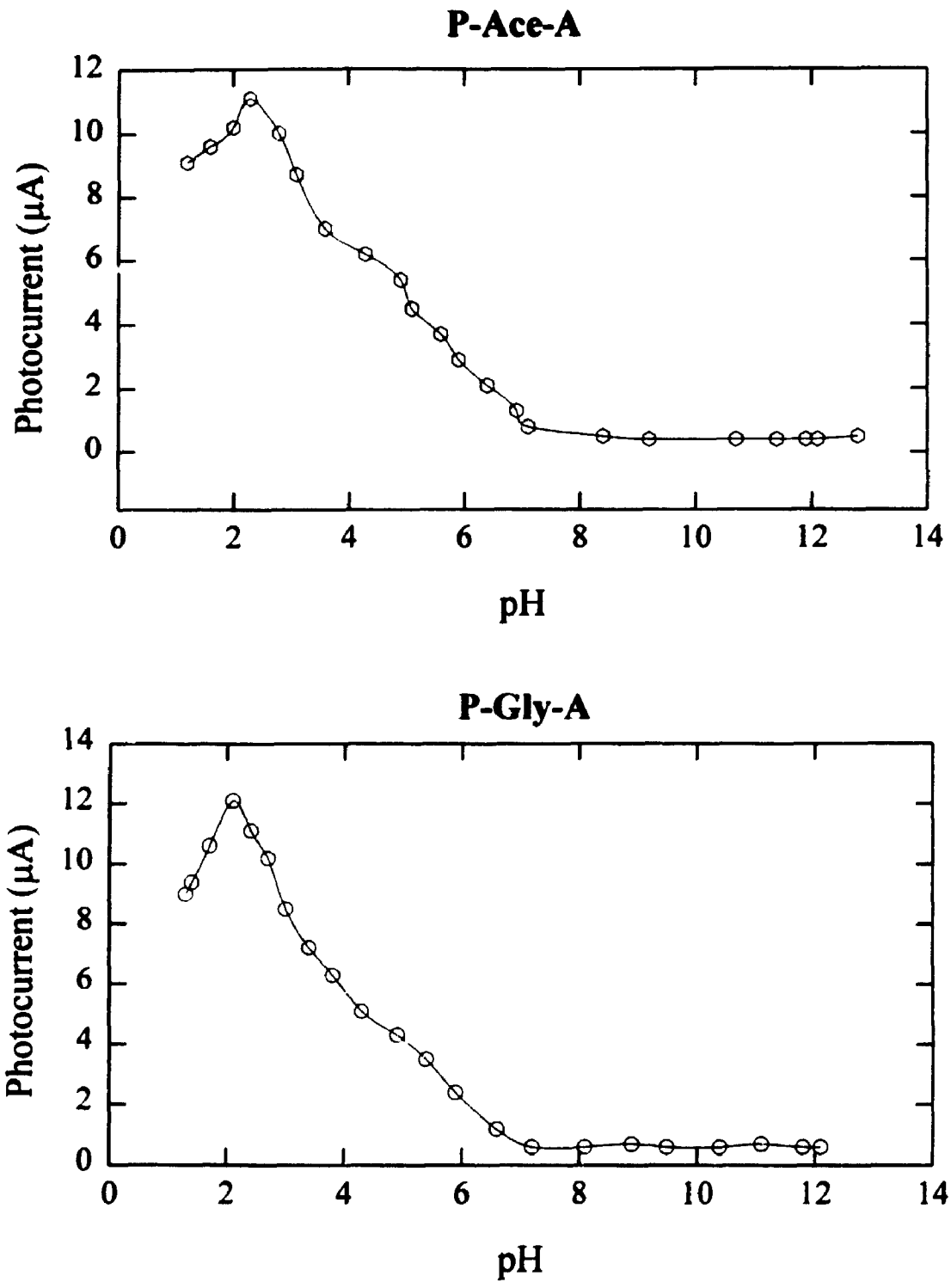

Figure 5.19 : Plots of pH dependence of the photocurrent. Electrolyte composition: 1 M TU, 0.25 M KH_2PO_4, 0.5 M NaCl, 0.1 M Na_2SO_3. Measurements were made at 22 ± 2^{0}C and at fixed offset potential (+400 mV) from the flatband potential of both compounds.

Two mechanisms have been suggested in the literature that include a pH dependent electron injection step. The first, which was referred to earlier,[30] predicts a logarithmic dependence with pH based on an increasing Helmholtz potential at low pH. Our results cannot be fit to this type of dependence. Rather they resemble sigmoidal functions. A second mechanism which predicts this type of dependence was proposed by Clark and Sutin.[51] They proposed that if the distribution of the oxidation potentials of the excited state overlap incompletely with the surface conduction band edge, the degree of overlap and hence the probability of isoenergetic electron transfer would be controlled by the position of the band edge. Since the overlap is pH controlled, this model predicts that the anodic photocurrent should increase at low pH. This does not seem likely for our system, since the oxidation potential of the first excited singlet state of the dye is well above the surface conduction band edge at any pH.

A mechanism similar to that proposed by Frippiat *et al.*[33] may be operating here, in which some of the electrons are injected directly into the bulk and others are captured by unoccupied surface states at the Fermi level. Indeed, surface states probably mediate the electron capture by adsorbed oxygen as well, since the pH dependence for both these currents is similar.

The pH dependence of the photocurrent due to capture by surface states may either arise from the pH dependence of the tunnelling probability from the surface into the bulk or the pH dependence of the population of trapping states at the Fermi level. The voltage dependence of the photocurrent suggests the latter. As the voltage is made more anodic a larger number of surface states are emptied and

become available to trap the electrons. The increasing slope of this dependence with reduction in pH agrees with this, since the number of surface states at each energy level would increase with decreasing pH. If forward tunnelling through the space charge barrier was rate limiting, the current should decrease with increasingly positive voltage due to the increasing thickness of the barrier at the Fermi level.

A pH dependence of the surface state population has been proposed by a number of authors for ionic semiconductors.[52] The equilibria are generally of the type;

$$M^{2+} + OH^- \rightleftharpoons M\text{-}OH^+ \qquad (5.37)$$

Here the metal cation M^{2+}, in our case Sn^{2+}, acts as the initial trap for photoinjected electrons.

Scheme 5.1 shows the electron injection scheme, which summarizes the various processes possible on the semiconductor surface. In this scheme, an electron injected into the semiconductor bulk may either be injected directly (Step 3) or trapped by a surface state at the Fermi level creating an oxidized dye, reduced surface state intermediate pair as proposed by Fromhertz[34] (Step 4). If the surface state is in the proximity of adsorbed oxygen, it will reduce it (Step 8). The oxidized dye is then reduced by an electron from the conduction band producing a cathodic photocurrent (Step 9). If the reduced surface state is not in the proximity of adsorbed oxygen, it may either recombine with the oxidized dye molecule (Step 6) or tunnel through the space-charge layer into the semiconductor bulk, if the oxidized dye is reduced by TU molecule (Steps 5,7). Steps 6 and 7 compete in the reduction of the oxidized dye.

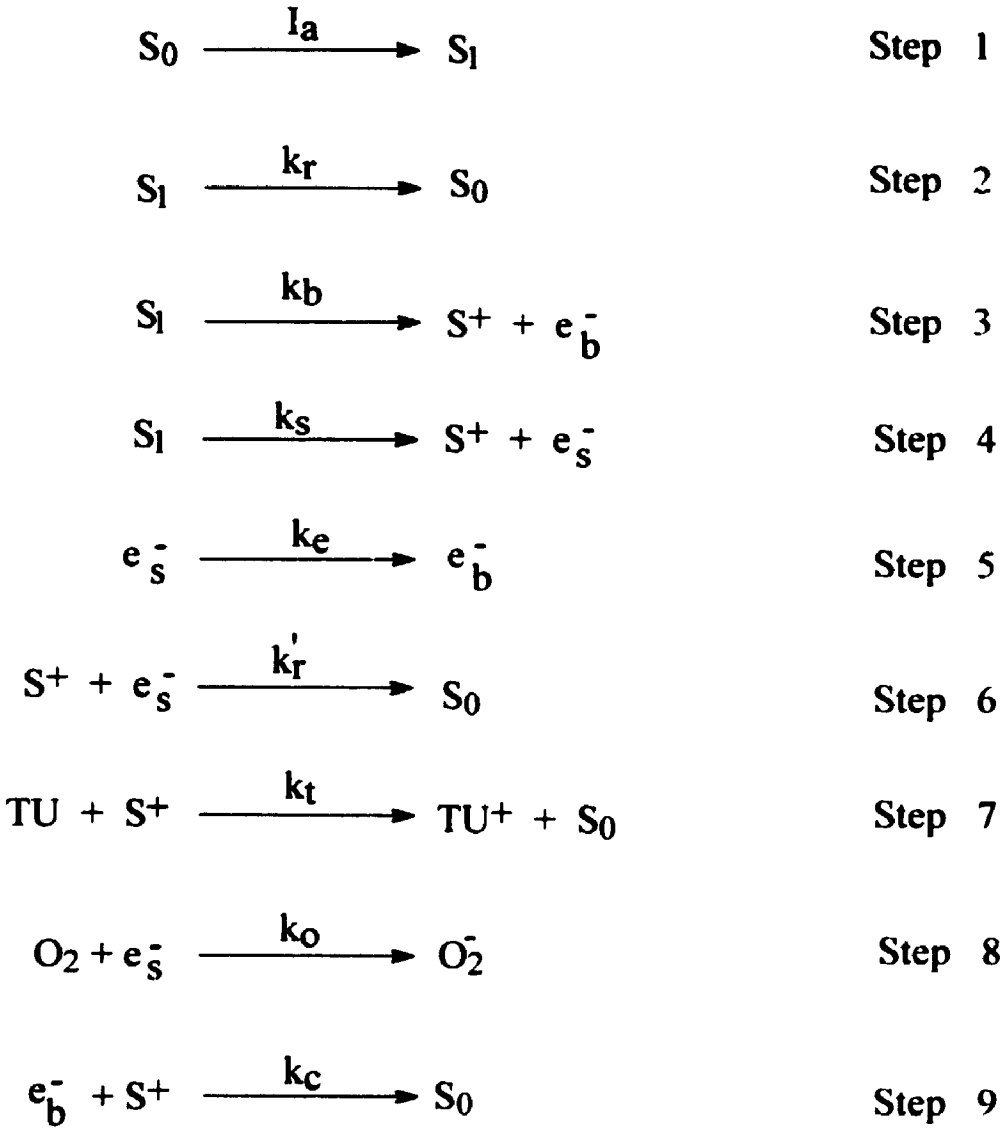

Scheme 5.1 : An electron injection scheme. The summarization of various electron transfer processes involved in the electrochemical cell.

We associate Step 3 with the pH independent part of the anodic photoresponse and Step 4 with the pH dependent part, which arises from trapping by Sn^{2+} atomic surface states. Regions where the Sn^{2+} surface concentration is high will favour this step. Such heterogeneity of response was observed by Frippiat *et al.*[33] and might also explain the occasional absence of the pH independent part of the anodic photoresponse for some samples.

5.11.5 Photocurrent Quantum Yield

The anodic photocurrent yield for all the model compounds, under identical cell, electrolyte and illumination conditions was determined. Normally narrow band monochromatic light conditions are suggested for photocurrent quantum yield determinations but in the present work an interference filter ($\lambda = 432 \pm 10$ nm) was used. This was done as measurement under narrow band monochromatic light was very difficult due to the low irradiance and high signal-to-noise ratio obtained for photocurrent signals.

The accurate estimation of the photocurrent quantum yield is important, in order to assess the relative importance of interfacial electron transfer and the energy loss by recombination processes in the semiconductor. The photocurrent quantum yield is defined as;

$$\phi_{PC} = \frac{R_{e^-}}{R_{Ph}} \qquad (5.38)$$

where R_{e^-} is the rate of electrons flowing through the circuit on illuminating a square centimeter area of the dye coated semiconductor photoelectrode and is expressed as

electrons s^{-1} cm^{-2}. R_{Ph} is the rate of photons absorbed per square centimeter area of the photoelectrode and is expressed as *photons* s^{-1} cm^{-2}. In the present work, the following expression was developed and used to determine the photocurrent quantum yields for all the model compounds.

$$\Phi_{PC} = \frac{i_{PC}}{e \times N_{Ph} \times B} \tag{5.39}$$

where i_{PC} is the photocurrent density (A cm^{-2}), e is the electronic charge, N_{Ph} is the incident photon flux (photons s^{-1} cm^{-2}) in a narrow wavelength band around the wavelength λ and B is the fraction of light absorbed in the porphyrin monolayer. B can be determined from the following relation, as suggested by Bolton *et al.*[53]

$$B = 1 - t - (1+t^2)\left(\frac{1-t_0}{1+t_0}\right) \tag{5.40}$$

where $t = I / I_{00}$ and $t_0 = I_0 / I_{00}$. I_{00}, I_0 and I are the measured irradiances (W cm^{-2}) for no slide, a bare SnO_2 slide and a porphyrin monolayer coated SnO_2 slide in the light beam coming through the interference filter, respectively. The photocurrent yields for all the model compounds were measured at a potential positive to their flatband potential, where they show the maximum yield. Table 5.2 shows the offset potentials from the flatband potentials, at which the measurements were made, and the photocurrent quantum yields for all the model compounds. From Figures 5.14-5.17, it is evident that porphyrins with different chains give the maximum photocurrent yields at different offset potentials. The photocurrent for all the compounds normally reach their plateau at different potentials, with respect to their flatband potentials. The potential at which the maximum photocurrent

Table 5.2 : Photocurrent quantum yields (ϕ_{PC}) of all the model porphyrin compounds.[a]

Compounds	V_{offset} / mV[b]	ϕ_{PC} (%)[c]
P-A	+508 ± 2	0.33 ± 0.02
P-Me-A	+522 ± 3	0.14 ± 0.01
P-Et-A	+518 ± 2	0.16 ± 0.01
P-Pr-A	+441 ± 3	0.21 ± 0.02
P-Ace-A	+641 ± 2	0.27 ± 0.02
P-Gly-A	+466 ± 2	0.27 ± 0.03
P-Glyco-A	+554 ± 3	0.11 ± 0.02

[a] Measurements were made at 22 ± 2°C. Electrolyte composition: 0.25 M KH_2PO_4, 0.5 M NaCl, 1 M TU, 0.1 M Na_2SO_3. pH ~ 2.0.

[b] Potentials at which photocurrent yields were determined.

[c] Narrow band light, λ = 432 (±10) nm was used.

output in a semiconductor photocell is produced normally depends on the position of the surface states. The presence of different chains attached to the porphyrin ring may be influencing the position of the surface states of the SnO_2 semiconductor and hence the maximum yields are observed at different potentials. Hence, for different model compounds that photocurrent yields were determined at different potentials, that is, at the potential at which the plateau region begins.

We have already discussed in the previous chapter (Chapter 4) that the fluorescence quenching of porphyrin compounds observed on the SnO_2 surface arises from two different deactivation pathways from the singlet excited species. The first path was the quenching due to the aggregate formation, which is also prominent on a quartz surface, and the second one was thought to be interfacial electron transfer from the S_1 excited state of the porphyrins to the conduction band of SnO_2. We have also accounted for the interfacial electron transfer rate (k_{et}) and it was found to be related to the relative fluorescence quantum yield of the compound.

In the previous chapter (Chapter 4) we have discussed the existing correlation between the fluorescence quantum yield (ϕ_f) and estimated rate of electron injection (k_{et}). Since the rate of photoelectron injection is responsible for the photocurrent production, there must be some correlation between them. Table 5.3 compares the photocurrent quantum yield (ϕ_{PC}) with the fluorescence quantum yield (ϕ_f) and the estimated electron transfer rate (k_{et}) on the SnO_2 semiconductor surface. As expected, the photocurrent yield (ϕ_{PC}) of all the compounds varies directly with the rate of electron transfer (k_{et}). It shows that the faster the electron is transferred to

Table 5.3: Comparison of photocurrent quantum yield (ϕ_{PC}), fluorescence quantum yield (ϕ_f) and rate of electron transfer (k_{et}) of all model porphyrin compounds on a SnO_2 semiconductor surface.[a]

Compounds	ϕ_{PC} (%)	ϕ_f (Rel)	$k_{et} \times 10^7$ (s^{-1})
P-A	0.33 ± 0.02	0.388 ± 0.001	1.5
P-Me-A	0.14 ± 0.01	0.332 ± 0.006	2.1
P-Et-A	0.16 ± 0.01	0.282 ± 0.006	1.2
P-Pr-A	0.21 ± 0.02	0.202 ± 0.002	6.9
P-Ace-A	0.27 ± 0.02	0.173 ± 0.004	20.4
P-Gly-A	0.27 ± 0.03	0.167 ± 0.004	10.9
P-Glyco-A	0.11 ± 0.02	0.380 ± 0.004	0.0[b]

[a] Measurements were done at 22 ± 2°C.

[b] Assumed to be zero.

the conduction band of the semiconductor, the larger is the photocurrent generated. The series P-A to P-Pr-A, P-Et-A nicely follows the trend of the change of photocurrent quantum yield as well as the fluorescence yield and in both cases it falls in between P-Me-A and P-Pr-A. The k_{et} value of P-Et-A does not follow the increasing trend. This may be due to the involvement of some kind of unusual deactivation process of its excited singlet state on the quartz surface, which leads to an inaccurate estimation of k_{et} for P-Et-A. Hence from the variation in the photocurrent quantum yield and electron transfer rate, it can be anticipated that the photoinjection process significantly contributes to the quenching process of the excited singlet state of all the compounds.

Going from P-A to P-Me-A the fluorescence yield decreases probably due to increased aggregate formation. This effect is also supported by the photocurrent yield of P-Me-A, which also decreases, indicating that quenching due to greater aggregation competes strongly over the photoinjection process. But as we move from P-Me-A to P-Et-A and then to P-Pr-A, a steady decrease is observed in the fluorescence yield and an increase in the photocurrent yield. Considering the fact that the long chain helps in the formation of a better aggregate, as we have seen from surface isotherm data of the model porphyrin compounds, a decrease in both photocurrent and fluorescence quantum yields should have occurred. The discrepancy in these results may be due to the quenching caused by an increase in the rate of the photoinjection process. Such an increase in photoinjection can be explained by the existence of *trans bond effect* in these compounds, as observed by Haran *et al.*[44] for long chain organic aliphatic compounds. As the chain length

increases, due to the increase in the conformational flexibility of the molecule, there is an overlap of the bonding and antibonding orbitals of the "inert" space layer of the alkyl chains, which increases the capability of through-bond tunnelling by the compound. This results in an enhanced rate constant for electron injection (k_{et}) on the SnO_2 surface by the molecule and hence a substantial increase in the photocurrent yield. Thus, by increasing the chain length, through-bond electron tunnelling becomes prominent due to the *trans bond effect* in the molecule and we observe a decrease in the fluorescence yield and a corresponding increase in the photocurrent yield of the molecule.

A similar trend in the photocurrent yield was observed for the series P-Pr-A, P-Ace-A, P-Gly-A and P-Glyco-A respectively. In P-Ace-A, due to the presence of a triple bond, an enhanced electron transfer rate is observed, which results in a high photocurrent quantum yield of the molecule and a low fluorescence yield. P-Gly-A also reflects a similar result, due to the presence of a lone pair of electrons on the central N-atom in the chain, which increases the electron mobility through the chain. Thus in P-Gly-A and P-Ace-A, the presence of an electron rich chain facilitates the rate of interfacial electron injection (k_{et}), which results in high photocurrent yields and low fluorescence yields, respectively. In the case of P-Glyco-A, due to the high electronegativity of the central oxygen atom, the rate of electron injection becomes esse ially zero, resulting in a small photocurrent yield and a high fluorescence yield.

5.11.6 Effect of Monolayer Deaggregation on Photocurrent Quantum Yield (ϕ_f)

It is a well established fact that the premature deactivation of the excited state of the dye, due to the involvement of any unwanted deactivation pathway, such as quenching due to aggregate formation, is at the cost of the photoinjection process. In order to maximize the photoinjection electron transfer rate (k_{et}), the rate of other quenching processes has to minimized. In the present study, we have seen that the porphyrin molecules with long chains tend to aggregate more strongly in the monolayer, due to their conformational freedom, and considerable fluorescence quenching on quartz and SnO_2 surfaces is observed. Hence, it is quite obvious that the photocurrent quantum yield observed for the aggregated monolayer does not reflect the actual photoinjection capability of the model compounds, as the aggregation quenching process is competing with it. To obtain the independent photoinjection behaviour of the monolayers of all the model compounds, the removal of aggregate mediated quenching is necessary. Hence, the quantum yields of diluted monolayers of some of the model compounds were studied.

Dioleylphosphatidylcholine (DOPC), a non fluorophor, surface active lipid, was used to dilute the monolayers. DOPC acts as a blocking molecule and helps the porphyrin rings to separate from each other and deaggregate in the monolayer. An increase in the fluorescence lifetime by diluting the monolayer of P-A, using DOPC has been reported earlier by Dick *et al.*[54] They have reasoned that the increase of the fluorescence lifetime is due to the decrease in the quenching rate, in the absence of fluorophor aggregation. Hence, in the present case it is expected that the fluorescence lifetime of the porphyrin molecules will increase, due to the decrease in

the quenching rate and will show an enhanced photocurrent yield. Table 5.4 summarizes the estimated photocurrent quantum yields of P-A, P-Pr-A, P-Ace-A and P-Gly-A in the presence (0:100) 0%, (1:9) 10%, (3:7) 30% and (1:1) 50% molar ratio of DOPC and porphyrin mixture embedded in the monolayer.

From Table 5.4 and Figures 5.20 and 5.21, it is evident that P-A, P-Pr-A P-Ace-A and P-Gly-A show almost identical effects under dilution, that is, a steady increase in the photocurrent quantum yield is observed. At a higher dilution, the photocurrent yield virtually levels off, indicating the presence of a monomer conformation of the molecules in the monolayer and the absence of any form of aggregation in the system. This clearly shows that in the presence of DOPC, photoinjection kinetics dominates over other quenching process. Under high dilution, the aggregation quenching effect virtually is minimized, and there is no effective competition against the photoinjection process. Hence, the excited singlet state effectively contributes to the photoinjection kinetics, which results in a higher photocurrent quantum yield. Similar effects were observed by Grätzel *et al.*,[41] using cholanic acid as the diluting agent. They observed a significant improvement in the photocurrent yield of copper chlorophyll sensitized TiO_2 solar cells on dilution of the monolayer. Therefore, it is concluded that the presence of aggregation decreases the photocurrent quantum yield uniformly for all four compounds (i.e., P-A, P-Pr-A, P-Et-A and P-Gly-A) under study.

P-Pr-A, which possess the maximum aggregated conformation in the monolayer among all the compounds of Series-I (Figure 1.1), shows a significant increase in the photocurrent yield on a small dilution of its monolayer (Figure 5.20).

Table 5.4: Effect of monolayer dilution on photocurrent yield (ϕ_{PC}), using 10%, 30%, and 50% DOPC. Electrolyte composition: 0.25 KH_2PO_4, 0.5 M NaCl, 0.1 M Na_2SO_4, 1 M TU at pH = 2.0 and at 22 ± 2°C.

Compounds	ϕ_{PC} (0% DOPC)	ϕ_{PC} (10% DOPC)	ϕ_{PC} (% Change)
P-A	0.33	0.35	6
P-Pr-A	0.21	0.23	10
P-Ace-A	0.27	0.29	7
P-Gly-A	0.27	0.29	7
Compounds	ϕ_{PC} (0% DOPC)	ϕ_{PC} (30% DOPC)	ϕ_{PC} (% Change)
P-A	0.33	0.37	12
P-Pr-A	0.21	0.25	19
P-Ace-A	0.27	0.32	19
P-Gly-A	0.27	0.31	15
Compounds	ϕ_{PC} (0% DOPC)	ϕ_{PC} (50% DOPC)	ϕ_{PC} (% Change)
P-A	0.33	0.38	15
P-Pr-A	0.21	0.26	24
P-Ace-A	0.27	0.33	22
P-Gly-A	0.27	0.32	19

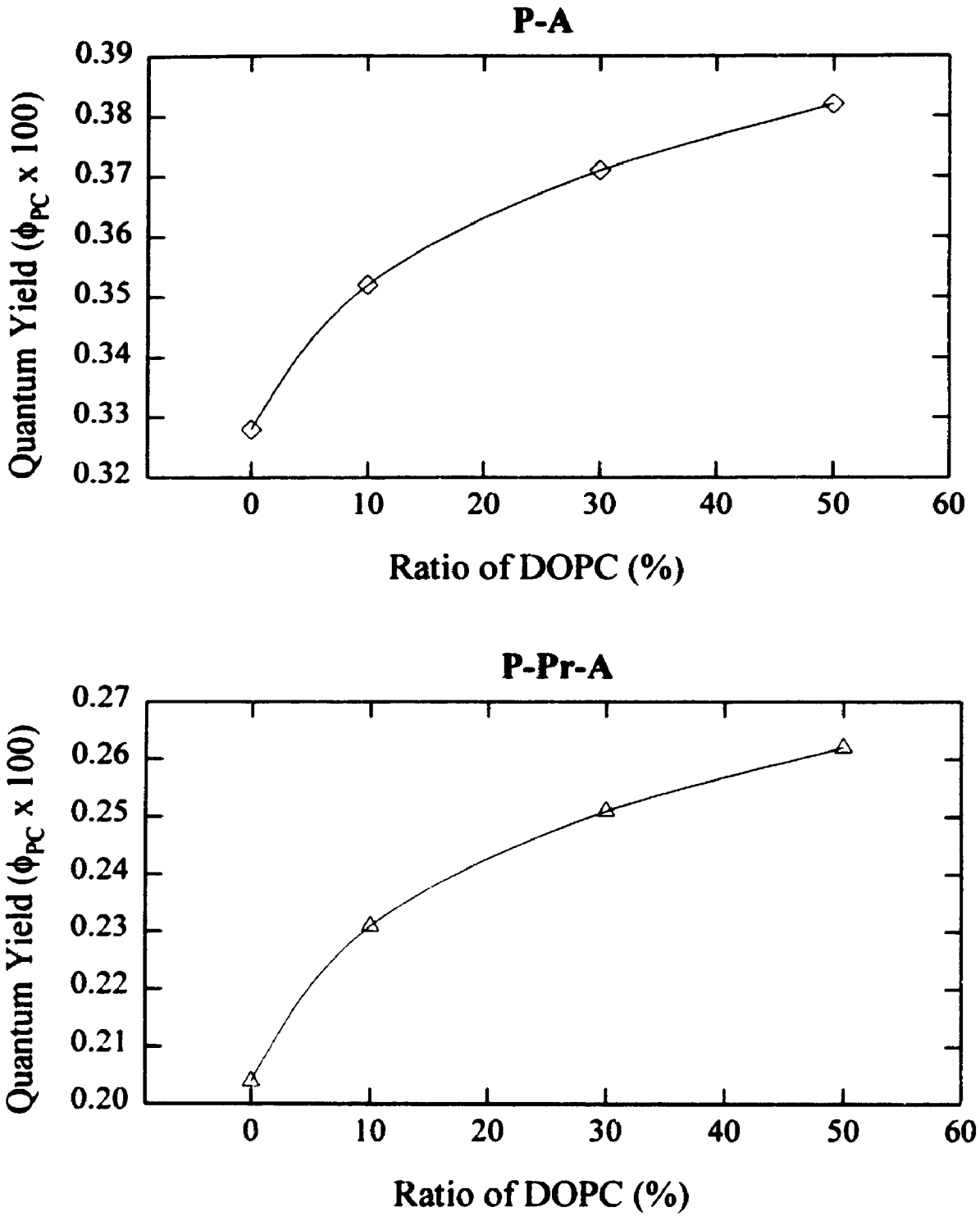

Figure 5.20 : Effect of monolayer deaggregation on photocurrent quantum yield. Electrolyte composition: 0.25 M KH_2PO_4, 0.5 M NaCl, 1 M TU, 0.1 M Na_2SO_3. Measurements were made at $\lambda = 432 \pm 10$ nm and at 22 ± 2^0C.

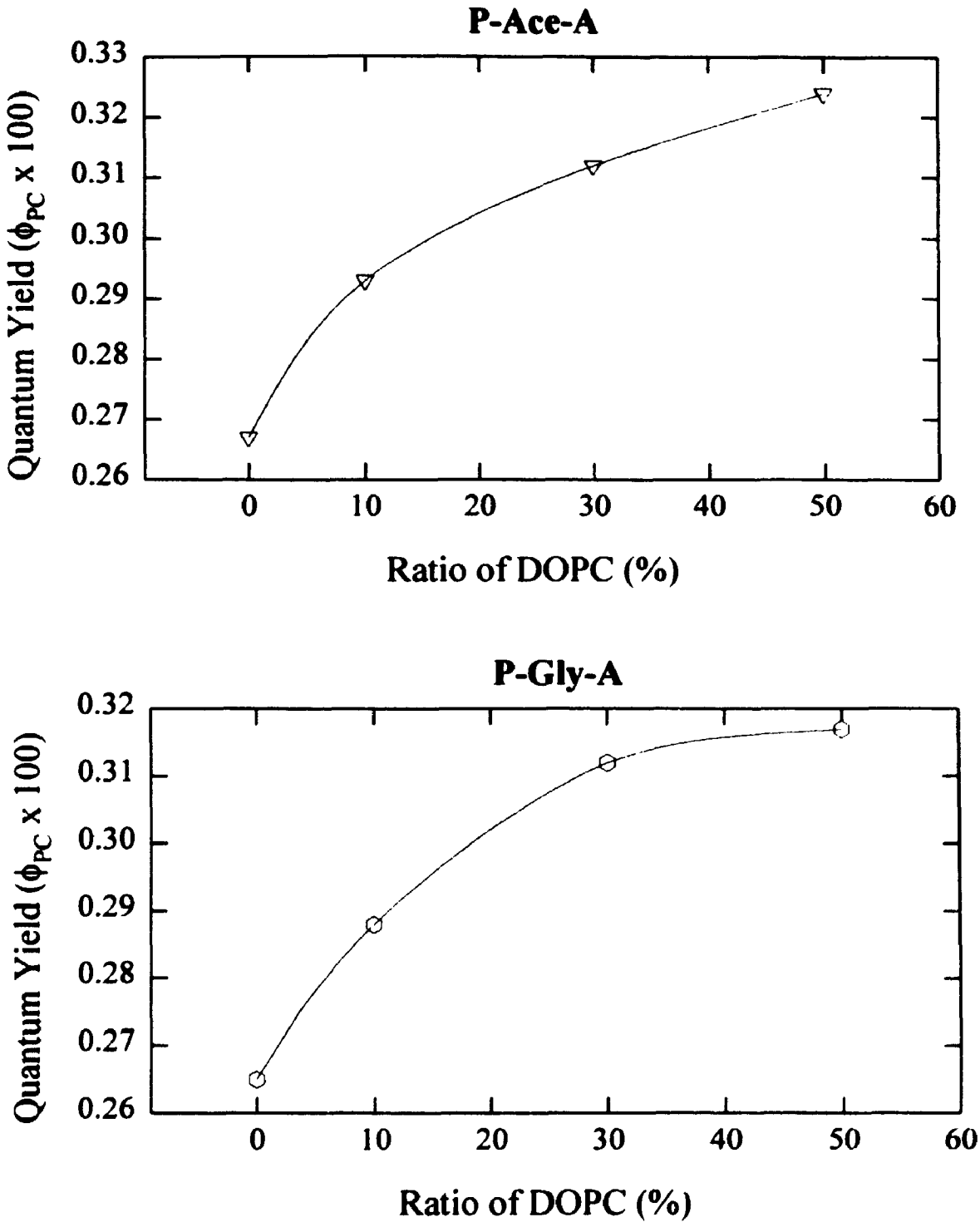

Figure 5.21 : Effect of monolayer deaggregation on photocurrent quantum yield. Electrolyte composition: 0.25 M KH_2PO_4, 0.5 M NaCl, 1 M TU, 0.1 M Na_2SO_3. Measurements were made at $\lambda = 432 \pm 10$ nm and at 22 ± 2^0C.

Almost a 10% increase in the photocurrent yield was observed by diluting the monolayer by a factor of only 10%. This shows that in this case, quenching due to aggregation is an effective competent of the photoinjection process and its decrease helps to increase the injection kinetics. As we go to higher dilution of the monolayer of P-A and P-Pr-A, the photocurrent yield is increased and almost a 24% increase for 50% dilution was observed in the case of P-Pr-A. For P-A a 50% dilution increased the photocurrent yield by only 15%. This shows that P-Pr-A being more aggregated system, experiences a larger change as compared to P-A. Hence, it can be seen that the aggregate initiated quenching is a serious drawback in the dye sensitization process and its minimization is an important requirement for increasing the efficiency of dye sensitized photoelectrochemical cells.

Interestingly both P-Ace-A and P-Gly-A show an increase of ~7% in photocurrent yield on 10% dilution. A large increase in the photocurrent yield on dilution was expected for P-Gly-A, as it possesses the maximum aggregated conformation among all the compounds studied and hence suffers the maximum aggregated mediated quenching. An explanation may be that in P-Ace-A, due to the presence of a triple bond, it possess a better electron injection capability than P-Gly-A and efficiently competes with P-Gly-A. Hence, it shows a similar increase as P-Gly-A on 10% dilution. The better electron injection capability of P-Ace-A, due to the triple bond, is obvious from the photocurrent yields observed at higher dilutions. Both under 30% and 50% dilution, it shows a higher effect as compared to P-Gly-A. Hence, it was concluded that the presence of triple bond in the chain (as in P-Ace-A) makes the compound a better sensitizer than the presence of a mobile lone pair of

electron (as in P-Gly-A) in the central part of the chain.

Therefore from all the obtained results (Table 5.4), it is obvious that the dilution of the monolayer did not have a large effect on the photocurrent quantum yield (only 24% increase at most on 50% dilution). This may be due to the fact that the aggregate formation, although contributing somewhat to the quenching, is not the dominant factor in the present model compounds. The nature of the electronic environment of the side chain seems to be the dominant factor for the photoinjection process in the present model compounds.

REFERENCES

1. For a review, see: (a) Dolphin, D., ed. *The Porphyrins*; Academic Press: New York, **1978**; Vol. I-VII. (b) Gouterman, M.; Rentzepis, P. M.; Straub, K. D., eds. *Porphyrins, Excited States and Dynamics*, ACS Symposium Series 321; American Chemical Society: Washington, D. C., **1986**.

2. For a review, see: Moser, F. H.; Thomas, A. C. *The Phthalocyanines*; CRC Press: Florida; **1983**; Vols. I and II.

3. (a) Hopf, F. R.; Whitten, D. G. In Reference 1a, Vol. II. (b) Felton, R. H. In reference 1a, Vol III. (c) Davis, D. G. In reference 1a, Vol. III. (d) Loutfy, R. O.; Hsiao, C. K.; Ho, R. *Can. J. Phys.* **1983**, *61*, 1416. (e) Menzel, E. R.; Loutfy, R. O. *Chem. Phys. Lett.* **1980**, *72*, 522. (f) Yamashita, K.; Harima, Y.; Iwashima, H. J. *J. Phys. Chem.* **1987**, *91*, 3055. (g) Kampas, F. J.; Gouterman M. *J. Phys. Chem.* **1977**, *81*, 690. (h) Stanberry, B. J.; Gouterman, M.; Burgess, R. M. *J. Phys. Chem.* **1985**, *89*, 4950. (i) Tanimura, K.; Kawai, T.; Sakata, T. *J. Phys. Chem.* **1980**, *84*, 751. (j) Wang, J. H. *Proc. Natl. Acad. Sci.* **1969**, *62*, 653. (k) Harima, K.; Yamashita, K. *J. Phys. Chem.* **1985**, *89*, 5325. (l) Panayotatos, P.; Parikh, D.; Sauers, R.; Bird, G.; Piechowski, A.; Husain, S. *Solar Cells*, **1986**, *18*, 71. (m) Tollin, G.; Kearns, D. R.; Calvin, M. *J. Chem. Phys.* **1960**, *32*, 1013. (n) Fan, F. -R.; Faulkner, L. R. *J. Chem. Phys.* **1978**, *69*, 3334. (o) Fan, F. -R.; Faulkner, L. R. *J. Chem. Phys.* **1978**, *69*, 3341. (p) Loutfy, R. O.; Sharp, J. H.; Hsiao, C. K.; Ho, R. *J. Appl. Phys.* **1981**, *52*, 5218. (q) Loutfy, R. O.; Sharp, J. H. *J. Chem. Phys.* **1979**, *71*, 1211. (r) Loutfy, R. O.; Hsiao, C. K. *Can. J. Phys.* **1981**, *59*, 727. (s) Tang, C. W.;

Albrecht, A. C. *J. Chem. Phys.* **1975**, *62*, 2139. (t) Ghosh, A. K.; Morel, D. L.; Feng, T.; Shaw, R. F.; Rowe, C. A. *J. Appl. Phys.* **1974**, *45*, 230.

4. (a) Jaeger, C. D.; Fan, F. -R. F.; Bard, A. J. *J. Am. Chem. Soc.* **1980**, *102*, 2592. (b) Giraudeau, A.; Fan, F. -R. F.; Bard, A. J. *J. Am. Chem. Soc.* **1980**, *102*, 5137. (c) Buttner, W. J.; Riecke, P. C.; Armstrong, N. R. *J. Phys. Chem.* **1985**, *89*, 1116. (d) Buttner, W. J.; Riecke, P. C.; Armstrong, N. R. *J. Am. Chem. Soc.* **1985**, *107*, 3738. (e) Inganas, O.; Lundstrom, I. *J. Appl. Phys.* **1983**, *54*, 4185. (f) Leempoel, P.; Fan, F. -R. F.; Bard, A. J. *J. Phys. Chem.* **1983**, *87*, 2948. (g) Klofta, T. J.; Danziger, J.; Lee, P.; Pankow, J.; Nebesny, K. W.; Armstrong, N. R. *J. Phys. Chem.* **1987**, *91*, 5646. (h) Fan, F. -R. F.; Faulkner, L. R. *J. Am. Chem. Soc.* **1979**, *101*, 4779. (i) Loutfy, R. O., McIntyre, L. F. *Can. J. Chem.* **1983**, *61*, 72. (j) Kearns, D. R.; Tollin, G.; Calvin, M. *J. Chem. Phys.* **1960**, *32*, 1020. (k) Klofta, T. J.; Rieke, P. C.; Linkous, C. A.; Buttner, W. J.; Nanthakumar, A.; Mewborn, T. D.; Armstrong, N. R. *J. Electrochem. Soc.* **1985**, *132*, 2134. (l) Kampas, F. J.; Yamashita, K.; Fajer, J. *Nature* **1980**, *284*, 40.

5. (a) Hackett, C. F. *J. Chem. Phys.* **1971**, *55*, 3178. (b) Meier, H.; Albrecht, W. *Ber. Bunsenges. Phys. Chem.* **1969**, *73*, 86. (c) Law, K. Y. *J. Phys. Chem.* **1988**, *92*, 4226.

6. (a) Fujishima, A.; Honda, K. *Bull. Chem. Soc. Jpn.* **1971**, *44*, 1148. (b) Fujishima, A.; Honda, K. *Nature* **1972**, *238*, 37.

7. (a) Myamlin, V. A.; Pleskov, Y. V. *Electrochemistry of semiconductors*, Plenum Press, New York, 1967. (b) Morrison, S. R. *Electrochemistry at Semiconductor and Oxidized Metal Electrodes*, Plenum Press, New York, 1980. (c) Green, M. In *Modern aspects of Electrochemistry*, Bockris, J. O'M. (ed), Vol II, Butterworth: London, **1959**, 343. (d) Dewald, J. F. In *Semiconductors*, Hannay, N. B. (ed.), Rheinhold: New York, **1960**, 727. (e) Gerischer, H. In *Physical Chemistry: An Advanced Treatise*, Eyring, H.; Henderson, D.; Jost, W. (eds.), Vol. IXA, Academic Press, New York, **1970**, 463. (f) Memming, R. In *Electroanalytical Chemistry*, Bard, A. J. (ed.), Vol. II, Marcel Dekker, New York, **1979**, 1. (g) Sze, S. M. *Physics of Semiconductor Devices*, 2nd ed., John Wiley & Sons: New York, **1981**.

8. Gutmann, F.; Lyons, L. E. *Organic Semiconductors*, Wiley, New York, **1967**.

9. Bolton, J. R. *Science* **1978**, *202*, 705.

10. Dare-Edwards, P. M.; Goodenough, J. B.; Hamnet, A.; Seddon, K. R.; Wright, D. R. *Faraday Discussions of the Chemical Society* **1980**, #70, 285.

11. Tributsch, H.; Gerischer, H. *Ber. Bunsenges. Phys. Chem.* **1969**, *73*, 251.

12. Memming, F. S.; Bringmann, U. *J. Electroanal. Chem.* **1979**, *100*, 307.

13. Kuhn, H. *Pure Appl. Chem.* **1979**, *51*, 341.

14. Kuhn, H. *J. Phys. Chem.* **1970**, *53*, 101

15. Bradwell, J. A. *Ph.D. Dissertation*, The University of Western Ontario, London, Ontario, **1982**, 63.

16. McTigue, P.; Farrell, J. *J. Electroanal. Chem.* **1982**, *37*, 139.

17. Ioffe, A. F. *Physics of Semiconductors*; Academic Press: New York, **1960**, 125.

18. (a) Erdey-Gruz, T. *Kinetics of Electrode Processes*, Akademiai Kiodo, Budapest: **1972**. (b) Gerischer, H.; Kolb, D.; Sass, J. K. *Adv. Phys.* **1978**, *27*, 437. (c) Vijh, K. A. *Electrochemistry of Metals and Semiconductors*, Marcel Dekker: New York, **1973**.

19. (a) Brattain, W. H.; Garret, C. G. B. *Bell. Syst. Tech. J.* **1955**, *34*, 129. (b) Brattain, W. H.; Garret, C. G. B. *Phys. Rev.* **1955**, *99*, 376.

20. Bolton, J. R.; Archer, M. D. *Photoconversion of Solar Energy*, section C.5.6; John Wiley & Sons. to be published.

21. Bockris, J. O'M.; Reddy, A. K. N. *Modern Electrochemistry*; Plenum Publishing Co.: New York, **1977**, 623.

22. Bulkowski, J. E. *Report 1983 from Energy Res. Abstr.* **1984**, *9*, #22, Abstract #45717.

23. (a) Ref. 7e. (b) Khan, S. U. M.; Bockris, J. O'M. *J. Phys. Chem.* **1983**, *87*, 2599.

24. Blok, L.; De Bruyn, P. L. *J. Coll. Interf. Sci.* **1970**, *32*, 518.

25. Gerischer, H. *Top. Appl. Phys.* **1977**, *31*. 115.

26. Memming, R. *Ber. Busenges. Phys. Chem.* **1987**, *91*, 353.

27. Lewis, N. S. *Annu. Rev. Mater. Sci.* **1984**, *14*, 95.

28. Honda, K.; Nakao, M.; Itoh, K.; Watanabe, T. *Ber. Busenges. Phys. Chem.* **1985**, *89*, 134.

29. (a) Memming, R. *Progress in Surface Chemistry* **1984**, *17*, 7. (b) Gerischer, H.; Michael-Beyerle, M. E.; Rebentrost, F.; Tributsch, H. *Electrochem. Acta* **1968**,

13, 1509. (c) Miyasaka, T.; Watanabe, T. Fujishima, A.; Honda, K. *J. Am. Chem. Soc.* **1978**, *100*, 6657.

30. Watanabe, T.; Fujishima, A.; Tatsuoki, O.; Honda, K. *Bull. Chem. Soc. Jpn.* **1976**, *49*, 8.

31. Regan, B. O.; Grätzel, M. *Nature* **1991**, *353*, 737.

32. Grätzel, M.; Kalyanasundaram, K. *Photosensitization and Photocatalysis Using Inorganic and Organometallic Compounds*, Kluwer Academic Press: Dordrecht, Netherlands, **1993**.

33. Frippiat, A.; Kirsch-De MesMaeker, A. *J. Electrochem. Soc.* **1987**, *134*, 66.

34. (a) Fromhertz, P.; Arden, W. *J. Am. Chem. Soc.* **1980**, *102*, 6211. (b) Fromhertz, P.; Arden, W. *J. Electrochem. Soc.* **1980**, *127*, 370.

35. (a) Watanabe, T.; Fujishima, A.; Honda, K. In *Energy Resources Through Photochemistry and Catalysis*, Grätzel, M. (ed.), Academic Press: New York, **1983** and references therein. (b) Miyasaka, T.; Honda, H. In *Photoeffects at Semiconductor-Electrolyte Interfaces*, Nozik, A. J. (ed.), ACS Symposium Series **1981**, *146*, 231.

36. Matsumura, M.; Mitsuda, K.; Yoshizawa, N.; Tsubomura, H. *Bull. Chem. Soc. Jpn.* **1981**, *54*, 692.

37. Minami, N.; Ichimura, K. *J. Electroanal. Chem.* **1984**, *165*, 181.

38. Chandrasekaran, K.; Giannotti, C.; Monserrat, J.; Otruba, J. P.; Whitten., D. G. *J. Am. Chem. Soc.* **1982**, *104*, 6200.

39. Breddels, P. A.; Blasse, G. *J. Chem. Soc. Faraday Trans.* **1984**, *80*, 1053.

40. Biesmans, G.; Van der Auweraer, M.; Cathry, C.; Meerschaut, D.; De Schryver, F. C.; Strock, W.; Willig, F. *J. Phys. Chem.* **1991**, *95*, 3771.

41. Kay, A.; Grätzel, M. *J. Phys. Chem.* **1993**, *97*, 6272.

42. Armstrong, N. R.; Parkinson, B. A. (to be published, quoted in reference 41).

43. (a) Spitler, M. T.; Parkinson, B. A. *Langmuir* **1986**, *2*, 549. (b) Spitler, M. T. *J. Electroanal. Chem.* **1987**, *228*, 69. (c) Parkinson, B. A. *Langmuir*, **1988**, *4*, 967.

44. Haran, A.; Waldeck, D. H.; Naaman, R.; Moons, E.; Cahen, D. *Science* **1994**, *263*, 948.

45. (a) Newton, M. D. *Chem. Rev.* **1991**, *91*, 767. (b) Ratner, M. A. *J. Phys. Chem.* **1990**, *94*, 4877. (c) Jordan, K. D.; Paddon-Row, M. N. *Chem. Rev.* **1992**, *92*, 395.

46. Dick, H. A. *Ph.D. Dissertation*, The University of Western Ontario, London, Ontario, **1988**.

47. Sprunken, H. R.; Schumaker, R.; Schindler, R. N. *Ber. Bunsenges. Phys. Chem.* **1980**, *84*, 1040.

48. Davis, D. G. In *The Porphyrins*, Dolphin, D (ed.), Academic Press: New York, **1978**, 143.

49. Finklea, H. O. In *Semiconductor Electrodes*, Finklea, H. O. (ed.), Elsevier: Amsterdam, **1988**, 30.

50. Memming, R. *Progress in Surface Chemistry* **1984**, *17*, 55.

51. Clark, W. D. K.; Sutin, N. *J. Am. Chem. Soc.* **1977**, *99*, 4676.

52. Morrison, S. R. *Electrochemistry at Semiconductor and Oxidized Metal Electrodes*; Plenum Press: New York, **1980**, 158.

53. Bolton, J. R.; Clayton, R. K.; Reed, D. W. *J. Photochem. Photobiol.* **1969**, *9*, 209.

54. Dick, H. A.; Bolton, J. R.; Picard, G.; Munger, G.; Leblanc, R. M. *Langmuir* **1988**, *4*, 133.

CHAPTER 6

EXPERIMENTAL METHODS FOR SYNTHESIS OF MODEL COMPOUNDS

6.1 GENERAL

^{1}H-NMR spectra were recorded at 200 MHz in $CDCl_3$ or CD_3OD on Varian XL 200 or Varian Gemini 200 instruments, or at 300 MHz in $CDCl_3$ on a Varian Gemini 300 instrument. ^{13}C-NMR spectra in $CDCl_3$ were recorded on a Varian XL 300 (75 MHz) or a Varian Gemini 200 (50 MHz) instrument. Chemical shifts (δ) are given in ppm downfield from TMS (0.00 ppm). Data for ^{1}H-NMR spectra are reported as follows: δ (multiplicity, coupling constant(s) in Hz, assignment of proton(s), integration). Data for ^{13}C-NMR spectra are given as follows: δ (degree of substitution).

Infrared spectra (film or Nujol mull) were recorded on a Bruker IFS 32/IBM system 9000 FT-IR instrument; bands are stated in cm^{-1}. Melting points were determined on a Koffler hot stage melting point apparatus.

Ultraviolet absorption spectra in chloroform or dichloromethane were obtained on a Hewlett-Packard 8450A diode array spectrophotometer or a Shimadzu UV-160 spectrophotometer. Data are reported as follows: λ_{max} in nm (ϵ).

Gas chromatography coupled mass spectroscopy was performed using a Varian 3400 gc equipped with a 30 m DB-5 capillary column attached to a Finnegan MAT 8230 mass spectrometer. Conventional mass spectroscopy was performed using the same mass spectrometer. Ionization was achieved by electron impact (EI; 25 or 70

eV), by chemical ionization (isobutane; CI) or by fast atomic bombardment (FAB).

Analytical gas chromatography was performed on a Hewlett-Packard 5880 GC equipped with a 30 m DB-5 capillary column (He carrier). Flame ionization detectors were used.

All solvents and chemicals were commercially available and used without further purification, except where noted. Tetrahydrofuran for Grignard reagents and for other moisture sensitive reactions was dried by refluxing over and distilling from sodium metal and benzophenone under a nitrogen atmosphere. All anhydrous reactions were performed under a dry nitrogen atmosphere with all glassware being dried overnight in a drying oven at 150°C prior to use. Assembly of the dry reaction apparatus was conducted under a flow of dry nitrogen. The drying reagents were reagent grade potassium carbonate (K_2CO_3) or sodium sulphate (Na_2SO_4).

Absorbents free from fluorescing agents were used for thin layer chromatography (tlc) to prevent the absorption of the zinc fluorescor by free-base porphyrins. Mallinckrodt 60-200 mesh silica gel (zinc free) was used for column chromatography.

All the literature references have been numbered following the reference list given in Chapter 2.

6.2 PREPARATION OF P-A (1)

This compound was prepared using a published procedure.[1] A solution of p-carboxybenzaldehyde (12.052 g, 80 mmol) and p-tolualdehyde (28.844 g, 240 mmol) in propionic acid (600 mL) was heated to reflux. Distilled pyrrole (21.471 g, 320

mmol) was added to it. After refluxing for thirty minutes the heat source was removed and 300 mL of ethylene glycol was added to the reaction mixture. This solution was refrigerated overnight. The solid material which had precipitated was filtered off, washed with 1:1 methanol water mixture and dried to give 8.472 g of a dull purple solid. This mixture of porphyrins was separated by column chromatography using 70 g of silica gel. Elution with chloroform removed tetratolylporphyrin from the column. Changing the solvent composition to 4% methanol in chloroform caused a dark impurity band to elute from the column. This was followed by the desired compound, which was collected as a 1250 mL fraction. Solid TTPa (1) was obtained by removing the solvent using a rotory evaporator. The TTPa (1) obtained was purified again by column chromatography in order to remove any remaining tetratolylporphyrin. Finally 2.705 g (3.86 mmol, 4.8%) of TTPa (1) was obtained. The mass spectrum showed the expected parent ion at m/e = 700 and confirmed that the compound was free from contamination by any di, tri or tetra (4-carboxyphenyl) substituted porphyrins. Exact mass: observed 700.2834 amu, calculated for $C_{48}H_{36}N_4O_2$ 700.2838 amu.

^{1}H-NMR [$CDCl_3/CD_3OD$, 200 MHz, δ(ppm)]: 8.71-8.80 (broad singlet, β-pyrrole protons, 8H), 8.34 (doublet, J = 8 Hz, benzoyl aromatic protons closer to porphyrin ring, 2H), 8.18 (doublet, J = 8 Hz, benzoyl aromatic protons farther from porphyrin ring, 2H), 7.97 (doublet, J = 8.6 Hz, tolyl aromatic protons closer to porphyrin ring, 6H), 7.44 (doublet, J = 8.6 Hz, tolyl aromatic protons farther from porphyrin ring, 6H), 2.58 (singlet, tolyl methyl protons, 9H), -2.78 (broad singlet, pyrrole N-H, 2H). The carboxylic acid (-COOH) proton was not observed separately,

as it was hydrogen bonded with water contamination in the solvent and appeared at δ = 1.13.

IR (Nujol mull): 3314.0 cm^{-1} (O-H stretch)

1691.8 cm^{-1} (>C=O stretch)

1605.0 cm^{-1} (>C=C< stretch)

3312.4 cm^{-1} (pyrrole N-H stretch)

6.3 PREPARATION OF TTP-OH (2)

The compound was made by adaption of a procedure published by Nystrom and Brown.[3] Lithium aluminium hydride (LAH) (1.731 g, 45.65 mmol) was taken in 200 mL dry THF and stirred at 0°C. A solution of TTPa (1) (0.523g, 0.75 mmol) in 150 mL dry THF was added dropwise to the LAH suspension in 15 min., keeping the temperature around 0°C. During addition, the colour of the solution changed from purple to green. After stirring for 2 hours at room temperature the reaction was terminated via careful addition of 30 mL saturated NH_4Cl solution in water. The product was filtered off and the precipitate was washed with chloroform until the washings were no longer purple. The combined washings (800 mL) were evaporated to yield a purple coloured solid crude product (0.601 g).

The crude product was purified using column chromatography. A column was packed using 75 g of silica gel. Elution with 2% methanol in chloroform caused a purple band of TTP-OH (2) to elute from the column. The product was collected as a 1300 mL fraction. Solvent evaporation gave TTP-OH (2) (0.473 g, 0.69 mmol, 92%) as a purple coloured solid. A pure sample was obtained by recrystallisation

from chloroform/methanol, m.p. > 300°C. The expected molecular ion (m/e = 686) was observed in the mass spectrum. Exact mass: observed 686.3041 amu, calculated for $C_{48}H_{38}N_4O$ 686.3045 amu.

^{1}H-NMR [$CDCl_3$, 200 MHz, δ(ppm)]: 8.84 (singlet superimposed on a multiplet, J = 5 Hz, β-pyrrole protons, 8H), 8.19 (doublet, J = 8 Hz, benzyl aromatic protons closer to porphyrin ring, 2H), 8.08 (doublet, J = 8 Hz, tolyl aromatic protons closer to porphyrin ring, 6H), 7.73 (doublet, J = 8 Hz, benzyl aromatic protons farther from porphyrin ring, 2H), 7.54 (doublet, J = 8 Hz, tolyl aromatic protons farther from porphyrin ring, 6H), 5.05 (doublet, J = 4.8 Hz, methylene protons of benzyl group, 2H), 2.69 (singlet, tolyl methyl protons, 9H), -2.78 (broad singlet, pyrrole N-H, 2H). The hydroxyl (-O<u>H</u>) proton was not observed separately, as it was hydrogen bonded with water contamination in the solvent and appeared at δ = 1.54.

IR (Nujol Mull): 3314.1 cm^{-1} (O-H stretch)

6.4 PREPARATION OF TTP-Cl (<u>3</u>)

The standard procedure[4] for preparing aliphatic chlorides from aliphatic alcohols using thionyl chloride was followed. The standard procedure suggests that TTP-OH (<u>2</u>) should be refluxed with thionyl chloride in chloroform for a few hours, depending on the nature of the alcohol. Trial reactions indicated that such vigorous conditions are not necessary and in fact result in some chlorination of the porphyrin ring. Consequently TTP-OH (<u>2</u>) (0.224 g, 0.33 mmol) was taken in 200 mL chloroform and stirred at room temperature. Thionyl chloride (1.191 g, 10 mmol) was added dropwise at a very slow rate. The colour of the reaction mixture changed

from purple to green immediately. The progress of the reaction was monitored by tlc. After stirring for 12 hours at room temperature, the reaction was terminated by distilling out the solvent from the reaction mixture. Excess thionyl chloride was distilled out by forming the azeotrope with benzene. Protonated TTP-Cl was obtained as a blue-green solid after removing all solvent under reduced pressure. The solid mass was dissolved in chloroform (100 mL) to give a green solution. The chloroform solution was washed with water (2 × 50 mL) in order to deprotonate the porphyrin. When this was done, the green solution turned purple, which is characteristic of a free-base porphyrin. TTP-Cl (3) (0.211 g, 0.29 mmol, 91%) was obtained as a purple solid after solvent evaporation. The expected molecular ion (m/e = 704) was not observed in the mass spectra; instead a prominent peak at m/e = 670 was observed. This is ascribed to rapid loss of $Cl^{\bullet}$ from TTP-Cl (3) so that the highest mass ion observed corresponds to tetratolylporphyrin (TTP).

^{1}H-NMR [$CDCl_3$, 200 MHz, δ(ppm)]: 8.84 (singlet superimposed on multiplet, J = 4.6 Hz, β-pyrrole protons, 8H), 8.19 (doublet, J = 8.1 Hz, benzyl aromatic protons closer to porphyrin ring, 2H), 8.08 (doublet, J = 7.7 Hz, tolyl aromatic protons closer to porphyrin ring, 6H), 7.76 (doublet, J = 8.1 Hz, benzyl aromatic protons farther from porphyrin ring, 2H), 7.54 (doublet, J = 7.7 Hz, tolyl aromatic protons farther from porphyrin ring, 6H), 4.93 (singlet, methylene protons of benzyl chloride group, 2H), 2.69 (singlet, tolyl methyl protons, 9H), -2.81 (broad singlet, pyrrole N-H, 2H). UV ($CHCl_3$): 418(490000), 516(17100), 552(8600), 590(5300), 646(4300).

IR (Nujol Mull): 694 cm^{-1} (C-Cl stretch)

6.5 PREPARATION OF ZnTTP-Cl (4)

The preparation of this compound was adapted from a known procedure.[5] Zinc acetate dihydrate (0.108 g, 0.49 mmol) in 10 mL methanol was added to a solution of TTP-Cl (3) (0.226 g, 0.32 mmol) in 50 mL of chloroform. The reaction was monitored by absorption spectroscopy. Insertion of the zinc ion into the porphyrin ring was complete after stirring for 30 minutes at room temperature, as evidenced by the collapse of the four-banded spectrum characteristic of a free-base porphyrin into the two-banded spectrum characteristic of a metallated porphyrin. The solution was washed with water (3 × 50 mL). Occasionally an emulsion formed, together with precipitation of solid in the organic layer. In this case, addition of some methanol to the mixture dissolved the precipitated material and gave clean separation into two layers. Finally, the organic layer was dried over anhydrous sodium sulphate and evaporation of the solvent gave 0.254 g of a purple solid compound.

Purification of the recovered crude compound was done by flash chromatography on 5 g of silica gel, eluting with chloroform. Pure ZnTTP-Cl (4) (0.238 g, 0.31 mmol, 97%) was isolated as shiny pinkish purple solid, which gave a clean single spot on tlc. The expected molecular ion (m/e = 767) was not observed in the mass spectra; instead a highest mass ion with m/e = 732 was observed. This is assigned to loss of $Cl^{\bullet}$ from ZnTTP-Cl (4) so that an ion for zinc tetratolyl-porphyrin (ZnTTP) was observed.

^{1}H-NMR [$CDCl_3$, 200 MHz, δ(ppm)]: 8.91 (singlet superimposed on a multiplet, J = 4.6 Hz, β-pyrrole protons, 8H), 8.28 (doublet, J = 8 Hz, benzyl aromatic protons closer to porphyrin ring, 2H), 8.16 (doublet, J = 7.8 Hz, tolyl

aromatic protons closer to porphyrin ring, 6H), 7.82 (doublet, J = 8 Hz, benzyl aromatic protons farther from porphyrin ring, 2H), 7.60 (doublet, J = 7.8 Hz, tolyl aromatic protons farther from porphyrin ring, 6H), 4.98 (singlet, methylene protons of benzyl chloride group, 2H), 2.70 (singlet, tolyl methyl protons, 9H). No resonances due to pyrrole protons were observed at ~ -2.8 ppm, consistent with the insertion of a metal ion into the center of the porphyrin ring. UV ($CHCl_3$): 420(495000), 550(14900), 594(4300).

IR (Nujol Mull): 695 cm^{-1} (C-Cl stretch)

6.6 PREPARATION OF P-Me-A (7)

6.6.1 Preparation of ZnTTP-CN (5)

The published literature procedure[6] for the preparation of a cyanoporphyrin from the corresponding haloporphyrin was followed for the preparation of this compound. ZnTTP-Cl (0.258 g, 0.34 mmol) dissolved in 40 mL DMF was mixed with powdered sodium cyanide (0.452 g, 9.23 mmol) and heated at 80°C under a nitrogen atmosphere. The progress of the reaction was monitored by tlc. After 1 hour, the starting material disappeared. The reaction was terminated by pouring the mixture into 100 mL 2% aqueous HCl solution. The product was extracted with ether, washed with water (3 × 50 mL) and then dried over anhydrous sodium sulphate. Crude ZnTTP-CN (0.246 g), a shiny purple coloured solid was obtained by evaporating the solvent to dryness.

Crude ZnTTP-CN was purified by column chromatography on 70 g silica gel, using chloroform as eluting agent. A faint pink band eluted first and this was

assumed to be unreacted starting material. The desired product eluted from the column following the starting material. Solvent evaporation gave ZnTTP-CN (5) (0.212 g, 0.28 mmol, 83%) as a shiny pinkish purple solid. Demetallation of ZnTTP-CN (5) by 10% aqueous HCl solution gave TTP-CN, m.p > 300°C. The expected molecular ion (m/e = 695) was observed in mass spectrum of this compound. Exact mass: observed 695.3046 amu, calculated for $C_{49}H_{37}N_5$ 695.3048 amu.

For TTP-CN ^{1}H-NMR [$CDCl_3$, 200 MHz, δ(ppm)]: 8.88 (singlet superimposed on doublet, J = 5.4 Hz, β-pyrrole protons farther from benzyl aromatic ring, 6H), 8.78 (doublet, J = 5 Hz, β-pyrrole protons closer to benzyl aromatic ring, 2H), 8.24 (doublet, J = 8.1 Hz, benzyl aromatic protons closer to porphyrin ring, 2H), 8.10 (doublet, J = 7.9 Hz, tolyl aromatic protons closer to porphyrin ring, 6H), 7.72 (doublet, J = 8.1 Hz, benzyl aromatic protons farther from porphyrin ring, 2H), 7.56 (doublet, J = 7.9 Hz, tolyl aromatic protons farther from porphyrin ring, 6H), 4.12 (singlet, methylene protons of benzyl group, 2H), 2.71 (singlet, tolyl methyl protons, 9H), -2.81 (broad singlet, pyrrole N-H, 2H).

IR (Nujol Mull): 2253 cm^{-1} (C≡N stretch)

6.6.2 Preparation of P-Me-OMe (6)

ZnTTP-CN (5) was converted to P-Me-OMe (6) by methanolysis of the cyano-porphyrin according to literature procedures.[6a] Saturated methanolic HCl was generated by bubbling hydrochloric acid gas through ice cold methanol until the solution reached constant weight. ZnTTP-CN (5) (0.245 g, 0.32 mmol) was added to methanolic HCl and stirred at room temperature for 30 minutes to get a green

suspension. The mixture was set aside at room temperature for 16 days. It was then neutralised with 28% aqueous ammonia solution. The precipitated purple mass was dissolved in 150 mL chloroform. The solution was washed with 5% aqueous HCl solution (2 × 30 mL), saturated sodium bicarbonate solution (2 × 50 mL) and water (3 × 60 mL). The organic layer was dried over anhydrous sodium sulphate and solvent evaporation gave 0.237 g of purple solid compound. Upon purification by flash chromatography on 15 g silica gel using chloroform as eluting agent pure P-Me-OMe (6) (0.197, 0.27 mmol, 84%), m.p.> 300°C, was obtained. The expected parent mass ion (m/e = 728) was observed in the mass spectrum. Exact mass: observed 728.3027 amu, calculated for $C_{50}H_{40}N_4O_2$ 728.3051 amu.

^{1}H-NMR [$CDCl_3$, 200 MHz, δ(ppm)]: 8.85 (singlet superimposed on multiplet, J = 4.5 Hz, β-pyrrole protons, 8H), 8.16 (doublet, J = 7.9 Hz, benzyl aromatic protons closer to porphyrin ring, 2H), 8.08 (doublet, J = 8.1 Hz, tolyl aromatic protons closer to porphyrin ring, 6H), 7.65 (doublet, J = 7.9 Hz, benzyl aromatic protons farther from porphyrin ring, 2H), 7.54 (doublet, J = 8.1 Hz, tolyl aromatic protons farther from porphyrin ring, 6H), 3.97 (singlet, methylene protons of benzyl group, 2H), 3.87 (singlet, methyl protons of carbomethoxy group, 3H), 2.69 (singlet, tolyl methyl protons, 9H), -2.78 (broad singlet, pyrrole N-H, 2H).

IR (Nujol Mull): 1741.4 cm^{-1} (>C=O stretch).

6.6.3 Preparation of P-Me-A (7)

P-Me-A (7) was prepared from P-Me-OMe (6) by base hydrolysis of the carbomethoxy group. Aqueous sodium hydroxide solution (0.5 N), 15 mL was added

to a solution of P-Me-OMe (6) (0.279 g, 0.38 mmol) in 100 mL THF. The resulting mixture was refluxed at 85°C for 1 hour. The reaction mixture was acidified with 50 mL of 5% aqueous HCl solution and extracted with chloroform. The organic layer was washed with water (3 × 100 mL), dried over anhydrous sodium sulphate and evaporated to dryness to give 0.271 g of a purple solid compound.

The crude product was purified by column chromatography on 75 g of silica gel. Elution with chloroform removed a faint pink band of unreacted starting material. The desired product was eluted by changing the solvent composition to 10% methanol in chloroform. The compound was recrystallised from chloroform/ methanol to give pure P-Me-A (0.250 g, 0.35 mmol, 91%), m.p.> 300°C. The expected mass ion (m/e = 714) was observed in the mass spectrum. Exact mass: observed 714.2962 amu, calculated for $C_{49}H_{38}N_4O_2$ 714.2994 amu.

^{1}H-NMR [$CDCl_3$, 200 MHz, δ(ppm)]: 8.85 (singlet superimposed on multiplet, J = 2.6 Hz, β-pyrrole protons, 8H), 8.20 (doublet, J = 8 Hz, benzyl aromatic protons closer to porphyrin ring, 2H), 8.09 (doublet, J = 7.9 Hz, tolyl aromatic protons closer to porphyrin ring, 6H), 7.70 (doublet, J = 8 Hz, benzyl aromatic protons farther from porphyrin ring, 2H), 7.55 (doublet, J = 7.9 Hz, tolyl aromatic protons farther from porphyrin ring, 6H), 4.04 (singlet, methylene protons of benzyl group, 2H), 2.71 (singlet, tolyl methyl protons, 9H), -2.81 (broad singlet, pyrrole N-H, 2H). The carboxylic acid (-COOH) proton was not observed separately, as it was hydrogen bonded with the water contamination in the solvent and appeared at δ = 1.17.

IR (Nujol Mull): 3421.6 cm^{-1} (O-H stretch)

1689.5 cm^{-1} (>C=O stretch)

6.7 PREPARATION OF P-Et-A (9)

6.7.1 Preparation of P-Et-OEt (8)

A published procedure[9] for the preparation of diethyl benzyl malonate from benzyl chloride was followed for the preparation of this compound. In the present synthesis benzyl chloride was replaced with TTP-Cl (3). Sodium ethoxide was prepared by addition of 77 mg (3.34 mmol) of sodium to 4 mL of absolute ethanol. Diethyl malonate (0.585 g, 3.65 mmol) dissolved in 5 mL dry THF was added dropwise with stirring to the sodium ethoxide solution in order to generate diethyl sodiomalonate. TTP-Cl (3) (0.181 g, 0.26 mmol) dissolved in 50 mL dry THF was added to the diethyl sodiomalonate. The mixture was refluxed at 90°C for 2 hours under a nitrogen atmosphere. After this time, analytical tlc indicated complete disappearance of the starting material. The reaction was terminated by adding 50 mL water followed by 100 mL chloroform. The organic layer was washed with saturated sodium bicarbonate solution (2 × 20 mL), water (2 × 30 mL) and then dried over anhydrous sodium sulphate. 0.214 g of crude product was obtained by evaporating the solvent to dryness.

The product was purified by column chromatography on 78 g silica gel using chloroform as eluting solvent. A very small amount of unreacted TTP-Cl (3) eluted as a faint pink band. The desired product eluted as a dark band when the solvent composition was changed to 3% methanol in chloroform. Pure P-Et-OEt (8) (0.191 g, 0.23 mmol, 89%), mp > 300°C, was obtained as a purple solid by evaporating the solvent to dryness. The expected molecular ion (m/e = 828) was observed in the mass spectrum. Exact mass: observed 828.3605 amu, calculated for $C_{55}H_{48}N_4O_4$

828.3675 amu.

^{1}H-NMR [$CDCl_3$, 300 MHz, δ(ppm)]: 8.85 (singlet superimposed on doublet, J = 4.6 Hz, β-pyrrole protons farther from benzyl aromatic ring, 6H), 8.78 (doublet, J = 4.6 Hz, β-pyrrole protons closer to benzyl aromatic ring, 2H), 8.12 (doublet, J = 8.1 Hz, benzyl aromatic protons closer to porphyrin ring, 2H), 8.08 (doublet, J = 8.1 Hz, tolyl aromatic protons closer to porphyrin ring, 6H), 7.58 (doublet, J = 8.1 Hz, benzyl aromatic protons farther from porphyrin ring, 2H), 7.54 (doublet, J = 8.1 Hz, tolyl aromatic protons farther from porphyrin ring, 6H), 4.31 (quartet, J = 7 Hz, ester methylene protons of diethyl malonate group, 4H), 3.96 (triplet, J = 7.8 Hz, methine proton of diethyl malonate group, 1H), 3.56 (doublet, J = 7.8 Hz, methylene protons of benzyl group, 2H), 2.69 (singlet, tolyl methyl protons, 9H), 1.35 (triplet, J = 7 Hz, ester methyl protons of diethyl malonate group, 6H).

IR (Nujol Mull): 1688.6 cm^{-1} (>C=O stretch)

1150.4 cm^{-1} (C-O stretch)

6.7.2 Preparation of P-Et-A (9)

The preparation of this compound was adapted from the standard literature procedure[10] for malonate hydrolysis and decarboxylation. P-Et-OET (8) was converted to the corresponding diacid by base hydrolysis. P-Et-OEt (8) (0.144 g, 0.17 mmol) was dissolved in 30 mL THF and mixed with 10 mL aqueous sodium hydroxide (0.5 N) solution. This mixture was refluxed at 85°C for 2 hours. A purple solid mass separated during the reaction. After cooling to room temperature 100 mL of 5% aqueous hydrochloric acid solution was added and the product was extracted

with chloroform. The organic layer was washed with water (3 × 50 mL), dried over anhydrous sodium sulphate and evaporated to dryness to yield porphyrin diacid (0.106 g) as a purple solid.

The porphyrin diacid (0.106 g) was dissolved in 50 mL glacial acetic acid and heated at 100°C for 1 hour. The mixture was then cooled and added to 100 mL chloroform. The solution was washed with water (5 × 100 mL), dried over anhydrous sodium sulphate and evaporated to give 0.102 g of purple crystals. The product was purified on 70 g silica gel using chloroform as eluting solvent. The desired product eluted as a dark band using a solvent composition of 10% methanol in chloroform. Evaporation of solvent yielded P-Et-A (9) (0.080 g, 0.11 mmol, 65%), mp > 325°C, as a purple fine crystalline solid.

The expected parent mass ion (m/e = 728) was seen in the mass spectrum. Exact mass: observed 728.3051 amu, calculated for $C_{50}H_{40}N_4O_2$ 728.3056 amu. The ^{1}H-NMR spectrum of P-Et-A (9) could not be obtained due to its poor solubility in all solvents examined.

IR (Nujol Mull): 3421.9 cm^{-1} (O-H stretch)

1689.5 cm^{-1} (>C=O stretch)

6.8 PREPARATION OF P-Gly-A (11)

6.8.1 Preparation of P-Gly-OMe (10)

Methyl glycinate was generated by bubbling anhydrous ammonia through an ice-cold suspension of the hydrochloride salt (2.530 g, 20.16 mmol) in 60 mL dichloromethane. The organic layer was filtered to remove precipitated NH_4Cl,

washed with water (2 × 50 mL) and then dried over anhydrous sodium sulphate. Evaporation of the solvent gave methyl glycinate (1.612 g, 18.11 mmol) as a colourless oily liquid. TTP-Cl (3) (0.279 g, 0.40 mmol) was dissolved in 25 mL chloroform and added to the solution of methyl glycinate. Silver nitrate (0.327 g, 1.92 mmol) was added to the reaction mixture and it was refluxed at 55°C for 20 hours. The progress of the reaction was monitored by analytical tlc. The reaction mixture was diluted with chloroform, washed with 10% HCl solution (2 × 20 mL) and water (3 × 50 mL), then dried over anhydrous sodium sulphate. Upon evaporation of the solvent the crude product (0.189 g) was obtained as a purple coloured solid. The product was separated from by-products by column chromatography using 70 g silica gel. Elution with chloroform removed unreacted TTP-Cl (3) from the column followed by the desired product, which was collected as a 200 mL fraction. Evaporating the solvent under reduced pressure gave pure P-Gly-OMe (10) (0.092 g, 0.122 mmol 30%), mp > 300°C, which was obtained as a purple coloured solid. The expected molecular ion (m/e = 757) was observed in the mass spectrum. Exact mass: observed 757.3424 amu, calculated for $C_{51}H_{43}N_5O_2$ 757.3416 amu.

^{1}H-NMR [$CDCl_3$, 200 MHz, δ(ppm)]: 8.85 (singlet superimposed on multiplet, J = 4.4 Hz, β-pyrrole protons, 8H), 8.17 (doublet, J = 7.9 Hz, benzyl aromatic protons closer to porphyrin ring, 2H), 8.09 (doublet, J = 7.8 Hz, tolyl aromatic protons closer to porphyrin ring, 6H), 7.69 (doublet, J = 7.9 Hz, benzyl aromatic protons farther from porphyrin ring, 2H), 7.54 (doublet, J = 7.8 Hz, tolyl aromatic protons farther from porphyrin ring, 6H), 4.14 (singlet, methylene protons of benzyl group, 2H), 3.91 (multiplet, J = 4 Hz, secondary N-H proton of methyl glycine chain,

1H), 3.83 (singlet, methyl ester protons, 3H), 3.67 (singlet, glycyl methylene protons, 2H), 2.69 (singlet, tolyl methyl protons, 9H), -2.79 (broad singlet, pyrrole N-H, 2H).

IR (Nujol Mull): 3316.0 cm^{-1} (secondary >N-H stretch)

1741.9 cm^{-1} (>C=O stretch)

6.8.2 Preparation of P-Gly-A (11)

P-Gly-OMe (10) was converted to P-Gly-A (11) by base hydrolysis of the carbomethoxy group. A solution of P-Gly-OMe (10) (0.088 g, 0.12 mmol) in 20 mL THF was mixed with 15 mL of aqueous sodium hydroxide (0.5 N) solution. A small amount of water (10 mL) was also added. The reaction mixture was boiled on a steam bath for 15 minutes and deposition of P-Gly-A (11) as a purple precipitate was observed.

The reaction mixture was acidified with 25 mL of aqueous 5% HCl. The product was extracted using chloroform, and the extract was washed with water (3 × 50 mL) and dried over anhydrous sodium sulphate. Upon evaporation of the solvent the crude product (0.074 g) was obtained as a purple solid. P-Gly-A (11) was purified by column chromatography using 75 g of silica gel. Elution with chloroform yielded unreacted P-Gly-OMe (10). Changing the solvent composition to 30% methanol in chloroform resulted in elution of P-Gly-A (11) (0.057 g, 0.08 mmol, 64%).

The ^{1}H-NMR spectrum of P-Gly-A (11) could not be obtained due to its poor solubility in all solvents examined. In addition, the expected molecular ion (m/e = 743) was not obtained in the mass spectrum. A mass ion at m/e = 699 appeared in

the spectra, which is 44 mass units less than the molecular mass of P-Gly-A (11). The loss of 44 mass units suggests the loss of CO_2 from the carboxylic acid group.

IR (Nujol Mull): 3422.1 cm^{-1} (O-H stretch)

1689.2 cm^{-1} (>C=O stretch)

6.9 PREPARATION OF TTP-Br (12)

The preparation of TTP-Br (12) from TTP-OH (2) was adapted from the standard literature procedure.[12] Thionyl bromide (1.342 g, 6.46 mmol) was added dropwise to a solution of TTP-OH (2) (0.124 g, 0.18 mmol) in 80 mL chloroform. The solution turned green immediately. The flask was covered with aluminium foil to prevent any light initiated side reaction by HBr, which is the reaction by-product. Progress of the reaction was monitored by tlc and after stirring for 12 hours at room temperature no sign of TTP-OH (2) was found. The reaction was terminated by evaporating the solvent to dryness on a rotory evaporator. A green coloured solid mass was obtained.

The green solid was dissolved in 100 mL chloroform and washed with saturated sodium bicarbonate solution (2 x 20 mL), water (3 x 50 mL) and then dried over anhydrous sodium sulphate. The crude product (0.131 g), a purple coloured solid, was obtained by evaporating the solvent. Purification of the crude product was carried out by flash chromatography on 10 g silica gel using chloroform as eluting solvent. Solvent evaporation gave pure TTP-Br (12) (0.127 g, 0.17 mmol, 94%) as a shiny purple coloured solid. The expected molecular ion (m/e = 748) was not observed in mass spectra; instead a prominent peak with m/e = 670 was observed.

This is assigned to the loss of Br$^{\bullet}$ from TTP-Br (12).

^{1}H-NMR [$CDCl_3$, 200 MHz, δ(ppm)]: 8.86 (singlet superimposed on multiplet, J = 5 Hz, β-pyrrole protons, 8H), 8.18 (doublet, J = 8.2 Hz, benzyl aromatic protons closer to porphyrin ring, 2H), 8.09 (doublet, J = 7.9 Hz, tolyl aromatic protons closer to porphyrin ring, 6H), 7.75 (doublet, J = 8.2 Hz, benzyl aromatic protons farther from porphyrin ring, 2H), 7.54 (doublet, J = 7.9 Hz, tolyl aromatic protons farther from porphyrin ring, 6H), 4.82 (singlet, methylene protons of benzyl group, 2H), 2.70 (singlet, tolyl methyl protons, 9H), -2.77 (broad singlet, pyrrole N-H, 2H). ^{13}C-NMR [$CDCl_3$, 50 MHz, δ(ppm)]: 143.4, 140.1, 138.2, 138.1, 131.9 (broad), 121.3, 121.1, 119.7 (aromatic C), 135.8, 135.4, 128.3 (aromatic CH), 30.6 (CH_2), 22.4 (tolyl CH_3). UV($CHCl_3$): 418(510000), 517(17100), 551(8700), 592(5300), 643(4300).

IR (Nujol Mull): 551 cm^{-1} (C-Br stretch)

6.10 PREPARATION OF ZnTTP-Br (13)

Preparation of this compound was performed following the synthetic procedure used for the preparation of ZnTTP-Cl (4).[5] TTP-Br (12) (0.129 g, 0.17 mmol) was dissolved in 50 mL chloroform and a solution of zinc acetate dihydrate (0.117 g, 0.53 mmol) in 10 mL methanol was added. The progress of the reaction was monitored by visible absorption spectroscopy. After stirring for 30 minutes at room temperature insertion of the zinc ion into the porphyrin ring was complete. This was confirmed by the collapse of the four-banded spectrum, characteristic of a free-base porphyrin into the two-banded spectrum characteristic of a metallated porphyrin. The solution was diluted with chloroform and washed with water (3 × 50

mL). Occasionally an emulsion formed together with precipitation of solid in the organic layer. Addition of some methanol to the mixture dissolved all precipitated product and gave a clean separation into two layers. Finally the organic layer was dried over anhydrous sodium sulphate and solvent evaporation on a rotory evaporator gave 0.142 g of dark purple coloured solid.

The recovered solid was purified by flash chromatography on 10 g silica gel, eluting with chloroform. Pure ZnTTP-Br (13) (0.131 g, 0.16 mmol, 94%), a shiny pinkish purple coloured solid, was isolated by evaporating the solvent. The expected molecular ion (m/e = 812) was not observed in the mass spectra; instead an ion of m/e = 732 was observed. This could be due to the loss of $Br^{\bullet}$ from ZnTTP-Br (13).

^{1}H-NMR [$CDCl_3$, 200 MHz, δ(ppm)]: 8.92 (singlet superimposed on multiplet, J = 5 Hz, β-pyrrole protons, 8H), 8.27 (doublet, J = 8 Hz, benzyl aromatic protons closer to porphyrin ring, 2H), 8.17 (doublet, J = 7.8 Hz, tolyl aromatic protons closer to porphyrin ring, 6H), 7.81 (doublet, J = 8 Hz, benzyl aromatic protons farther from porphyrin ring, 2H), 7.61 (doublet, J = 7.8 Hz, tolyl aromatic protons farther from porphyrin ring, 6H), 4.84 (singlet, methylene protons of benzyl group, 2H), 2.69 (singlet, tolyl methyl protons, 9H). No resonances due to pyrrole N-H protons are observed at ~ -2.8 ppm, consistent with the insertion of a metal ion into the center of the porphyrin ring. UV($CHCl_3$): 420(494000), 551(14875), 592(4262).

IR (Nujol Mull): 552 cm^{-1} (C-Br stretch)

6.11 PREPARATION OF P-Glyco-A (16)

6.11.1 Preparation of Sodium salt of Ethyl Glycolate (14)

The sodium salt of ethyl glycolate was made by following a published literature procedure.[15] Sodium ethoxide was prepared from sodium (0.262 g, 11.39) and 15 mL absolute ethanol under a nitrogen atmosphere. To this ethyl glycolate (2.178 g, 20.92 mmol) dissolved in 20 mL absolute ethanol was added dropwise. The mixture was stirred at room temperature for 1 hour. The organic layer was then diluted with pentane. A white precipitate was formed immediately. The precipitate was filtered, washed with pentane (3 × 20 mL) and dried in a vacuum dessicator. The sodium salt of ethyl glycolate (14) (1.092 g, 8.66 mmol, 76%) was recovered as a white solid.

6.11.2 Preparation of ZnP-Glyco-OEt (15)

The procedure is similar to the one reported[15] except that ZnTTP-Br (13) was used instead of benzyl chloride as the starting material. To a stirring solution of ZnTTP-Br (13) (0.309 g, 0.35 mmol) in 50 mL dry DMF was added the sodium salt of ethyl glycolate (0.188 g, 1.49 mmol) and the mixture was heated at 90°C under nitrogen. The progress of the reaction was monitored by tlc. After heating for 1 hour, the starting material had disappeared and a new spot had developed. The reaction was terminated by adding 20 mL water. The organic layer was diluted with ether, washed with 5% aqueous HCl solution (30 mL) to get a clear separation, followed by water (3 × 30 mL). It was then dried on anhydrous sodium sulphate and evaporated to dryness to yield 0.196 g of a purple coloured solid compound. Considerable hydrolysis was observed upon slow elution of ZnP-Glyco-OEt (15) by

3% methanol in chloroform through a column packed with 70 g silica gel. Due to this problem the entire crude mass was not subjected to column purification in order to avoid hydrolysis of the ethoxycarbonyl group within the column. A small analytical quantity was purified by flash chromatography on 2 g silica gel using chloroform as eluting agent. The unreacted starting material came down first followed by the desired product. Pure ZnP-Glyco-OEt (15) was obtained as shiny purple solid. The expected molecular ion (m/e = 835) was observed in the mass spectrum. Exact mass: observed 835.2671 amu, calculated for $C_{52}H_{43}N_4O_3Zn$ 835.2625 amu.

^{1}H-NMR [$CDCl_3$, 200 MHz, δ(ppm)]: 8.97 (singlet superimposed on multiplet, J = 3.8 Hz, β-pyrrole protons, 8H), 8.26 (doublet, J = 8.1 Hz, benzyl aromatic protons closer to porphyrin ring, 2H), 8.11 (doublet, J = 7.9 Hz, tolyl aromatic protons closer to porphyrin ring, 6H), 7.78 (doublet, J = 8.1 Hz, benzyl aromatic protons farther from porphyrin ring, 2H), 7.56 (doublet, J = 7.9 Hz, tolyl aromatic protons farther from porphyrin ring, 6H), 5.58 (singlet, methylene protons of the benzyl ether group, 2H), 3.71 (quartet, J = 7 Hz, methylene protons of ethyl ester group, 2H), 3.49 (singlet, methylene protons of ethyl glycolate chain, 2H), 2.72 (singlet, tolyl methyl protons, 9H), 1.21 (triplet, J = 7 Hz, methyl protons of ethyl ester group, 3H). Resonances at ~ -2.8 ppm were not found, consistent with the presence of a metal ion in the center of the porphyrin ring. ^{13}C-NMR [$CDCl_3$, 50 MHz, δ(ppm)]: 151.2 (C=O), 142.3, 139.9, 137.5, 131.9, 131.7, 121.8, 121.1, 120.6 (aromatic C), 137.0, 134.4, 127.2, 125.8 (aromatic CH), 72.7 (ester CH_2), 66.1 (ether CH_2), 29.7 (Ar-$\underline{C}H_2$), 21.5 (tolyl CH_3), 15.3 (ester CH_3).

IR (Nujol Mull): 1729.4 cm^{-1} (>C=O stretch)

6.11.3 Preparation of P-Glyco-A (16)

ZnP-Glyco-OEt (15) was converted to P-Glyco-A (16) by base hydrolysis of the carboxyethoxy group. Crude ZnP-Glyco-OEt (15) (0.180 g) dissolved in 50 mL THF was mixed with 10 mL sodium hydroxide solution (0.5 N) and refluxed at 85°C for 30 minutes. The mixture was washed with 5% aqueous HCl solution (3 × 50 mL), and a green organic layer was formed due to the formation of demetallated protonated porphyrin. This layer was washed with water (4 × 50 mL), dried over anhydrous sodium sulphate, and the solvent was removed on a rotory evaporator to give 0.178 g of crude P-Glyco-A (16). The crude compound was purified by column chromatography using 76 g of silica gel. Eluting with chloroform yielded traces of ZnTTP-Br (13) followed by a small impurity band. The desired product was eluted from the column by changing the solvent composition to 3% methanol in chloroform. Solvent evaporation gave pure P-Glyco-A (16) (0.163 g, 0.22 mmol, 58% based on ZnTTP-Br (13) used), mp > 320°C, as a shiny purple coloured solid. In the mass spectrum, the expected molecular ion (m/e = 744) was observed. Exact mass: observed 744.3101 amu, calculated for $C_{50}H_{40}N_4O_3$ 744.3059 amu.

^{1}H-NMR [$CDCl_3$, 200 MHz, δ(ppm)]: 8.98 (singlet superimposed on a doublet, J = 3.5 Hz, β-pyrrole protons farther from porphyrin ring, 6H), 8.91 (doublet, J = 4.8 Hz, β-pyrrole protons closer to porphyrin ring, 2H), 8.23 (doublet, J = 7.6 Hz, benzyl aromatic protons closer to porphyrin ring, 2H), 8.12 (doublet, J = 7.9 Hz, tolyl aromatic protons closer to porphyrin ring, 6H), 7.68 (doublet, J = 7.6 Hz, benzyl aromatic protons farther from porphyrin ring, 2H), 7.57 (doublet, J = 7.9 Hz, tolyl aromatic protons farther from porphyrin ring, 6H), 5.46 (singlet, methylene

protons of benzyl group, 2H), 3.89 (doublet, J = 3.9 Hz, methylene protons of glycolic acid part, 2H), 2.72 (singlet, tolyl methyl protons, 9H), -2.80 (broad singlet, pyrrole N-H, 2H). The carboxylic acid (-COOH) proton was not observed separately, as it was hydrogen bonded with water contamination in the solvent and appeared at δ = 1.15.

IR (Nujol Mull): 3310.1 cm^{-1} (O-H stretch)

1692.3 cm^{-1} (>C=O stretch)

6.12 PREPARATION OF 4-phenyl-2-butyn-1-ol (18)

6.12.1 Preparation of Protected Propargyl Alcohol (17)

Protection of the alcohol group of propargyl alcohol was done according to the available literature procedure.[21] Freshly distilled ethyl vinyl ether (34.684 g, 0.48 mol) was cooled to -5°C and 0.233 g p-toluene sulphonic acid (monohydrate) was added with efficient stirring. Propargyl alcohol (18.097 g, 0.32 mol) was then added dropwise keeping the temperature between 0-5°C. An acetone/dry ice cooling bath was used because of its flexibility in controlling the temperature. The mixture was stirred for an additional 30 minutes at 5-10°C. It was then cooled to 0°C and an additional 0.198 g p-toluene sulphonic acid was added. The mixture was stirred for an additional 15 minutes. The reaction was then terminated by adding 50 mL aqueous potassium carbonate (5 g) solution and the product was extracted with ether. The organic layer was washed with water (2 x 50 mL) dried over anhydrous potassium carbonate and evaporated on a rotary evaporator to yield the protected propargyl alcohol (17) (39.682 g, 0.31 mol, 97%), bp = 42°C at 15 mm Hg. GC

analysis showed a new peak for the product with a retention time 4.66 min (98% pure). The expected molecular ion (m/e = 128) was not observed in GC-MS. Exact mass: observed 127.0754 amu, calculated for $C_7H_{11}O_2$ (for M - H fragment) 127.0759 amu.

^{1}H-NMR [$CDCl_3$, 200 MHz, δ(ppm)]: 4.73 (slightly split quartet, J = 5.4 Hz, O-C<u>H</u><, 1H), 4.08 (slightly split doublet of doublets, J = 1.8 Hz, 2.4 Hz, ≡C-C<u>H</u>$_2$-O, 2H), 3.61-3.31 (multiplet, O-C<u>H</u>$_2$-CH_3, 2H), 2.32 (slightly split triplet, J = 2.4 Hz, <u>H</u>-C≡C, 1H), 1.20 (slightly split doublet, J = 5.4 Hz, >CH-C<u>H</u>$_3$, 3H), 1.08 (slightly split triplet, J = 7 Hz, O-CH_2-C<u>H</u>$_3$, 3H).

IR (film): 3294.8 cm^{-1} (≡C-H stretch)
2209.4 cm^{-1} (C≡C stretch)
1132.4 cm^{-1} (C-O-C stretch)

6.12.2 Preparation of 4-Phenyl-2-Butyn-1-ol (<u>18</u>)

The method used for the preparation of this compound was adapted from published literature procedures.[20] The Grignard reagent was prepared from Mg (0.659 g, 27.11 mmol) and ethyl bromide (2.574 g, 23.62 mmol) in 25 mL dry THF. The solution obtained was decanted from excess Mg into another flask which was previously filled with nitrogen. The protected propargyl alcohol (<u>17</u>) (3.213 g, 25.10 mmol) dissolved in 5 mL dry THF was added dropwise to the Grignard reagent over 5 minutes. During addition of the alcohol an exothermic reaction was observed and the THF began to reflux. When the exothermic reaction had subsided the mixture was warmed at 55°C for 30 minutes. The solution was then cooled to room

temperature and freshly purified[13] powdered CuCl (0.138 g, 1.39 mmol) was added. After stirring for 15 minutes at room temperature a pale yellowish-green solution was obtained. Freshly distilled benzyl bromide (2.546 g, 23.36 mmol) was added dropwise and the mixture was refluxed at 85°C for 3 hours. Progress of the reaction was monitored by GC. GC analysis revealed a new peak with higher retention time. The reaction was terminated by adding 50 mL saturated ammonium chloride solution containing 0.6 g of sodium cyanide. The organic layer was diluted with ether, washed with water (2 × 30 mL) and dried over anhydrous sodium sulphate. Evaporation of the solvent on rotary evaporator gave 2.841 g of a yellowish oily compound.

To deprotect the alcohol group, the oily product (2.841 g) was dissolved in 100 mL of a 1:1 mixture of chloroform and methanol. Four drops of conc. HCl was added and the mixture was heated at 50°C for 30 minutes. The organic layer was then washed with saturated sodium bicarbonate solution (2 × 20 mL), water (3 × 50 mL) and dried over anhydrous sodium sulphate. Solvent evaporation gave 0.242 g of oily product. GC analysis showed disappearance of the peak for the product with the protected alcohol group and formation of a new peak.

Purification of the crude product was done on a silica gel column (70 g). Unreacted benzyl bromide was eluted with hexane. Changing the solvent composition to a 1:1 mixture of ether and hexane yielded the desired product. Solvent evaporation gave pure 4-phenyl-2-butyn-1-ol (18) (2.114 g, 14.48 mmol, 62%), as a colourless liquid. The expected molecular ion (m/e = 146) was observed in GC-MS. Exact mass: observed 146.0735 amu, calculated for $C_{10}H_{10}O$ 146.0732 amu.

^{1}H-NMR [$CDCl_3$, 200 MHz, δ(ppm)]: 7.28 (singlet, phenyl protons, 5H), 4.62 (singlet, benzyl methylene protons, 2H), 4.18 (singlet, methylene protons of propargyl alcohol, 2H), 3.12 (broad singlet, alcohol O-H proton, 1H).

IR (Thin Film): 3311.9 cm^{-1} (O-H stretch)

2208.5 cm^{-1} (C≡C stretch)

6.13 PREPARATION OF P-Ace-A (23)

6.13.1 Preparation of P-Ace-OH (20)

The procedure used for the preparation of P-Ace-OH (20) was identical to that used for the preparation of 4-phenyl-2-butyn-1-ol (18) except that benzyl bromide was replaced by ZnTTP-Br (13).[20] The Grignard reagent was prepared from Mg (1.695 g, 69.72 mmol) and ethyl bromide (5.914 g, 54.27 mmol) in 50 mL dry THF. A 21 mL sample of the prepared Grignard solution (22.79 mmol) was transferred to a flask previously filled with nitrogen gas. Protected propargyl alcohol (17) (5.292 g, 41.34 mmol) dissolved in 10 mL dry THF was added. An exothermic reaction was observed and the THF began to reflux. The mixture was heated at 55°C for 30 minutes and then cooled to room temperature. Freshly purified[13] powdered CuCl (0.581 g, 5.87 mmol) was added and the mixture was stirred at room temperature for 15 minutes to obtain a pale yellowish-green solution. ZnTTP-Br (13) (0.121 g, 0.15 mmol) dissolved in 10 mL dry THF was added to the yellowish-green solution and the mixture was refluxed at 85°C. The progress of the reaction was monitored by analytical tlc and it showed that the starting material had almost disappeared after 40 hours.

The reaction was terminated by adding 60 mL saturated aqueous ammonium chloride solution containing 3 g of sodium cyanide. The organic layer was diluted with 100 mL chloroform, washed with water (2 x 50 mL) and dried over anhydrous sodium sulphate. Crude ZnP-Ace-OR (19) (5.946 g) was obtained as a purple coloured thick liquid following evaporation of excess solvent. It was then dissolved in 100 mL of a 1:1 mixture of chloroform and methanol and 5 drops of conc. HCl. The solution turned green immediately. The solution was heated at 55°C for 30 minutes. The organic layer was diluted with chloroform (50 mL), washed with saturated sodium bicarbonate solution (2 x 20 mL), water (3 x 50 mL) and dried over anhydrous sodium sulphate. Solvent evaporation gave a purple coloured thick liquid as the crude product. 400 mL hexane was added to this thick liquid to dissolve the liquid impurities. Being insoluble in hexane, porphyrin compounds were precipitated out. The precipitate was filtered, washed with hexane (50 mL) and then dissolved in 100 mL chloroform. Solvent evaporation gave 0.174 g of a purple coloured solid as the crude product.

The crude product was purified by column chromatography on 85 g silica gel, using chloroform as eluting agent. A small band of unreacted starting material eluted first followed by the desired product. Solvent evaporation gave pure P-Ace-OH (20) (0.029 g, 0.04 mmol, 27%) as a dark purple coloured solid with mp > 300°C. The mass spectra showed the expected mass ion (m/e = 724). Exact mass: observed 724.3168 amu, calculated for $C_{51}H_{40}N_4O$ 724.3201 amu.

^{1}H-NMR [$CDCl_3$, 200 MHz, δ(ppm)]: 8.89 (singlet superimposed on a multiplet, J = 3.4 Hz, β-pyrrole protons, 8H), 8.19 (doublet, J = 8 Hz, benzyl

aromatic protons closer to porphyrin ring, 2H), 8.13 (doublet, J = 8.1 Hz, tolyl aromatic protons closer to porphyrin ring, 6H), 7.73 (doublet, J = 8 Hz, benzyl aromatic protons farther from porphyrin ring, 2H), 7.58 (doublet, J = 8.1 Hz, tolyl aromatic protons farther from porphyrin ring, 6H), 4.47 (broad singlet, benzyl methylene protons, 2H), 4.02 (broad singlet, methylene protons from propargyl alcohol part, 2H), 2.73 (singlet, tolyl methyl protons, 9H), -2.79 (broad singlet, pyrrole N-H protons, 2H). The hydroxyl (-O<u>H</u>) proton was not observed separately, as it was hydrogen bonded with the water contamination in the solvent and appeared at δ = 1.56. ^{13}C-NMR [$CDCl_3$, 75 MHz, δ(ppm)]: 141.7, 140.2, 136.7, 135.6, 131.8 (broad), 121.2, 121.1, 120.4 (aromatic C), 138.2, 135.4, 128.3, 127.1 (aromatic CH), 84.9 (≡C-), 81.8 (-C≡), 52.5 (<u>C</u>H_2-OH), 26.1 (Ar-<u>C</u>H_2), 22.4 (tolyl CH_3).

IR (Nujol Mull): 3312.4 cm^{-1} (O-H stretch)

2208.8 cm^{-1} (C≡C stretch)

6.13.2 Preparation of P-Ace-CHO (<u>21</u>)

A published literature procedure[26] for the oxidation of unsaturated alcohols to the corresponding aldehydes was followed for the preparation of P-Ace-CHO (<u>21</u>). The alcohol P-Ace-OH (<u>20</u>) (0.111 g, 0.15 mmol) was dissolved in 20 mL dichloromethane and pyridinium dichromate (0.805 g, 2.14 mmol) was added. The mixture was stirred at room temperature and the progress of the reaction was monitored by analytical tlc. After 12 hours, no sign of the starting material was found and a new spot was observed on tlc. The reaction mixture was diluted with ether (120 mL), washed with water (5 × 100 mL) to remove all pyridinium dichromate and then dried

over anhydrous sodium sulphate. Solvent evaporation gave 0.043 g of a purple coloured solid, which was purified by flash chromatography on 5 g silica gel. The desired product came out by eluting with chloroform. Pure P-Ace-CHO (21) (0.021 g, 0.03 mmol, 20%), a purple coloured solid, was recovered by evaporating all solvent. Expected mass ion (m/e = 722) was observed in GC-MS. Exact mass: observed 722.3127 amu, calculated for $C_{51}H_{48}N_4O$ 722.3045 amu.

^{1}H-NMR [$CDCl_3$, 200 MHz, δ(ppm)]: 9.41 (triplet, J = 0.6 Hz, aldehyde C<u>H</u>O proton, 1H), 8.88 (singlet superimposed on a doublet, J = 4.6 Hz, β-pyrrole protons farther from benzyl ring, 6H), 8.83 (doublet, β-pyrrole protons closer to benzyl ring, 2H), 8.22 (doublet, J = 8.4 Hz, benzyl aromatic protons closer to porphyrin ring, 2H), 8.11 (doublet, J = 7.8 Hz, tolyl aromatic protons closer to porphyrin ring, 6H), 7.73 (doublet, J = 8.4 Hz, benzyl aromatic protons farther from porphyrin ring, 2H), 7.57 (doublet, J = 7.8 Hz, tolyl aromatic protons farther from porphyrin ring, 6H), 4.20 (broad singlet, methylene protons of benzyl group, 2H), 2.72 (singlet, tolyl methyl protons, 9H), -2.78 (broad singlet, pyrrole N-H, 2H). ^{13}C-NMR [$CDCl_3$, 50 MHz, δ(ppm)]: 173.8 (<u>C</u>HO), 141.5, 139.2, 134.9, 133.3, 130.8 (broad), 129.4, 120.3, 120.2, 118.8 (aromatic C), 137.3, 134.5, 127.4, 126.3 (aromatic CH), 84.6 (≡C-), 82.2 (-C≡), 29.7 (CH_2), 21.5 (tolyl CH_3).

IR (Nujol Mull): 2820.4 cm^{-1} (Aldehyde C-H stretch)

1695.7 cm^{-1} (>C=O stretch)

6.13.3 Preparation of P-Ace-OMe (22)

A published literature procedure[27] for selective oxidation of a conjugated aldehyde to the corresponding ester was followed. P-Ace-CHO (21) (0.065 g, 0.09 mmol) dissolved in 15 mL THF was mixed with 82 mg of sodium cyanide (1.67 mmol), 30 mg of acetic acid and 570 mg of active manganese dioxide. Methanol (15 mL) was added and the mixture was stirred at room temperature for 24 hours. The progress of the reaction was monitored by analytical tlc. The solution was filtered to remove all insoluble matter and then it was diluted with 100 mL chloroform. It was then washed with water (3 × 30 mL), dried over anhydrous sodium sulphate and evaporated to dryness to yield 0.094 g of a purple solid compound. The crude product was purified by flash chromatography on 6 g of silica gel using chloroform as eluting agent. Pure P-Ace-OMe (22) (0.062 g, 0.082 mmol, 91%), a purple solid compound, was obtained. In the mass spectra the expected molecular ion (m/e = 752) was observed in the mass spectrum. Exact mass: observed 752.3151 amu, calculated for $C_{52}H_{40}N_4O_2$ 752.3132 amu.

^{1}H-NMR [$CDCl_3$, 200 MHz, δ(ppm)]: 8.84 (singlet superimposed on a multiplet, J = 3 Hz, β-pyrrole protons, 8H), 8.15 (doublet, J = 7.9 Hz, benzyl aromatic protons closer to porphyrin ring, 2H), 8.05 (doublet, J = 8.1 Hz, tolyl aromatic protons closer to porphyrin ring, 6H), 7.64 (doublet, J = 7.9 Hz, benzyl aromatic protons farther from porphyrin ring, 2H), 7.51 (doublet, J = 8.1 Hz, tolyl aromatic protons farther from porphyrin ring, 6H), 4.01 (singlet, methylene protons of benzyl group, 2H), 3.86 (singlet, methyl protons of methyl ester group, 3H), 2.69 (singlet, tolyl methyl protons, 9H), -2.79 (broad singlet, pyrrole N-H, 2H).

IR (Nujol Mull): 2209.4 cm^{-1} (C≡C stretch)

1741.4 cm^{-1} (>C=O stretch)

6.13.4 Preparation of P-Ace-A (23)

P-Ace-OMe (22) was converted to P-Ace-A (23) by base hydrolysis of the carbomethoxy group. A solution of P-Ace-OMe (22) (0.051 g, 0.068 mmol) in 20 mL THF was mixed with 10 mL of aqueous sodium hydroxide solution (0.5 M) and refluxed at 80°C for 1 hour. The progress of the reaction was checked by analytical tlc.

A 5% aqueous HCl solution (50 mL) was added to the reaction mixture and the product was extracted with chloroform. The chloroform layer was washed with water (3 × 60 mL), dried over anhydrous sodium sulphate and evaporated to dryness to give 0.045 g of a purple solid compound. Purification of the crude compound was done by column chromatography on 60 g silica gel. A faint pink band came down upon eluting with chloroform. Changing the solvent composition to 10% methanol in chloroform caused the desired product to elute from the column. Solvent evaporation gave P-Ace-A (23) (0.036 g, 0.049 mmol, 72%), mp > 300°C, as a purple coloured solid compound. The expected molecular ion (m/e = 738) was not observed in the mass spectrum. A mass ion at m/e = 694 appeared in the spectra, which is 44 mass units less than the molecular mass of P-Ace-A (23). The loss of 44 units suggests the loss of CO_2 from the carboxylic acid group.

^{1}H-NMR [$CDCl_3$, 300 MHz, δ(ppm)]: 9.43 (triplet, J = 0.9 Hz, -COOH, 1H), 8.89 (singlet superimposed on a multiplet, J = 5 Hz, β-pyrrole protons, 8H), 8.59

(doublet, J = 8.1 Hz, benzyl aromatic protons closer to porphyrin ring, 2H), 8.49 (doublet, J = 8.2 Hz, tolyl aromatic protons closer to porphyrin ring, 6H), 7.98 (doublet, J = 8.1 Hz, benzyl aromatic protons farther from porphyrin ring, 2H), 7.82 (doublet, J = 8.2 Hz, tolyl aromatic protons farther from porphyrin ring, 6H), 4.26 (singlet, methylene protons of benzyl group, 2H), 2.79 (singlet, tolyl methyl protons, 9H), -2.79 (broad singlet, pyrrole N-H, 2H). The carboxylic acid (-COOH) proton was not observed separately, as it was hydrogen bonded with the water contamination present in the solvent and appeared at δ = 1.14.

IR (Nujol Mull): 3313.9 cm^{-1} (O-H stretch)

2208.9 cm^{-1} (C≡C stretch)

1692.1 cm^{-1} (>C=O stretch)

6.14 PREPARATION OF P-Pr-A (25)

6.14.1 Preparation of P-Pr-OH (24)

P-Pr-OH (24) was prepared from P-Ace-OH (20) by adapting a published literature procedure[27] for catalytic hydrogenation of unsaturated alcohols. A solution of P-Ace-OH (20) (0.064 g, 0.088 mmol) in 20 mL THF was mixed with 6 mg of 10% palladium on charcoal and stirred at room temperature while hydrogen was bubbled through it. The reaction was monitored by tlc. After 3 hours the starting material disappeared and a new spot developed on tlc. The reaction was terminated by flowing nitrogen through the flask. The solution was filtered to remove the catalyst and then evaporated to dryness to recover 0.068 g of crude P-Pr-OH (24). The crude product was purified by flash chromatography on 5 g silica gel using

chloroform as eluting agent. Pure P-Pr-OH (24) (0.063 g, 0.086 mmol, 98%), mp > 300°C was obtained as a purple coloured solid. The expected mass ion (m/e = 728) was observed in the mass spectrum. Exact mass: observed 728.3507 amu, calculated for $C_{51}H_{44}N_4O$ 728.3515 amu.

^{1}H-NMR [$CDCl_3$, 200 MHz, δ(ppm)]: 8.87 (singlet, β-pyrrole protons, 8H), 8.13 (doublet superimposed on another doublet, J = 8 Hz, benzyl aromatic protons closer to porphyrin ring, 2H), 8.11 (doublet superimposed on another doublet, J = 8 Hz, tolyl aromatic protons closer to porphyrin ring, 6H), 7.56 (doublet, J = 8 Hz, benzyl and tolyl aromatic protons farther from porphyrin ring, 8H), 3.82 (triplet, J = 6.2 Hz, methylene protons next to alcohol group, 2H), 2.99 (triplet, J = 7.8 Hz, methylene protons of benzyl group, 2H), 2.08-1.76 (multiplet, methylene protons generated by the hydrogenation of -C≡C- group, 4H), 2.71 (singlet, tolyl methyl protons, 9H), -2.78 (broad singlet, pyrrole N-H, 2H). The hydroxyl (-O<u>H</u>) proton was not observed separately, as it was hydrogen bonded with water contamination in the solvent and appeared at δ = 1.55. ^{13}C-NMR [$CDCl_3$, 50 MHz, δ(ppm)]: 142.6, 140.6, 140.2, 135.6, 131.8 (broad), 121.0, 120.9 (aromatic C), 138.2, 135.4, 128.3, 128.1, 127.6 (aromatic CH), 63.9 ($\underline{C}H_2OH$), 36.6 ($\underline{C}H_2$-CH_2OH), 33.5 (Ar-CH_2-$\underline{C}H_2$), 28.6 (Ar-$\underline{C}H_2$), 22.4 (tolyl CH_3).

IR (Nujol Mull): 3311.9 cm^{-1} (O-H stretch)

6.14.2 Preparation of P-Pr-A (25)

A published literature procedure[26] for the oxidation of a primary alcohol to corresponding acid was followed. The application of this procedure required

protection of the porphyrin ring as its Zn derivative. To a solution of P-Pr-OH (24) (0.087 g, 0.12 mmol) in 50 mL chloroform was added a solution of zinc acetate (0.258 g, 1.18 mmol) in 5 mL methanol. The mixture was stirred at room temperature for 30 minutes. The progress of the reaction was monitored by visible absorption spectroscopy. Insertion of the zinc ion into the porphyrin ring was confirmed by the collapse of the four-banded spectrum characteristic of a free-base porphyrin into the two-banded spectrum characteristic of a metallated porphyrin. The organic layer was diluted with chloroform and washed with water (2 × 50 mL). Occasionally an emulsion was formed together with precipitation of a solid in the organic layer. The precipitated product was dissolved by adding some methanol to the mixture. A clear separation was then obtained. Finally the organic layer was dried over anhydrous sodium sulphate and solvent evaporation on a rotary evaporator gave 0.092 g of a shiny pinkish purple solid. The crude compound was purified by flash chromatography on 5 g silica gel using chloroform as eluting agent and pure ZnP-Pr-OH (0.087 g, 0.11 mmol, 92%), a shiny pinkish purple coloured solid was obtained.

^{1}H-NMR [$CDCl_3$, 200 MHz, δ(ppm)]: 8.91 (singlet, β-pyrrole protons, 8H), 8.19 (doublet superimposed on another doublet, J = 8 Hz, benzyl aromatic protons closer to porphyrin ring, 2H), 8.16 (doublet superimposed on another doublet, J = 8 Hz, tolyl aromatic protons closer to porphyrin ring, 6H), 7.59 (doublet, J = 8 Hz, benzyl and tolyl aromatic protons farther from porphyrin ring, 8H), 3.84 (triplet, J = 6.1 Hz, terminal methylene protons next to alcohol group, 2H), 3.01 (triplet, J = 7.8 Hz, methylene protons of benzyl group, 2H), 2.10-1.77 (multiplet, methylene protons generated by the hydrogenation of -C≡C- group, 4H), 2.72 (singlet, tolyl

methyl protons, 9H). The hydroxyl (-OH) proton was not observed separately, as it was hydrogen bonded with water contamination in the solvent and appeared at δ = 1.52. No resonances due to pyrrole N-H protons were observed at ~ -2.8 ppm, consistent with the insertion of a metal ion into the center of the porphyrin ring.

ZnP-Pr-OH (0.087 g, 0.11 mmol) was dissolved in 20 mL DMF and 0.403 g pyridinium dichromate (1.07 mmol) was added. The mixture was stirred at room temperature and the progress of the reaction was monitored by tlc. After 7 hours no sign of starting material was noticed on tlc. The mixture was diluted with chloroform (80 mL) and washed with water (5 × 100 mL) to remove excess pyridinium dichromate. It was diluted with 100 mL chloroform and acidified with four drops of conc. HCl to remove zinc from porphyrin. The organic layer was then washed with water (3 × 50 mL) and dried over anhydrous sodium sulphate. Solvent evaporation on a rotary evaporator gave 0.082 g of purple solid. The crude compound was purified by column chromatography on 70 g of silica gel. A faint pink coloured band, presumably unreacted P-Pr-OH (24), was eluted with chloroform. Changing the solvent composition to 15% methanol in chloroform gave the desired product. Pure P-Pr-A (25) (0.046 g, 0.062 mmol, 56%), mp > 310°C, a purple coloured solid, was obtained by evaporating the solvent.

The ^{1}H-NMR spectrum of P-Pr-A (25) could not be obtained due to its poor solubility in all the solvents tested. The expected molecular ion (m/e = 742) was seen in the mass spectrum. Exact mass: observed 742.3302 amu, calculated for $C_{51}H_{42}N_4O_2$ 742.3307 amu.

IR (Nujol Mull): 3315.6 cm^{-1} (O-H stretch), 1693.4 cm^{-1} (>C=O stretch)

CHAPTER 7

CONCLUSIONS AND SUGGESTIONS FOR FURTHER RESEARCH

7.1 CONCLUSIONS

7.1.1 Spectroscopic Properties of Porphyrin Solutions

The presence different linkages attached to the porphyrin ring has very little influence on the spectroscopic properties of the porphyrin model compounds studied. By changing the solvent system, various degrees of aggregation were experienced by all the compounds, which leads them to absorb at higher wavelength and give different fluorescence yields. Aggregated species were found in sodium hydroxide solution, and the degree of aggregation was found to be independent of the nature of the chain attached to the porphyrin ring. In addition, all the compounds showed almost identical fluorescence quenching, as evidenced from their fluorescence yield data. In chlorinated solvents, all the compounds showed a similar degree of quenching of the excited singlet state, indicating the absence of any influence of the side chains on the fate of the excited state of the porphyrin. Hence it is concluded that the nature of the side chain does not influence the fate of the excited state of the porphyrin, and so the porphyrin ring can exhibit its own spectroscopic properties.

7.1.2 Surface and Photophysical Properties of the Monolayers

The model porphyrin compounds exhibit a significant variation in their surface-pressure area isotherms, which appears to arise from the presence of different

side chains attached to the porphyrin ring. The compounds with longer side chains were found to possess a smaller area per molecule, as compared to those with shorter chains. This is perhaps due to the presence of greater conformational flexibility of the porphyrin ring, which allows them to compact into a tight arrangement in the monolayer and hence occupy a smaller area. Thus P-A, where there is no side chain, possesses a higher surface area per molecule, and P-Gly-A, where the side chain is considerably longer, occupies a very small surface area.

The nature of the packing of these porphyrin compounds is also reflected in the absorption characteristics of their monolayers deposited onto quartz and SnO_2 surfaces, respectively. An increasing red shift in λ_{max} was observed, as the attached chain length was increased, which probably arises from the increasing compactness of the porphyrin structure in the monolayer. On changing the substrate from quartz to SnO_2 a blue shift was observed for λ_{max} of the monolayers of all the compounds. This probably arises from the rough surface of SnO_2, on which the compounds cannot make a perfectly compact matrix as they can do on the smooth quartz surface. The more "open" monolayer on SnO_2 thus leads to a blue shift of λ_{max} for monolayers on SnO_2, as compared to λ_{max} on a quartz surface.

The fluorescence quantum yield data indicate a considerable quenching of all the monolayers on a quartz surface. The degree of quenching was found to be directly related to the extent of molecular aggregation of the molecules in the monolayer. Hence, compounds with long side chain, such as P-Pr-A, show a very high fluorescence quenching on a quartz surface. On a SnO_2 surface, a smaller quenching effect was expected for all the compounds, as the molecular packing is not

as good as it is on a quartz surface. Instead, an enhanced quenching was observed. We have postulated that this is due to the occurrence of isoenergetic electron transfer from the excited singlet state of the porphyrin to the conduction band of the semiconductor. This process serves as an additional deactivation pathway of the excited singlet state and results in an enhanced fluorescence quenching. P-Ace-A and P-Gly-A showed the maximum quenching due to the presence of an electron rich chain system, which resulted in a higher isoenergetic electron transfer and more quenching of the excited state for these molecules.

7.1.3 Photovoltaic Effects of the Monolayer Modified Photoelectrodes

LB monolayers of all the model compounds, deposited onto SnO_2 semiconductor slides, were found to produce an anodic photocurrent, corresponding to electron injection into the semiconductor. Contrary to expectation, the compounds with long alkane linkages showed a higher photocurrent, which increased with the length of the alkane linkage. The compounds with electron rich linkages also showed significant anodic photocurrent production.

An increasing anodic photocurrent quantum yield was observed for the compounds with long alkane chain, such as P-Pr-A, and also compounds with an electron rich side chain, such as P-Gly-A and P-Ace-A. In the alkane linkage, it is postulated that this is due to the presence of a *trans bond effect*, and in electron rich linkage it is due to the presence of mobile electrons, which allow the excited singlet state of the porphyrin to undergo an efficient electron tunnelling to surface states of the semiconductor, resulting in a high anodic photocurrent yield.

On diluting the monolayers with DOPC, a surface active non fluorescent lipid, an increase in the photocurrent yield was observed. This is perhaps caused by increasing the isoenergetic electron transfer rate due to the minimization of the aggregate mediated quenching of the excited state of the porphyrin. A significant increase in the photocurrent yield was observed for P-Ace-A, on dilution of its monolayer. This is probably due to the combination of two favourable effects experienced by P-Ace-A. First the decrease in the aggregate mediated deactivation of the excited singlet state, and the second due to a higher rate of isoenergetic electron tunnelling through the electron rich triple bond system to the surface states of the semiconductor.

7.2 SUGGESTIONS FOR THE FURTHER RESEARCH

In the present work, the rate of isoenergetic electron transfer, carried out by the model compounds, was estimated on the basis of their photocurrent quantum yields. It would be interesting to carry out a series of fluorescence lifetime experiments, using the monolayers of these model compounds deposited onto quartz and SnO_2 surfaces. From their lifetimes, the extent of quenching possessed by different monolayers can be estimated. By carrying out the lifetime experiments with the diluted monolayers of these model compounds, the rate of the isoenergetic electron photoinjection can also be evaluated more accurately.

It will be interesting to study the fluorescence lifetime distribution of a range of DOPC/porphyrin model compounds mixing ratios at various temperatures, which might shed some light on the question of whether the quenching is diffusional or

static. Variation of the redox potential of the supersensitizer might help to pin down the dynamics of the low pH supersensitization process. Variation of the surface character by controlled etching might also be helpful.

Experiments have indicated that it is possible to deposit LB films of porphyrin-quinone compounds linked by an amide linkage. Here the quinone is thought to be the hydrophillic portion of the molecule. Deposition of the monolayer onto a semiconductor would sandwich the quinone between the porphyrin and the semiconductor producing an intermediate photoelectron acceptor site. It would be interesting to synthesize some new porphyrin model systems to study the effect of the presence of an intermediate acceptor site. This can be done by modifying the present model porphyrin compounds by replacing the carboxylic acid group with a quinone system. Comparing the fluorescence quenching data from the studies of these molecules in solution with the photocurrent quantum yield for electrodes modified by the attachment of these molecules, a clear picture of the interfacial electron transfer can be obtained. The presence of such an acceptor might profoundly increase the quantum yield of photoelectron injection, by stabilizing the fluorescence quenching process.

APPENDIX I

PROGRAM WRITTEN IN ASYST 3.0 FOR INTERFACING WITH THE OSCILLOSCOPE AND FOR PHOTOELECTROCHEMICAL ANALYSIS.

```
\
\
\
\
\
\
\
ECHO.OFF
\
\
\
\
\
\
\
\
\
```

Program to acquire and analyse photoelectrochemical data

NICOLET.PRG
Program to transfer data from NICOLET 2090 to PC

```
integer dim[ 1024 ]  array nic.buff      \ creates array for GPIB buffer
                     scalar a.base       \ right side of peak to integrate
                     scalar b.base       \ left side of peak to integrate
                     scalar niv          \ # of point in integrated peak
                     scalar b2           \ index of 1 point of peak
dp.real              scalar ground       \ slope of base line
                     scalar f(a)
                     scalar f(b)

token integrated.peak                    \ peak to integrated
exp.mem> integrated.peak

bus.init                                 \ initializes GPIB bus
send.interface.clear
remote.enable.on

14 gpib.device nicout                    \ NICOLET 2090 output address is 14
```

```
nicout listener                    \ assign nicout to this address
selected.device.clear

unlisten
nic.buff []gpib.buffer
2048 listen.limit                  \ set the limit of bytes to be
                                   \ received as neither EOI or EOS seem
                                   \ to work with NICOLET 2090
                                   \ # bytes = 2 * (dim of nic.buff)

15 gpib.device nicin               \ NICOLET 2090 input address is 15
nicin listener                     \ assign nicin to this address
selected.device.clear
unlisten
vuport vunorm
: vuport.setup \ set up VUPORT VUNORM
      vunorm
      0.0 0.25 vuport.orig
      1.0 0.75 vuport.size
      0 vuport.color
      9 label.color
      10 color
      15 axis.color
      13 cursor.color
      inten.off
;

: nic.read          \ nic.read reads a Waveform from NICOLET 2090 from
                    \ the memory positions Q1, Q2, Q3 or Q4. If any other
                    \ positions are going to be read change the dimension
                    \ of nic.buff and the number of listen.limit accordingly

    unlisten untalk
    0 nic.buff :=                  \ set buffer to 0
    me talker
    nicin listener
    " D3D2 " talk                  \ tell NICOLET 2090 to send binary
                                   \ data
    me listener
    nicout talker
    buffer.listen                  \ read data
    nic.buff byte.swap 1 + nic.buff :=   \ convert received data so it
                                   \ corresponds to screen of
                                   \ NICOLET 2090

    graphics.display vunorm
```

```
    nic.buff
    y.auto.plot                          \ plot data
;
\
\                    STORE.PRG
\                Program to store waveforms as
\                received from NICOLET 2090
\
\
\
      integer scalar indx                \ Index-# to subfile
14          string filename
64          string commstr
                                         \ Array NIC.BUFF was declared
                                         \ in NICOLET.PRG


15 set.file.parse                        \ set default path to subdirectory
data.file c:\asyst\data\dummy.dat        \ c:\asyst\data\*.dat


: new.file                               \ creates new file
      regular.datafile
      file.template                      \ template for datafile with 10
        20 comments                      \ subfiles
        integer dim[ 1024 ] subfile
        10 times
      end
      cr ." Filename .....: "
      "input filename ":=
      filename defer> file.create        \ create file "filename".dat
      3 indx :=
;

: yesno  \ leaves true on stack if string = " y"
      "input 1 "left
      " y" "=
;

: find.place  \ evaluate if there is space left in opened file
      filename defer> file.open          \ open file "filename".dat
      1 indx :=                          \ search for empty space for
      begin                              \ subfile
          indx 1 + comment> "null "=
          indx 2 + indx :=
          indx 21 = or
      until
```

```
        file.close                          \ indx is 2 too large when leaving
                                            \ find.place. It has to be reset
                                            \ before using
;

: nic.store                                 \ stores data into file *.dat
        normal.display
        cr ." All files are stored with the extension .DAT "
        cr ." in the subdirectory c:\ASYST\DATA " cr cr
        cr ." Do you want to create a new file ? "
        yesno if new.file
        else
           cr ." Old filename .....: "
           "input filename ":=
           find.place
           indx 21 = if cr ." Not enough room in file ! "
           cr ." Create new file !! " cr cr
           new.file then
        then
        indx 2 - indx :=                    \ reset indx to correct value
        filename defer> file.open
        screen.clear
        cr ."      Your file contains following data " cr cr
        10 0 do                             \ Read comment strings from file
            i 2 * 1 + comment> -trailing i . "type  cr
            "      Created..: "
            i 2 * 2 + comment> -trailing "cat "type cr
        loop
        cr ." C mment ..... : "
        "input indx >comment
        "date indx 1 + >comment
        indx 1 + 2 / subfile nic.buff array>file
        file.close
;
\
\                  GET.PRG
\          Program to retrive waveforms
\            stored with STORE.PRG
\
\
                                            \ FILNAME, NIC.BUFF, INDX
                                            \ were declared above

: nic.file  \ Read stored data
        normal.display
        cr ." Filename .....: "
```

```
        "input filename ":=
        filename defer> file.open
        screen.clear
        cr ."      Your file contains following data " cr cr
        10 0 do                                  \ Read comment strings from file
            i 2 * 1 + comment> -trailing i 1 + . "type  cr
            "      Created..: "
            i 2 * 2 + comment> -trailing "cat "type cr
        loop
        cr ." File-# to read .....: "
        #input indx :=
        indx subfile
        nic.buff file>array
        graphics.display vunorm
        nic.buff y.auto.plot
        file.close
;
\
\
\
\
\
\
```

PLOT.PRG
Program to plot waveforms on screen

```
: integer.label.format                   \ sets x-axis labels to integer
                                         \ see G1.4.19
        ?horizontal if
        drop fix "."                     \ drop y-value and put the Integer
                                         \ value on symbol stack
        else label.string then
;

dp.real dim[ 1024 ] array  xax
dp.real dim[ 1024 ] array  yax
                scalar maxx
                scalar maxy
                scalar minx
                scalar miny
                scalar volt
                scalar ohms
integer          scalar delta
                scalar plt.indx

: axis.setup                             \ set up optimized axis for I-V plots
        cr ." Start potential....: " #input minx :=
        cr ." End potential.....: " #input maxx :=
        cr ." Voltage setting of NICOLET in mV ...: "  \ might be replaced
```

```
                                        \ by direct reading from
                                        \ the NICOLET
                    #input volt :=
cr ." Measuring resistance....: "       \ Can be read off the
                                        \ potentiostat

          #input 1000. /       ohms :=  \ As NICOLET reading is
                                        \ read in mV and we want
                                        \ the current in uA the
                                        \ resistance has to be
                                        \ divided by 1000
nic.buff                          yax :=
yax 2048. / volt * ohms /           yax :=
1024 ramp maxx minx - 1024 / * minx +   xax :=
axis.defaults
vertical axis.fit.off grid.off
label.scale.off
horizontal axis.fit.off grid.off
label.scale.off
normal.coords
0.13 0.12 axis.orig
0.13 0.12 axis.point
0.8 0.8  axis.size
50                        delta :=  \ Change delta if other
                                    \ spacing between x-tics
                                    \ is desired
maxx dup delta modulo -             maxx :=
horizontal minx maxx world.set
vertical yax []min/max world.set
maxx minx - delta /
8 axis.divisions
horizontal 0 1 label.points
vertical -1. 0 5 label.format
0.007 0.005  tick.size
0 0 tick.just
install integer.label.format in label.string.xeq
vuport.clear
xy.axis.plot
normal.coords
7 label.color
0.02 0.3 position 90 char.dir 90 label.dir
" Current [1E-6 A]" label
.37 .02 position 0 char.dir 0 label.dir
" Potential vs Ag/AgCl [mV]" label
10 color
9 label.color
```

```
        world.coords
;

: iv.plot
        axis.setup
        maxx xax [ 1 ] -
        1024 xax [ 1024 ] xax [ 1 ] - / * plt.indx :=
        xax sub[ 1 , plt.indx ]                         \ cut off data at the end
        yax sub[ 1 , plt.indx ] xy.data.plot            \ to fit plot into range
        cursor.off
        screen.clear
        pause
;
\
\                    ACTION.PRG
\                Program to plot action spectra
\                      on screen
\
\
\
dp.real                 scalar sens
: axis2.setup  \ set up optimized axis for action spectra
        cr ." Start wavelength...: " #input minx :=
        cr ." End wavelength.....: " #input maxx :=
        cr ." Voltage setting of NICOLET in V ....: "     \ might be replaced
                                                          \ by direct reading from
                                                          \ the NICOLET
                                #input volt :=
        cr ." Measuring resistance....: "                 \ Can be read off the
                                                          \ potentiostat
                            #input 1000. / ohms :=        \ Divide by 1000 to
                                                          \ get uA as resulting
                                                          \ current
        cr ." lock-in sensitivity in mV : ...: "          \ Can be read off the
                                                          \ lock-in amplifier
                            #input 10. / sens :=          \ SENS has to be
                                                          \ divided
                                                          \ as the full output
                                                          \ from the lock-in is
                                                          \ 10 V


        nic.buff                            yax :=
        yax 2048. / volt * sens * ohms /      yax :=
        yax dup []min/max drop -              yax :=
        yax 1000 *                          yax :=        \ To get current in nA
```

```
        1024 ramp maxx minx - 1024 / * minx +    xax  :=
        axis.defaults
        vertical axis.fit.off grid.off
        label.scale.off
        horizontal axis.fit.off grid.off
        label.scale.off
        normal.coords
        0.13 0.12 axis.orig
        0.13 0.12 axis.point
        0.8 0.8  axis.size
        25                          delta :=          \ Change delta if other
                                                      \ spacing between x-tics
                                                      \ is desired
        maxx dup delta modulo - delta +       maxx :=
        horizontal minx maxx world.set
        vertical yax []min/max world.set
        maxx minx - delta /
        8 axis.divisions
        maxx minx - delta /
        10. > if 0 2 horizontal label.points then   \ If the x-values are too
                                                    \ narrowly spaced print
                                                    \ only every second label
        1 1 vertical label.points
        vertical -1. 0 5 label.format
        0.007 0.005  tick.size
        0 0 tick.just
        install integer.label.format in label.string.xeq
        vuport.clear
        xy.axis.plot
        normal.coords
        7 color
        0.02 0.3 position 90 char.dir 90 label.dir
        ' Current [nA]" label
        .37 .02 position 0 char.dir 0 label.dir
        " Wavelength [nm] " label
        10 color
        world.coords
;

: action.plot
        axis2.setup
        xax yax xy.data.plot
        cursor.off
        screen.clear
;
```

```
\ Peak.find finds peaks in any wave form
token max.points
exp.mem> max.points
40 set.#.points

: peak.find
        cr ." Number of peaks in your waveform.....: "
        #input 1 + set.#.optima
        nic.buff local.maxima swap dup becomes> max.points
        swap
        13 color " *" symbol
        xy.data.plot
        10 color solid
;
\
\
\
\
\
\
\
: nic.123
        load.ov . ay c:\asyst\123io.sov
        cr ." Files are stored in C:\SIGMA" cr
        cr ." Name of SIGMA PLOT file ....:"
        "input " .cal" "cat filename ":=
        chdir c:\sigma
        filename defer> 123file.create
        filename defer> 123file.open
        2 1 123write.down
        xax array>123file
        2 2 123write.down
        yax array>123file
        123file.close
        chdir c:\asyst\
;
\
\
\
\
\
\
: nic.hp7475.A \ Plot Actionspectrum
        def.vuport
        load.overlay hpplotr.sov
        hp7475
```

LOTUS.PRG
Program to store waveforms in a file
that can be read by Sigma Plot

Plotting routines for HP 7475A plotter
NIC.HP7475.A & NIC.HP7475.B

```
        device.init
        plotter.defaults
        7.8 10.15 plotter.size
        1 color
        normal.coords
        0.13 0.17 axis.orig
        0.13 0.17 axis.point
        0.8 0.75 axis.size
        horizontal minx maxx world.set
        vertical yax []min/max yax []min/max - abs 10 / +
        world.set
        maxx minx - delta /
        8 axis.divisions
        maxx minx - delta /
        10. > if 0 2 horizontal label.points
        else 0 1 horizontal label.points then
        1 1 vertical label.points
        vertical -1. 0 5 label.format
        0.007 0.005  tick.size
        0 0 tick.just
        install integer.label.format in label.string.xeq
        xy.axis.plot
        normal.coords
        0.03 0.4 position 90 char.dir 90 label.dir
        " Current /nA" label
        .37 .1 position 0 char.dir 0 label.dir
        " Wavelength /nm" label
        0.13 0.92 position                    \ Draw box
        0.93 0.92 draw.to
        0.93 0.17 draw.to
        world.coords
        xax yax xy.data.plot
        graphics.display
        vunorm vuport.clear
        vuport.setup
;

: nic.hp7475.B \ Plot IV-plot
        def.vuport
        load.overlay hpplotr.sov
        hp7475
        device.init
        plotter.defaults
        7.8 10.15 plotter.size
        1 color
        normal.coords
```

```
        0.13 0.17 axis.orig
        0.13 0.17 axis.point
        0.8 0.75 axis.size
        horizontal minx maxx world.set
        vertical yax []min/max yax []min/max - abs 20 / +
        world.set
        maxx minx - delta /
        8 axis.divisions
        maxx minx - delta /
        10. > if 0 2 horizontal label.points
        else 0 1 horizontal label.points then
        1 1 vertical label.points
        vertical -1. 0 5 label.format
        0.007 0.005  tick.size
        0 0 tick.just
        install integer.label.format in label.string.xeq
        xy.axis.plot
        normal.coords
        0.03 0.4 position 90 char.dir 90 label.dir
        " Current /uA" label
        .37 .1 position 0 char.dir 0 label.dir
        " Potential vs. Ag/AgCl /mV" label
        0.13 0.92 position                    \ Draw box
        0.93 0.92 draw.to
        0.93 0.17 draw.to
        world.coords
        xax sub[ 1 , plt.indx ]
        yax sub[ 1 , plt.indx ] xy.data.plot
        graphics.display
        vunorm vuport.clear
        vuport.setup
;

: p.t.i \ sets display in array.readout mode with two cursors
        array.readout
        normal.coords 0.7 0.95 readout>position   \ defines readout position
                                                  \ on the screen
        world.coords
        3 array.readout.type                      \ defines cursor type
        stack.clear
        screen.clear
        cr ." See Manual MODULE 1 Glossaries G1-4-26 "
        cr ." for cursor key movements"
        cr ." When the two cursors are placed on both sides of the"
        cr ." peak you want to integrate press Ctrl B to get integral"
        cr ." Press F10 when finished"
```

```
        cr
;

: base.lin                              \ integrates peak between cursors
        screen.clear cr cr ."           "
        readout.indices
                        a.base :=
                        b.base :=
        a.base b.base - niv :=
        b.base          b2 :=
        nic.buff a.base lookup      f(a) :=
        nic.buff b.base lookup      f(b) :=
        f(a) f(b) > if f(b) else f(a) then
                                ground  :=
        nic.buff sub[ b2 , niv ] becomes> integrated.peak
        integrated.peak ground -
        1000. / integrate.data
        []max .
;
\
\                  Menu Structure : Set Up
\
\
\
INTEGER DIM[ 4 ] ARRAY FLAG
: MENU1  \ ******************************************************
SCREEN.CLEAR
CR ." ------------------------------------------------------------- "
                                        \ Menu 1
CR ."       F5  : Data acquisition "    \ Menu 1.1
CR ."       F6  : Data analysis "       \ Menu 1.2
CR ."       F10 : Bye           "       \ Exits ASYST
0 FLAG [ 1 ] :=
;

: MENU1.1  \ ****************************************************
SCREEN.CLEAR
CR ." ------------------------------------------------------------- "
                                                    \ Menu 1.1
CR ."       F5 : Read Data from Nicolet 2090 "      \ Does Nic.read
CR ."       F6 : Store Data in file "               \ Does Nic.file
CR ."       F10: Exit           "                   \ Menu 1
1 FLAG [ 1 ] :=
0 FLAG [ 2 ] :=
;
```

```
: MENU1.2  \ ******************************************************
SCREEN.CLEAR
CR ." ------------------------------------------------------------------ "
            \ Menu 1.2
CR ."       F5 : Read Data from file "                    \ Does Nic.get
CR ."       F6 : I-V plot  (hit any key to pause) "       \ Menu 1.2.1
CR ."       F7 : Action Spectrum "                        \ Menu 1.2.2
CR ."       F10: Exit "                                   \ Menu 1
2 FLAG [ 1 ] :=
0 FLAG [ 2 ] :=
;
: MENU1.2.1  \ ****************************************************
SCREEN.CLEAR
CR ." ------------------------------------------------------------------ "
                                                          \ Menu 1.2.1
CR ."       F5  : Find flatband potential "               \ Does Flat.find
CR ."       F6  : Plot IV curve on HP7475 "               \ Does nic.hp7475.B
CR ."       F7  : Store x-y in SIGMA file "                     \ Does nic.123
CR ."       F10 : Exit    "                               \ Menu 1.2
1 FLAG [ 2 ] :=
;
: MENU1.2.2  \ ****************************************************
SCREEN.CLEAR
CR ." ------------------------------------------------------------------ "
                                                          \ Menu 1.2.2  "
CR ."       F5  : Find Peak   "                           \ Does Peak.find
CR ."       F6  : Plot spectrum on HP7475                 \ Does nic.hp7475.A
CR ."       F7  : Store x-y in SIGMA file "                     \ Does nic.123
CR ."       F8  : Integrate Peak                          \ Does P.T.I
CR ."       F10 : Exit "                                  \ Menu 1.2
2 FLAG [ 2 ] :=
;

: F10.MENU.OUT
FLAG [ 1 ]
CASE
   0 OF BYE    ENDOF                                      \ In Menu1
   1 OF MENU1  ENDOF                                      \ In Menu 1.1
   2 OF FLAG [ 2 ]
     CASE
        0 OF MENU1   ENDOF                                \ From Menu 1.2
        1 OF MENU1.2 ENDOF                                \ From Menu 1.2.1
        2 OF MENU1.2 ENDOF                                \ From Menu 1.2.2
     ENDCASE
           ENDOF
ENDCASE
```

```
;

: F5.MENU.IN  \ Determines the action of F5 at different Menu levels
FLAG [ 1 ]
CASE
   0 OF MENU1.1 ENDOF                                    \ In Menu 1
   1 OF
     NIC.READ MENU1.1  ENDOF                             \ In Menu 1.1
   2 OF FLAG [ 2 ]
     CASE
        0 OF NIC.FILE MENU1.2 ENDOF                      \ In Menu 1.2
        1 OF NOP ENDOF  \  FLAT.FIND   ENDOF             \ In Menu 1.2.1 *****
        2 OF PEAK.FIND MENU1.2.2  ENDOF                  \ In Menu 1.2.2
     ENDCASE
           ENDOF
ENDCASE
onerr:
F10.MENU.OUT
;

: F6.MENU.IN  \ Determines the action of F6 at different Menu levels
FLAG [ 1 ]
CASE
   0 OF MENU1.2 ENDOF                                \ In Menu 1
   1 OF
     NIC.STORE MENU1.1 ENDOF                         \ In Menu 1.1
   2 OF FLAG [ 2 ]
     CASE
        0 OF IV.PLOT  MENU1.2.1     ENDOF            \ In Menu 1.2
        1 OF NIC.HP7475.B MENU1.2.1 ENDOF            \ In Menu 1.2.1
        2 OF NIC.HP7475.A MENU1.2.2 ENDOF            \ In Menu 1.2.2
     ENDCASE
           ENDOF
ENDCASE
onerr:
F10.MENU.OUT
;

: F7.MENU.IN
FLAG [ 1 ]
CASE
   0 OF NOP      ENDOF                               \ In Menu 1
   1 OF NOP      ENDOF                               \ In Menu 1.1
   2 OF FLAG [ 2 ]
     CASE
        0 OF ACTION.PLOT MENU1.2.2 ENDOF             \ In Menu 1.2
```

```
        1 OF NIC.123 MENU1.2.1     ENDOF          \ In Menu 1.2.1
        2 OF NIC.123 MENU1.2.2     ENDOF          \ In Menu 1.2.2
     ENDCASE     ENDOF
ENDCASE
onerr:
F10.MENU.OUT
;

: F8.MENU.IN
FLAG [ 1 ]
CASE
   0 OF NOP      ENDOF                            \ In Menu 1
   1 OF NOP      ENDOF                            \ In Menu 1.1
   2 OF FLAG [ 2 ]
     CASE
        0 OF NOP              ENDOF               \ In Menu 1.2
        1 OF NOP              ENDOF               \ In Menu 1.2.1
        2 OF P.T.I            ENDOF               \ In Menu 1.2.2
     ENDCASE     ENDOF
ENDCASE
onerr:
F10.MENU.OUT
;


: MENU.MAIN
F5  FUNCTION.KEY.DOES F5.MENU.IN
F6  FUNCTION.KEY.DOES F6.MENU.IN
F7  FUNCTION.KEY.DOES F7.MENU.IN
F8  FUNCTION.KEY.DOES F8.MENU.IN
F10 FUNCTION.KEY.DOES F10.MENU.OUT
02 control.key.does base.lin                    \ set CTRL B to perform base.lin
;

MENU.MAIN
GRAPHICS.DISPLAY
VUNORM
MENU1
```

PROGRAM TO PLOT TWO SIGNALS AND THEIR DIFFERENCE TOGETHER

```
\
\                    DIFFERENCE.PRG
\                  Program to plot two signals and
\                 their differences together
\
\
\
\
\
ECHO.OFF
Integer dim[ 1024 ] array nic1.buff        \ creates array for GPIB buffer
Integer dim[ 1024 ] array nic2.buff        \ Two arrays were created

vuport vunorm
: vuport.setup                             \ set up VUPORT VUNORM
      vunorm
      0.0 0.25 vuport.orig
      1.0 0.75 vuport.size
      0 vuport.color
      9 label.color
      10 color
      15 axis.color
      13 cursor.color
      inten.off
;
: Menu.bild
SCREEN.CLEAR
CR ." ------------------------------------------------------------------ "
CR ."      F5  : Plot spectrum on screen "
CR ."      F6  : Plot spectrum on HP7475 "
CR ."      F7  : Read file "
CR ."      F8  : Store x-y as ASCII File "
;

      integer scalar indx                  \ Index-# to subfile
20          string filename
50          string title                   \ String length for title
64          string commstr
                                           \ Array NIC.BUFF was declared
                                           \ in NICOLET.PRG

15 set.file.parse                          \ set default path to subdirectory
data.file c:\data3\dummy.dat               \ c:\asyst\data\*.dat

: yesno
```

```
                                                    \ leaves true on stack if
                                                    \ string = " y"
        "input 1 "left
        " y" "=
;
\
\
\
\
\
\
\
\
\
: nic.file                                          \ Read stored data
        stack.clear
        normal.display
        CR ." Filename .....: "
        "input filename ":=
        filename defer> file.open
        screen.clear
        CR ."       Your file contains following data " CR CR
        10 0 d-                                     \ Read comment strings from file
            i 2 * 1 + comment> -trailing i 1 + . "type  CR
            "      Created...: "
            i 2 * 2 + comment> -trailing "cat "type CR
        loop
        CR ." file-# to read .....: "
        #input indx :=
        indx subfile
        nic1.buff file>array
        CR ." file-# to read .....: "
        #input indx :=
        indx subfile
        nic2.buff file>array
        graphics.display vunorm
        file.close
        menu.bild
;
```

GET.PRG
Program to retrive waveforms
stored by STORE.PRG

```
\
\
\
\
\
\
\
```

PLOT.PRG
Program to plot waveforms on the screen

```
: integer.label.format                          \ sets x-axis labels to integer
                                                \ see G1.4.19
      ?horizontal if
      drop fix "."                              \ drop y-value and put the integer
                                                \ value on symbol stack
      else label.string then
;

dp.real dim[ 1024 ] array xax
dp.real dim[ 1024 ] array yax1
dp.real dim[ 1024 ] array yax2
dp.real dim[ 1024 ] array yax3
                scalar maxx
                scalar minx
                scalar maxy1
                scalar miny1
                scalar maxy2
                scalar miny2
                scalar volt
                scalar ohms
                scalar y1
                scalar y2
                scalar y3
                scalar y4
                scalar ydiv1
                scalar ydiv2
integer          scalar delta
                scalar plt.indx

: axis.setup                                    \ set up optimized axis for I-V plots
      CR ." Start Potential.....: " #input minx :=
      CR ." F id Potential.....: " #input maxx :=
      CR ." Voltage setting of NICOLET in mv ... : "   \ can be replaced by
                                                \ direct reading from
                                                \ the NICOLET
                              #input volt :=
      CR ." Measuring resistance .....: "       \ can be read off the
                                                \ potentiostat
```

```
#input 1000. /      ohms :=      \ As NICOLET reading is
                                 \ read in mv and we want
                                 \ the current in uA the
                                 \ resistance has tto be
                                 \ divided by 1000

CR ." Title.....: "
"input title ":=

nic1.buff                        yax1 :=
yax1 2048. / volt * ohms /          yax1 :=
nic2.buff                        yax2 :=
yax2 2048. / volt * ohms /          yax2 :=

1024 ramp maxx minx - 1024 / * minx +     xax :=
yax1 yax2 -                       yax3 :=       \ Diff. of two
                                                \ arrays
axis.defaults
vertical axis.fit.off grid.off
label.scale.off
horizontal axis.fit.off grid.off
label.scale.off
normal.coords
0.13 0.12 axis.orig
0.13 0.12 axis.point
0.7 0.7 axis.size
50                          delta :=      \ Change delta if other
                                          \ spacing between x-tics
                                          \ is desired
maxx dup delta modulo -          maxx :=
horizontal minx maxx world.set
vertical yax1 []min/max world.set
maxx minx - delta /
8 axis.divisions
horizontal 0 1 label.points
vertical -1. 0 5 label.format
0.007 0.005 tick.size
0 0 tick.just
install integer.label.format in label.string.xeq
vuport.clear
xy.axis.plot
normal.coords
0.83 0.82 axis.point                    \ Second axis defining
horizontal minx maxx world.set
vertical yax3 []min/max world.set
maxx minx - delta /
```

```
        8 axis.divisions
        0.1 0 5 label.format
        1 1 tick.just
        horizontal no.labels
        xy.axis.plot
        normal.coords
        7 label.color
        0.02 0.3 position 90 char.dir 90 label.dir
        " Total current/uA" label
        0.48 0.02 position 0 char.dir 0 label.dir
        " Potential/mv (vs. Ag/AgCl)" centered.label
        0.93 0.66 position 270 char.dir 270 label.dir
        " Photocurrent/uA" label
        0.49 0.86 position 0 char.dir 0 label.dir
        \ " I-V PLOT :          " centered.label
        title centered.label
        10 color
        9 label.color
        world.coords
;

: iv.plot
        axis.setup
        vertical yax1 []min/max world.set
        solid
        maxx xax [ 1 ] -
        1024 xax [ 1024 ] xax [ 1 ] - / * plt.indx :=
        xax sub[ 2 , plt.indx ]                    \ cut off data at the end
        yax1 sub[ 2 , plt.indx ] xy.data.plot      \ to fit plot into range
        3 color
        0.01 0.05 0.01 0.05 dashed
        xax sub[ 2 , plt.indx ]
        yax2 sub[ 2 , plt.indx ] xy.data.plot
        vertical yax3 []min/max world.set
        solid
        xax sub[ 2 , plt.indx ]
        yax3 sub[ 2 , plt.indx ] xy.data.plot
        cursor.off
        screen.clear
        MENU.BILD
        yax1 []min .                               \ To see these values on the screen
        yax1 []max .
        yax2 []min .
        yax2 []max .
        yax3 []min .
        yax3 []max .
```

```
;
\
\
\
\
\
\
\
```

ASCII.PRG
Program to save plot as ASCII file

```
: nic.asc
        CR ." Start Potential.....: " #input minx :=
        CR ." End Potential.....: " #input maxx :=
        CR ." Voltage setting of NICOLET in mv ... : "  \ can be replaced by
                                                        \ direct reading from
                                                        \ the NICOLET
                              #input volt :=
        CR ." Measuring resistance .....: "             \ can be read off the
                                                        \ potentiostat
                #input 1000. /      ohms :=             \ As NICOLET reading is
                                                        \ read in mv and we want
                                                        \ the current in uA the
                                                        \ resistance has tto be
                                                        \ divided by 1000

        nic1.buff                           yax1 :=
        yax1 2048. / volt * ohms /             yax1 :=
        nic2.buff                           yax2 :=
        yax2 2048. / volt * ohms /             yax2 :=

        1024 ramp maxx minx - 1024 / * minx +      xax :=
        yax1 yax2 -                             yax3 :=     \ Diff. of two
                                                            \ arrays
        normal.display
        cr ." Files are stored on b:\ " cr
        cr ." Name of ASCII File (No Extension) ....."
        "input " .asc" "cat filename ":=
        chdir b:\
        filename defer> out>file console.off
        -1 5 fix.format
        1024 1 + 1
        do cr xax [ I ] .
             yax1 [ I ] .
             yax2 [ I ] .
             yax3 [ I ] .
        loop
        console
        out>file.close
```

```
        chdir c:\asyst
        menu.bild
;

: nic.hp7475.B                                  \ Plot IV-Plot
        CR ." yax1 min.....: " #input y1 :=     \ Input from the screen
        CR ." yax1 max.....: " #input y2 :=
        CR ." yax3 min.....: " #input y3 :=
        CR ." yax3 max.....: " #input y4 :=
        CR ." ydiv1.....: " #input ydiv1 :=
        CR ." ydiv2.....: " #input ydiv2 :=
        def.vuport
        load.overlay c:\asyst\hpplotr.sov
        hp7475
        device.init
        plotter.defaults
        7.8 10.15 plotter.size
        1 color
        normal.coords
        0.13 0.17 axis.orig
        0.13 0.17 axis.point
        0.72 0.7 axis.size
        horizontal minx maxx world.set
        vertical y1 y2 world.set
        maxx minx - delta /
        8 ydiv1 axis.divisions                  \ variable axis divisions for y-axis
        maxx minx - delta /
        10. > if 0 2 horizontal label.points
        else 0 1 horizontal label.points then
        1 1 vertical label.points
        vertical -1. 0 5 label.format
        0.007 0.005 tick.size
        0 0 tick.just
        install integer.label.format in label.string.xeq
        xy.axis.plot
        normal.coords
        0.85 0.87 axis.point                    \ Difining second set of axes
        horizontal minx maxx world.set
        vertical y3 y4 world.set
        maxx minx - delta /
        8 ydiv2 axis.divisions                  \ variable axis divisions for y-axis
        maxx minx - delta /
        10. > if 0 2 horizontal label.points
        else 0 1 horizontal label.points then
        1 1 vertical label.points
        vertical 0.2 0 5 label.format
```

```
        1 1 tick.just
        horizontal no.labels
        xy.axis.plot
        normal.coords
        0.04 0.4 position 90 char.dir 90 label.dir
        " Total current/uA" label
        0.49 0.1 position 0 char.dir 0 label.dir
        " Potential/mv (vs. Ag/AgCl)" centered.label
        0.95 0.63 position 270 char.dir 270 label.dir
        " Photocurrent/uA" label
        0.49 0.89 position 0 char.dir 0 label.dir
        \ " I-V PLOT :                " centered.label
        title centered.label
        world.coords
        vertical yax1 []min/max world.set
        \ 0.01 0.01 0.01 0.01 dashed
        solid
        xax sub[ 2 , plt.indx ]                    \ first data point is neglected
        yax1 sub[ 2 , plt.indx ] xy.data.plot
        \ 0.001 0.01 0.001 0.01 dashed
        solid
        xax sub[ 2 , plt.indx ]
        yax2 sub[ 2 , plt.indx ] xy.data.plot
        vertical yax3 []min/max world.set
        solid
        xax sub[ 2 , plt.indx ]
        yax3 sub[ 2 , plt.indx ] xy.data.plot
        graphics.display
        vunorm vuport.clear
        vuport.setup
        Menu.bild
;

: MENU.MAIN
   F5  FUNCTION.KEY.DOES IV.PLOT
   F6  FUNCTION.KEY.DOES NIC.HP7475.B
   F7  FUNCTION.KEY.DOES NIC.FILE
   F8  FUNCTION.KEY.DOES NIC.ASC
;
MENU.MAIN
GRAPHICS.DISPLAY
VUNORM
MENU.BILD
```